

Copyright
by
Hamed Darabi
2014

**The Dissertation Committee for Hamed Darabi Certifies that this is the approved
version of the following dissertation:**

**Development of a Non-Isothermal Compositional Reservoir Simulator
to Model Asphaltene Precipitation, Flocculation, and Deposition and
Remediation**

Committee:

Kamy Sepehrnoori, Supervisor

Ekwere J. Peters

Mojdeh Delshad

Kishore Mohanty

Walter G. Chapman

**Development of a Non-Isothermal Compositional Reservoir Simulator
to Model Asphaltene Precipitation, Flocculation, and Deposition and
Remediation**

by

Hamed Darabi, B.E.; M.S.

Dissertation

Presented to the Faculty of the Graduate School of
The University of Texas at Austin
in Partial Fulfillment
of the Requirements
for the Degree of

Doctor of Philosophy

The University of Texas at Austin

May 2014

Dedication

To my wife,

Rojan,

for her never-ending love, patience, and encouragement.

To my parents,

Kobra and Gholamreza,

without their support none of this would have been possible.

Acknowledgements

This dissertation would not have been possible without the support of many people.

First, I would like to express my sincere gratitude to my supervising professor, Dr. Kamy Sepehrnoori, for his continuous guidance, support, and encouragement. I have learned a lot from his profound insight, keen observations, and vast knowledge. I am privileged to have had an opportunity to work with him. He was a true guide for getting through some of the challenges familiar to many graduate students.

This dissertation would not be what it is today without the additional guidance provided to me by the other members of my graduate committee, Dr. Ekwere J. Peters, Dr. Mojdeh Delshad, Dr. Kishore Mohanty, and Dr. Walter G. Chapman. I also would like to thank Dr. Chowdhury Mamun for careful review of my work and comments on my dissertation.

I would like to thank the staff of the Petroleum and Geosystems Engineering Department at The University of Texas at Austin, Dr. Roger Terzian, Michelle Mason, Joanna Castillo, Cheryl Kruzic, and Frankie Hart for their technical and administrative support.

Special thanks to my friends Mahdy Shirdel, Abolghasem Kazeminia, Mohsen Taghavifar, Mohsen Rezaveisi, Saeedeh Mohebbinia and Amin Ettehad for their indispensable help and knowledge sharing. I enjoyed technical discussions with Dr. Abdoljalil Varavei and Dr. Mohammad H. Kalaei. I would also like to thank my great colleagues and friends Ali Abouei, Ali Goudarzi, Mahdy Haddad, Reza Ganjdanesh, Amir Reza Rahmani, Mehdi Haghshenas, Behdad Aminzadeh, Hassan Dehghanpour, Ali

Afsharpour, Ali Moinfar, Javad Behseresht, Mehran Hosseini, Shayan Tavassoli, and Amir Frooqnia.

I sincerely thank the financial support provided by Abu Dhabi National Oil Company and Reservoir Simulation JIP at the Center for Petroleum and Geosystem Engineering Department at The University of Texas at Austin.

Development of a Non-Isothermal Compositional Reservoir Simulator to Model Asphaltene Precipitation, Flocculation, and Deposition and Remediation

Hamed Darabi, Ph.D.

The University of Texas at Austin, 2014

Supervisor: Kamy Sepehrnoori

Asphaltene precipitation, flocculation, and deposition in the reservoir and producing wells cause serious damages to the production equipment and possible failure to develop the reservoirs. From the field production prospective, predicting asphaltene precipitation, flocculation, and deposition in the reservoir and wellbore may avoid high expenditures associated with the reservoir remediation, well intervention techniques, and field production interruption. Since asphaltene precipitation, flocculation, and deposition strongly depend on the pressure, temperature, and composition variations (e.g. phase instability due to CO₂ injection), it is important to have a model that can track the asphaltene behavior during the entire production system from the injection well to the production well, which is absent in the literature.

Due to economic concerns for asphaltene related problems, companies spend a lot of money to design their own asphaltene inhibition and remediation procedures. However, due to the complexity and the lack of knowledge on the asphaltene problems, these asphaltene inhibition and remediation programs are not always successful. Near-wellbore asphaltene inhibition and remediation techniques can be divided into two

categories: changing operating conditions, and chemical treatment of the reservoir. Although, the field applications of these procedures are discussed in the literature, a dynamic model that can handle asphaltene inhibition and remediation in the reservoir is missing.

In this dissertation, a comprehensive non-isothermal compositional reservoir simulator with the capability of modeling near-wellbore asphaltene inhibition and remediation is developed to address the effect of asphaltene deposition on the reservoir performance. This simulator has many additional features compared to the available asphaltene reservoir simulators. We are able to model asphaltene behavior during primary, secondary, and EOR stages. A new approach is presented to model asphaltene precipitation and flocculation. Adsorption, entrainment, and pore-throat plugging are considered as the main mechanisms of the asphaltene deposition. Moreover, we consider porosity, absolute permeability, and oil viscosity reductions due to asphaltene.

It is well known that the asphaltene deposition on the rock surface changes the wettability of the rock towards oil-wet condition. Although many experiments in the literature have been conducted to understand the physics underlying wettability alteration due to asphaltene deposition, a comprehensive mathematical model describing this phenomenon is absent. Based on the available experimental data, a wettability alteration model due to asphaltene deposition is proposed and implemented into the simulator.

Furthermore, the reservoir simulator is coupled to a wellbore simulator to model asphaltene deposition in the entire production system, from the injection well to the production well. The coupled reservoir/wellbore model can be used to track asphaltene deposition, to diagnose the potential of asphaltene problems in the wellbore and reservoir, and to find the optimum operating conditions of the well that minimizes asphaltene problems.

In addition, the simulator is capable of modeling near-wellbore asphaltene remediation using chemical treatment. Based on the mechanisms of the asphaltene-dispersant interactions, a dynamic modeling approach for the near-wellbore asphaltene chemical treatments is proposed and implemented in the simulator. Using the dynamic asphaltene remediation model, we can optimize the asphaltene treatment plan to reduce asphaltene related problems in a field.

The results of our simulations show that asphaltene precipitation, flocculation, and deposition in the reservoir and wellbore are dynamic processes. Many parameters, such as oil velocity, wettability alteration, pressure, temperature, and composition variations influence the trend of these processes. In the simulation test cases, we observe that asphaltene precipitation, flocculation, and deposition can occur in primary production, secondary production, or EOR stages. In addition, our results show that the wettability alteration has the major effect on the performance of the reservoir, comparing to the permeability reduction. During CO₂ flooding, asphaltene precipitation occurs mostly at the front, and asphaltene deposition is at its maximum close to the reservoir boundaries where the front velocity is at its minimum. In addition, the results of the coupled reservoir/wellbore simulator show that the behavior of asphaltene in the wellbore and reservoir are fully coupled with each other. Therefore, a standalone reservoir or wellbore simulator is not able to predict the asphaltene behavior properly in the entire system. Finally, we show that the efficiency of an asphaltene chemical treatment plan depends on the type of dispersant, amount of dispersant, soaking time, number of treatment jobs, and the time period between two treatment jobs.

Table of Contents

List of Tables	xiv
List of Figures.....	xvii
Chapter 1: Introduction.....	1
1.1 Description of the Problem	1
1.2 Research Objectives.....	3
1.3 Brief Description of the Chapters	4
Chapter 2: Background and Literature Review.....	7
2.1 Asphaltene Definition	7
2.2 Solubility in Crude Oil.....	8
2.3 Conditions of Asphaltene Precipitation	9
2.4 Asphaltene Precipitation Models	10
2.5 Asphaltene Flocculation.....	13
2.6 Asphaltene Deposition	16
2.7 Wettability Alteration	17
2.8 Reservoir Models	21
2.9 Field Experiences.....	23
Chapter 3: Review of UTCOMP Simulator	29
3.1 Introduction to UTCOMP	29
3.2 Governing Equations	31
3.2.1 Mass Conservation Equations.....	31
3.2.2 Pressure Equation.....	34
3.2.3 Phase Behavior Calculation	35
3.3 Solution Methods	36
3.3.1 Phase Behavior Calculation Algorithm	36
3.3.2 Overall Computational Procedure of UTCOMP.....	38

Chapter 4: Implementation of Energy Equation in UTCOMP.....	40
4.1 Review of Thermal Simulators	40
4.2 Energy Balance Equation.....	41
4.3 Enthalpy and Internal Energy	42
4.4 Heat Loss Term.....	43
4.5 Physical Properties.....	45
4.5.1 Viscosity	45
4.5.2 Density	47
4.6 Discretization of Energy Equation.....	48
4.7 Solution Procedure of Energy Equation	49
4.8 Overall Computational Procedure of the Non-Isothermal UTCOMP ..	50
4.9 Automatic Time-Step Selection.....	52
4.10 Validation of the Enthalpy Calculation.....	54
4.11 Case Studies of the Non-Isothermal model	55
Chapter 5: Asphaltene Model.....	87
5.1 Asphaltene Precipitation Model.....	87
5.2 Asphaltene Flocculation Model	91
5.3 Asphaltene Deposition Model.....	93
5.4 Porosity and Permeability Reductions	95
5.5 Oil Viscosity	96
5.5 Wettability Alteration Model.....	97
5.6 Modifications of the Governing Equations of UTCOMP.....	101
5.6.1 Mass Conservation Equation	102
5.6.2 Pressure Equation.....	102
5.7 Overall Procedure of the Asphaltene Model in UTCOMP.....	103
5.8 Verification of the Asphaltene Precipitation Model	105
5.9 Verification of the Asphaltene Deposition Model	105
5.10 Summary.....	107
Chapter 6: Results	119
6.1 Fluid Characterization.....	119

Appendix A: Peng-Robinson Equation-of-State	253
Nomenclature	257
References	259

List of Tables

Table 4.1	Comparison of UTCOMP and CMG for the enthalpy change calculation and z -Factor for case 1 at $T=150$ °F and $P=3100$ psi.....	65
Table 4.2	Overall composition of the mixture for case 2.....	65
Table 4.3	Liquid and gas compositions (mole percent) from the flash calculations performed by UTCOMP and CMG for case 2 at $T=150$ °F and $P=1000$ psi.....	65
Table 4.4	Comparison of UTCOMP and CMG for the enthalpy change calculation and z -Factor for case 2 at $T=150$ °F and $P=1000$ psi.....	66
Table 4.5	Reservoir properties and the simulation input data for case 1 (comparison with analytical solution).....	66
Table 4.6	Properties of the fluid used in case 2 (comparison with UTCHEM).67	
Table 4.7	Reservoir properties and the simulation input data for case 2 (comparison with UTCHEM).	67
Table 4.8	Relative permeability data for case 2 (comparison with UTCHEM).68	
Table 4.9	Overall composition of the mixture for case 3 (comparison with CMG).	68
Table 4.10	Reservoir properties and the simulation input data for case 3.	68
Table 4.11	Relative permeability data for case 3 (comparison with CMG).	69
Table 4.12	Overall composition of the mixture for case 4 (comparison with CMG).	69
Table 4.13	Reservoir properties and the simulation input data for case 5.	69

Table 5.1	Properties of the five crude oils that are used in the Al-Maameri and Buckley (2003) set of experiments.	108
Table 5.2	Properties of the brines that are used in the Al-Maameri and Buckley (2003) set of experiments.....	108
Table 5.3	Tuned parameters of proposed wettability alteration model for the five crude oils that are used in the Al-Maameri and Buckley (2003) set of experiments.....	108
Table 5.4	Mixture properties and overall composition of the Burke et al. (1990) fluid.....	109
Table 5.5	Binary interaction coefficients for the Burke et al. (1990) fluid.....	109
Table 5.6	Weyburn dead oil composition (Kohse and Nghiem, 2004).....	110
Table 5.7	Oil core flood data of Minssieux (1997) experiments.	110
Table 5.8	Deposition model parameters for oil core flood simulations (Kohse and Nghiem, 2004).	111
Table 5.9	Necessary parameters of the asphaltene model of UTCOMP.	111
Table 6.1	Overall composition of the Middle East oil.....	142
Table 6.2	Properties of the Middle East oil.	142
Table 6.3	Binary interaction coefficients for the Middle East oil.....	143
Table 6.4	Reservoir properties and the simulation input data for case 1.	144
Table 6.5	Relative permeability data for case 1.....	144
Table 6.6	Operating conditions of the production well for case 2.....	145
Table 6.7	Reservoir properties and the simulation input data for case 4.	145
Table 6.8	Reservoir properties and the simulation input data for case 6.	146
Table 7.1	Simulation input data.	207
Table 8.1	Reservoir properties and the simulation input data for case study 1.237	

Table 8.2	Relative permeability data for case study 1.....	237
-----------	--	-----

List of Figures

Figure 2.1	Schematic of the process of asphaltene flocculation, reproduced from Akbarzadeh et al. (2007).....	28
Figure 4.1	Phase envelope of the mixture generated by UTCOMP.....	70
Figure 4.2	Schematic views of the reservoir and the wells for case 1 (comparison with analytical solution).....	70
Figure 4.3	Comparison of the results (dimensionless temperature versus dimensionless distance) of UTCOMP with the analytical solution. .	71
Figure 4.4	Comparison of the results (dimensionless temperature of grid-block 3) of UTCOMP with the analytical solution.	71
Figure 4.5	Comparison of the results (dimensionless temperature versus dimensionless distance) of UTCOMP with UTCHEM.	72
Figure 4.6	Comparison of oil production rate of UTCOMP with CMG for case 3.	72
Figure 4.7	Comparison of temperature and pressure profiles of UTCOMP with CMG after 2000 days of simulation for case 3.....	73
Figure 4.8	Comparison of temperature and pressure profiles of UTCOMP with CMG after 4000 days of simulation for case 3.....	74
Figure 4.9	Comparison of water saturation profiles of UTCOMP with CMG after 2000 and 4000 days of simulation for case 3.....	75
Figure 4.10	Comparison of temperature variations during simulation for grid-block (20,1,1) of UTCOMP with CMG for case 3.	76

Figure 4.11	Comparison of pressure variations during simulation for grid-block (20,1,1) of UTCOMP with CMG for case 3.	76
Figure 4.12	Comparison of water saturation variations during simulation for grid-block (20,1,1) of UTCOMP with CMG for case 3.	77
Figure 4.13	Comparison of oil production rate of UTCOMP with CMG for case 4.	77
Figure 4.14	Comparison of temperature and pressure profiles of UTCOMP with CMG after 2000 days of simulation for case 4.	78
Figure 4.15	Comparison of temperature and pressure profiles of UTCOMP with CMG after 4000 days of simulation for case 4.	79
Figure 4.16	Comparison of temperature variations during simulation for grid-block (20,1,1) of UTCOMP with CMG for case 4.	80
Figure 4.17	Comparison of pressure variations during simulation for grid-block (20,1,1) of UTCOMP with CMG for case 4.	80
Figure 4.18	Comparison of water saturation variations during simulation for grid-block (20,1,1) of UTCOMP with CMG for case 4.	81
Figure 4.19	Schematic views of the reservoir for case 5.	81
Figure 4.20	Water viscosity versus temperature calculated using the Brill and Beggs correlation.	82
Figure 4.21	Water mass density versus temperature calculated using the Kell correlation.	82
Figure 4.22	Comparison of oil production rate resulted from the isothermal UTCOMP with the non-isothermal UTCOMP for case 5.	83
Figure 4.23	Comparison of cumulative oil production resulted from the isothermal UTCOMP with the non-isothermal UTCOMP for case 5.	83

Figure 4.24	Temperature profile resulted from the non-isothermal UTCOMP after 1000 and 2000 days of simulation for case 5.....	84
Figure 4.25	Pressure profile resulted from the non-isothermal UTCOMP after 1000 and 2000 days of simulation for case 5.....	84
Figure 4.26	Water saturation profile resulted from the non-isothermal UTCOMP after 1000 and 2000 days of simulation for case 5.	85
Figure 4.27	Water viscosity profile resulted from the non-isothermal UTCOMP after 1000 and 2000 days of simulation for case 5.....	85
Figure 4.28	Water mass density profile resulted from the non-isothermal UTCOMP after 1000 and 2000 days of simulation for case 5.	86
Figure 5.1	Schematic views of the P-T diagram of a fluid and the asphaltene precipitation envelope (APE).....	112
Figure 5.2	Schematic views of asphaltene precipitation curve at a constant temperature.	112
Figure 5.3	Asphaltene particle size distribution, reproduced from Kraiwattanawong et al., 2009.....	113
Figure 5.4	Results of the Al-Maamari and Buckley experiments for the five mentioned crude oils in the presence of the unstable brine (pH = 4 and $M = 0.01$).....	113
Figure 5.5	Comparison of the proposed wettability alteration model's prediction and the experimental data for the A-93 oil.	114
Figure 5.6	Comparison of the proposed wettability alteration model's prediction and the experimental data for the Marse-Yellow oil.	114
Figure 5.7	Comparison of the proposed wettability alteration model's prediction and the experimental data for the Mars-Pink oil.....	115

Figure 5.8	Comparison of the proposed wettability alteration model's prediction and the experimental data for the Legrave-97 oil.	115
Figure 5.9	Comparison of the proposed wettability alteration model's prediction and the experimental data for the Tensleep oil.	116
Figure 5.10	Comparison of the results of Al-Maamery and Buckley (2003) experiments for the A-93 oil in the presence of two different brines: (1) unstable brine (pH = 4 and $M = 0.01$), and (2) stable brine (pH = 8 and $M = 1.00$).	116
Figure 5.11	Comparison of asphaltene precipitation model of UTCOMP with Burke al. (1990) experimental data and WinProp module of CMG.	117
Figure 5.12	Permeability resistance factor for the GF3 sample; comparison between experimental data, UTCOMP, and Kohse and Nghiem (2004).	117
Figure 5.13	Permeability resistance factor for the GF1 sample; comparison between experimental data, UTCOMP, and Kohse and Nghiem (2004).	118
Figure 5.14	Permeability resistance factor for the GV5 sample; comparison between experimental data, UTCOMP, and Kohse and Nghiem (2004).	118
Figure 6.1	Asphaltene precipitation curve at reservoir temperature (212 °F) for the Middle East oil, generated by batch calculation of UTCOMP.	147
Figure 6.2	Experimental onset points, and calculated bubble points and offset points at different temperatures.	147
Figure 6.3	Comparison of asphaltene precipitation curves at various temperatures that are calculated using the batch calculation of UTCOMP.	148
Figure 6.4	Experimental onset points, and calculated bubble points and offset points at different CO ₂ mole fractions.	148

Figure 6.5	Comparison of asphaltene precipitation curves at various CO ₂ concentrations that are calculated using the batch calculation of UTCOMP.....	149
Figure 6.6	Well-block pressures for simulations of two cases of considering and ignoring asphaltene modeling.....	149
Figure 6.7	Results after 300 days of simulation for case 1: (a) pressure, (b) asphaltene precipitation, (c) asphaltene flocculation, (d) asphaltene deposition, (e) porosity, (f) horizontal permeability, and (g) oil viscosity profiles.	151
Figure 6.8	Results after 100 days of simulation for case 2: (a) pressure, (b) asphaltene deposition, (c) porosity, and (d) horizontal permeability profiles.	152
Figure 6.9	Results after 200 days of simulation for case 2: (a) pressure, (b) asphaltene deposition, (c) porosity, and (d) horizontal permeability profiles.	153
Figure 6.10	Results after 300 days of simulation for case 2: (a) pressure, (b) asphaltene deposition, (c) porosity, and (d) horizontal permeability profiles.	154
Figure 6.11	Results after 400 days of simulation for case 2: (a) pressure, (b) asphaltene deposition, (c) porosity, and (d) horizontal permeability profiles.	155
Figure 6.12	Results after 500 days of simulation for case 2: (a) pressure, (b) asphaltene deposition, (c) porosity, and (d) horizontal permeability profiles.	156

Figure 6.13	Average reservoir pressures for simulations of two cases of considering and ignoring asphaltene modeling; case 2.	157
Figure 6.14	Oil rates for simulations of two cases of considering and ignoring asphaltene modeling; case 2.	157
Figure 6.15	Cumulative oil productions for simulations of two cases of considering and ignoring asphaltene modeling; case 2.	158
Figure 6.16	Initial and final water/oil relative permeability curves for case 3; initial contact angle is (θ_i) is 30° and final contact angle (θ_f) is 60°	158
Figure 6.17	Comparison of the average reservoir pressures of three scenarios: ignoring asphaltene, considering asphaltene with no wettability alteration, and considering asphaltene with wettability alteration from $\theta_i=30^\circ$ to $\theta_f=60^\circ$	159
Figure 6.18	Comparison of the oil productions of three scenarios: ignoring asphaltene, considering asphaltene with no wettability alteration, and considering asphaltene with wettability alteration from $\theta_i=30^\circ$ to $\theta_f=60^\circ$	159
Figure 6.19	Comparison of the cumulative oil productions of three scenarios: ignoring asphaltene, considering asphaltene with no wettability alteration, and considering asphaltene with wettability alteration from $\theta_i=30^\circ$ to $\theta_f=60^\circ$	160
Figure 6.20	Initial and final water/oil relative permeability curves for case 3; initial contact angle is (θ_i) is 30° and final contact angle (θ_f) is 90°	160

Figure 6.21	Comparison of the average reservoir pressures of three scenarios: ignoring asphaltene, considering asphaltene with no wettability alteration, and considering asphaltene with wettability alteration from $\theta_i = 30^\circ$ to $\theta_f = 90^\circ$.	161
Figure 6.22	Comparison of the oil productions of three scenarios: ignoring asphaltene, considering asphaltene with no wettability alteration, and considering asphaltene with wettability alteration from $\theta_i = 30^\circ$ to $\theta_f = 90^\circ$.	161
Figure 6.23	Comparison of the cumulative oil productions of three scenarios: ignoring asphaltene, considering asphaltene with no wettability alteration, and considering asphaltene with wettability alteration from $\theta_i = 30^\circ$ to $\theta_f = 90^\circ$.	162
Figure 6.24	Initial and final water/oil relative permeability curves for case 3; initial contact angle is (θ_i) is 30° and final contact angle (θ_f) is 150° .	162
Figure 6.25	Comparison of the average reservoir pressures of three scenarios: ignoring asphaltene, considering asphaltene with no wettability alteration, and considering asphaltene with wettability alteration from $\theta_i = 30^\circ$ to $\theta_f = 150^\circ$.	163
Figure 6.26	Comparison of the oil productions of three scenarios: ignoring asphaltene, considering asphaltene with no wettability alteration, and considering asphaltene with wettability alteration from $\theta_i = 30^\circ$ to $\theta_f = 150^\circ$.	163

Figure 6.27	Comparison of the cumulative oil productions of three scenarios: ignoring asphaltene, considering asphaltene with no wettability alteration, and considering asphaltene with wettability alteration from $\theta_i=30^\circ$ to $\theta_f=150^\circ$	164
Figure 6.28	Comparison of the cumulative oil productions of five scenarios: ignoring asphaltene, considering asphaltene, and considering asphaltene with wettability alteration from $\theta_i=30^\circ$ to $\theta_f=60^\circ, 90^\circ$, and 150°	164
Figure 6.29	Results after 500 days of simulation for case 4; (a) pressure, (b) water saturation, (c) temperature, (d) asphaltene deposition, (e) asphaltene concentration, (f) horizontal permeability, (g) water viscosity, and (h) oil viscosity maps.....	166
Figure 6.30	Results after 1000 days of simulation for case 4; (a) pressure, (b) water saturation, (c) temperature, (d) asphaltene deposition, (e) asphaltene concentration, (f) horizontal permeability, (g) water viscosity, and (h) oil viscosity maps.....	168
Figure 6.31	Results after 1500 days of simulation for case 4; (a) pressure, (b) water saturation, (c) temperature, (d) asphaltene deposition, (e) asphaltene concentration, (f) horizontal permeability, (g) water viscosity, and (h) oil viscosity maps.....	170
Figure 6.32	Oil rates for simulations of two scenarios of considering and ignoring asphaltene modeling; case 4.....	171
Figure 6.33	Water/oil ratios for simulations of two scenarios of considering and ignoring asphaltene modeling; case 4.....	171
Figure 6.34	Cumulative oil productions for simulations of two scenarios of considering and ignoring asphaltene modeling; case 4.....	172

Figure 6.35	Comparison of the oil production rates of five scenarios: ignoring asphaltene, considering asphaltene, and considering asphaltene with wettability alteration from $\theta_i=30^\circ$ to $\theta_f=60^\circ, 90^\circ$, and 150°	172
Figure 6.36	Comparison of the water/oil ratios of five scenarios: ignoring asphaltene, considering asphaltene, and considering asphaltene with wettability alteration from $\theta_i=30^\circ$ to $\theta_f=60^\circ, 90^\circ$, and 150°	173
Figure 6.37	Comparison of the cumulative oil productions of five scenarios: ignoring asphaltene, considering asphaltene, and considering asphaltene with wettability alteration from $\theta_i=30^\circ$ to $\theta_f=60^\circ, 90^\circ$, and 150°	173
Figure 6.38	Results after 500 days of simulation for case 5 when $\theta_f=60^\circ$: (a) water saturation, (b) temperature, (c) water relative permeability, and (d) oil relative permeability maps.....	174
Figure 6.39	Results after 500 days of simulation for case 5 when $\theta_f=90^\circ$: (a) water saturation, (b) temperature, (c) water relative permeability, and (d) oil relative permeability maps.....	175
Figure 6.40	Results after 500 days of simulation for case 5 when $\theta_f=150^\circ$: (a) water saturation, (b) temperature, (c) water relative permeability, and (d) oil relative permeability maps.....	176
Figure 6.41	Results after 100 days of simulation for case 6: (a) pressure, (b) CO ₂ concentration, (c) asphaltene precipitation, (d) asphaltene flocculation, (e) asphaltene concentration, (f) asphaltene deposition, and (g) horizontal permeability maps.....	178

Figure 6.42	Results after 420 days of simulation (around CO ₂ breakthrough) for case 6: (a) pressure, (b) CO ₂ concentration, (c) asphaltene precipitation, (d) asphaltene flocculation, (e) asphaltene concentration, (f) asphaltene deposition, and (g) horizontal permeability maps.....	180
Figure 6.43	Results after 1000 days of simulation for case 6: (a) CO ₂ concentration, (b) asphaltene concentration, (c) asphaltene deposition, and (d) horizontal permeability maps.....	181
Figure 6.44	Comparison of the oil production rates in the presence and absence of the asphaltene deposition.	182
Figure 6.45	Comparison of the cumulative oil productions in the presence and absence of the asphaltene deposition.	182
Figure 6.46	Comparison of the after breakthrough cumulative oil productions in the presence and absence of the asphaltene deposition.	183
Figure 6.47	Comparison of the oil production of the five scenarios: ignoring asphaltene, considering asphaltene and ignoring wettability alteration, and considering asphaltene with wettability alteration to $\theta_f=60^\circ$, 90° , and 150°	183
Figure 6.48	Comparison of the cumulative oil productions of the five scenarios: ignoring asphaltene, considering asphaltene and ignoring wettability alteration, and considering asphaltene with wettability alteration to $\theta_f=60^\circ$, 90° , and 150°	184
Figure 6.49	Comparison of the cumulative oil production of the three scenarios: ignoring asphaltene, considering asphaltene and ignoring gas override, and considering asphaltene with gas override.	184

Figure 6.50	Results after 300 days of simulation for case 8: (a) CO ₂ concentration, (b) top layer permeability, (c) middle layer permeability, and (d) bottom layer permeability maps.....	185
Figure 6.51	Results after 1000 days of simulation for case 8: (a) CO ₂ concentration, (b) top layer permeability, (c) middle layer permeability, and (d) bottom layer permeability maps.....	186
Figure 7.1	Schematic views of the deposition mechanisms: (a) diffusion, (b) inertia, and (c) impaction.	208
Figure 7.2	Illustration of the reservoir model.....	208
Figure 7.3	Oil and water relative permeability curves.....	209
Figure 7.4	(a) Asphaltene deposition and (b) permeability maps after 6 months in the reservoir.	209
Figure 7.5	(a) Pressure, (b) temperature, (c) oil superficial velocity, (d) asphaltene concentration, and (e) asphaltene thickness profiles in the wellbore after 1, 10, 50, and 100 days of simulation.	211
Figure 7.6	Oil production rates over six months of production.	211
Figure 7.7	Bottom-hole pressures over six months of production.	212
Figure 7.8	Cumulative oil productions over six months of production.....	212
Figure 7.9	Pressure response of the reservoir because of asphaltene deposition in the wellbore after 10, 50, 100 days of production; (a) no workover, (b) with workover.....	213
Figure 7.10	(a) CO ₂ concentration, (b) asphaltene precipitation, (c) asphaltene deposition, and (d) permeability maps of the reservoir after 300 days of simulation.....	214

Figure 7.11	(a) CO ₂ concentration, (b) asphaltene precipitation, (c) asphaltene deposition, and (d) permeability maps of the reservoir after 800 days of simulation.....	215
Figure 7.12	(a) CO ₂ concentration and (b) permeability maps of the reservoir after 900 days of simulation.....	216
Figure 7.13	(a) Pressure, (b) temperature, (c) oil superficial velocity, (d) asphaltene concentration, and (e) asphaltene thickness profiles in the wellbore after 800, 850, and 900 days of simulation.....	217
Figure 7.14	Oil production rates after 100 days of CO ₂ breakthrough.....	218
Figure 7.15	Cumulative oil productions after 100 days of CO ₂ breakthrough...	218
Figure 8.1	Oil production profile for the well in case history 2, reproduced from Newberry and Barker (2000).....	238
Figure 8.2	Oil production profile for the well in case history 3, reproduced from Newberry and Barker (2000).....	238
Figure 8.3	Oil production profile for the well in case history 4, reproduced from Newberry and Barker (2000).....	239
Figure 8.4	Adsorption isotherms for DBSA, NP, DP, and NPE6 dispersants, reproduced from Leon et al. (1999).....	239
Figure 8.5	Adsorption isotherms for TBP, SBT, and TOP dispersants, reproduced from Leon et al. (1999).....	240
Figure 8.6	Amount of DBSA adsorbed on the asphaltene particles versus weight ratio of asphaltene over DBSA, reproduced from Chang and Fogler (1994(b)).....	240

Figure 8.7	Specific dissolution rate constant, k , as a function of DBSA concentration in solution, reproduced from Permsukarome et al. (1997).	241
Figure 8.8	Oil production rates for three scenarios of ignoring asphaltene, considering asphaltene, and considering asphaltene with chemical treatment, case 1.....	241
Figure 8.9	Permeability maps after (a) 200 days, (b) 202 days (after treatment), (c) 400 days, and (d) 600 days for case 1.....	242
Figure 8.10	Comparison of oil production rates for three different soaking times of 6 hrs, 1 day, and 2 days for case 2.	243
Figure 8.11	Oil production rates for three scenarios of ignoring asphaltene, considering asphaltene, and considering asphaltene with three chemical treatment jobs.....	243
Figure 8.12	Cumulative oil productions for three scenarios of ignoring asphaltene, considering asphaltene, and considering asphaltene with three chemical treatment jobs.....	244

Chapter 1: Introduction

In this chapter, we discuss the main objectives and the overall scope of this dissertation. Moreover, we briefly review each of the chapters of the dissertation.

1.1 DESCRIPTION OF THE PROBLEM

Asphaltenes are the heavy components of the oil that are sometimes referred to as the “cholesterol of petroleum”. As doctors recommend cholesterol testing every five years to avoid severe medical problems such as heart attack and stroke, we need to track the behavior of the asphaltene in the lifespan of a field to avoid severe asphaltene related problems. Asphaltene precipitation, flocculation, and deposition in the reservoir and producing wells are complex problems that cause serious damages to the production equipment and possible failure to develop the reservoirs. Asphaltene related problems have been observed in different fields around the world such as Ventura field in California, Hassi-Messaoud field in Algeria, Lake Maracaibo field in Venezuela, Little Creek Field in Mississippi, Ula Field in Norway; Villafortuna-Trecate (VF-TR) field in Italy, Comalcalco field in Mexico, various fields in Kuwait, etc. These problems have been observed during primary production, secondary production, and EOR stages.

Asphaltene deposition in the reservoir and wellbore plugs the wellbore and production facilities and reduces the rock porosity and permeability. Asphaltene related problems usually follow costly workover jobs, well interventions, and in severe cases complete shutdown of a field. For instance, Kuwait Oil Company reported that many fields in Kuwait suffered from asphaltene deposition problems from moderate to severe (Al-Qabandi and Al-Naqi, 2003). It was estimated that approximately 100,000 barrels of

oil were lost daily due to the asphaltene related problems. They even shut down one of their fields completely because of asphaltene problems.

Due to the economic concerns about the asphaltene related problems, chemical treatments of the near-wellbore region to control asphaltene deposition have become important in the oil and gas industry. For instance, it was reported that a single asphaltene chemical treatment job in a major producer in Mexico resulted in \$9.3 million revenue over a sixteen-month period with the oil price of \$15 per barrel of oil (Newberry and Barker, 2000). In another well in Mexico, similar chemical treatment job resulted in \$6.5 million over a four-month period (Newberry and Barker, 2000). However, due to the complexity and the lack of knowledge on the asphaltene problems, the asphaltene inhibition and remediation programs are not always successful. The success of an asphaltene treatment plan requires optimization of the amount of injected dispersant, soaking time, number of treatment jobs, and the time period between two treatment jobs.

In this dissertation, we develop a comprehensive non-isothermal compositional reservoir simulator with a capability of modeling near wellbore asphaltene inhibition and remediation to address the effect of asphaltene deposition on the reservoir performance. Since asphaltene precipitation, flocculation, and deposition strongly depend on the pressure, temperature, and composition variations (e.g. phase instability due to CO₂ injection), we track the asphaltene behavior during the entire production system from the injection well to the production well. The coupled reservoir/wellbore model can be used to track asphaltene deposition, to diagnose the potential of asphaltene problems in the wellbore and reservoir, and to find the optimum operating conditions of the well that minimizes asphaltene problems. From the field production perspective, predicting asphaltene precipitation, flocculation, and deposition in the reservoir and wellbore essentially avoids high expenditures associated with the reservoir remediation, well

intervention techniques, and field production interruption. In addition, using the developed asphaltene remediation model, we can design an optimum asphaltene treatment plan to reduce asphaltene related problems in a field.

To the best of our knowledge, our simulator has many additional features compared to the commonly available asphaltene reservoir simulators. These features include modeling the wettability alteration due to asphaltene deposition, considering the effects of pressure, temperature, and composition variations simultaneously on asphaltene behavior, addressing the reservoir-wellbore interactions on the asphaltene deposition, and dynamic modeling of the near-wellbore chemical treatment for asphaltene remediation purpose.

1.2 RESEARCH OBJECTIVES

The main objective of this dissertation is the modeling of asphaltene precipitation, flocculation, and deposition and near-wellbore asphaltene remediation. The asphaltene reservoir simulator that is developed in this dissertation is embedded in UTCOMP, The University of Texas Compositional Simulator.

We summarize the objectives of this research are as follows:

- Implementation of Energy Equation in UTCOMP.
- Dynamic modeling and implementation of asphaltene precipitation, flocculation, and deposition in the reservoir.
- Dynamic modeling and implementation of wettability alteration due to asphaltene deposition.

- Studying the behavior of asphaltene during primary production, secondary production, and EOR stages.
- Addressing the reservoir/wellbore interactions on asphaltene behavior in the entire production system from the production well to the injection well.
- Dynamic modeling and implementation of the near-wellbore asphaltene chemical treatment for asphaltene remediation.

1.3 BRIEF DESCRIPTION OF THE CHAPTERS

In Chapter 2, we present background information about definition of asphaltene, its solubility in crude oil, and conditions of asphaltene precipitation. In addition, we review the related papers for asphaltene precipitation, flocculation and deposition models, and developed asphaltene reservoir simulators. Moreover, some issues on the field experiences of asphaltene around the world will be presented.

In Chapter 3, we present an overview of UTCOMP and its formulation, assumptions, and features, since the asphaltene reservoir simulator that is developed in this study is embedded in UTCOMP.

In Chapter 4, we present the formulation and results of the non-isothermal UTCOMP. Since asphaltene precipitation depends on temperature, pressure, and composition variations and UTCOMP is an isothermal simulator, we implemented the energy equation in UTCOMP to consider the effect of temperature variations on asphaltene behavior. We verify the results of the non-isothermal UTCOMP against the experimental data and other non-isothermal simulators.

In Chapter 5, we present details on the asphaltene model that is implemented in UTCOMP. Details on the asphaltene precipitation, flocculation, and deposition models will be provided. In addition, we will present various models that consider porosity, absolute permeability, oil viscosity, and wettability alterations due to asphaltene precipitation, flocculation, and deposition. At the end of this chapter, we will discuss the solution scheme and the modifications that have been done in the governing equations of UTCOMP.

In Chapter 6, we present various case studies of the asphaltene model in UTCOMP. First, the characterization process of a Middle East oil will be discussed. Then, different case studies will be presented to investigate the effects of pressure variations, temperature variations, composition variations, and wettability alteration on the dynamics of asphaltene precipitation, flocculation, and deposition. The cases studies include the behavior of asphaltene during primary production, secondary production, and EOR stages.

In Chapter 7, a comprehensive non-isothermal compositional coupled wellbore/reservoir simulator with the capability of modeling asphaltene phase behavior in the reservoir and the wellbores will be presented to address the wellbore/reservoir interaction, the effect of asphaltene deposition on the flow prediction and long-term reservoir performance. We present primary production and CO₂ flood simulation cases to investigate the effect of asphaltene deposition on oil recovery.

In Chapter 8, we review available asphaltene inhibition and remediation procedures for the wellbore and reservoir. Then, we present various field case trials of chemical remediation for the reservoirs that have experienced asphaltene deposition problems. In addition, we discuss the mechanisms of asphaltene-dispersant interactions and related reactions. Afterward, we introduce the first near wellbore asphaltene

remediation model that is developed in this work and implemented in UTCOMP. Finally, we present different simulation cases to investigate the effectiveness of chemical treatment jobs on asphaltene remediation.

Finally, in Chapter 9, we present the summary of the dissertation and the concluding remarks. In addition, we recommend the future works that can be accomplished for asphaltene modeling in the reservoir.

Chapter 2: Background and Literature Review

In this chapter, we present background information about definition of asphaltene, its solubility in crude oil, and conditions of asphaltene precipitation. Also, we review the related papers for asphaltene precipitation, flocculation and deposition models, and developed asphaltene reservoir simulators. At the end of this chapter, some issues on the field experiences of asphaltene around the world will be presented.

2.1 ASPHALTENE DEFINITION

The term asphaltene originated in 1837. J.B. Boussingault (1837) defined the residue of the distillation of bitumen as asphaltenes, which are soluble in turpentine while insoluble in alcohol. Today, asphaltenes are defined in the Standard Test Method for n-Heptane Insolubles (ASTM D3279-97, 2001). According to this new definition, asphaltenes are insoluble in alkanes with low molecular weight (specifically n-heptane) and are soluble in benzene. They can be derived from coal, shale oil, and petroleum. The definition of asphaltenes as solubility class makes them much more challenging to study compared to lighter components in crude oil, which have defined chemical structures. Although, the exact chemical structures of asphaltenes are not known, it is fairly well accepted that asphaltenes are the most polarizable and heaviest components of the crude oil, with an average carbon number of 40 to 80 and H/C ratio of 1.1 to 1.2 (Carnahan, 2000). According to Scotti and Montanari (1998), asphaltenes are composed of a polydisperse mixture of molecules, which may contain a few percent of oxygen, sulfur, nitrogen, iron, nickel, vanadium, and polynuclear aromatic components. Lighter components of hydrocarbon can be characterized by standard laboratory methods, such as gas chromatography. However, these standard methods are not applicable for

asphaltenes, and exceptional measurements are usually required for characterizing asphaltenes. Some of the methods that are used to determine asphaltene molecular weight and size include field-ionization mass spectrometry (Boduszynski, 1981), atmospheric pressure photo-ionization mass spectrometry (Merdrignac et al., 2004), field-desorption/field-ionization mass spectrometry (Qian et al., 2007), laser desorption ionization (Hortal et al., 2006), time-resolved fluorescence depolarization (Groenzin and Mullins, 2000), fluorescence correlation spectroscopy (Andrews et al., 2006), and Taylor dispersion diffusion (Wargadalam et al., 2002).

2.2 SOLUBILITY IN CRUDE OIL

The solubility factor of a non-polar molecular mixture is a function of density and electronic polarizability of the mixture components (Ting, 2003). Most of the observed cases of the asphaltene precipitation are explained by these two parameters.

Density has a direct effect on the solubility factor. If density of a mixture increases, the solubility factor will increase and vice versa. For example, if the amount of light hydrocarbons dissolved in the liquid phase is high, the solubility factor will be low due to low density of the mixture. Therefore, asphaltene will precipitate from the liquid phase. Composition variations that decrease density may decrease asphaltene solubility. However, composition variations that increase density may have the opposite effect.

Despite density, polarizability has a reverse effect on the solubility factor. Mixing oil with species that have low polarizability (e.g. methane or lighter oils) will decrease the oil solubility factor. However, higher polarizability materials (e.g. toluene) will increase the solubility factor of crude oil.

2.3 CONDITIONS OF ASPHALTENE PRECIPITATION

Precipitation of asphaltene in crude oil depends on a number of factors such as pressure, temperature, and composition of fluid.

Pressure variations. Asphaltene precipitation is observed within a range above and below the bubble point, during pressure depletion at a constant temperature. During production from an undersaturated reservoir, as pressure drops, density of oil decreases. Therefore, the solubility factor decreases, and asphaltene may precipitate consequently. The maximum amount of precipitation takes place at or around the bubble point pressure. Below the bubble point, the light gases come out of the solution, increasing the density and decreasing the amount of asphaltene precipitation (Ting, 2003). In reservoirs that experience asphaltene precipitation in normal pressure depletion, the oil is usually light to medium with small asphaltene content. Heavy crude oils that contain a large amount of asphaltene have less asphaltene precipitation problems, because solubility factor is high in this case (De Boer et al., 1995). Leontaritis and Mansoori (1988) reviewed some field cases that experienced asphaltene precipitation problems during primary depletion.

Temperature variations. The effect of temperature variations on asphaltene precipitation is more complicated compared to pressure variations. As temperature increases, the oil density decreases, but at the same time the entropy of the solution increases, resulting in a counter balancing effect (Ting, 2003). Temperature change can occur in transportation of oil in offshore fields. The wellhead flowing temperatures are typically between 110-140 °F for shallow reservoirs. In addition, temperature of sea-bottom is often near or below 40 °F. Therefore, temperature of the oil decreases during the transportation which may cause asphaltene precipitation (Moritis, 2001).

Composition variations. Oil composition changes during artificial gas lifting or during gas injection processes such as miscible flooding with CO₂, N₂, and natural gas.

Injected gas decreases the density of crude oil, and therefore, decreases the asphaltene solubility (Verdier et al., 2006). Numerous articles including field reports and laboratory studies on this aspect have been published (Novosad and Costain, 1990; Srivastava et al., 1995; Turta et al., 1997). Variations in composition of crude oil that results in asphaltene precipitation, may also arise from the presence of oil-based muds (Muhammad et al., 2004), or come from the relative proportions of mixing fluids (Moritis, 2001).

2.4 ASPHALTENE PRECIPITATION MODELS

The mechanism of asphaltene precipitation has not been fully understood because of the complex physical behavior of asphaltene. Many thermodynamic models have been proposed to predict the onset point of asphaltene precipitation and the amount of precipitation. We divide these models into three groups: solubility models, solid models, and thermodynamic micellization model.

Solubility models. The base of these models is the Flory-Huggins theory (Flory, 1942). Asphaltene stability is described in terms of reversible solution equilibrium. According to the Flory-Huggins theory, the chemical equilibrium condition between the asphaltene-rich phase A and solvent-rich phase B is $\mu_i^A = \mu_i^B$, where μ_i is the chemical potential of component i . Hirschenberg model (Hirschenberg et al., 1984), Cimino model (Cimino et al., 1995), and Nor-Azlan model (Nor-Azlan and Adewumi, 1993) are in this category. These models are usually easy to implement, but their performances are not very good. They are usually unable to match the experimental data quantitatively.

Hirschenberg model (Hirschenberg et al., 1984) assumes that asphaltene precipitation is reversible, and uses a thermodynamic approach to calculate amount of asphaltene precipitation. In this model, composition of liquid phase is calculated by

Soave Equation-of-State (Soave, 1972), assuming that there is no asphaltene precipitation. Then, the amount of asphaltene precipitation is calculated using modified Flory-Huggins theory. It is assumed that asphaltene precipitation does not change the vapor-liquid equilibrium calculations. According to this model, asphaltene precipitation will increase with a decrease in pressure above the bubble point. On the other hand, below the bubble point, the amount of asphaltene precipitation will decrease with a decrease in pressure. These results are consistent with experiments of asphaltene precipitation, but the prediction of this model is poor to reproduce the experimental data.

Cimino et al. (1995) proposed an asphaltene precipitation model based on polymer solution thermodynamics. One assumption of this model is that an asphaltene nucleus contains both asphaltene class components and the solvent. This model can represent the behavior of asphaltene very well, but it requires several experimental data to determine the model parameters. In addition, this model is not applicable when the composition of original fluid changes (e.g. during gas injection).

Nor-Azlan and Adewumi (1993) proposed a precipitation model that is also based on the thermodynamics of polymer solutions. In this model, a vapor-liquid equilibrium flash calculation is performed using an equation of state. Then, using Flory-Huggins theory, a liquid-liquid equilibrium calculation will be made to calculate the amount of asphaltene precipitation, assuming that the precipitated asphaltene does not affect the vapor-liquid equilibrium calculation in the previous step. This model is a good tool for screening purposes, but it does not match the experimental data quantitatively.

In addition to these models, there are some models that are not based on the Flory-Huggins theory, but can still be considered as solubility models. These models assume that asphaltenes are dissolved in the crude oil. Gonzales Rodriguez (2008) used Perturbed Chain Statistical Association Fluid Theory (PC-SAFT) Equation-of-State to

model asphaltene precipitation. In this model, it is assumed that asphaltene precipitation is a reversible process, asphaltene associates to form pre-aggregates, and asphaltene rich phase contains some amount of the other crude oil components. It is known that the Statistical Association Fluid Theory (SAFT) is able to handle asymmetric mixtures and associating molecules (e.g. asphaltenes) that most of the Equation-of-States could not handle (Chapman et al., 1990). Recently, a modified version of the SAFT was introduced by Gross and Sadowski (2001), which is called the Perturbed Chain Statistical Association Fluid Theory (PC-SAFT). It is believed that the PC-SAFT can represent the behavior of asphaltene properly (Gonzales Rodriguez, 2008). Another Equation-of-state that is used recently for modeling asphaltene is the Cubic Plus Association (CPA) Equation-of-State. CPA, introduced by Kontogeorgis et al. (1996), a combination of a cubic equation of state with association parameter. Similar to PC-SAFT, CPA can predict asphaltene precipitation more accurately, because of the association term, compared to a simple cubic Equation-of-State. However, they are computationally more expensive than cubic Equation-of-States, which makes the cubic Equation-of-States more favorable in large simulation case studies.

Solid models. In these models, oil and gas are modeled with a cubic Equation-of-State, while asphaltene is treated as a single component existing in the solid phase. Gupta's model (Gupta, 1986) and Thomas's model (Thomas et al., 1992) are the two first simple models in this category. To use these models, a large number of parameters should be determined empirically. In addition, matching the experimental data requires a lot of tuning for interaction coefficients and asphaltene fugacity (Thomas et al., 1992). Thomas et al. (1992) extended their single component asphaltene model to multi-component solid phase, but this model is inapplicable due to large number of parameters.

Ngheim et al. (1993) extended Gupta's model to model asphaltene precipitation more efficiently. They proposed a new approach to characterize the asphaltene component. In both models by Gupta and Thomas, it is assumed that asphaltene is the heaviest component in the oil. However, in Neighm's model (Nghiem et al., 1993), it is assumed that the heaviest component in the oil phase splits into a non-precipitating component and a precipitating component. All the properties of these two components (e.g. critical properties, acentric factors, and parachor) are identical, except their interaction coefficients with lighter components. Generally, the precipitating component has a larger interaction coefficient with light components, compared to the non-precipitating component. This means more incompatibility of the precipitating component with the lighter components, resulting in transfer of the precipitating component into the solid phase.

Thermodynamic micellization model. This model, which was developed by Pan and Firoozabadi (1996), assumes asphaltene molecules form a micelle core and the resin molecules adsorb on the surface of this core. Gibbs free energy minimization principle is used to determine the structure and concentration of the micelle. The calculated size of asphaltene micelles in crude oils predicted by this model matched the experimental data. However, the results on the amount of precipitation have not been presented (Pan and Firoozabadi, 1996).

2.5 ASPHALTENE FLOCCULATION

Asphaltene formation in crude oils is a two-step process: first, phase separation and second, asphaltene particle growth (flocculation). Once asphaltene precipitates from the oil, the small asphaltene particles flocculate (aggregate) into larger aggregates.

Precipitated asphaltenes are very small (less than 1 μm diameter size) particles (Kraiwattanawong et al., 2009). On the other hand, flocculated asphaltenes are very large asphaltene particles ranging from a few microns to hundreds of microns (Ferworn et al., 1993). Figure 2.1 illustrates the process of flocculation (Akbarzadeh et al., 2007). As it can be seen in this figure, asphaltene molecules aggregate to form nano-aggregates and clusters of nano-aggregates, respectively. Depending on the nature of the solution and asphaltene, these clusters of nano-aggregates may stay in the fluid and form viscoelastic network, or flocculate into larger particles. In this section, we review some of the works that have been done to study the physics of flocculation process, the flocs size, and the aggregation rate.

Ferworn et al. (1993) measured asphaltene particle size distributions in six different crude oils diluted with n-heptane, using a laser particle analyzer. Since the minimum time required for the laser particle analyzer experiment was greater than asphaltene flocculation time, they could only measure the final flocs size. The results showed that asphaltene flocs have a unimodal, log-normal distribution with mean flocs size ranging from 4.5 to 291 μm .

Nielson et al. (1994) studied the effects of pressure and temperature variations on the asphaltene particle size distribution. They performed a set of experiments on four different crude oils diluted with n-pentane, using a laser particle analyzer. The results showed that average flocculated asphaltene particles size is in the range of 266 to 495 μm . They claimed that asphaltene flocs size increases with an increase in pressure, and slightly decreases with an increase in temperature.

Anisimov et al. (1995) studied the process of asphaltene flocculation in hydrocarbon solutions using photon correlation spectroscopy. Results of their experiments show that basic aggregates size in solutions is in the order of 1 μm , which

eventually transform into flocs of size of about 4-5 μm . They claimed that the nature of the solvent strongly affects the kinetics of flocculation and the stability of asphaltene aggregates in the solution.

Burya et al. (2001) used dynamic light scattering to study asphaltene aggregation in crude oils. They observed a diffusion-limited and a reaction-limited aggregation regime with a crossover regime between them. They showed that an addition of a precipitant to crude oil increases asphaltene aggregation. In addition, they claimed that we may have a fast formation of stable-in-size asphaltene particles or an exponential-in-time flocculation of asphaltene particles into huge flocs, depending on the nature of the precipitant and crude oil.

Joshi et al. (2001) studied the processes of asphaltene precipitation and flocculation during pressure depletion using light scattering and the sedimentation rate. They claimed that the initial asphaltene precipitates, which are small asphaltene particles, are not problematic for the field during production. They showed that different asphaltene flocs will be formed during depressurization of crude oil and that flocculation is a reversible process.

Kraiwatanawong et al. (2009) investigated the effect of different dispersants on the aggregate size distribution and growth of asphaltene particles. They added various chemicals to different crude oils and monitored asphaltene precipitation and flocculation. They showed that none of the chemicals were able to stop asphaltene phase separation (precipitation). However, some of the chemicals were successful in delaying or inhibiting asphaltene flocculation. Based on the asphaltene particle size distribution measurements, they suggested that three different types of asphaltenes exist in crude oils: stable asphaltenes, colloidal asphaltenes, and flocculated asphaltenes. They showed that

asphaltene dispersants can stabilize colloidal asphaltenes and inhibit or delay asphaltene flocculation.

2.6 ASPHALTENE DEPOSITION

Asphaltene may deposit on the rock surface after it precipitates from oil. Civan (1996) proposed the first asphaltene deposition model, which is an extension of the Gruesbeck and Collins (1982) model for fines deposition. Gruesbeck and Collins (1982) used a simple concept (partitioning the porous media into parallel plugging and non-plugging pathways) and developed a robust model for deposition of fine particles. Deposition and entrapment were introduced as two main mechanisms that control decline in production. The model was verified with matching multiple experimental data. Later, Civan (1996) modified the Gruesbeck and Collins (1982) model for deposition of asphaltene and paraffin in porous media. He added a source term to the material balance equation to consider asphaltene or paraffin precipitation. He also included the energy balance equation and dispersion in his model.

Minssieux (1997) performed wide-ranging experiments on different asphaltic oils and found that asphaltene deposition causes permeability reduction up to 90 % of initial permeability, depending on the asphaltene content of oil and rock properties. Different asphaltic fluids from Weyburn, Lagrave, Hassi-Messaoud, and Boscan fields have been tested. Asphaltene content of these fluids was reported between 0.1 to 0.6 % (weight percent). Different rock samples (porosity range: 0.071 to 0.247, permeability range: 0.67 to 107 md) were used in these sets of experiments. The author claimed that permeability reduction because of asphaltene deposition is similar to the process of fines

migration during brine injection. Therefore, the fine migration models would be applicable for permeability reduction due to asphaltene.

Ali and Islam (1998) performed a series of experiments to study permeability reduction due to asphaltene deposition in carbonate rocks. The authors used artificial core samples, with oil samples consisting of dead oil and 3% asphaltene concentration. A deposition model, including adsorption and mechanical entrapment was proposed for asphaltene deposition. The model matched the experimental data provided by Ali and Islam (1998) reasonably well. They stated that asphaltene plugging strongly depends on flow rate, and the maximum plugging occurs near the wellbore.

Wang (2000) presented a more comprehensive model for the asphaltene deposition process. This model is an extension of the Gresbeck and Collin (1982) model. Surface deposition, pore throat plugging, and entrainment of deposits were considered in this model. Experimental and theoretical approaches were provided to determine model parameters. This model matches the experimental data very well, and it is the most reliable model for asphaltene deposition in the literature.

2.7 WETTABILITY ALTERATION

Wettability is a key property that controls multiphase fluid flow in oil recovery processes. It is known that asphaltene deposition on the surface of the rock changes the wettability of the rock toward oil-wet condition. Although many experiments in the literature have been conducted to understand the physics underlying wettability alteration because of asphaltene deposition (e.g. Kim et al., 1990; Buckley, 1996; Al-Maameri and Buckley, 2003), a mathematical model describing this phenomenon is absent. In this

section, we review some of the works that have been done to study wettability alteration due to asphaltene deposition.

Kim et al. (1990) studied the role of asphaltene deposition in wettability alteration. They gradually added n-heptane to four different crude oils and measured the oil/water interfacial tension and the oil surface tension on a solid surface. Addition of n-heptane reduces asphaltene solubility factor; as a result increases asphaltene precipitation and deposition. They found that asphaltene deposition significantly affects interfacial properties of oil/water systems. A sudden change in the oil/water interfacial tension has been observed at the start of asphaltene deposition, while oil surface tension remained unchanged due to asphaltene deposition. Based on the results, Kim et al. (1990) concluded that asphaltene deposition has a substantial role in wettability reversal of a solid surface.

Buckley (1996) performed a comprehensive research on the mechanisms of wettability alteration in crude oil/brine/rock (COBR) systems. She measured the wettability of various crude oils in the presence of different brines on the surface of a glass. The effect of temperature variation was also included in these sets of experiments. Buckley (1996) identified four distinct categories of interactions in COBR systems that affect the wettability: polar interactions, surface precipitation, acid/base interactions, and ion binding. Polar interactions are dominant in the absence of water film on the rock surface. In this case, a monolayer of asphaltene, rich in nitrogen, oxygen, and sulfur, deposits on the surface of the rock. Surface precipitation depends on the solubility factor of asphaltene in crude oils. If the asphaltene solubility factor is low in a crude oil, more asphaltene precipitates from oil, and as a result, a greater change in wettability is expected. Acid/base interactions explain the effects of brine on the oil/water and the rock/water surface charges. In the presence of brine, the oil and rock surfaces will be

charged and the polar components on these surfaces will act as acids or bases. These surface charges affect the stability of the brine film on the rock surface as well as the amount of asphaltene deposition on the rock surface. Ion binding is the interaction between charged surfaces and the high valency ions (e.g. Ca^{2+}). Depending on the type of the interaction, ion bonding can either limit or promote wettability alteration. Based on the results of the experiments, Buckley (1996) concluded that the wettability of rock in a COBR system depends on the composition of the rock, brine, and oil. She showed that asphaltene deposition has a significant effect on the wettability of the rock. Her work became the base of many studies that have been conducted subsequently.

Yan et al. (1997) studied the effect of asphaltene adsorption on the wettability of a sandstone rock. They performed a set of water flood tests on Berea sandstone cores using two different asphaltic oils. They added n-hexane to both oils to increase asphaltene precipitation and measured the wettability of the core using Amott tests. The results showed that wettability of the rock significantly changed toward oil wet condition because of asphaltene deposition. In addition, effects of initial water saturation, brine salinity, and type of brine (NaCl , CaCl_2 , AlCl_3) on wettability were investigated. Results showed that sandstone rock wettability considerably changed toward oil-wet condition due to a decrease in the initial water saturation, or an increase in ionic strength and cation valency (e.g. Na^+ , Ca^{2+} , Al^{3+}) of the brine.

Kaminsky and Radke (1997) presented a model for diffusion of asphaltene particles from surface of oil/water through the water film, followed by asphaltene deposition on the rock surface. They calculated diffusion time of asphaltene particles in the brine film for a crude oil with a very low asphaltene solubility factor. They showed that one reaches adsorption equilibrium in couples of hours, even if the asphaltene solubility factor is extremely low. As a result, they concluded that asphaltene deposition

is not massive in the presence of a thin brine film on the rock surface. They claimed that the significant wettability alteration because of asphaltene deposition is due to rupture of the brine film and direct contact of asphaltene particles with the rock surface.

Armoun and Tiab (2001) reported that the wettability of Rhourd-Nouss Sud Est field in Algeria changed to intermediate condition (very close to neutral condition) because of asphaltene deposition. They measured the wettability of different core samples from this field using the USBM test. They concluded that the rock has a higher tendency to become neutral wet at higher concentration of asphaltene. In addition, they claimed that the wettability alteration due to asphaltene deposition is an irreversible process.

Al-Maamari and Buckley (2003) performed a set of experiments in COBR systems to measure wettability changes due to asphaltene deposition. They gradually added n-heptane to six different crude oils and measured the contact angle at different conditions. The tests were performed in the presence of brine on the surface of mica. Refractive index (RI) was measured to quantify the stability of asphaltene in the mixture. Buckley (1996) demonstrated that there is a correlation between the refractive index of a mixture and the onset of asphaltene precipitation. Asphaltene starts to precipitate at a certain refractive index called P_{RI} . If the RI of the mixture is greater than P_{RI} , asphaltene is stable; otherwise, asphaltene precipitates. Al-Maamari and Buckley (2003) observed that the wettability of rock changes significantly toward oil-wet condition if the brine film on the rock surface is unstable. They concluded that in the presence of a stable water film, asphaltene will be poorly absorbed on the rock surface and the wettability of a water-wet rock will remain unchanged.

2.8 RESERVOIR MODELS

Asphaltene precipitation and deposition occurs in the reservoir during primary production and miscible gas flooding, such as CO₂ injection. Asphaltene deposition may plug pores, change the porosity and permeability in reservoirs, alter rock wettability and affect all aspects of oil production, processing, and transportation. Although many researchers studied fundamentals of asphaltene precipitation, flocculation and deposition, only a few attempts have been made to develop a reservoir simulator to model asphaltene behavior.

Leontaritis (1998) developed a single well simulator to model asphaltene deposition around the wellbore. It was assumed that the well is producing at a constant rate and the flow regime is pseudo-steady state. Asphaltene deposition far from the wellbore was neglected, and thermodynamic colloidal model was used to model asphaltene precipitation. This model is very simple and it is not applicable to real field cases.

Qin (1998) and Qin et al. (2000) implemented an asphaltene model into the UTCOMP (UTCOMP Technical Documentation, 2003), The University of Texas Compositional Reservoir Simulator, which is a three-dimensional compositional simulator that can be used for miscible gas flooding processes. This model is able to simulate asphaltene precipitation and deposition during the primary production. The Nghiem et al. (1993) solid model was used for asphaltene precipitation. Also, permeability and porosity reduction models were included in the model. It was assumed that all the precipitated asphaltene deposits on the rock surface and asphaltene particles cannot move inside the reservoir. Moreover, flocculation (aggregation) of asphaltene and the effect of wettability alteration due to asphaltene deposition were not considered.

Nghiem (1999) developed a reservoir model that can model asphaltene precipitation and deposition during primary production and CO₂ flooding. A solid model is used to model precipitation, and it is assumed that asphaltene flows inside the reservoir with oil. Physical deposition is assumed the dominant asphaltene deposition mechanism as Leontaritis (1998) stated in his model. This was the first three-dimensional asphaltene reservoir model that could handle primary production and EOR processes.

Wang (2000) also proposed a reservoir model for asphaltene deposition during primary production. This model, which is a three-dimensional three-phase black oil simulator, was used for both vertical wells and horizontal wells. Surface deposition, pore throat plugging, and entrainment were included in the deposition model. In addition, permeability and porosity reduction models were incorporated. The solubility model proposed by Hirschberg et al. (1984) was used to calculate the amount of precipitation.

Kohse and Nghiem (2004) extended the reservoir model developed by Nghiem (1999) to consider asphaltene precipitation, flocculation, and deposition. In this model, it is assumed that only flocculated asphaltene can deposit on the rock surface. Both flocculated and precipitated asphaltene have the same properties (e.g. molecular weight and density). Also, the old deposition model is substituted by the Wang (2000) deposition model to consider surface deposition, pore throat plugging, and entrainment. This is a fully implicit simulator that can be used during both primary production and EOR processes.

Fazelipour et al. (2008) developed an asphaltene model embedded in the General Purpose Adaptive Compositional Reservoir Simulator called GPAS (GPAS 3.5 Technical Documentation, 2005). GPAS is a fully implicit compositional reservoir simulator, developed by the reservoir simulation group of PGE Department at The University of Texas at Austin. The asphaltene model uses a solid model for precipitation and is used

during primary production and water flooding. Permeability and porosity reduction are considered. Also, it is assumed that precipitated asphaltene adsorb on the surface of the rock and the asphaltene particles do not flow inside the reservoir.

2.9 FIELD EXPERIENCES

Asphaltene precipitation and deposition have been observed in many fields around the world (Leontaritis and Mansoori, 1988; Kokal and Sayegh, 1995; Newberry and Barker, 2000; Cenegy, 2001). In this section, we review some of these experiences in oil and gas industry.

Ventura field, California. During the early stages of production, significant problems occurred because of asphaltene deposition (Tuttle, 1983). It is reported that asphaltene deposition occurred during primary production, secondary production, and EOR stages. The deposited asphaltene plugged the wellbore and tubing. First, oil was circulated to dilute the crude oil and reduce the amount of precipitation. Then, various solvents such as toluene, pyridine, and carbon disulphide were injected to remove the deposited asphaltene. However, none of these methods were successful to stop the asphaltene problems. It turned out that reducing the bottom-hole pressure below the bubble point pressure reduces asphaltene problems in the wellbore and tubing significantly. The wells that were drilled after finding this solution produced oil with no asphaltene problems in the wellbore and pipelines. However, it took the Ventura field team around 25 years to come up with this solution, which affected the economics of the field significantly. They were forced to re-drill most of the wells.

Prinos field, North Aegean Sea. Asphaltene precipitation and deposition have been seen in the first well that was drilled in the Prinos field (Adialalis, 1982). At the

early stages, the company wanted to shut down the project because it was thought that the severe asphaltene problems observed in the first well will affect the economics of the project drastically. However, the team working on this field took some beneficial steps to reduce the asphaltene problems, and the project continued. Many laboratory experiments were performed to come up with the best production methods and special solvents to diminish asphaltene problems. Among these works, French Institute of Petroleum (IFP) produced a valuable plot to identify the precipitation envelope of the Prinos fluid. This plot identified stable conditions (temperature and pressure) of asphaltene; it was concluded that high well-head pressure will decrease asphaltene problems significantly. In addition to these laboratory works, the wells were completed with a dual completion that helped to reduce the asphaltene problems. A second tubing string is used for oil circulation, solvent injection, running production testing devices, sometimes for oil production when the main string was shut in due to cleaning of asphaltene deposition. Also, based on production surveys, the Prinos field team decided to produce from the upper layer of the reservoir first. The studies showed that the upper layer has less asphaltene problems, and therefore, with this decision, they could reduce the asphaltene problems significantly.

Hassi-Messaoud field, Algeria. Asphaltene precipitation and deposition was observed in the early stage of production in Hassi-Messaoud field (Haskett and Tartera, 1965). Asphaltene deposition in the tubing strings caused up to 25 % of wellhead pressure reduction in some wells in less than 20 days, which ultimately caused drastic reduction in oil production. The Hassi-Messaoud field team started to wash the tubing strings with solvents. This program was successful to some extent, but later on developments of asphaltene deposition profile helped them to reduce the problems more efficiently. The asphaltene deposition profile identified the conditions (pressure and

temperature) at which asphaltene deposits in the tubing and provided the progress of the shape of deposited asphaltene. Using this profile, it was found that maintaining the well-head pressure below the bubble point reduces asphaltene deposition problems significantly in the tubing strings. They have tested this idea on some of the wells, and it was observed that the amount of asphaltene deposition reduced in these wells.

Lake Maracaibo field, Venezuela. Asphaltene deposition problems have been observed in the Lake Maracaibo, which is the major play in Venezuela (Von Albrecht et al., 1977). Most of the early wells that have been completed in Cretaceous layers have undergone costly workovers to reduce the asphaltene problems. These costly workovers drastically affected the economics of the field, consequently Venezuela oil industry. It is reported that in some parts of the field asphaltene content of the oil is up to 10 %. Based on the studies conducted, it was found that asphaltene precipitation is reduced, as either the dissolved gas oil ratio of the hydrocarbon fluid decreases or the temperature increases. Setting the well-head pressure in a way that the tubing pressure becomes very low (much less than bubble point) and insulating the tubing strings reduced the asphaltene problems a lot in this field.

Mata-Acerna and Boscan fields, Venezuela. Mata-Acerna is another field in Venezuela that has experienced serious asphaltene problems in many wells (Lichaa, 1977). The asphaltene content of Mata-Acerna oil is low in most parts of the reservoir. The highest reported asphaltene content is 9.8 %. However, this amount of asphaltene was enough to completely plug some of the wells in the Mata-Acerna field. On the other hand, experiments show that asphaltene content of Boscan oil is approximately 17.2 %, but no asphaltene deposition problem was observed. Studies suggested that Boscan oil has components that act as asphaltene precipitation and deposition preventing agents

(Lichaa, 1975; Lichaa, 1977). No precipitation has been observed even when Mata-Acerna and Boscan fluid were mixed with each other.

Little Creek Field, Mississippi. Little Creek is an example of a field that had no asphaltene problem during primary and secondary productions, but experienced serious asphaltene deposition problems during CO₂ flooding (Tuttle, 1983; Leontaritis et al., 1988). Not only acidizing and well stimulation was not helpful in remedying the asphaltene problems, but in fact in most cases, it enhanced asphaltene precipitation and deposition. It was found that mechanical cleaning of the wells and tubing strings is the most efficient way to reduce the asphaltene problems in this field.

Ula Field, Norway. Asphaltene deposition was observed in Ula field in the well tubing, processing facilities, and separators (Thawer et al., 1990). Asphaltene problems were not so much of concern in most cases and the solvent cleaning was positively effective. Experiments showed that the asphaltene content of the Ula fluid is about 0.57 %, and asphaltene precipitation window is between bubble point and about 400 psi above bubble point. No asphaltene precipitation has been observed below the bubble point.

Villafortuna-Treccate (VF-TR) field, northern Italy. Asphaltene deposition within the tubing strings reduced production of many wells from the beginning of production (Galoppini and Tambini, 1994). VF-TR asphaltene content is only 0.4 %, but this small amount of asphaltene was enough to cause abnormal production decline in many wells. Experiments identified that a special solvent can stabilize asphaltene in the crude oil, but field results of this solvent treatment was not reported. Galoppini and Tambini (1994) suggested that the most efficient way to reduce asphaltene problems in this field is as follows: first, cleaning of tubing strings; second, asphaltene removal technique; and third, shut down the well for a complete flowback of solvent.

Comalcalco, Mexico. Quick decline in production (about 35 %) was reported in one of the wells in the Comalcalco area of Mexico (Newberry and Barker, 2000; Wang, 2000). The asphaltene problems were largely controlled by taking the following steps: first, dispersant and solvent were injected into the well following over-flush solvent injection; then, the well was shut down for 24 hours for flow-back of solvent. Newberry and Barker (2000) reported that the extra revenue that came from this asphaltene treatment job was approximately \$9.3 million over sixteen months.

Kuwait. Kuwait Oil Company reported that many fields in Kuwait suffered from asphaltene precipitation and deposition problems from moderate to severe (Al-Qabandi and Al-Naqi, 2003). The company reported that they lost approximately 100,000 BOPD, because of asphaltene precipitation and deposition. The company even shut down one of the fields completely because of asphaltene problems. After unsuccessful attempts to reduce the asphaltene problems, the company started a project named Downhole Asphaltene Remediation Treatment (DART). The outcome of this project was development of the DART chemical to diminish asphaltene precipitation and deposition. The chemical was tested in some of the wells and it was successful to some extent. After the chemical injection, asphaltene precipitation was still observed in the tubing and surface facilities, but the amount of deposition was reduced significantly.

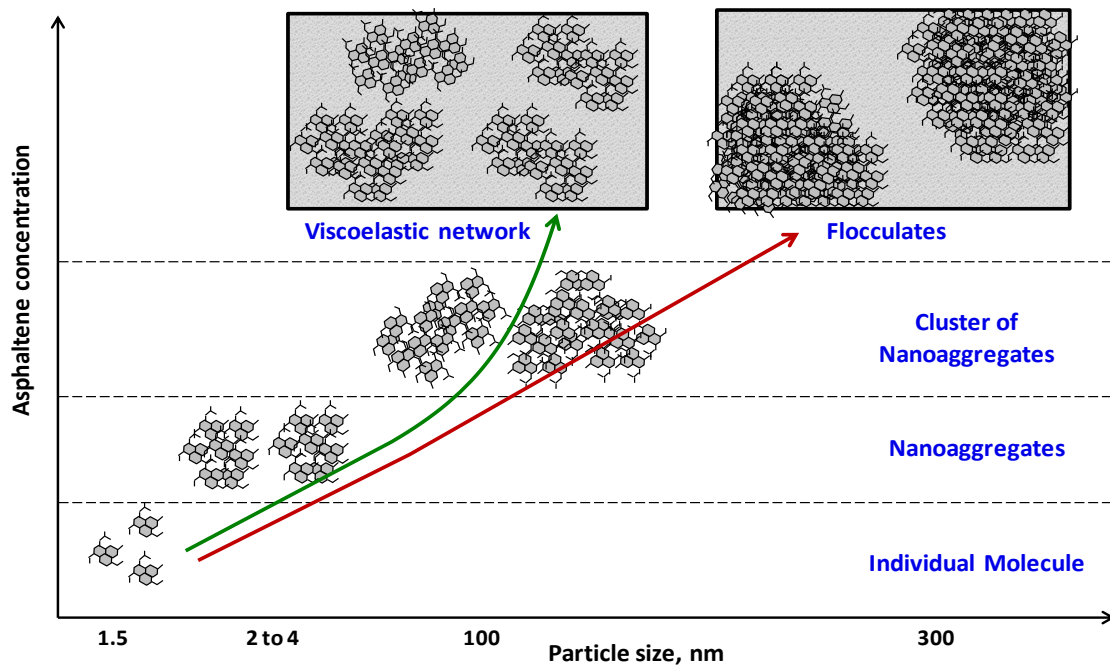


Figure 2.1 Schematic of the process of asphaltene flocculation, reproduced from Akbarzadeh et al. (2007).

Chapter 3: Review of UTCOMP Simulator

The asphaltene reservoir simulator developed in this study is embedded in UTCOMP, The University of Texas Compositional Simulator. In this chapter, we present an overview of UTCOMP and its formulation, assumptions, and features. More details on these topics can be found in Chang's dissertation (Chang, 1990), Chang et al. (1990), and the UTCOMP Technical Manual (2003).

3.1 INTRODUCTION TO UTCOMP

UTCOMP is an isothermal, three-dimensional, Equation-of-State (EOS) IMPEC (Implicit Pressure and Explicit Compositions) compositional reservoir simulator capable of modeling primary, secondary, and some important EOR processes (such as immiscible and miscible flooding). The first version of UTCOMP was developed by Chang (1990). He modified the volume-balanced approach presented by Acs et al. (1985). The solution scheme is similar to IMPES (Implicit Pressure and Explicit Saturations), but instead of saturations, overall composition of the fluid will be updated explicitly. We summarize the main features of UTCOMP as follows:

- Three-dimensional EOS IMPEC compositional
- Rigorous and simplified flash calculations (including three-phase flash-calculation capability)
- K-value method for phase-behavior calculations
- Higher-order total variation diminishing (TVD) finite-difference method
- Full physical-dispersion tensor
- Variable-width cross-section option

- Vertical or horizontal well capability
- Tracer-flood capability
- Polymer-flood capability
- Dilute-surfactant option with both equilibrium and non-equilibrium mass transfer
- Gas-foam-flood capability (Pc* model and table-look-up approach)
- Black-oil model
- Asphaltene precipitation model
- CO₂ sequestration in aquifers

UTCMP allows existence of up to four phases in the reservoir: aqueous phase, oil phase, gas phase, and a second non-aqueous liquid phase. Phase equilibrium calculations can be made using the Peng-Robinson EOS (Peng and Robinson, 1976) or a modified version of the Redlich-Kwong EOS (Turek et al., 1984). In addition to advection, physical dispersion is considered by using the full dispersion tensor. Various relative permeability models such as Baker's model (Delshad and Pope, 1989), modified Stone's model II (Stone, 1973), Pope's model (Delshad and Pope, 1989), Corey's model (Corey et al., 1956), and Corey's Model with trapping (Pope et. al., 2000) are included in this simulator. The basic assumptions of UTCMP include

- Reservoir is isothermal
- Local thermodynamic equilibrium exists
- No-flow boundary condition exists on the edges of the reservoir
- Advection follows Darcy's law
- Physical dispersion follows Fick's law

- Formation is slightly incompressible
- Injection and production wells handled by source/sink terms
- Permeability tensor is diagonal
- Adsorption is neglected

3.2 GOVERNING EQUATIONS

In this section, the mathematical formulation of UTCOMP (specifically those parts that are important in asphaltene modeling) is presented. We introduce mass conservation equations, pressure equation, and phase behavior calculation, respectively.

3.2.1 Mass Conservation Equations

The general mass conservation equation for component i in multi-component, multiphase flow in an isothermal porous medium can be written as

$$\frac{\partial W_i}{\partial t} + \vec{\nabla} \bullet \vec{F}_i - R_i = 0, \quad i = 1, 2, \dots, n_c, \quad (3.1)$$

where W_i is the accumulation term, F_i is the flux term, and R_i is the source term (Lake et al., 1984). The Equation (3.1) is expressed in terms of moles per unit bulk volume per unit time.

Neglecting the adsorption, the accumulation term (W_i) in Equation (3.1) can be determined by

$$W_i = \phi \sum_{j=2}^{n_p} \xi_j S_j x_{ij}, \quad i = 1, 2, \dots, n_c, \quad (3.2)$$

where ϕ is porosity, ξ_j is the molar density of phase j , S_j is the saturation of phase j , and x_{ij} is the mole fraction of the component i in phase j . In UTCOMP, water can be included as a component in the hydrocarbon feed or as a separate phase. If we consider water as a separate phase and assume that no hydrocarbon components exist in the water phase, the accumulation term for water (W_{n_c+1}) can be expressed as

$$W_{n_c+1} = \phi \xi_1 S_1. \quad (3.3)$$

In Equations (3.2) and (3.3), the following phase index labeling is used: (1) aqueous phase, (2) oil phase, (3) gas phase, and (4) a second non-aqueous liquid phase. The hydrocarbon components are shown by indexes from 1 through n_c , and the water component is shown by index n_c+1 .

The flux term (\bar{F}_i) in Equation (3.1) can be expressed as

$$\bar{F}_i = \sum_{j=1}^{n_p} \left(\xi_j x_{ij} \left(-\frac{\bar{k} k_{rj}}{\mu_j} (\nabla P_j - \gamma_j \nabla D) \right) - \phi \xi_j S_j \bar{\bar{K}} \nabla x_{ij} \right), \quad i = 1, 2, \dots, n_c. \quad (3.4)$$

In Equation (3.4), the first term is for advection and the second term is for physical dispersion. \bar{k} is the absolute permeability tensor, k_{rj} is the relative permeability of phase j , μ_j is the viscosity of phase j , P_j is the pressure of phase j , and $\bar{\bar{K}}$ is the full dispersion tensor.

The accumulation term (R_i) in Equation (3.1) can be written as

$$R_i = \frac{q_i}{V_b}, \quad i = 1, 2, \dots, n_c, n_c + 1, \quad (3.5)$$

where V_b is the bulk volume of a grid-block, and q_i is the molar flow rate of the component i . q_i is zero for the non-well blocks, positive for the injection well blocks, and negative for the production well blocks.

By substituting Equations (3.2) through (3.5) into Equation (3.1), the final form of the material balance equation for the component i becomes

$$\frac{\partial \left(\phi \sum_{j=1}^{n_p} \xi_j S_j x_{ij} \right)}{\partial t} + \vec{\nabla} \cdot \left[\sum_{j=1}^{n_p} \left(\xi_j x_{ij} \left(-\frac{\vec{k} k_{rj}}{\mu_j} (\nabla P_j - \gamma_j \nabla D) \right) - \phi \xi_j S_j \vec{K} \nabla x_{ij} \right) \right] - \frac{q_i}{V_b} = 0, \quad (3.6)$$

$$i = 1, 2, \dots, n_c, n_c + 1.$$

Equation (3.6) is a set of nonlinear partial differential equations with $n_c n_p + 6n_p + 2$ degrees of freedom. The unknown variables include ϕ (1 variable), S_j (n_p variables), ξ_j (n_p variables), x_{ij} ($n_c(n_p-1)$ variables), k_{rj} (n_p variables), μ_j (n_p variables), P_j (n_p variables), γ_j (n_p variables), and q_i (n_c+1 variables). Equation (3.6) is coupled with a set of additional equations to solve for these ($n_c n_p + 6n_p + 2$) unknown variables. The additional equations include (1) phase equilibrium equations, (2) saturation constraint, (3) phase composition constraint, (4) formation porosity as a function of pressure, (5) hydrocarbon phase molar density, mass density, and viscosity as functions of pressure and phase composition, (6) aqueous phase molar density and mass density as functions of pressure, (7) constant aqueous phase viscosity, (8) relative permeability as a function of saturation, (8) phase pressure related to capillary pressure and reference pressure, and (9) well model for computing q_i . Details on each of these equations are provided in Chang's dissertation (Chang, 1990).

3.2.2 Pressure Equation

The pressure equation in UTCOMP is derived on the basis that the formation pore volume is filled completely by the total fluid volume. Mathematically,

$$V_p(P) = V_t \left(P, \vec{N} \right), \quad (3.7)$$

where V_p is the pore volume, V_t is the total fluid volume, and N_i is the total number of moles of the component i . Here, V_t is a function of pressure and the total number of moles of each component, while V_p is only a function of pressure.

If we differentiate from both sides of Equation (3.7) with respect to time and use the chain rule, we obtain

$$\left(\frac{dV_p}{dP} \right) \left(\frac{\partial P}{\partial t} \right) = \left(\frac{\partial V_t}{\partial P} \right)_{N_i} \left(\frac{\partial P}{\partial t} \right) + \sum_{i=1}^{n_c+1} \left(\frac{\partial V_t}{\partial N_i} \right)_{P, N_k(k \neq i)} \left(\frac{\partial N_i}{\partial t} \right). \quad (3.8)$$

Assuming slightly compressible formation, the pore volume and its derivative with respect to pressure can be expressed as

$$V_p = V_p^0 \left[1 + c_f (P - P^0) \right], \quad (3.9)$$

$$\left(\frac{dV_p}{dP} \right) = V_p^0 c_f, \quad (3.10)$$

where V_p^0 and ϕ_0 are the pore volume and porosity at the reference pressure P^0 and c_f is the fluid compressibility.

The derivatives of the total fluid volume with respect to pressure and total mole of the component i in Equation (3.8) are calculated based on the fact that the total fluid volume is equal to sum of the volumes of all phases, including water. Mathematically,

$$V_t = \sum_{j=1}^{n_p} n_j v_j, \quad (3.11)$$

where n_j is the number of moles in phase j and v_j is the molar volume of phase j . Details on the calculations of the derivatives of the total fluid volume with respect to pressure and total mole of the component i are provided in Chang's dissertation (Chang, 1990).

Considering N_i is equal to $V_b W_i$ and by substituting Equations (3.6) and (3.10) into Equation (3.8), the final form of the pressure equation becomes

$$\begin{aligned} & \left(\phi V_b c_f - \frac{\partial V_t}{\partial P} \right) \left(\frac{\partial P}{\partial t} \right) - V_b \sum_{i=1}^{n_c+1} \bar{V}_{ii} \bar{\nabla} \cdot \sum_{j=1}^{n_p} \bar{k} \lambda_{rj} \xi_j x_{ij} \nabla P \\ & = V_b \sum_{i=1}^{n_c+1} \bar{V}_{ii} \bar{\nabla} \cdot \sum_{j=1}^{n_p} \bar{k} \lambda_{rj} \xi_j x_{ij} (\nabla P_{c2j} - \gamma_j \nabla D) + V_b \sum_{i=1}^{n_c+1} \bar{V}_{ii} \bar{\nabla} \cdot \sum_{j=1}^{n_p} \phi_{S_j}^{\xi} S_j \bar{K} \nabla x_{ij} + \sum_{i=1}^{n_c+1} \bar{V}_{ii} q_i. \end{aligned} \quad (3.12)$$

3.2.3 Phase Behavior Calculation

The phase-equilibrium calculation is a key step in any compositional reservoir simulator, which determines the numbers, amounts, and compositions of all equilibrium phases. In UTCOMP, the equilibrium solution must satisfy three conditions: (1) the material balance constraint must be preserved, (2) the chemical potentials for each component must be the same in all phases, (3) the Gibbs free energy at a constant temperature and pressure must be a minimum. The Gibbs energy minimization criterion results in the equality of component fugacities among all phases,

$$f_i^j - f_i^r = 0, \quad (i = 1, 2, \dots, n_c; j = 1, 2, \dots, n_p - 1), \quad (3.13)$$

where f_i^j is the fugacity of the component i in phase j , and f_i^r is the fugacity of the component i in the reference phase. Equation (3.13) is a set of $(n_p-1)n_c$ equations, considered to be the governing equations for the flash calculation. The fugacity of each component in hydrocarbon phases can be calculated using the Peng-Robinson, or the modified version of the Redlich-Kwong EOSs. The solution of Equation (3.13) satisfies the first and the second conditions stated above; moreover, it is the necessary condition of the third criterion. The phase composition constraints are

$$\sum_{i=1}^{n_c} x_{ij} - 1 = 0 \quad (j = 1, 2, \dots, n_p), \quad (3.14)$$

and the equations for determining the phase amounts for two hydrocarbon phases are

$$\sum_{i=1}^{n_c} \frac{z_i(K_i - 1)}{1 + v(K_i - 1)} = 0, \quad (3.15)$$

which are implicitly used in the solution of Equation (3.13).

3.3 SOLUTION METHODS

In this section, we briefly review the overall solution scheme for the phase behavior calculation and the overall procedure of UTCOMP. More detailed discussion can be found in Chang (1990).

3.3.1 Phase Behavior Calculation Algorithm

In UTCOMP, pressure equation is solved at each time-step followed by updating the concentration of each component in every grid-block. Then, the phase equilibrium

calculation will be performed in order to determine the number of phases (oil, gas, and second liquid) and the composition of each phase (Chang, 1990). The phase equilibrium calculation is a two-step process: first, the phase stability analysis; second, the flash calculation.

In order to determine the number of existing phases at any condition, a phase stability analysis will be performed at each grid-block. A trial phase is stable, if the overall Gibbs free energy of the mixture is lower than the single phase Gibbs free energy (Chang, 1990). Mathematically,

$$\Delta G = \sum_{i=1}^{n_c} y_i [\mu_i(\bar{y}) - \mu_i(\bar{z})], \quad (3.16)$$

where y_i is the mole fraction of the component i in the trial phase, \bar{z} is the overall mole fraction of the single phase mixture, and μ_i is the chemical potential of component i . Two different phase stability analysis algorithms were incorporated in the simulator. One method is the Michelson (1982) algorithm that searches for stationary points of ΔG and infers the stability of the trial phase based on the analysis of the solutions of these stationary points. The second method is the Trangenstein (1987) approach that minimizes ΔG with respect to \bar{y} . Details on these algorithms can be found in Chang's dissertation (Chang, 1990).

If the stability analysis shows that more than one phase exists in a grid-block, flash calculation will be performed to calculate the amount and composition of each phase.

Two different flash calculation methods are incorporated in UTCOMP:

- (1) Flash formulation using K-values with an accelerated successive substitution, ACSS (Mehra et al., 1983).
- (2) Gibbs free energy minimization approach (Trangenstein, 1987).

Details on both methods can be found in Perschke (1988).

3.3.2 Overall Computational Procedure of UTCOMP

The overall solution scheme of UTCOMP follows a two-step procedure, which is determined by the nature of the governing equations and solution strategy:

- Solve implicitly the pressure equation, Equation (3.12), which involves the variables in the adjacent grid-blocks for the pressures of all the grid-blocks using explicit saturation- and phase-composition-dependent terms; those terms are computed using the physical properties at the previous time level.
- Compute the overall number of moles for each component in each of the grid-blocks using the component molar-balance equation, Equation (3.6). The flash calculations are then performed to determine the phase amounts and compositions.

It should be noted that a set of linear equations is formed in the first step, because pressure is the only unknown in Equation (3.12). This distinct feature results in the formulation of UTCOMP being non-iterative over a time-step. The detailed solution procedure over a time-step is given below:

- (1) Compute the derivatives and coefficients necessary for Equation (3.12).
- (2) Solve Equation (3.12) implicitly for pressure at each of the grid-blocks.
- (3) Update grid-block porosity at the new pressure.

- (4) Compute the overall number of moles of each component in every grid-block using Equation (3.6) with the new pressure and porosity.
- (5) Determine the equilibrium phase compositions and molar amount in each of the grid-blocks using flash calculation.
- (6) Evaluate the phase saturations using the phase molar amounts and molar densities.
- (7) Compute all other physical properties and desired injection/production streams.
- (8) Check if further calculation is needed by applying user-provided termination criteria. If continuation is permitted, go to step (1) for the next time-step; otherwise, terminate the simulation.

Chapter 4: Implementation of Energy Equation in UTCOMP

As discussed in Chapter 2, asphaltene precipitation depends on temperature, pressure, and composition variations. Since UTCOMP is an isothermal simulator, we implemented the energy equation in UTCOMP to consider the effect of temperature variations on asphaltene behavior. In this chapter, we present the formulation and the results of the non-isothermal UTCOMP.

4.1 REVIEW OF THERMAL SIMULATORS

Hot/cold fluid injection and electrical heating are the most frequent thermal processes. Shulter (1969) developed the first simulator to model steam flooding. This simulator was based on a three-phase, one-dimensional model. Abdalla and Coats (1971) presented a simulator to model steam drive. This simulator was three-phase and two-dimensional, and was based on an implicit pressure explicit saturations model. This model was extended to a three-dimensional model by Coats et al. (1974), and to a three-dimensional compositional model by Coats (1976). Vinsome (1974) developed an implicit pressure explicit saturation simulator to model steam-drive and steam-soak processes. Ferrer (1977) developed a two-dimensional, compositional simulator for steam flooding with similar formulation to the Coats (1976) model. Coats (1978) introduced a three-dimensional compositional simulator with implicit formulation to model steam flooding. Abou-Kassem (1981) developed a two-dimensional, fully implicit compositional simulator for steam injection. Rubin and Buchanan (1985) presented a general, fully implicit, multi-component, multi-dimensional steam simulator that can handle up to four phases. This reservoir model was coupled with a fully implicit well model. Hilbert (1986) introduced a reservoir simulator to model electrical pre-heating and

steam flooding. Ishimoto et al. (1987) developed the first Equation-of-State based thermal simulator. Later, Chien et al. (1989) developed a general purpose thermal simulator that has K-values and Equation-of-State options for calculating fluid properties. Brantferger et al. (1991) modified the Ishimoto et al. (1987) model and used an Equation-of-State to calculate thermodynamic properties of each phase. They used enthalpy as the primary variable in place of temperature. Godderij et al. (1999) developed a three-dimensional steam flooding simulator using an interface model. It was assumed that a steam condensation drive front separates the single-phase steam zone from the two-phase liquid region. Cicek (2005) developed a fully implicit, compositional thermal simulator to model steam displacement in naturally fractured reservoirs. Varavei (2009) presented a fully implicit, parallel, compositional, EOS-based reservoir simulator to model hot fluid injection, electrical heating, and hot chemical injection.

In this study, a compositional EOS-based, non-isothermal reservoir simulator is developed to model hot/cold fluid injection. We calculate the equilibrium conditions among all phases and the physical properties using the Peng-Robinson EOS.

4.2 ENERGY BALANCE EQUATION

Governing equations for the non-isothermal model in UTCOMP consist of equilibrium equations, mass conservation equations, pore volume constraint, and the energy equation. The first three sets of equations are presented in Chapter 2. The energy balance equation is defined as follows:

$$V_b \frac{\partial U^T}{\partial t} + V_b \nabla \cdot \sum_{j=a,v,o} (\zeta_j h_j \vec{v}_j) - V_b \nabla \cdot (\lambda_T \nabla T) = -\dot{Q}_L + \dot{q}_H + \hat{H}_r, \quad (4.1)$$

where U^T is the sum of internal energy of rock and total fluid per bulk volume,

$$U^T = (1-\phi)\zeta_r u_r + \phi \sum_{j=a,v,o} \zeta_j S_j u_j. \quad (4.2)$$

In Equations (4.1) and (4.2), λ_T is the effective conductive coefficient, h_j is the phase molar enthalpy, ζ_j is the phase fluid density, ζ_r is the rock density, ϕ is porosity, T is temperature, u_j is the internal energy of phase j , u_r is the internal energy of the rock, S_j is the saturation of the phase j , \vec{v}_j is the phase flux, Q_L is the heat loss, q_H is the enthalpy of the injection fluid, H_r is the heat of reaction, and the dot in the equation stands for rate. In Equation (4.1), the first term in the left side is the accumulation term, the second one is the heat convection term, and the third one is the heat conduction term. On the right side of Equation (4.1), the first term is the heat-loss term, the second one is the source/sink term, and the third one is the heat of reaction term.

4.3 ENTHALPY AND INTERNAL ENERGY

We calculate enthalpy and internal energy of each phase directly from the Peng-Robinson EOS. The enthalpy and internal energy of each phase are functions of mole fraction, temperature, and pressure, which can be calculated by

$$H_j = f(x_{ij}, T, P), \quad (4.3)$$

$$H_j = \frac{T \frac{\partial a_{m,j}}{\partial T} - a_{m,j}}{2\sqrt{2}b_{m,j}} \ln \left(\frac{Z_j + (\sqrt{2} + 1)B_j}{Z_j - (\sqrt{2} - 1)B_j} \right) + RT(Z_j - 1) + H_j^\circ, \quad (4.4)$$

$$H_j^\circ = \sum_{i=1}^n x_i h_i^\circ, \quad (4.5)$$

$$U_j = H_j - PV_j, \quad (4.6)$$

where H_j is the enthalpy of phase j , H_j° is the enthalpy of phase j at the reference condition, a and b are parameters of the Peng-Robison EOS, and U_j is the internal energy of phase j . Details on the Peng-Robinson EOS and the enthalpy (or internal energy) calculation can be found in Appendix A.

4.4 HEAT LOSS TERM

In Equation (4.1), Q_L is the heat loss term that considers the exchange of heat by conduction between the reservoir and its surrounding layers. Since the heat transfer between the reservoir and the adjacent layers can be very high, the heat loss term (Q_L) should be included in the numerical simulation of thermal processes. In this study, we use the Vinsome and Westerveld (1980) method for calculating heat loss to overburden and underburden layers. Vinsome and Westerveld (1980) assumed that temperature in the underburden and overburden rock is a function of time and vertical distance from the reservoir boundary. Temperature profile in the adjacent conductive layer is assumed in the form of the following function:

$$T_s(t, z) = (T - T^0 + b_1 z + b_2 z^2) \exp(-z / d) + T^0. \quad (4.7)$$

In Equation (4.7), z is the distance from the boundary, $T_s(t, z)$ is overburden/underburden temperature at time t at a distance of z from the reservoir boundary. The interface between the reservoir and the underburden/overburden rock is defined to be at $z = 0$. The coefficients b_1 and b_2 are time-dependent parameters and are different in each grid-block. T_0 is initial temperature in a grid-block, T is temperature in a grid-block, and d is penetration depth for heat conduction, defined as

$$d = \frac{1}{2} \sqrt{\eta t}, \quad (4.8)$$

where $\eta = \frac{\lambda_r}{c_r \xi_r}$ is the thermal diffusivity, λ_r is the thermal conductivity of the rock, and c_r is the heat capacity of the rock.

In equation (4.7), b_1 and b_2 can be determined using the following simple physical principles: (1) at the boundaries, temperature follows the heat conduction equation for the underburden/overburden rocks, and (2) the total rate of change of heat content in total underburden/overburden rocks is equal to heat flux at the boundary. After implementing these two simple principles, b_1 and b_2 can be expressed as

$$b_1^{n+1} = \frac{\frac{\eta \Delta t (T^{n+1} - T^0)}{d^{n+1}} + \tau^n - \frac{(d^{n+1})^3 (T^{n+1} - T^n)}{\eta \Delta t}}{3(d^{n+1})^2 + \eta \Delta t}, \quad (4.9)$$

$$b_2^{n+1} = \frac{2b_1^{n+1} (d^{n+1}) + (T^{n+1} - T^0) - \frac{(d^{n+1})^2 (T^{n+1} - T^n)}{\eta \Delta t}}{2(d^{n+1})^2}, \quad (4.10)$$

where Δt is the time-step size, n is the notation for time, and

$$\tau^n = \left[(T - T^0) d + b_1 d^2 + 2b_2 d^3 \right]^n. \quad (4.11)$$

Heat loss term (Q_l) in Equation (4.1) can be calculated using

$$Q_l = \lambda_r A \left[\frac{(T^{n+1} - T^0)}{d^{n+1}} - b_1^{n+1} \right], \quad (4.12)$$

where A is the cross-sectional area for heat loss to overburden and underburden layers.

4.5 PHYSICAL PROPERTIES

Considering density and viscosity of water, oil, and gas phases change in each grid-block during simulation of thermal recovery processes, due to temperature variations. In this section, we present the density and viscosity models that are used in UTCOMP to consider the effect of temperature.

4.5.1 Viscosity

We use the Brill and Beggs (1978) correlation to calculate the viscosity of water phase as a function of temperature,

$$\mu_w = \exp(1.003 - 1.479 \times 10^{-2} T + 1.982 \times 10^{-5} T^2), \quad (4.13)$$

where T is temperature in $^{\circ}F$ and μ_w is water viscosity in cp .

We use the Lohrenz et al. (1964) correlation to calculate the viscosity of hydrocarbon (oil and gas) phases. First, the low-pressure, pure-component viscosity at the desired temperature is calculated as

$$\begin{cases} \hat{\mu}_i = \frac{0.00034T_{ri}^{0.094}}{\xi_i}, & T_{ri} \leq 1.5 \\ \hat{\mu}_i = \frac{0.0001776(4.58T_{ri} - 1.67)^{5/8}}{\xi_i}, & T_{ri} > 1.5 \end{cases} \quad (4.14)$$

where T_{ri} is the grid-block temperature over the critical temperature of component i , and

$$\xi_i = \frac{5.44T_{ci}^{1/6}}{MW_i^{1/2} P_{ci}^{2/3}}. \quad (4.15)$$

Then we calculate the low-pressure, mixture viscosity as

$$\mu_j^* = \frac{\sum_{i=1}^{n_c} x_{ij} \hat{\mu}_i \sqrt{MW_i}}{\sum_{i=1}^{n_c} x_{ij} \sqrt{MW_i}}. \quad (4.16)$$

The viscosity of phase j at the desired pressure is expressed as follows:

$$\begin{cases} \mu_j = \mu_j^* + 0.000205 \frac{\xi_{jr}}{\eta_j}, & \xi_{jr} \leq 0.18 \\ \mu_j = \frac{\mu_j^* + (\chi_j^4 - 1)}{10^4 \eta_j}, & \xi_{jr} > 0.18 \end{cases} \quad (4.17)$$

where,

$$\xi_{jr} = \xi_j \sum_{i=1}^{n_c} x_{ij} V_{ci}, \quad (4.18)$$

$$\eta_j = \frac{5.44 \left[\sum_{i=1}^{n_c} x_{ij} T_{ci} \right]^{1/6}}{\left[\sum_{i=1}^{n_c} x_{ij} \sqrt{MW_i} \right]^{1/2} \left[\sum_{i=1}^{n_c} x_{ij} P_{ci} \right]^{2/3}}, \quad (4.19)$$

$$\chi_j = 1.023 + 0.23364 \xi_{jr} + 0.58533 \xi_{jr}^2 - 0.40758 \xi_{jr}^3 + 0.093324 \xi_{jr}^4. \quad (4.20)$$

4.5.2 Density

We use the Kell (1975) correlation to calculate the density of water phase as a function of temperature,

$$\zeta_w = \frac{E_0 + E_1 T + E_2 T^2 + E_3 T^3 + E_4 T^4 + E_5 T^5}{1 + E_6 T} e^{C_{pw}(P - E_7)}, \quad (4.21)$$

where T is temperature in $^{\circ}C$, ζ_w is water density in kg/m^3 , P is pressure in MPa , and C_{pw} is water compressibility factor in MPa^{-1} . The coefficients E_1 through E_7 are as follows: $E_0=999.83952$, $E_1=16.955176$, $E_2=-7.987 \times 10^{-3}$, $E_3=-46.170461 \times 10^{-6}$, $E_4=105.56302 \times 10^{-9}$, $E_5=-280.54353 \times 10^{-12}$, $E_6=16.87985 \times 10^{-3}$, and $E_7=10.2$.

We use the Peng-Robinson EOS to calculate the density of each hydrocarbon phase,

$$\xi_j = \frac{P}{Z_j RT}, \quad (4.22)$$

where ξ_j and Z_j are the density and compressibility factor of phase j , respectively.

4.6 DISCRETIZATION OF ENERGY EQUATION

One important step in solving any Partial Differential Equation (PDE) numerically is linearization of the equations and approximation of the time and spatial derivatives. In this section, the discretized form of the energy equation (Equation (4.1)) is presented. We use a first-order finite difference approximation for the time derivative term and a second-order centered finite difference approximation for the spatial derivatives. Neglecting the heat of reaction, the residual, three-dimensional, discretized form of Equation (4.1) can be expressed as

$$R_E = \frac{1}{\Delta t} \left(U_{i,j,k}^{n+1} - U_{i,j,k}^n \right) + \left\{ \frac{\left(E_{i+1/2,j,k}^x - E_{i-1/2,j,k}^x \right)^{n+1}}{\Delta x_i} + \frac{\left(E_{i,j+1/2,k}^y - E_{i,j-1/2,k}^y \right)^{n+1}}{\Delta y_i} + \frac{\left(E_{i,j,k+1/2}^z - E_{i,j,k-1/2}^z \right)^{n+1}}{\Delta z_i} \right\} - \frac{\dot{q}_{H_{i,j,k}}}{V_b} + \frac{\dot{Q}_l}{V_b} = 0, \quad (4.23)$$

where R_E is the residual of energy at each grid-block and E is the sum of convective and conductive heat fluxes at the grid-block faces. The term E is given by

$$E_{i+1/2,j,k}^x = E_{conv.} + E_{cond.} = \left\{ \sum_{j=1}^{n_p} \left(H_j T \right)_{i+1/2,j,k} u_{j,i+1/2,j,k} - K_{T_{i+1/2,j,k}} \left(T_{i+1,j,k} - T_{i,j,k} \right) \right\}, \quad (4.24)$$

where H_j is the enthalpy of phase j , and K_T is the thermal conductivity coefficient. The heat content ($H_j T$) at each face of the grid-block is calculated using a single-point upstream weighting method. For instance, in x direction,

$$\begin{cases} \left(H_j T \right)_{i+1/2,j,k} = \left(H_j T \right)_{i,j,k}, & \text{if } \Phi_{i,j,k} > \Phi_{i+1,j,k} \\ \left(H_j T \right)_{i+1/2,j,k} = \left(H_j T \right)_{i+1,j,k}, & \text{if } \Phi_{i,j,k} < \Phi_{i+1,j,k} \end{cases} \quad (4.25)$$

where $\Phi_{i,j,k}$ is the potential at the grid-block (i,j,k) . Similarly, we evaluate (H_jT) at different faces of a grid-block. Thermal conductivity coefficient (K_T) is an average value of the thermal conductivities of two adjacent grid-blocks. For instance, in x direction,

$$K_{T_{i+1/2,j,k}} \Big|_{i \rightarrow i+1} = \frac{(2\Delta y_i \Delta z_i \lambda_i \lambda_{i+1})}{(\Delta x_i \lambda_i + \Delta x_{i+1} \lambda_{i+1})}. \quad (4.26)$$

Likewise, we evaluate K_T at different faces of a grid-block.

4.7 SOLUTION PROCEDURE OF ENERGY EQUATION

We solve energy equation implicitly, isolated from pressure equation and material balance equations. The primary variables for the energy equation in the non-isothermal model are temperatures at all grid-blocks. Writing Equation (4.3) for every grid-block, we have a system of n_b (number of grid-blocks) equations with n_b independent variables. Using the residual form of the energy equation, temperature of each grid-block at a desired time-step can be calculated using

$$\delta T = T^{n+1} - T^n = -\vec{\vec{J}}^{-1} \cdot R_E^n, \quad (4.27)$$

where $\vec{\vec{J}}$ is the Jacobian matrix. The expanded form of Equation (4.27) is

$$\begin{pmatrix} \Delta T_1 \\ \Delta T_2 \\ \vdots \\ \Delta T_{n_b} \end{pmatrix} = - \begin{pmatrix} J_{1,1} & J_{1,2} & \cdots & J_{1,n_b} \\ J_{2,1} & J_{2,2} & \cdots & J_{2,n_b} \\ \vdots & & & \vdots \\ J_{n_b,1} & J_{n_b,2} & \cdots & J_{n_b,n_b} \end{pmatrix}^{-1} \cdot \begin{pmatrix} R_{E1} \\ R_{E2} \\ \vdots \\ R_{En_b} \end{pmatrix}, \quad (4.28)$$

where,

$$J_{I,J} = \frac{\partial R_{EI}}{\partial T_J}. \quad (4.29)$$

Since the time-steps are small in our IMPEC simulator (around 1 day), we approximate $\frac{\partial R_{EI}}{\partial T_J}$ numerically.

4.8 OVERALL COMPUTATIONAL PROCEDURE OF THE NON-ISOTHERMAL UTCOMP

The overall solution scheme of the non-isothermal UTCOMP is an iterative, sequential, semi-implicit scheme. At a specific time-step, the solution scheme follows an iterative three-step procedure which is determined based on the nature of the governing equations and the solution strategy:

- Solve implicitly the pressure equation (Equation (3.12)) that involves the variables in the adjacent grid-blocks for the pressures of all the grid-blocks.
- Compute overall number of moles for each component in each of the grid-blocks using the component molar-balance equations, Equation (3.6).
- Solve implicitly the energy equation (Equation (4.23)) that involves the variables in the adjacent grid-blocks for the temperatures of all the grid-blocks. Physical properties at a given time-step are calculated at the previous time level.
- Iterate on the above three steps until the solution converges. The convergence criteria are based on the relative errors in pressure, temperature, saturations, and compositions.

The detailed solution procedure over a time-step is given below.

- (1) Compute the derivatives and coefficients necessary for Equation (3.12).
- (2) Solve implicitly Equation (3.12) for pressure at each of the grid-blocks.
- (3) Update grid-block porosity at the new pressure.
- (4) Compute overall number of moles of each component in each of the grid-blocks with the new pressure and porosity.
- (5) Determine the equilibrium phase composition and the molar amount in each of the grid-blocks using the flash calculation.
- (6) Evaluate the phase saturation using the phase molar amount and the molar density.
- (7) Compute all other physical properties and desired injection/production streams.
- (8) Solve implicitly the energy equation, Equation (4.23).
- (9) Determine the equilibrium phase composition and molar amount in each of the grid-blocks from the flash calculation.
- (10) Check if the relative errors in pressure, temperature, saturations and compositions are less than the user-defined values. If the errors are high, go to (1) and solve the pressure equation again.
- (11) March to the next time-step.

4.9 AUTOMATIC TIME-STEP SELECTION

Automatic time-step selection is very important to avoid numerical instability, save computational time, and save time in selecting time-step size by trial and error. We use the Jensen (1980) method of relative changes to select a suitable time-step size as simulation proceeds. Chang (1990) considered relative changes in pressure, saturations, volume error, and component mole numbers to select the time-step size in UTCOMP. Since temperature is not constant in the non-isothermal UTCOMP, we include relative changes of temperature to the set of time-step selection criteria. The computational procedure is summarized below:

- (1) Read the first (Δt_{start}), maximum (Δt_{max}), and minimum (Δt_{min}) time-step sizes from input data.
- (2) Calculate the relative changes in pressure, temperature, saturations, volume error, and component mole numbers between the current time-step and the previous time-step:

$$(\Delta P)_i = \frac{|P_i^{n+1} - P_i^n|}{P_i^n}, \quad (4.30)$$

$$(\Delta T)_i = \frac{|T_i^{n+1} - T_i^n|}{T_i^n}, \quad (4.31)$$

$$(\Delta S_j)_i = |(S_j)_i^{n+1} - (S_j)_i^n|, \quad (4.32)$$

$$(\Delta V)_i = \frac{|(V_t)_i^{n+1} - (V_p)_i^n|}{(V_p)_i^n}, \quad (4.33)$$

$$(\Delta N_k)_i = \frac{|(N_k)_i^{n+1} - (N_k)_i^n|}{(N_k)_i^n}, \quad (4.34)$$

where V_i is the total fluid volume, and V_p is the pore volume.

(3) Calculate the maximum change for each of the variables (ΔP , ΔT , ΔS , ΔV , and ΔN) on all of the grid-blocks.

(4) Calculate Δt for next time-step using

$$\Delta t = \min(\Delta t_p, \Delta t_T, \Delta t_S, \Delta t_V, \Delta t_N), \quad (4.35)$$

where

$$\Delta t_p = \Delta t^{n+1} \frac{\Delta P_{\text{lim}}}{\Delta P_{\text{max}}}, \quad (4.36)$$

$$\Delta t_T = \Delta t^{n+1} \frac{\Delta T_{\text{lim}}}{\Delta T_{\text{max}}}, \quad (4.37)$$

$$\Delta t_S = \Delta t^{n+1} \frac{\Delta S_{\text{lim}}}{\Delta S_{\text{max}}}, \quad (4.38)$$

$$\Delta t_V = \Delta t^{n+1} \frac{\Delta V_{\text{lim}}}{\Delta V_{\text{max}}}, \quad (4.39)$$

$$\Delta t_N = \Delta t^{n+1} \frac{\Delta N_{\text{lim}}}{\Delta N_{\text{max}}}, \quad (4.40)$$

where ΔP_{lim} , ΔT_{lim} , ΔS_{lim} , ΔV_{lim} , and ΔN_{lim} are user defined parameters.

(5) Check if the new time-step size is limited by the minimum and maximum time-step sizes (Δt_{min} and Δt_{max}).

4.10 VALIDATION OF THE ENTHALPY CALCULATION

In this section, we present two cases to validate the enthalpy calculation of the non-isothermal UTCOMP. We compare the results of UTCOMP with the WinProp module of the CMG simulator (WinProp, 2011).

Case 1: Single Component, Single Phase Fluid. We perform flash calculation using UTCOMP and WinProp module of CMG for pure methane (C_1) using the Peng-Robinson EOS at pressure of 3100 psi and temperature of 150 °F. At this condition, methane is vapor. Table 4.1 presents the z-factor and the enthalpy changes (ΔH) at the specified condition calculated from UTCOMP and CMG simulators. The z-factor calculated by UTCOMP and CMG are 0.8884 and 0.8881, respectively. In addition, the enthalpy changes calculated by UTCOMP and CMG are -1057.79 and -1059.56, respectively. As can be seen, the results of UTCOMP are in good agreement with CMG.

Case 2: Multi-Component, Two-Phase Fluid. A mixture of hydrocarbons with six components is selected for this case. Table 4.2 presents the overall composition of the mixture. Figure 4.1 illustrates the two-phase envelope of the mixture generated by UTCOMP. We perform the flash calculation at temperature of 150 °F and pressure of 1000 psi. Figure 4.1 shows that both liquid and vapor phases exist at this condition. Table 4.3 shows the liquid and gas compositions from the flash calculations performed by UTCOMP and CMG. As can be seen, results of CMG and UTCOMP are not exactly the same, because the flash calculation algorithms are not exactly identical. However, the results are in good agreement. The largest difference is for the mole percent of methane in the liquid phase, which is estimated around 23 % by UTCOMP, and 21 % by CMG. For the vapor phase, the differences are not significant (less than 0.3 % for all

components). Table 4.4 presents the z-factor and the enthalpy changes (ΔH) at the specified condition for both liquid and gas phases calculated from UTCOMP and CMG. The liquid phase enthalpy changes calculated by UTCOMP and CMG are -17545.7 and -17696.1, respectively. Also, the gas phase enthalpy changes calculated by UTCOMP and CMG are -471.5 and -475.3, respectively. As can be seen, the results of UTCOMP and CMG for the enthalpy changes of liquid and vapor phases are very close. The minor differences are due to the small deviations in the results of the flash calculations of these two simulators.

4.11 CASE STUDIES OF THE NON-ISOTHERMAL MODEL

In this section, we present few case studies to validate the non-isothermal UTCOMP. We compare the results of the non-isothermal UTCOMP with the Lauwarier (1955) analytical solution, UTCHEM (UTCHEM-10 Technical Documentation, 2003), and GEM module of CMG (GEM, 2011).

Case 1: Comparison with Analytical Solution. Lauwarier (1955) proposed an analytical solution for one-dimensional hot water injection problem that considers heat loss to the overburden and underburden layers. In this case study, we compare the results of UTCOMP with the Lauwarier (1955) analytical solution to validate the Vinsome and Westerveld (1980) heat loss model that is implemented in the simulator. Lauwarier (1955) assumed (1) the reservoir has a constant thickness, porosity, and permeability, (2) the specific heat of the rock and the fluids are constant, (3) thermal conductivity of the reservoir and cap/base rock in z-direction are constant, (4) there is no heat conduction in the flow direction (x-direction) and there is no vertical temperature gradient, (5) there is

an instantaneous thermal equilibrium between the fluids and rock, and (6) water is injected at a constant rate and temperature. Lauwarier (1955) wrote the energy balance equations for reservoir and its surrounding as

$$h_t \rho_t C_t \left(\frac{\partial \theta_r}{\partial t} \right) + h_t V_f \rho_f C_f \left(\frac{\partial \theta_r}{\partial x} \right) - 2\lambda_s \left(\frac{\partial \theta_s}{\partial z} \right)_{z=h_t/2} = 0, \quad (4.41)$$

$$\rho_s C_s \left(\frac{\partial \theta_s}{\partial t} \right) - \lambda_s \left(\frac{\partial^2 \theta_s}{\partial z^2} \right) = 0, \quad (4.42)$$

where

$$\theta = \frac{T - T_{ini}}{T_{inj} - T_{ini}}. \quad (4.43)$$

In Equations (4.41) through (4.43), h_t is the thickness of the reservoir, V_f is the velocity of the fluid, ρ_f is the density of the fluid, C_f is the heat capacity of the fluid, λ_s is the heat conductivity of the surrounding, ρ_s is the density of the surrounding, C_s is the heat capacity of the surrounding, θ is the dimensionless temperature defined in Equation (4.43), T_{ini} is the initial temperature of reservoir, and T_{inj} is the injection temperature. ρ_t and C_t are the total density and compressibility, respectively, that are defined as

$$\rho_t C_t = (1 - \phi) \rho_r C_r + \phi \rho_w C_w S_w + \phi \rho_o C_o S_o, \quad (4.44)$$

where subscripts w , o and r represent water, oil, and rock, respectively.

The dimensionless form of Equations (4.41) and (4.42) are as follows:

$$\left(\frac{\partial \theta_s}{\partial t_D}\right) + \left(\frac{\partial \theta_s}{\partial x_D}\right) - \left(\frac{\partial \theta_s}{\partial z_D}\right) = 0 \quad (4.45)$$

$$\beta \left(\frac{\partial^2 \theta_s}{\partial z_D^2}\right) = \left(\frac{\partial \theta_s}{\partial t_D}\right) \quad (4.46)$$

where x_D is the dimensionless distance in x (flow)-direction, z_D is the dimensionless distance in z -direction, t_D is dimensionless time, and β is the dimensionless density-compressibility. These dimensionless parameters are defined as follows:

$$x_D = \frac{4\lambda_s x}{h_i^2 V_f \rho_f C_f}, \quad (4.47)$$

$$z_D = \frac{2z}{h_i}, \quad (4.48)$$

$$t_D = \frac{4\lambda_s t}{h_i^2 \rho_t C_t}, \quad (4.49)$$

$$\beta = \frac{\rho_t C_t}{\rho_s C_s}. \quad (4.50)$$

The initial and boundary conditions for the system of Equations (4.45) and (4.46) are defined as

$$\theta_r = \theta_s \quad \text{If } |z_D| = 1, \quad (4.51)$$

$$\theta_r = \theta_s = \begin{cases} 1 & \text{If } x_D < 0 \\ 0 & \text{If } x_D > 0 \end{cases} \quad \text{If } t_D = 0. \quad (4.52)$$

Lauwarier (1955) derived the following expressions for the dimensionless temperatures of the reservoir and the surrounding:

$$\theta_s = \begin{cases} 0 & \text{If } x_D \geq 0 \\ \operatorname{erfc}\left(\frac{x_D + |z_D| - 1}{2\sqrt{\beta(t_D - x_D)}}\right) & \text{If } x_D < 0 \end{cases}, \quad (4.53)$$

$$\theta_r = \begin{cases} 0 & \text{If } x_D \geq 0 \\ \operatorname{erfc}\left(\frac{x_D}{2\sqrt{\beta(t_D - x_D)}}\right) & \text{If } x_D < 0 \end{cases}. \quad (4.54)$$

In order to make a comparison between UTCOMP and the Lauwarier (1955) analytical solution, we set up a one-dimensional simulation case study of displacing cold water with hot water. Table 4.5 summarizes the reservoir properties and the simulation input data. The reservoir is one-dimensional and homogenous with the size of $1000 \times 10 \times 10 \text{ ft}^3$. Figure 4.2 shows a schematic view of the reservoir and wells. The rock porosity is 0.3 and the rock permeability is 100 md. Initial temperature and pressure of the reservoir are $60 \text{ }^\circ\text{F}$ and 1000 psi, respectively. The reservoir is divided into 100 grid-blocks in x -direction. Hot water is injected into the reservoir at a constant rate of 693.4 lb-mol/day and at a temperature of $120 \text{ }^\circ\text{F}$. The producer is a constant bottom-hole pressure well set at 1000 psi. In order to be consistent with the Lauwarier's assumptions, we neglect heat conduction in the flow direction in this case study. Furthermore, the volumetric heat capacity and thermal conductivity of the reservoir rock are assumed constant: $0.18 \text{ (Btu/lb-}^\circ\text{R)}$ and $67.2 \text{ Btu/(ft-day-}^\circ\text{R)}$, respectively. Similarly, the volumetric heat capacity and the thermal conductivity of the cap/base rock are $0.18 \text{ (Btu/lb-}^\circ\text{R)}$ and $67.2 \text{ Btu/(ft-day-}^\circ\text{R)}$. Figure 4.3 compares the results of UTCOMP with the analytical solution for the dimensionless temperature versus dimensionless distance at dimensionless times of 4, 8, 16, and 32. The dimensionless distance is calculated from the injection well, i.e. $x_D=0$ at the injector. Figure 4.4 compares UTCOMP with the

analytical solution for the dimensionless temperature of the grid-block number 3 (counted from the injection well) versus dimensionless time. As shown in Figures 4.3 and 4.4, there is good agreement between UTCOMP and the analytical solution.

Case 2: Comparison with UTCHEM. In this case study, we compare the results of the non-isothermal UTCOMP with UTCHEM (UTCHEM-10 Technical Documentation, 2003), The University of Texas Chemical Simulator. In the thermal model of UTCHEM, it is assumed that the heat capacities of the fluids are constant, and enthalpy and internal energy are approximated using the heat capacities. In addition, the energy equation is solved explicitly to calculate the temperature profile at each time-step. Furthermore, oil should be single component. We set up a one-dimensional simulation case study of displacing oil with hot water. In this case study, we consider the effect of heat conduction in the direction of the flow, which was neglected in case 1. Table 4.6 presents the properties of the oil which is a single component fluid (C_{20}). Table 4.7 summarizes the reservoir properties and the simulation input data, and Table 4.8 provides relative permeability data. The reservoir is homogenous with the size of $1000 \times 10 \times 10$ ft³. Initial water saturation is 0.3, and the rock porosity and permeability are 0.3 and 100 md, respectively. Initial temperature of the reservoir is 60 °F and initial pressure is 1000 psi. Hot water is injected into the reservoir at a constant rate of 693.4 lb-mol/day and a temperature of 120 °F. The producer is a constant bottom-hole pressure well set at 1000 psi. The heat capacity of the oil is assumed constant: 0.438 Btu/(lb-°R). Moreover, the volumetric heat capacity and thermal conductivity of the reservoir rock are assumed constant: 0.18 (Btu/lb-°R) and 67.2 Btu/(ft-day-°R), respectively. Similarly, the volumetric heat capacity and the thermal conductivity of the cap/base rock are 0.18 (Btu/lb-°R) and 72 Btu/(ft-day-°R). Figure 4.5 compares the results of UTCOMP with

UTCHEM for dimensionless temperature versus dimensionless distance at simulation times of 5, 50, and 365 days. Dimensionless distance is calculated from the injection well ($x_D=0$ at the injector and $x_D=1$ at the producer). Dimensionless temperature is calculated using Equation (4.43) considering that $T_{in}=60$ °F and $T_{inj}=120$ °F. Figure 4.5 shows that there is good agreement between the results of UTCOMP and UTCHEM.

Case 3: Comparison with CMG (GEM), Two-Component Fluid. In this case study, we compare the results of the non-isothermal UTCOMP with GEM module of CMG simulator (GEM, 2011). GEM is a three-dimensional, EOS, compositional simulator with the capability of modeling hot/cold fluid injection. Both GEM and UTCOMP use the Peng-Robinson EOS to calculate enthalpy and internal energy. In addition, both simulators can be used for multi-component and multi-phase flow in the porous media. However, the flash calculations of these simulators are not identical (see case 2 of the previous section). In addition, the solution scheme of the non-isothermal UTCOMP is semi-implicit, sequential, and iterative while GEM is a fully implicit simulator. We set up a two-dimensional simulation case study of displacing oil with hot water. Since the heat loss calculation of the UTCOMP is already validated in case studies 1 and 2, we neglect heat transfer between the reservoir and overburden/underburden layers in the current case. Table 4.9 presents the overall composition of oil, which is a two-component fluid (C₁-C₂₀). Table 4.10 summarizes the reservoir properties and the simulation input data, and Table 4.11 provides relative permeability data. The reservoir is homogenous with the size of 1000×1000×20 ft³. Initial water saturation is 0.3, and the rock porosity and horizontal permeability are 0.3 and 100 md, respectively. Initial temperature and pressure of the reservoir are 120 °F and 1500 psi, respectively. Hot water is injected into the reservoir with a constant pressure of 2200 psi and temperature of 180 °F. The producer is

a constant bottom-hole pressure well set at 1500 psi. Water density and viscosity are assumed constant: 62.4 lb /ft³ and 1 cp, respectively. The heat capacity and thermal conductivity of the reservoir rock are the same in case study 2 (Table 4.7). Figure 4.6 compares the oil rate profile calculated by UTCOMP with CMG over 4200 days of simulation. Although the flash calculation and solution scheme of these simulators are not identical, there is a complete match between the results of UTCOMP and CMG. Figure 4.7 compares the results of UTCOMP with CMG for the temperature and the pressure maps after 2000 days of simulation. The injection well is located on the top-left corner, and the production well is located on bottom-right corner of the reservoir. Similarly, Figure 4.8 compares the results of UTCOMP with CMG for the temperature and the pressure maps after 4000 days of simulation, which is around the water breakthrough time in the producer. Figure 4.9 compares the results of UTCOMP with CMG for the water saturation map after 2000 and 4000 days of simulation. We observe that the temperature and the water fronts are not necessarily at the same place, which is due to the heat exchange between the reservoir rock and the hot water. Figure 4.10 compares the results of UTCOMP with CMG for the temperature variations of the grid-block (20,1,1), counted from injection well (top-left corner). Temperature is almost constant at the beginning when the water front did not reach the grid-block. Afterwards, the temperature rapidly increases while the water front is passing the grid-block. Then, we have a gradual increase in temperature, which is stabilized around the injection temperature at the end of simulation. Similarly, Figure 4.11 and 4.12 compare the results of UTCOMP with CMG for the pressure variations and water saturation variations of the grid-block (20,1,1). As can be seen in Figures 4.7 through 4.12, the results of UTCOMP and CMG are compatible with one another.

Case 4: Comparison with CMG (GEM), Six-Component Fluid. In this case study, we set up a two-dimensional case of displacing a six-component oil with hot water. The overall composition of the fluid is presented in Table 4.12. The simulation input data and relative permeability curves are similar to case 3 (Tables 4.10 and 4.11). Figure 4.13 compares the oil rate profile calculated by UTCOMP with CMG over 4200 days of simulation. As can be observed, there is good agreement between the results of CMG and UTCOMP. The minor differences between the oil productions come from the dissimilarity in flash calculations of these two simulators. One can get a better match by tuning the flash calculation parameters of UTCOMP with CMG or vice versa. Figure 4.14 compares the results of UTCOMP with CMG for the temperature and the pressure maps after 2000 days of simulation. The injection well is located on the top-left corner, and the production well is located on bottom-right corner of the reservoir. Similarly, Figure 4.15 shows the temperature and the pressure maps after 4000 days of simulation, which is around the water breakthrough time. Figure 4.16 compares the results of UTCOMP with CMG for the temperature variations of the grid-block (20,1,1), counted from injection well (top-left corner). Similar to case 3, temperature is almost constant at the beginning of the simulation that is followed by a rapid increase and is stabilized at the end of the simulation. In addition, Figures 4.17 and 4.18 compare the results of UTCOMP with CMG for the pressure and water saturation variations at grid-block (20,1,1). As can be observed in Figures 4.14 through 4.18, the results of UTCOMP and CMG are in good harmony.

Case 5: Three-Dimensional Reservoir, Six-Component Fluid. In the previous cases, we assumed that water viscosity and density are constant in order to make a comparison between the results of UTCOMP with the analytical solution, UTCHEM, and GEM

module of CMG. In this case, we investigate the effect of temperature variations in the reservoir on water viscosity and density, and consequently on the performance of the hot water flooding. We set up a three-dimensional simulation case of displacing oil with hot water. Figure 4.19 illustrates schematic views of the reservoir. There is one production well at the left corner, and one injection well at the right corner of the reservoir. The relative permeability and fluid data are the same as case 4 (Tables 4.11 and 4.12). Table 4.13 summarizes the reservoir properties and the simulation input data. The reservoir is homogenous with the size of $400 \times 400 \times 80$ ft³. Initial water saturation is 0.3 and rock porosity and horizontal permeability are 0.3 and 100 md, respectively. Initial temperature of the reservoir is 120 °F and initial pressure is 1500 psi. Hot water is injected into the reservoir at a constant pressure of 1600 psi and a temperature of 180 °F. The producer is a constant bottom-hole pressure well set at 1500 psi. The cap/base rock properties and the reservoir rock density, heat capacity and thermal conductivity are the same as in case 2 (Table 4.7). Water viscosity is calculated using the Brill and Beggs correlation and the water density is calculated using the Kell correlation. Figures 4.20 and 4.21 present the water viscosity graph calculated using the Brill and Beggs correlation and water mass density graph calculated using the Kell correlation versus temperature, respectively. Figure 4.22 compares the results of the isothermal with non-isothermal UTCOMP for the oil production rate. Similarly, Figure 4.23 shows the comparison for cumulative oil production. The flow rate calculated using the non-isothermal UTCOMP is much higher (almost twice) at the early stage of simulation (before 2000 days). The non-isothermal UTCOMP estimates that water breakthroughs after about 2000 days, while the isothermal UTCOMP predicts the water breakthrough time of about 4000 days (almost twice). The ultimate recovery is the same, using both isothermal and non-isothermal UTCOMP. However, the non-isothermal UTCOMP predicts that the oil recovery reaches its

maximum at around 2000 days, while the isothermal UTCOMP predicts this value to be around 4000 days. The difference between the results of the isothermal and the non-isothermal UTCOMP is due to water viscosity and density reduction with temperature increase in the reservoir during hot water injection. Figures 4.24 through 4.28 present the results of the non-isothermal UTCOMP after 1000 and 2000 days of simulation for temperature, pressure, water saturation, water viscosity, and water mass density profiles, respectively. In Figure 4.24, we observe that the rock temperature is maximum at the injection well and it gradually decreases towards the production well. Temperatures in the upper and lower layers are less than the temperatures in the middle layers. This difference is due to heat exchange between the upper/lower layers with overburden/underburden layers. Figures 4.27 and 2.28 show that water viscosity and water density decreased considerably around the injection well. This reduction in water viscosity and density is due to the increase in the reservoir temperature around the injection well.

Table 4.1 Comparison of UTCOMP and CMG for the enthalpy change calculation and z -Factor for case 1 at $T=150$ °F and $P=3100$ psi.

	UTCOMP	CMG
z-Factor	0.8884	0.8881
ΔH [Btu/lb-mol]	-1057.79	-1059.56

Table 4.2 Overall composition of the mixture for case 2.

Component Name	Overall Composition
C ₁	0.5
C ₃	0.03
C ₆	0.07
C ₁₀	0.2
C ₁₅	0.15
C ₂₀	0.05

Table 4.3 Liquid and gas compositions (mole percent) from the flash calculations performed by UTCOMP and CMG for case 2 at $T=150$ °F and $P=1000$ psi.

UTCOMP		CMG	
Liquid	Vapor	Liquid	Vapor
22.87294	97.42818	20.49308	97.16292
3.623877	1.909231	3.53976	2.13726
10.6829	0.560917	11.00273	0.60217
31.38231	0.099489	32.45286	0.09574
23.57818	0.002158	24.38340	0.00188
7.85979	0.00002	8.12817	0.00003

Table 4.4 Comparison of UTCOMP and CMG for the enthalpy change calculation and z-Factor for case 2 at $T=150$ °F and $P=1000$ psi.

	UTCOMP		CMG	
	Liquid	Vapor	Liquid	Vapor
z-Factor	0.440	0.907	0.451	0.906
ΔH [Btu/lb-mol]	-17545.7	-471.5	-17969.1	-475.3

Table 4.5 Reservoir properties and the simulation input data for case 1 (comparison with analytical solution).

Parameters	Value
Number of grid-blocks (x,y,z)	100×1×1
Grid-block size	10 ×10×10 ft ³
Injection temperature	120 °F
Reservoir temperature	60 °F
Water viscosity	1 cp
Water density	62.46 lb/ft ³
Initial water saturation	1
Initial reservoir pressure	1000 psi
Injection rate	693.4 lb-mol/day
Bottom-hole pressure of producer	1000 psi
Reservoir thermal conductivity	67.2 Btu/(ft-day-°R)
Reservoir rock density	171.36 lb/ft ³
Reservoir rock heat capacity	0.18 Btu/(lb -°R)
Surrounding rock thermal conductivity	67.2 Btu/(ft-day-°R)
Surrounding rock density	171.36 lb/ft ³
Surrounding rock heat capacity	0.18 Btu/(lb -°R)
Water heat capacity	1 Btu/(lb -°R)
Porosity	0.3
Permeability	100 md

Table 4.6 Properties of the fluid used in case 2 (comparison with UTCHEM).

Parameters	Value
Molecular weight	282
Critical pressure	162 psi
Critical temperature	920 °F
Critical volume	19.484 ft ³ /(lb-mole)
Accentric factor	0.85

Table 4.7 Reservoir properties and the simulation input data for case 2 (comparison with UTCHEM).

Parameters	Value
Number of grid-blocks (x,y,z)	100×1×1
Grid-block size	10 ×10×10 ft ³
Injection temperature	120 °F
Reservoir temperature	60 °F
Water viscosity	1 cp
Water density	62.46 lb/ft ³
Initial water saturation	0.3
Initial reservoir pressure	1000 psi
Injection rate	693.4 lb-mol/day
Bottom-hole producer pressure	1000 psi
Reservoir rock thermal conductivity	67.2 Btu/(ft-day-°R)
Surrounding rock and reservoir rock density	171.36 lb/ft ³
Reservoir rock heat capacity	0.18 Btu/(lb -°R)
Surrounding rock thermal conductivity	72 Btu/(ft-day-°R)
Surrounding rock heat capacity	0.18 Btu/ (lb -°R)
Water heat capacity	1 Btu/(lb-°R)
Oil heat capacity	0.438 Btu/(lb-°R)
Porosity	0.3
Permeability	100 md

Table 4.8 Relative permeability data for case 2 (comparison with UTCHEM).

	Water	Oil	Gas
Residual saturation	0	0	0
End point	1	1	1
Exponent	2	2	2

Table 4.9 Overall composition of the mixture for case 3 (comparison with CMG).

Component Name	Overall Composition
C ₁	0.1
C ₂₀	0.9

Table 4.10 Reservoir properties and the simulation input data for case 3.

Parameters	Value
Number of grid-blocks (x,y,z)	50×50×1
Grid-block size	20 ×20×20 ft ³
Injection temperature	180 °F
Reservoir temperature	120 °F
Water viscosity	1 cp
Water density	62.4 lb/ft ³
Initial water saturation	0.3
Initial reservoir pressure	1500 psi
Bottom-hole injector pressure	2200 psi
Bottom-hole producer pressure	1500 psi
Reservoir rock thermal conductivity	67.2 Btu/(ft-day-°R)
Reservoir rock density	171.36 lb/ft ³
Reservoir rock heat capacity	0.18 Btu/(lb -°R)
Porosity	0.3
Vertical permeability	10 md
Horizontal permeability	100 md

Table 4.11 Relative permeability data for case 3 (comparison with CMG).

	Water	Oil	Gas
Residual saturation	0.3	0.1	0
End point	0.3	0.8	1
Exponent	2	2	2

Table 4.12 Overall composition of the mixture for case 4 (comparison with CMG).

Component Name	Overall Composition
C ₁	0.1
C ₂	0.1
C ₃	0.1
C ₇	0.1
C ₁₀	0.2
C ₂₀	0.4

Table 4.13 Reservoir properties and the simulation input data for case 5.

Parameters	Value
Number of grid-blocks (x,y,z)	20×20×4
Grid-block size	20 ×20×20 ft ³
Injection temperature	180 °F
Reservoir temperature	120 °F
Initial water saturation	0.3
Initial reservoir pressure	1500 psi
Bottom-hole injector pressure	1600 psi
Bottom-hole producer pressure	1500 psi
Porosity	0.3
Horizontal permeability	100 md
Vertical permeability	10 md

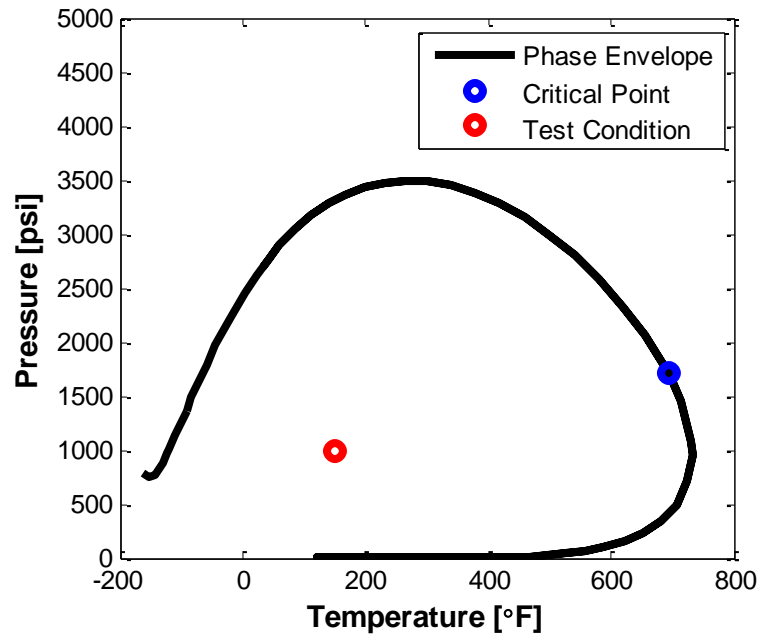


Figure 4.1 Phase envelope of the mixture generated by UTCOMP.

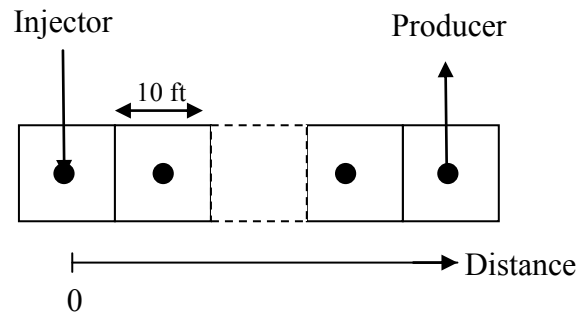


Figure 4.2 Schematic views of the reservoir and the wells for case 1 (comparison with analytical solution).

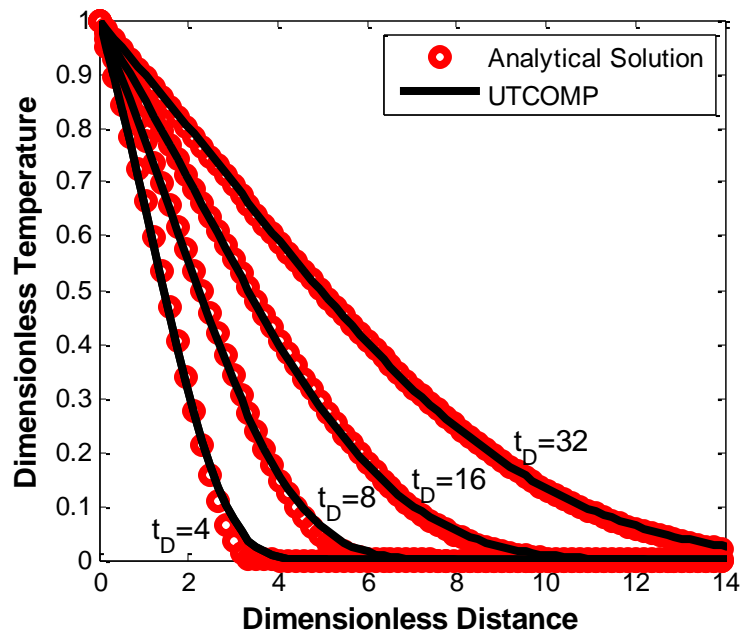


Figure 4.3 Comparison of the results (dimensionless temperature versus dimensionless distance) of UTCOMP with the analytical solution.

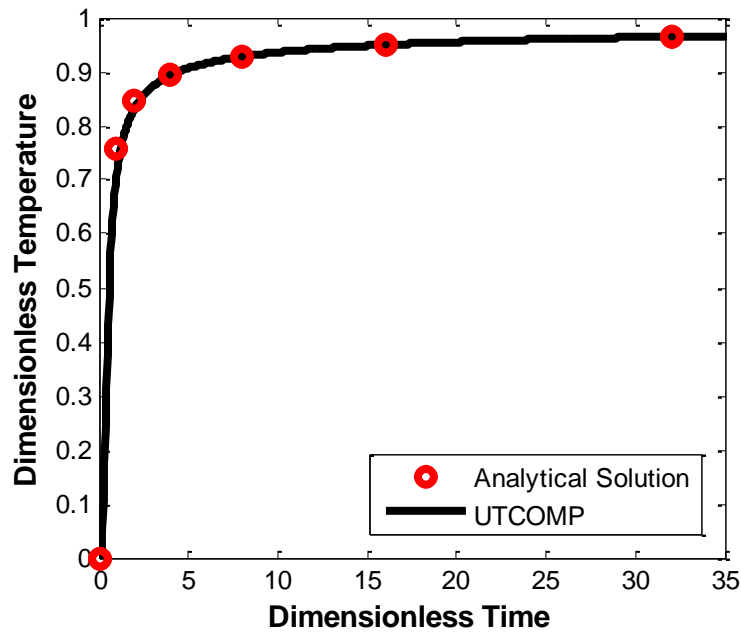


Figure 4.4 Comparison of the results (dimensionless temperature of grid-block 3) of UTCOMP with the analytical solution.

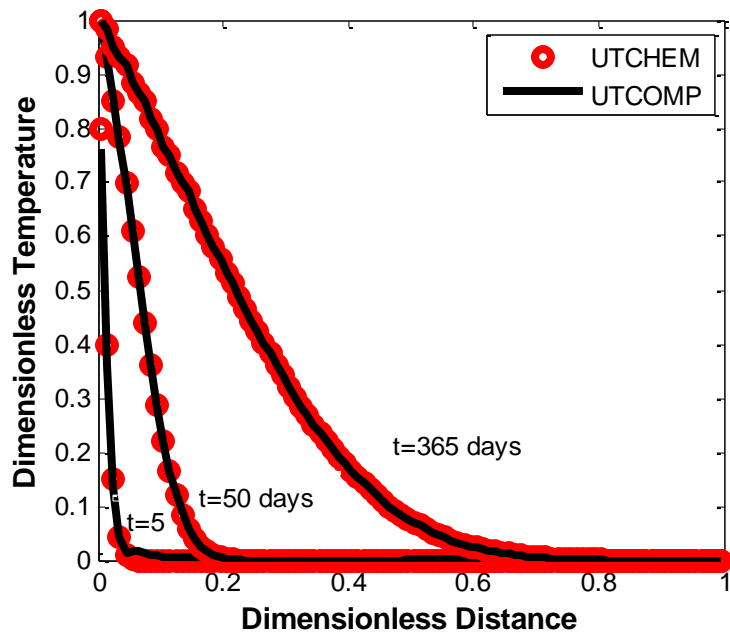


Figure 4.5 Comparison of the results (dimensionless temperature versus dimensionless distance) of UTCOMP with UTCHEM.

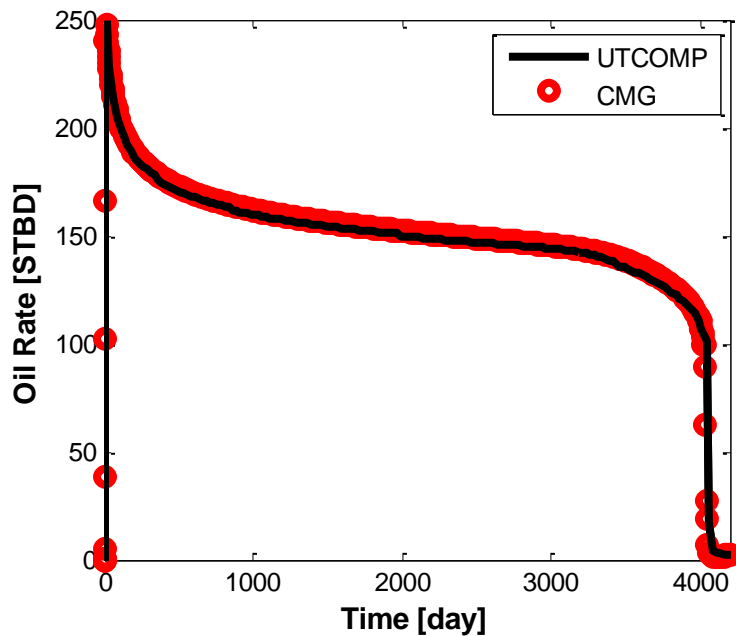


Figure 4.6 Comparison of oil production rate of UTCOMP with CMG for case 3.

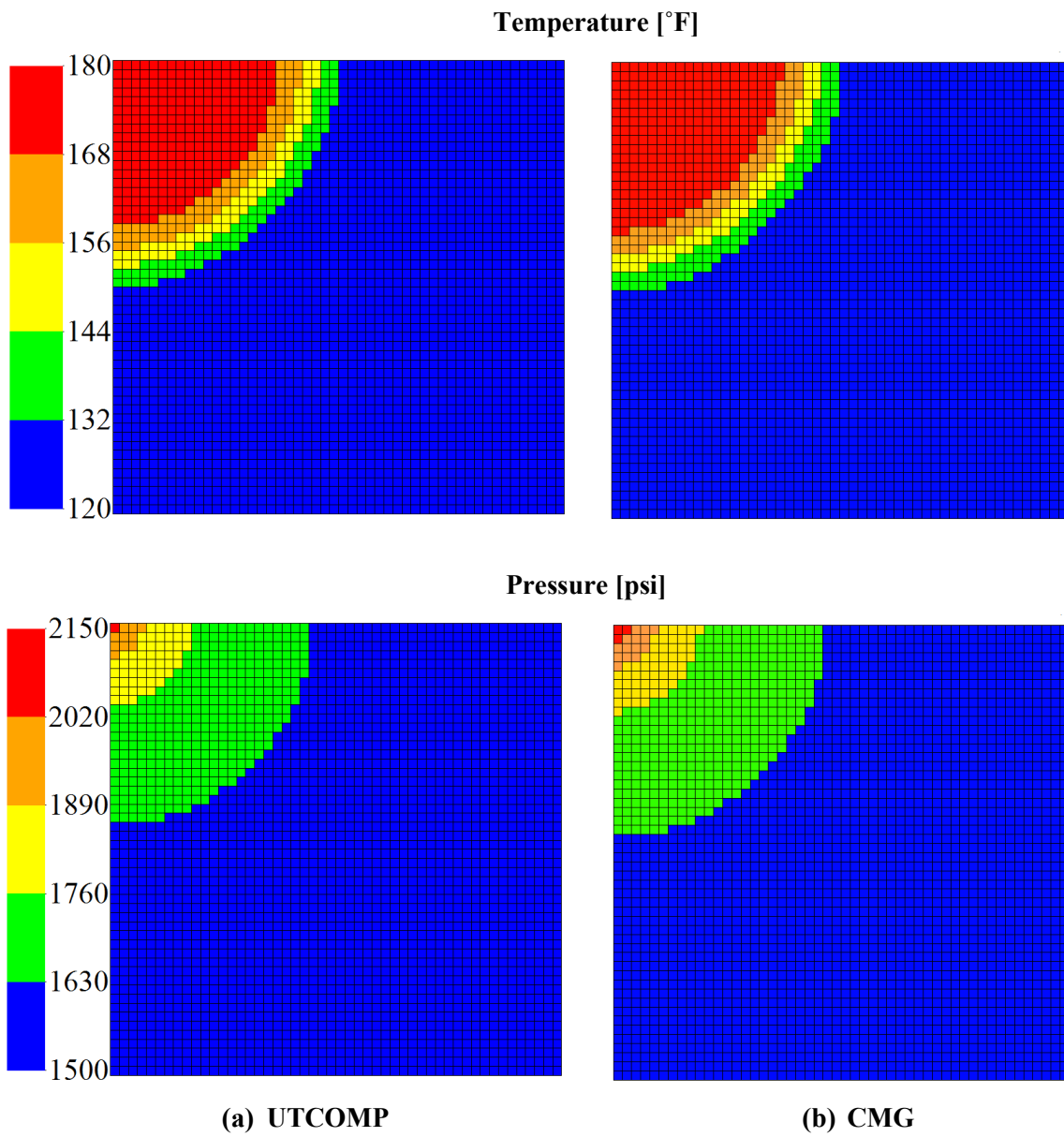


Figure 4.7 Comparison of temperature and pressure profiles of UTCOMP with CMG after 2000 days of simulation for case 3.

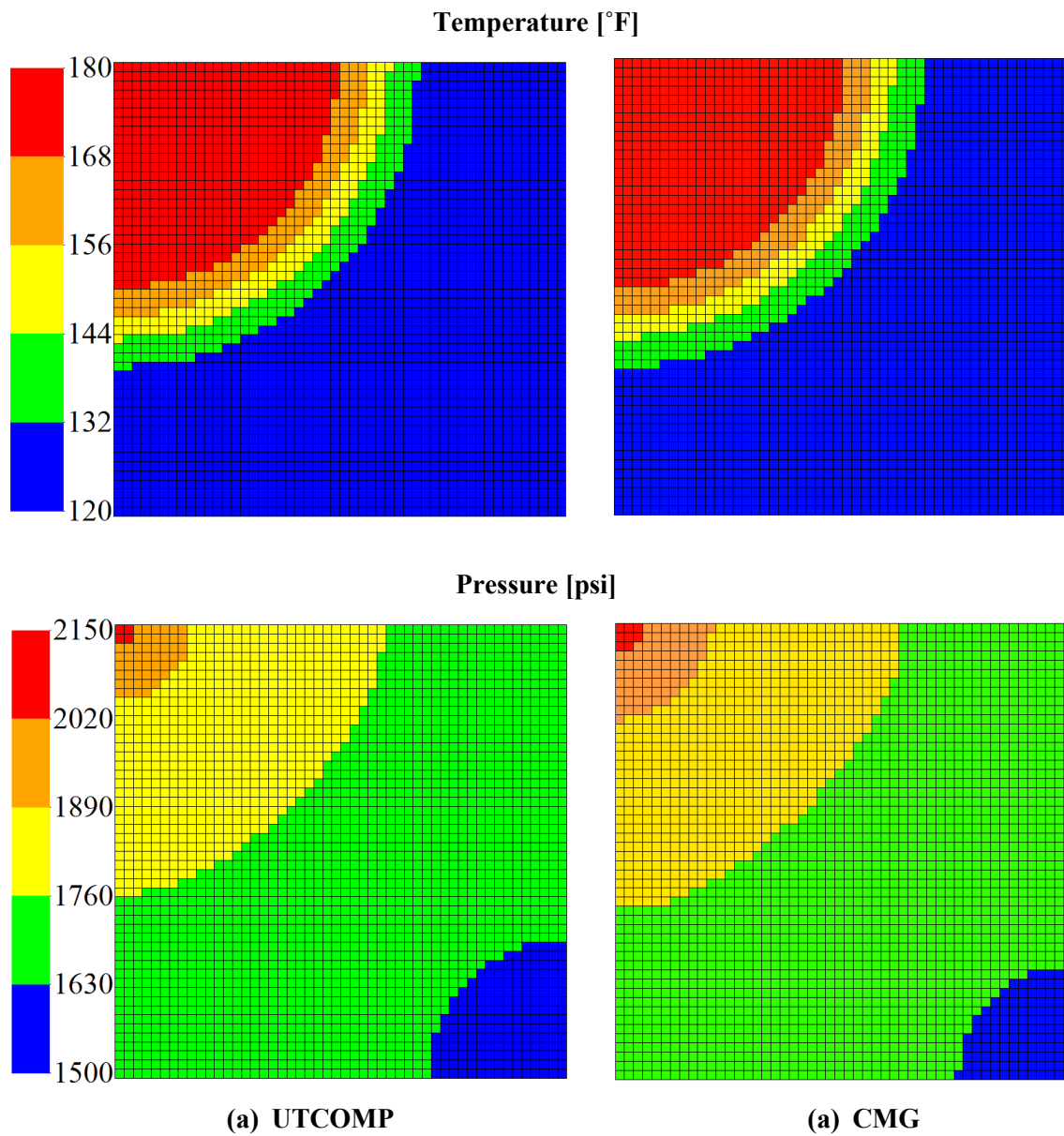
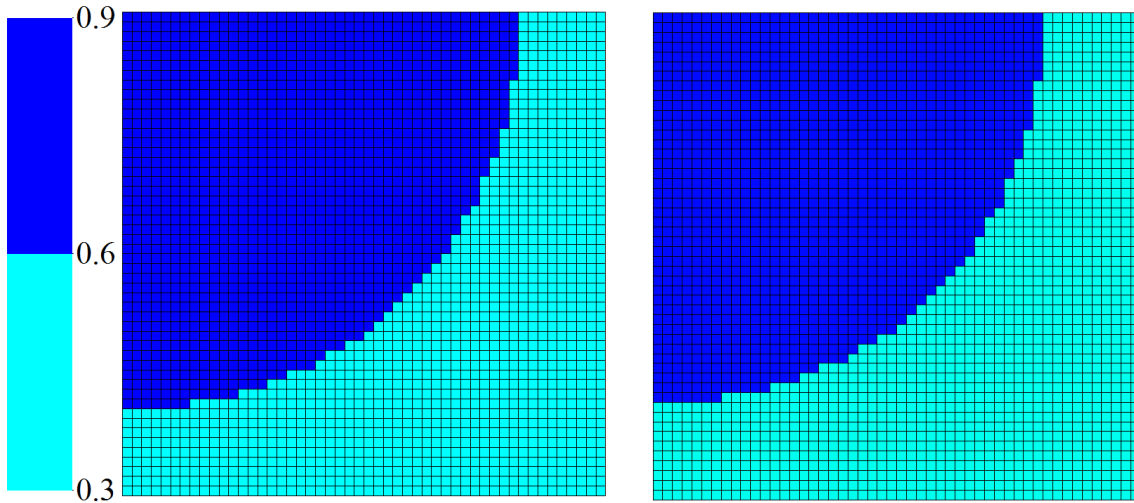
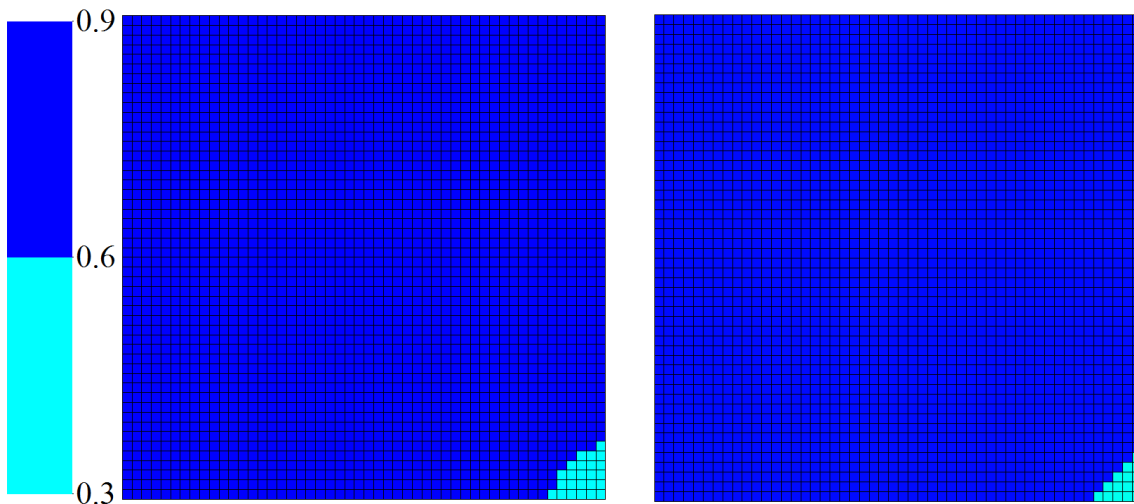


Figure 4.8 Comparison of temperature and pressure profiles of UTCOMP with CMG after 4000 days of simulation for case 3.

Water Saturation at 2000 days



Water Saturation at 4000 days



(a) UTCOMP

(b) CMG

Figure 4.9 Comparison of water saturation profiles of UTCOMP with CMG after 2000 and 4000 days of simulation for case 3.

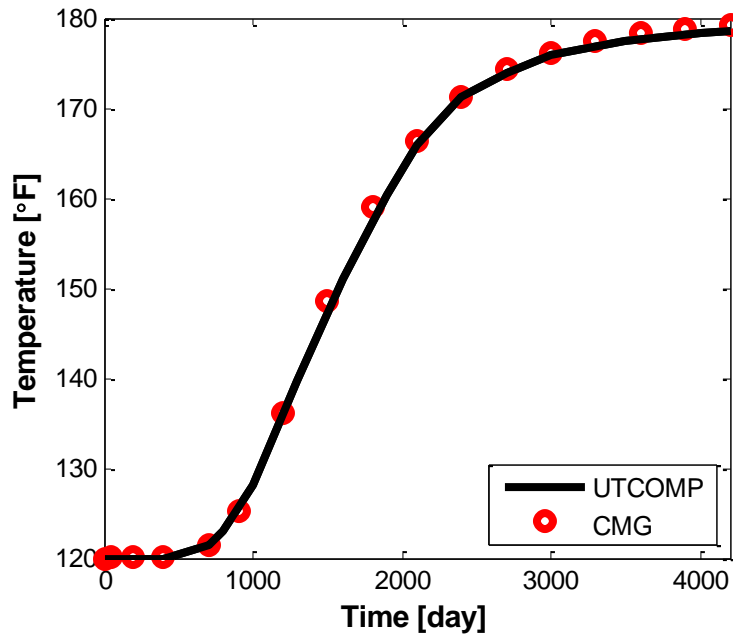


Figure 4.10 Comparison of temperature variations during simulation for grid-block (20,1,1) of UTCOMP with CMG for case 3.

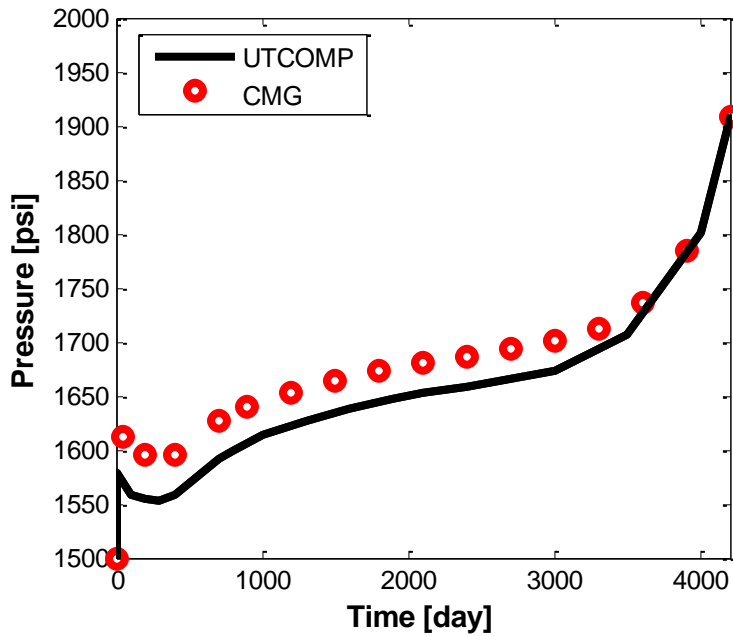


Figure 4.11 Comparison of pressure variations during simulation for grid-block (20,1,1) of UTCOMP with CMG for case 3.

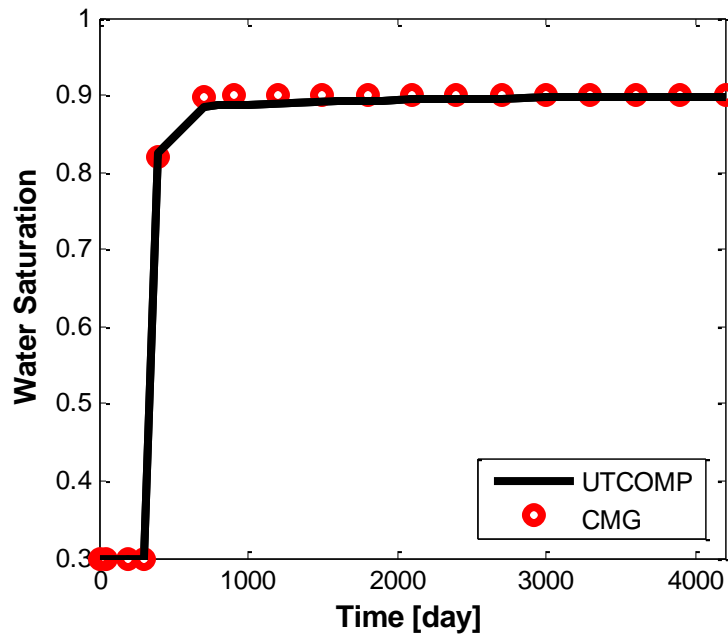


Figure 4.12 Comparison of water saturation variations during simulation for grid-block (20,1,1) of UTCOMP with CMG for case 3.

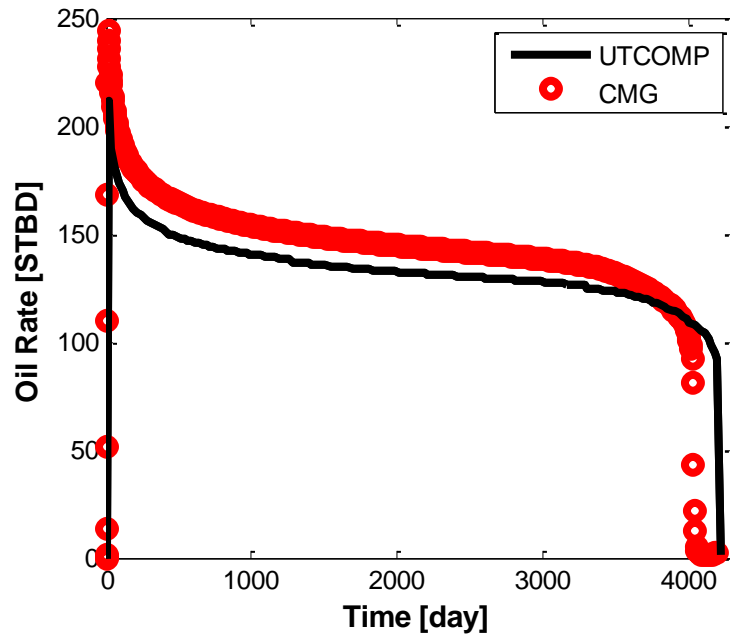


Figure 4.13 Comparison of oil production rate of UTCOMP with CMG for case 4.

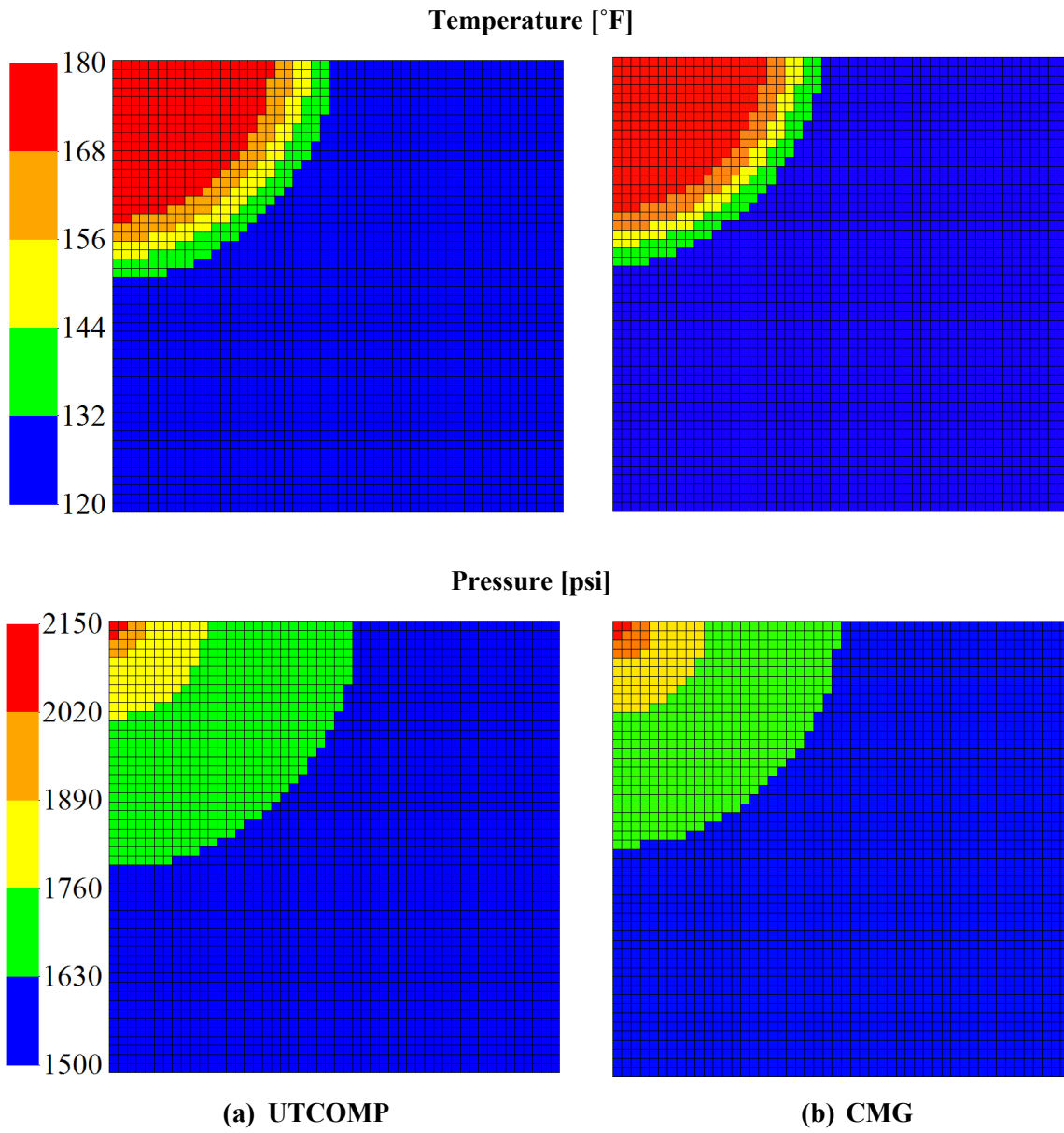


Figure 4.14 Comparison of temperature and pressure profiles of UTCOMP with CMG after 2000 days of simulation for case 4.

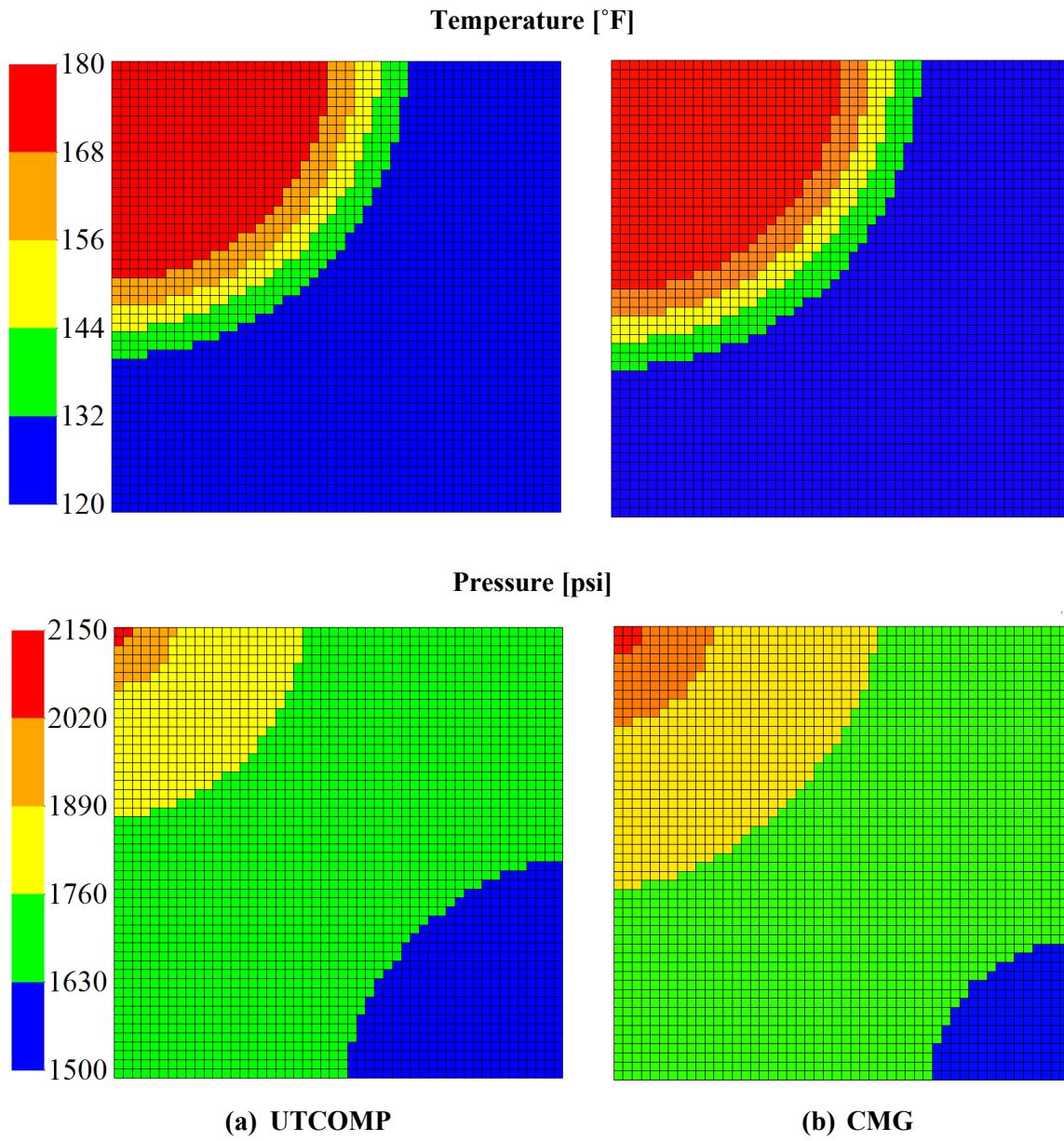


Figure 4.15 Comparison of temperature and pressure profiles of UTCOMP with CMG after 4000 days of simulation for case 4.

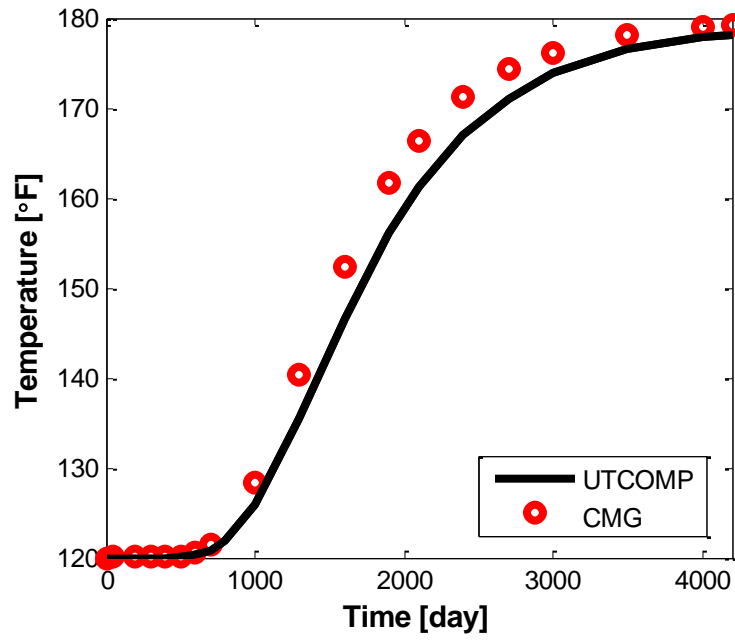


Figure 4.16 Comparison of temperature variations during simulation for grid-block (20,1,1) of UTCOMP with CMG for case 4.

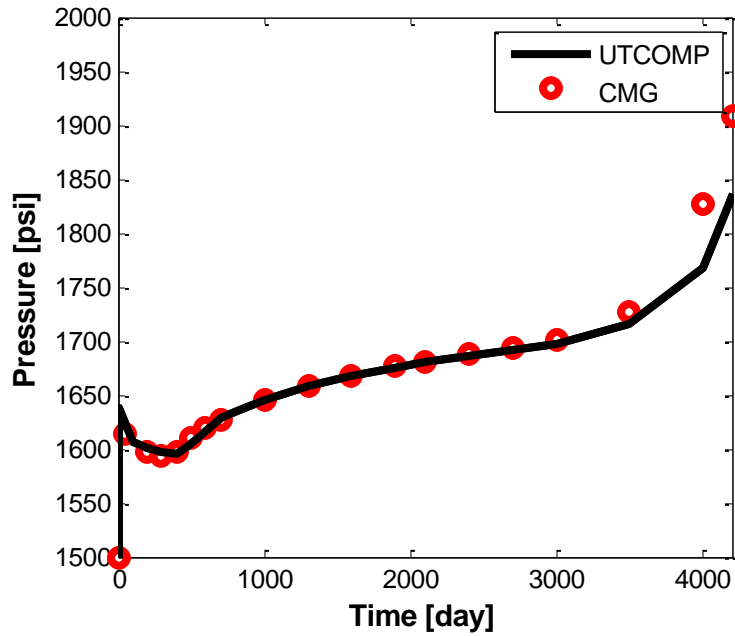


Figure 4.17 Comparison of pressure variations during simulation for grid-block (20,1,1) of UTCOMP with CMG for case 4.

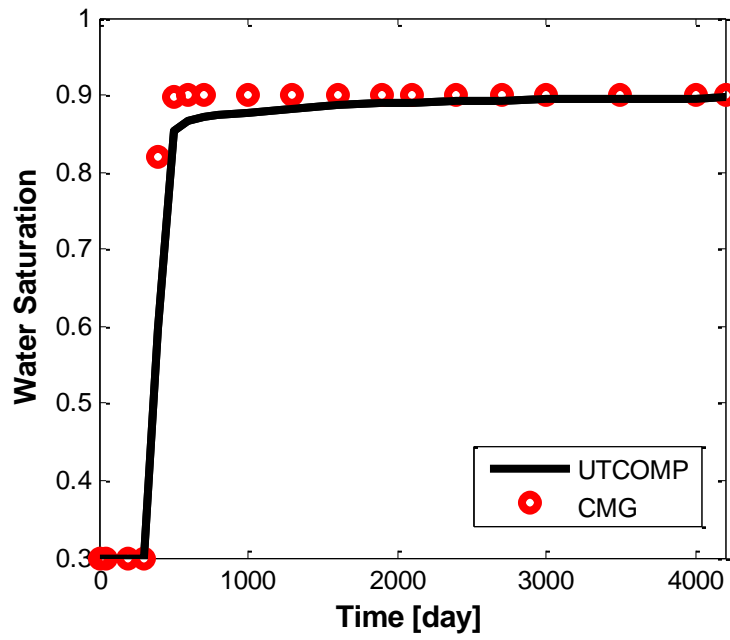


Figure 4.18 Comparison of water saturation variations during simulation for grid-block (20,1,1) of UTCOMP with CMG for case 4.

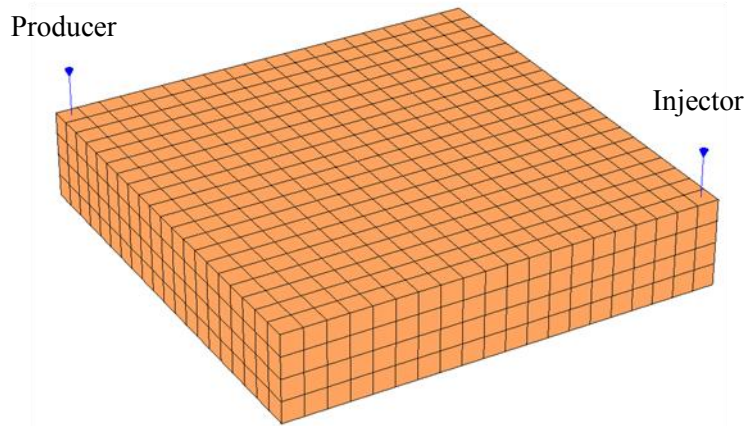


Figure 4.19 Schematic views of the reservoir for case 5.

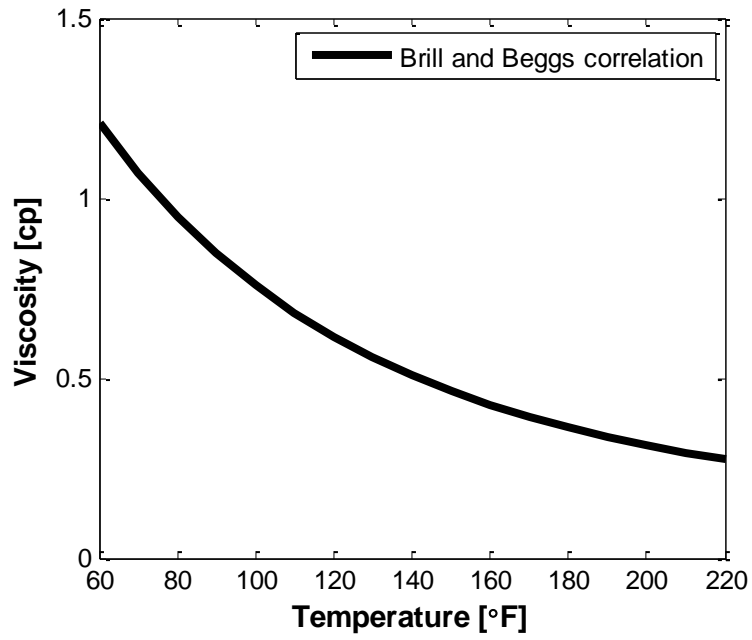


Figure 4.20 Water viscosity versus temperature calculated using the Brill and Beggs correlation.

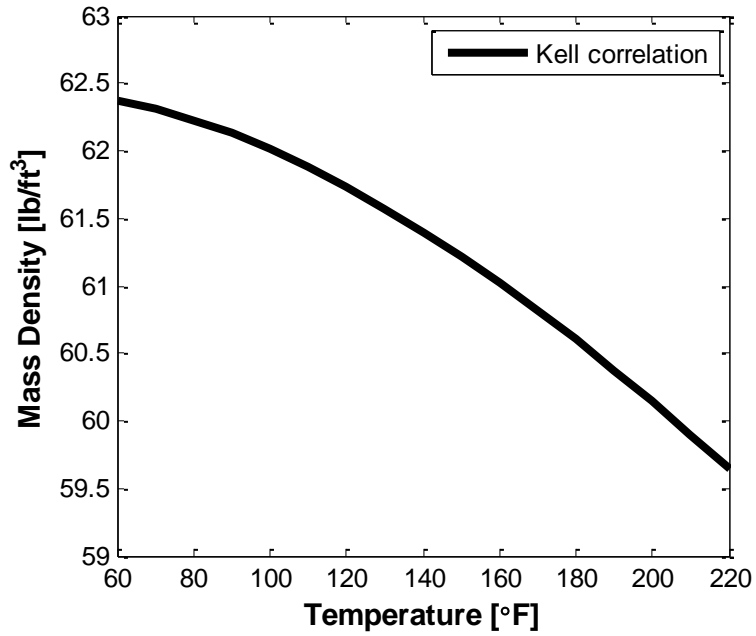


Figure 4.21 Water mass density versus temperature calculated using the Kell correlation.

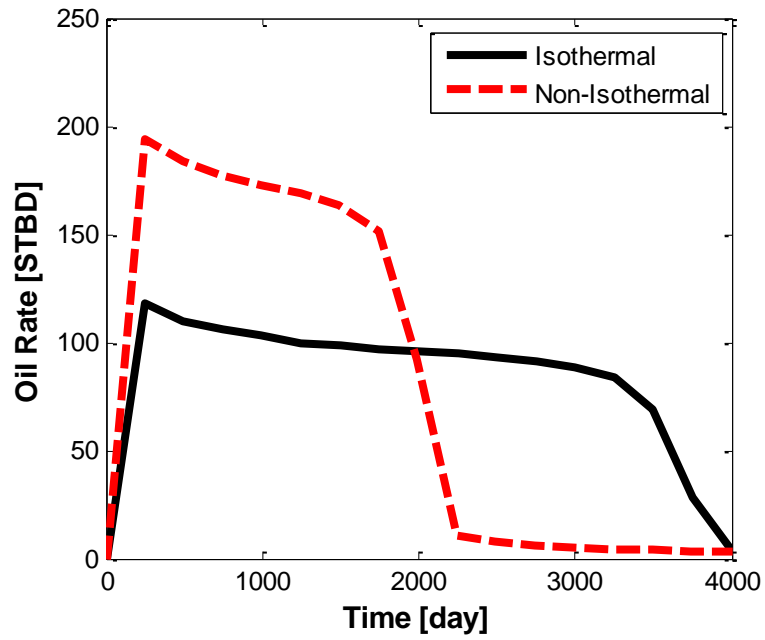


Figure 4.22 Comparison of oil production rate resulted from the isothermal UTCOMP with the non-isothermal UTCOMP for case 5.

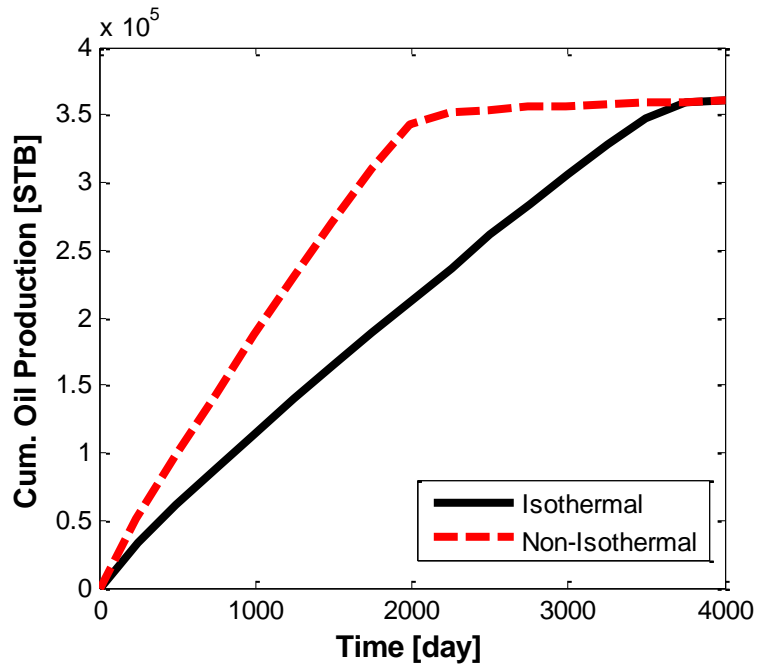


Figure 4.23 Comparison of cumulative oil production resulted from the isothermal UTCOMP with the non-isothermal UTCOMP for case 5.

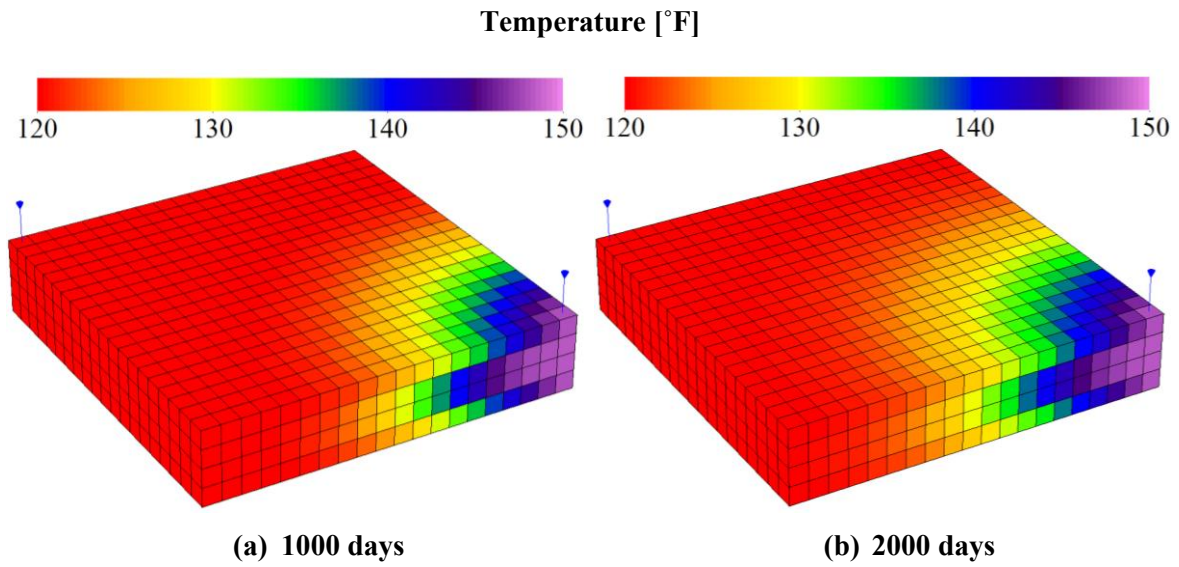


Figure 4.24 Temperature profile resulted from the non-isothermal UTCOMP after 1000 and 2000 days of simulation for case 5.

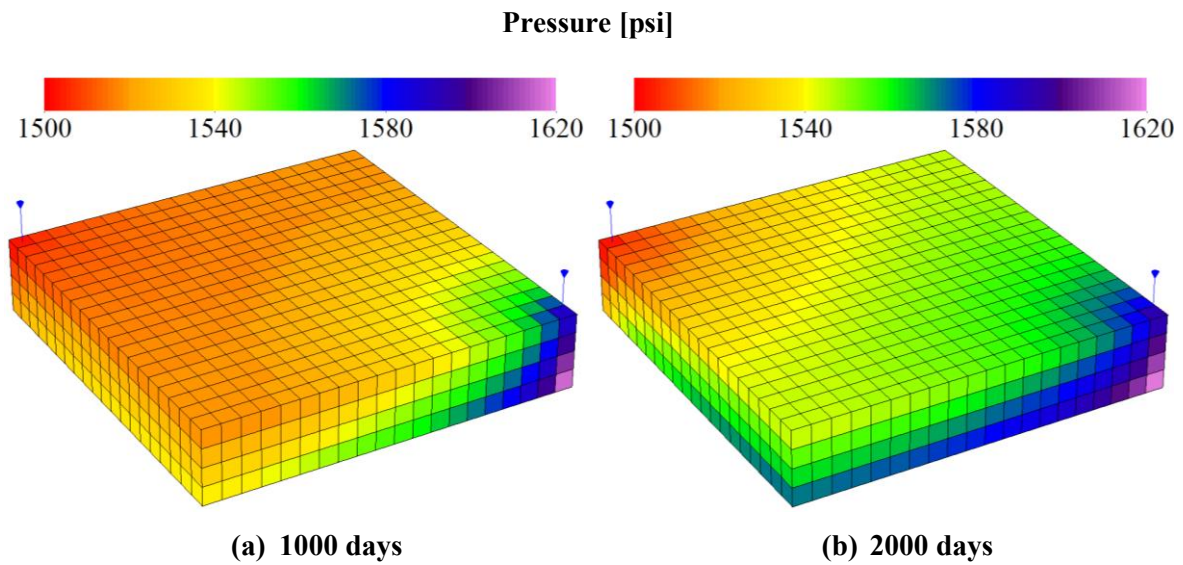


Figure 4.25 Pressure profile resulted from the non-isothermal UTCOMP after 1000 and 2000 days of simulation for case 5.

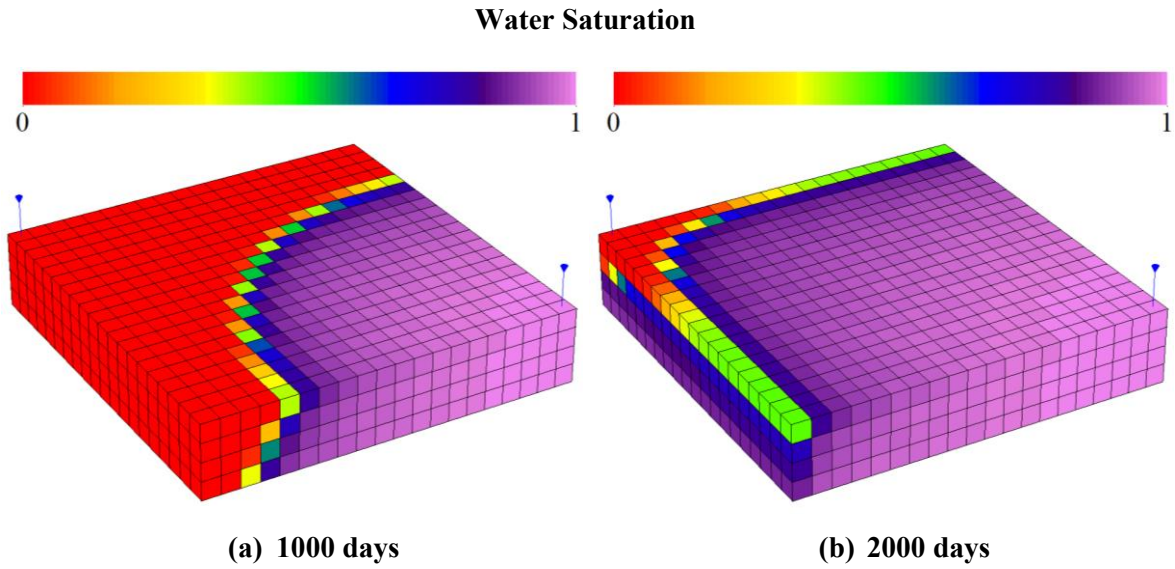


Figure 4.26 Water saturation profile resulted from the non-isothermal UTCOMP after 1000 and 2000 days of simulation for case 5.

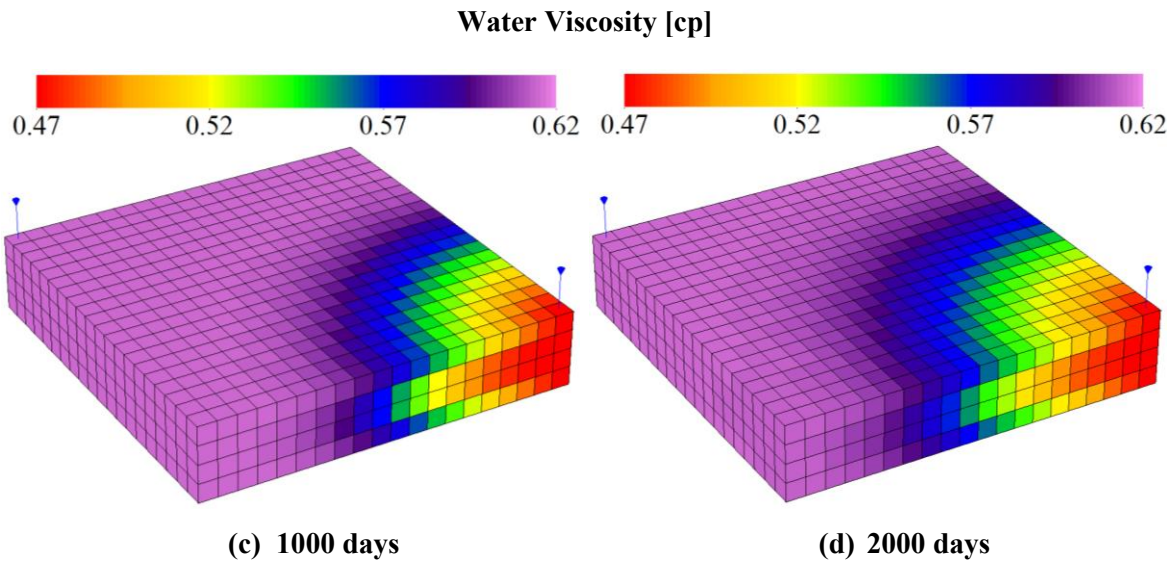


Figure 4.27 Water viscosity profile resulted from the non-isothermal UTCOMP after 1000 and 2000 days of simulation for case 5.

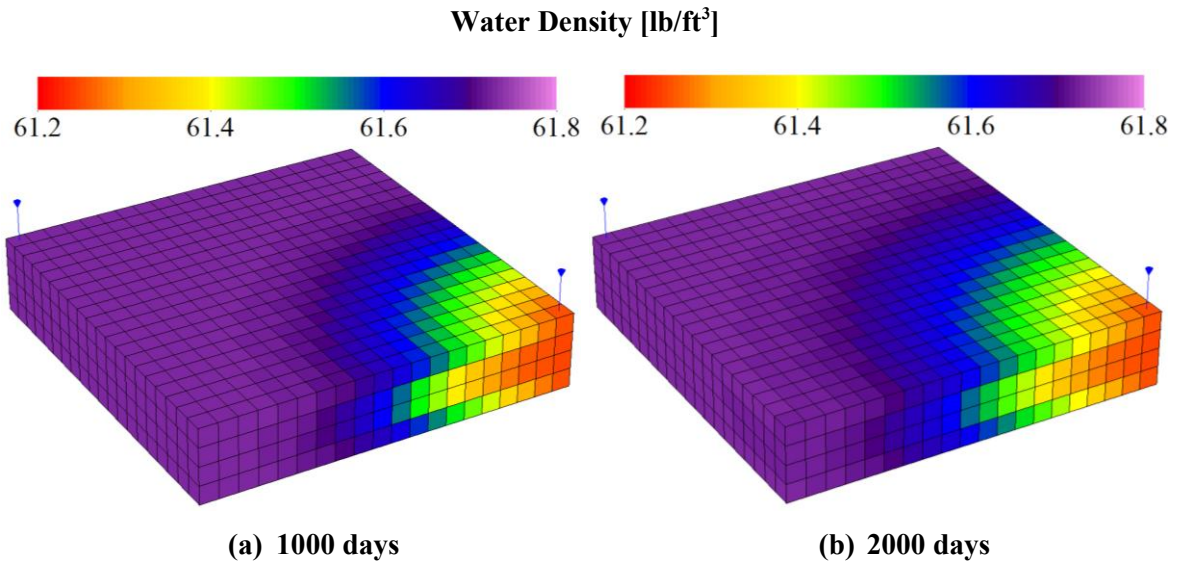


Figure 4.28 Water mass density profile resulted from the non-isothermal UTCOMP after 1000 and 2000 days of simulation for case 5.

Chapter 5: Asphaltene Model

In this chapter, we present the asphaltene model implemented in UTCOMP. First, details on the asphaltene precipitation, flocculation, and deposition models will be provided. Then, we will present various models that consider porosity, absolute permeability, oil viscosity, and wettability alterations due to asphaltene precipitation, flocculation, and deposition. At the end, we will discuss the solution scheme and the modifications that have been performed in the governing equations of UTCOMP.

5.1 ASPHALTENE PRECIPITATION MODEL

As discussed in Chapter 2, asphaltene precipitation depends on pressure, temperature, and composition variations. Figure 5.1 illustrates schematic views of the phase envelope of a crude oil. The green line is the saturation curve and brown area is the Asphaltene Precipitation Envelope (APE). At any condition inside the APE, asphaltene will precipitate from oil. Figure 5.2 shows schematic views of the asphaltene precipitation curve, which is the cross section of APE at a constant temperature (e.g. T^*). If we gradually decrease pressure at a constant temperature, asphaltene starts to precipitate at a certain pressure called onset pressure of asphaltene. Subsequently, the amount of precipitation increases, reaches to its maximum, and follows by a decrease. Finally, the amount of precipitation reaches zero at the offset pressure. As mentioned in Chapter 2, there are different methods available in the literature to model the phase behavior of asphaltene precipitation. In this study, we use a solid model (Gupta, 1986) to predict the amount of asphaltene precipitation. In addition, we use the Nghiem et al. (1993) method for characterizing the solid (asphaltene) phase. In the precipitation model, we assume that

- (1) Asphaltene precipitation is a reversible process.
- (2) Heaviest pseudo-component in oil splits into a non-precipitating and a precipitating (asphaltene) component.
- (3) All of the properties of the non-precipitating and precipitating components are identical (e.g. critical properties, acentric factors, and parachor), except their interaction coefficients with lighter components.
- (4) The precipitating component (asphaltene) may exist in the oil, gas, or solid phase.
- (5) Solid phase is only composed of asphaltene.
- (6) There is a thermodynamic equilibrium condition between oil, gas, and solid phases.

The amount of asphaltene precipitation at any condition is calculated using the thermodynamic equilibrium condition between oil, gas, and solid phases. The equilibrium condition is maintained when the fugacities of all the components in the phases are equal. Mathematically,

$$f_{i,o} = f_{i,g}, \quad i = 1, \dots, n_c, \quad (5.1)$$

$$f_{n_c,o} = f_{n_c,s}, \quad (5.2)$$

where $f_{i,o}$ is the fugacity of component i in the oil phase, $f_{i,g}$ is the fugacity of component i in the gas phase, and $f_{n_c,s}$ is the fugacity of asphaltene in the solid phase. Equation (5.1) shows the thermodynamic equilibrium condition between component i in the oil phase and component i in the gas phase. Similarly, Equation (5.2) shows the

thermodynamic equilibrium condition between the asphaltene component in the solid phase and the precipitating component in the oil phase (index n_c represents the heaviest component). The fugacity of each component in the oil or the gas phase is calculated from the Peng-Robinson EOS. Since the solid phase is only composed of the asphaltene component, the fugacity of asphaltene in the solid phase can be calculated analytically as follows:

$$\ln f_{n_c,s} = \ln f_{n_c,s}^* + \frac{v_{asph.}(P - P^*)}{RT}, \quad (5.3)$$

where P^* is the onset pressure of asphaltene at temperature T , $f_{n_c,s}^*$ is the fugacity of asphaltene in the solid phase at temperature T and pressure P^* , and $v_{asph.}$ is the molar volume of asphaltene. Having the onset pressure at a given temperature, we can use Equation (5.3) to calculate the fugacity of asphaltene in the solid phase. However, if the onset pressure data at different temperatures are not available, we use the following equation proposed by Kohse et al. (2000) for the asphaltene component fugacity in the solid phase:

$$\ln f_{n_c,s} = \ln f_{n_c,s}^* + \frac{v_{asph.}}{R} \left[\frac{(P - P_{tb})}{T} - \frac{(P^* - P_{tb})}{T^*} \right] - \frac{\Delta H_{tb}}{R} \left(\frac{1}{T} - \frac{1}{T^*} \right) - \frac{\Delta C_p}{R} \left(\ln \frac{T^*}{T} - T_{tp} \left(\frac{1}{T} - \frac{1}{T^*} \right) \right), \quad (5.4)$$

where ΔH_{tp} , ΔC_p , P_{tp} , and T_{tp} are the triple point parameters that can be calculated from correlations available in Won (1986).

As discussed in Chapter 3, the phase equilibrium calculation is a two-step process: first, the phase stability analysis and second, the flash calculation. Equations (5.1) and (5.2) create a set of $(2n_c+1)$ equations, which are the governing equations of the flash calculation in the presence of the solid phase. Before performing the flash calculation, a phase stability analysis should be performed at each grid-block in order to determine the number of existing phases. The stability analysis algorithms for the oil and gas phases in UTCOMP are discussed in Chapter 3. For the solid phase, we use the following criterion: the solid phase is stable if

$$\ln f_{n_c,o} \geq \ln f_{n_c,s}. \quad (5.5)$$

The overall phase behavior calculation procedure of UTCOMP over a time-step in a grid-block in the presence of the solid phase is as follows:

- (1) Perform phase behavior calculation for the oil and gas phases (including stability analysis and flash calculation), considering that solid phase does not exist.
- (2) Calculate fugacity of asphaltene in the solid phase using Equations (5.3) or (5.4).
- (3) Perform stability analysis for the solid phase using Equation (5.5).
- (4) Exit from phase behavior calculation, if the solid phase is not stable; otherwise, proceed to the next step.
- (5) Guess the amount of asphaltene precipitation in the solid phase. Subtract the amount of precipitation from the numbers of moles of the component n_c in the oil phase, and update the composition of the fluid.
- (6) Calculate fugacity of each component in the oil and gas phases using the Peng-Robinson EOS.

- (7) Check thermodynamic equilibrium condition (Equations (5.1) and (5.2)).
- (8) Exit from the phase behavior calculation if the thermodynamic equilibrium condition is satisfied; otherwise, compute the new amount of precipitation using the secant method and go to step (5).

Since the time-step size in UTCOMP is not large, pressure, temperature and composition in a grid-block do not change too much over one time-step. Therefore, we use the amount of precipitation calculated at the previous time-step as the initial guess (step (5) in the above procedure) in the current time-step to speed up the phase equilibrium calculation. When the pressure, temperature and composition variations are high or no asphaltene precipitated in the previous time-step, the initial guess for the amount of precipitation can be calculated using

$$w_a = \frac{f_{n_c,o} - f_{n_c,s}}{f_{n_c,o}}, \quad (5.6)$$

where w_a is the weight percentage of the asphaltene component in the solid phase.

5.2 ASPHALTENE FLOCCULATION MODEL

Based on the size of asphaltene particles, three different types of asphaltenes exist in crude oils: stable asphaltenes, colloidal asphaltenes, and flocculated asphaltenes (Kraiwanawong et al., 2009). Figure 5.3 illustrates the asphaltene particle size distribution in a crude oil (Kraiwanawong et al., 2009). Stable asphaltenes are small particles that are not visible in the precipitation tests. Colloidal asphaltenes are mid-size particles (less than 1 μm), which are visible in the precipitation tests, but are not

problematic in the deposition mechanism. Flocculated asphaltenes are the largest particles that are formed due to aggregation of colloidal asphaltenes. Flocculated asphaltenes deposit on the surfaces of the rock, wellbore, and pipelines and cause detrimental effects to the field. We use a reversible chemical reaction in order to model the flocculation process in the reservoir (Kohse and Nghiem, 2004). We assume that

- (1) Asphaltene precipitates in the form of colloidal asphaltenes.
- (2) Colloidal asphaltenes transform into flocculated asphaltenes, and vice versa.
- (3) Colloidal asphaltenes have a normal distribution and are represented by their average size.
- (4) Flocculated asphaltenes have a normal distribution and are represented by their average size.
- (5) Colloidal asphaltenes can dissolve in the oil instantaneously.
- (6) Flocculated asphaltenes cannot dissolve in the oil instantaneously.

The pseudo-reaction model for the process of flocculation is as follows:



where the asphaltene flocculation rate depends on the properties of the fluid and the concentration of colloidal and flocculated asphaltenes in the solution. The asphaltene flocculation rate is defined as

$$r = \frac{dC_{floc.}}{dt} = k_{cf} C_{coll.} - k_{fc} C_{floc.} \quad (5.8)$$

In Equation (5.8), $C_{coll.}$ is the concentration of the colloidal asphaltenes in the oil phase, $C_{floc.}$ is the concentration of the flocculated asphaltenes in the oil phase, k_{cf} is the forward rate of the formation of flocculated asphaltenes from colloidal asphaltenes, and k_{fc} is the reverse rate. k_{cf} and k_{fc} are determined using experimental data. It should be noted that both flocculation and precipitation are reversible processes in our model.

5.3 ASPHALTENE DEPOSITION MODEL

Due to Stokes law (Geankoplis, 1993), the size of an asphaltene particle dictates how fast a particle will deposit. Based on the calculations that have been made by Kraiwattanawong et al. (2009), an asphaltene particle with the size of about 1 μm has a settling velocity of 7.25×10^{-5} cm/s in heptanes, and will settle 5 cm within 19 h. Kraiwattanawong et al. (2009) concluded that the colloidal asphaltenes that are particles under 1 μm , have enough time to be transported in the porous media, and will not deposit on the rock surface. We assume that colloidal asphaltenes flow as suspended particles in the oil phase, and flocculated asphaltenes partially flow as suspended particles in the oil and partially deposit on the rock surface. We consider adsorption, pore throat plugging, and re-entrainment processes as explained by Wang and Civan (2001) as the main mechanisms of asphaltene deposition. Thus, we use the following equation for the deposition rate:

$$\frac{dV_{dep.}}{dt} = \alpha C_{floc.} \phi - \beta V_{dep.} (v_o - v_{cr,o}) + \gamma u_o C_{floc.} \quad (5.9)$$

In Equation (5.9), $V_{dep.}$ is the volume of the deposited asphaltene per grid-block volume, $C_{floc.}$ is the volumetric concentration of flocculated asphaltene per volume of oil, ϕ is

porosity, v_o is oil phase interstitial velocity, $v_{cr,o}$ is critical oil phase interstitial velocity (above this velocity re-entrainment occurs), and u_o is the oil phase Darcy velocity. In addition, α is the surface deposition rate coefficient, which is a positive constant value and depends on the rock type, β is the entrainment coefficient, which is set to zero when the interstitial oil phase velocity is smaller than the critical interstitial velocity, and γ is the pore-throat plugging coefficient. The value of β is set as

$$\begin{cases} \beta = \beta_i & \text{if } v_o > v_{cr,o} \\ \beta = 0 & \text{if } v_o \leq v_{cr,o} \end{cases}, \quad (5.10)$$

where β_i is the instantaneous entrainment rate coefficient, v_o is the interstitial velocity of the oil phase, and $v_{o,cr}$ is the critical interstitial velocity of the oil phase. The value of γ is defined as

$$\begin{cases} \gamma = \gamma_i (1 + \sigma V_{dep.}) & \text{if } D_{pt} \leq D_{pt,cr} \\ \gamma = 0 & \text{if } D_{pt} > D_{pt,cr} \end{cases}, \quad (5.11)$$

where γ_i is the instantaneous plugging deposition rate coefficient, σ is the snowball-effect deposition constant, D_{pt} is the average pore throat diameter, and $D_{pt,cr}$ is the critical pore throat diameter. Pore throat plugging occurs when the average pore throat diameter in the porous medium is less than the critical pore throat diameter.

5.4 POROSITY AND PERMEABILITY REDUCTIONS

Once Asphaltene deposits on the rock surface in a grid-block, porosity of that grid-block will be reduced. To consider porosity reduction, we simply subtract the amount of the deposited asphaltene from the pore volume,

$$\phi = \phi_i - V_{dep.}, \quad (5.12)$$

where ϕ_i is the initial porosity and $V_{dep.}$ is the volume of the deposited solid per grid-block volume.

Since porosity and permeability are correlated, decrease in porosity causes reduction in permeability as well. If experimental data for absolute permeability versus porosity is available, we use the experimental data as a table to calculate absolute permeability at each grid-block based on the value of porosity. Otherwise, we assume that there is a power law relationship between porosity and permeability (Reis and Acock, 1994) as follows:

$$k = a(\phi)^g, \quad (5.13)$$

where a and g are constant parameters that can be determined using experimental data. In our model, we use the following equation in order to update the permeability values based on the new porosity values:

$$\frac{k}{k_i} = \left(\frac{\phi}{\phi_i} \right)^g, \quad (5.14)$$

where k_i is the initial permeability, and the exponent g ranges from 3 to 7 (Reis and Acock, 1994).

5.5 OIL VISCOSITY

The asphaltene particles in the oil phase alter the viscosity of the oil phase. If experimental data for the oil viscosity at various concentrations of asphaltene particles is available, a table will be used to calculate the viscosity of the oil at each grid-block. Otherwise, we have the option to use the Einstein model (Eastman et al., 2004), semi-empirical Krieger and Dougherty (1959) model, or the generalized Nielson (1970) model to calculate the viscosity.

The Einstein model is expressed as

$$\frac{\mu}{\mu_0} = 1 + aC_p, \quad (5.15)$$

where C_p is the volume concentration of colloids and μ_0 is the oil viscosity at $C_p=0$. The default value for a is 2.5. The Einstein model is usually used for a suspension that has a low volume fraction of particles (less than 0.01); however, the power law based models are more appropriate for a higher concentration of particles (Krieger and Dougherty, 1959; Nielson, 1970).

The Krieger and Dougherty model is expressed as

$$\frac{\mu}{\mu_0} = \left(1 - \frac{C_p}{C_{p0}}\right)^{-[\eta] C_{p0}}, \quad (5.16)$$

where C_{p0} is the volumetric concentration of the maximum packing and $[\eta]$ is the intrinsic viscosity. For hard spheres, $[\eta] = 2.5$, and for randomly mono-dispersed spheres, $C_{p0} = 0.65$.

The Nielsen model is expressed as

$$\frac{\mu}{\mu_0} = (1 + 1.5C_p) e^{-C_p/(1-C_{p0})}. \quad (5.17)$$

5.5 WETTABILITY ALTERATION MODEL

As discussed in Chapter 2, Al-Maamari and Buckley (2003) performed a set of experiments in COBR systems to measure wettability changes due to asphaltene deposition. n-heptane was added to different crude oils to change the stability of asphaltene and the contact angle at different conditions was measured. Al-Maamari and Buckley (2003) measured refractive index (RI) at different conditions to quantify the stability of asphaltene in the mixture (by knowing that there is a correlation between the refractive index of a mixture and the onset of asphaltene precipitation (Buckley, 1996)). The refractive index at the onset point of asphaltene precipitation is called P_{RI} . Asphaltene precipitates from oil, if the RI of the mixture is less than P_{RI} . Al-Maamari and Buckley (2003) tested five different asphaltic crude oils: A-93, Marse-Yellow, Mars-Pink, Legrave-97, and Tensleep oils. Table 5.1 summarizes the properties of the crude oils that were used in those experiments. To avoid flocculation, they added α -methylnaphthalene (α -MN) to Legrave-97 and Tensleep oils. Table 5.2 presents the properties of the brines used in their set of experiments. The brine with pH of 4 and ionic strength (M) of 0.01 created an unstable water film on the surface, while the brine with

pH of 8 and ionic strength (M) of 1.00 created a stable water film on the surface. Figure 5.4 presents the results of the Al-Maamari and Buckley (2003) experiments for the five mentioned crude oils in the presence of the unstable brine (pH = 4 and $M = 0.01$). The vertical axis is contact angle and the horizontal axis is the refractive index difference, defined as

$$\Delta RI = P_{RI} - RI. \quad (5.18)$$

Positive ΔRI means asphaltene precipitates from oil and negative ΔRI means asphaltene is stable.

Based on the experimental data provided by Al-Maamari and Buckley (2003) and known physical mechanisms of asphaltene deposition on the rock in the COBR system, we propose the following equation to model wettability alteration due to asphaltene instability in a crude oil (Darabi et al., 2012):

$$\theta = \theta_i + \frac{\theta_f - \theta_i}{1 + \exp\left(\frac{b - ASI}{a}\right)}, \quad (5.19)$$

where θ is contact angle at desired condition, θ_i is the initial contact angle, θ_f is the final contact angle, a and b are matching parameters, and ASI is the asphaltene stability index. ASI can be any physical parameter that can define stability of asphaltene in the mixture. For example, ASI is equal to ΔRI for the Al-Maamari and Buckley (2003) experimental data set. To investigate the accuracy of the proposed model, we tuned the model parameters (a , b , and θ_f) to match the experimental data shown in Figure 5.4. Table 5.3 presents the tuned parameters for each of the oils that were used in the Al-Maamari and

Buckley (2003) experiments. In addition, Figures 5.5 through 5.9 compare the proposed model's prediction versus the experimental data for A-93, Marse-Yellow, Mars-Pink, Legrave-97, and Tensleep oils, respectively. As can be seen, the proposed model matches the experimental data very well.

In the Al-Maameri and Buckley (2003) experiments, flocculation of asphaltenes was inhibited by adding α -MN to the oils. In addition, enough aging time before measuring the contact angle was allowed to make sure that asphaltenes were deposited homogeneously on the surface at each condition. Therefore, ΔRI is a measure of deposition rather than precipitation in those experiments. During simulation, the suspended asphaltene particles in the oil can partially flow in the porous media and can partially deposit on the rock surface. To consider dynamics of asphaltene precipitation, flocculation, and deposition, we calculate ASI directly from the amount of deposited asphaltene in a grid-block. In addition, we assume that during deposition, a mono-layer of asphaltene particles coats the rock surface (homogenous deposition).

In Equation (5.19), θ_f and constants a and b depend on compositions of rock, oil, and brine. Composition of the rock is responsible for the adhesion forces between the asphaltene particles and the rock surface, and the degree of which the water film is dispersed. Composition of the oil dictates the amount of asphaltene precipitation at any condition (pressure and temperature) that can potentially deposit on the rock surface. Composition of brine dictates the degree of stability of brine film on the surface of the rock. For instance, Figure 5.10 compares the results of Al-Maamery and Buckley (2003) experiments for the A-93 oil in the presence of two different brines: (1) unstable brine (pH = 4 and $M = 0.01$), and (2) stable brine (pH = 8 and $M = 1.00$). As can be observed, the wettability of the rock changed from water-wet towards oil-wet in the presence of the unstable brine; however, the wettability remained unchanged in the presence of the stable

water film. In another study, Yan et al. (1997) used different types of brines (NaCl, CaCl₂, and AlCl₃) in their experiments to investigate the effect of asphaltene deposition on the wettability of the rock for the Wyoming '95 and Purdhoie Bay '95 asphaltic oils. They showed that in the presence of AlCl₃ salt (that has the highest cation valency among the salts used), the rock has the most tendency to become oil-wet compared to CaCl₂ and NaCl. In addition, the rock has the least tendency to become oil-wet in the presence of NaCl.

Based on the contact angle variations, we modify the relative permeabilities and capillary pressures at each grid-block during simulation. We use the following equations proposed by Adibhatia et al. (2005) to correlate the relative permeability of oil and water phases to the contact angle in Corey's (Corey et al., 1956) model:

$$k_{r_{w/o}} = k_{r_{w/o}}^* \left(\frac{S_o - S_{ro}}{1 - S_{ro} - S_{rw}} \right)^{e_{w/o}}, \quad (5.20)$$

$$k_{r_{w/o}}^* = 1 + \left[k_{r_w}^{*0} + \frac{\cos \theta - \cos \theta^0}{\cos(\pi - \theta^0) - \cos \theta^0} (k_{ro}^{*0} - k_{r_w}^{*0}) - 1 \right] \left(\frac{1 + T_{w/o}^0 N_{T_{w/o}}^0}{1 + T_{w/o} N_{T_{w/o}}} \right), \quad (5.21)$$

$$e_{w/o} = 1 + \left[e_w^0 + \frac{\cos \theta - \cos \theta^0}{\cos(\pi - \theta^0) - \cos \theta^0} (e_o^0 - e_w^0) - 1 \right] \left(\frac{1 + T_{w/o}^0 N_{T_{w/o}}^0}{1 + T_{w/o} N_{T_{w/o}}} \right). \quad (5.22)$$

All of the values with superscript "0" correspond to the initial condition. Note that in Equations (5.21) and (5.22), $(\pi - \theta)$ should be used instead of θ for the oil phase. T is the trapping parameter and N_T is the trapping number. The trapping number for a phase l displaced by l' is defined as

$$N_{T_i} = \frac{|k(\vec{\nabla}\Phi_{l'} + g(\rho_{l'} - \rho_l))|}{\sigma_{ll'}}, \quad (5.23)$$

where Φ is potential, ρ is density, and $\sigma_{ll'}$ is interfacial tension. Changing the wettability affects both $S_{rw/o}$ and $T_{w/o}$. The following equations correlate $S_{rw/o}$ and $T_{w/o}$ to contact angle:

$$\frac{\ln(T_{w/o}) - \ln(T_w^0)}{\ln(T_o^0) - \ln(T_w^0)} = \frac{\cos \theta - \cos \theta^0}{\cos(\pi - \theta^0) - \cos \theta^0}, \quad (5.24)$$

$$\frac{S_{r_{w/o}} - S_{r_w}^0}{S_{r_o} - S_{r_w}^0} = \frac{\cos \theta - \cos \theta^0}{\cos(\pi - \theta^0) - \cos \theta^0}. \quad (5.25)$$

We assume that asphaltene deposition does not affect the relative permeability of the gas phase.

The following equation correlates the capillary pressure to the contact angle:

$$p_{w/o}^c = C_{pc} \sigma_{w/o} \sqrt{\frac{\phi}{k}} (1 - \bar{S}_w)^{E_{pc}} \frac{\cos(\theta)}{\cos(\theta_0)}, \quad (5.26)$$

where the parameters C_{pc} and E_{pc} need to be determined by matching water/oil experimental capillary pressure curve.

5.6 MODIFICATIONS OF THE GOVERNING EQUATIONS OF UTCOMP

In the presence of asphaltene, we need to modify the governing equations of UTCOMP (pressure equation, material balance equation, and phase behavior calculation) that are presented in Chapter 3. Phase behavior calculation of oil, gas, and solid

(asphaltene) phases is discussed in Section 5.1. In this section, we present the modified pressure equation and material balance equation in the presence of asphaltene.

5.6.1 Mass Conservation Equation

In our asphaltene model, we assume that asphaltene is not a continuous phase and exists in the oil phase in the form of colloids. In addition, we assume that colloidal and flocculated asphaltene particles are carried in the crude oil and move with the same velocity of the oil phase. Based on these assumptions, the flux term in the mass conservation equation (Equation (3.1)) for the heaviest component (n_c) is modified as

$$\vec{F}_{n_c} = \sum_{j=1}^{N_p} \left(\xi_j x_{n_c,j} \vec{u}_j - \phi \xi_j S_j \vec{K} \nabla x_{n_c,j} \right) + \frac{1}{V_b} \left(N_{coll.} \vec{u}_o + N_{floc.} \vec{u}_o \right), \quad (5.27)$$

where $N_{coll.}$ is the number of moles of colloidal asphaltenes and $N_{floc.}$ is the number of moles of flocculated asphaltenes in a grid-block. The flux term for other components in the mixture is similar to Equation (3.4).

5.6.2 Pressure Equation

We modify the pressure equation (Equation (3.8)) of UTCOMP as follows to consider the flow of asphaltene particles and the effect of asphaltene deposition on pore volume:

$$\left(\frac{dV_p^{-asph.}}{dP} \right) \left(\frac{\partial P}{\partial t} \right) - \left(\frac{dV_{dep.}}{dt} \right) = \left(\frac{\partial V_t}{\partial P} \right)_{N_i} \left(\frac{\partial P}{\partial t} \right) + \sum_{i=1}^{N_c+1} \left(\frac{\partial V_t}{\partial N_i} \right)_{P, N_k (k \neq i)} \left(\frac{\partial N_i}{\partial t} \right), \quad (5.28)$$

where $V_p^{-asph.}$ is the pore volume of a grid-block neglecting asphaltene deposition. The term $\left(\frac{dV_{dep.}}{dt}\right)$ is evaluated at the previous time-step using Equation (5.9). In addition, the modified flux expression provided in Equation (5.27) is used to evaluate $\left(\frac{\partial N_i}{\partial t}\right)$.

5.7 OVERALL PROCEDURE OF THE ASPHALTENE MODEL IN UTCOMP

The overall procedure of the asphaltene model in UTCOMP over a time-step in a grid-block is as follows:

- (1) Compute the derivatives and coefficients necessary for Equation (5.28).
- (2) Solve implicitly Equation (5.28) for pressure at each of the grid-blocks.
- (3) Update grid-block porosity at the new pressure.
- (4) Compute the overall number of moles for each of the components including colloidal and flocculated asphaltenes with the new pressure and porosity using the modified mass conservation equation.
- (5) Add the number of moles of colloidal and flocculated asphaltenes to the total moles of the heaviest component, and update overall composition of the mixture.
- (6) Perform phase behavior calculation for oil and gas phase (including stability analysis and flash calculation), considering that the solid phase does not exist.
- (7) Calculate fugacity of asphaltene in the solid phase using Equation (5.3) or (5.4).
- (8) Perform stability analysis for the solid phase using Equation (5.5).
- (9) Go to 14, if the solid phase is not stable; otherwise, proceed to the next step.

- (10) Guess the amount of asphaltene precipitation in the solid phase. Subtract the amount of precipitation from the component n_c moles in the oil phase, and update the composition of the fluid.
- (11) Calculate fugacity of each component in the oil and gas phases using the Peng-Robinson EOS.
- (12) Check the thermodynamic equilibrium condition (Equations (5.1) and (5.2)).
- (13) If the thermodynamic equilibrium condition satisfies, go to (14); otherwise, compute the new amount of precipitation using the secant method and go to step (9).
- (14) If the new amount of precipitation is greater than the sum of colloidal and flocculated asphaltenes, add the difference to the colloidal asphaltene. If the new amount of precipitation is less than the sum of colloidal and flocculated asphaltenes, subtract the difference only from the colloidal asphaltene.
- (15) Calculate the new number of moles of flocculated asphaltenes and colloidal asphaltenes using Equation (5.8).
- (16) Compute the amount of deposition using Equation (5.9), and update the numbers of moles of flocculated asphaltenes.
- (17) Compute the new contact angle of the rock at a grid-block using Equation (5.19).
- (18) Update porosity, absolute permeability, oil viscosity, relative permeabilities, and capillary pressure.
- (19) March to the next time-step.

5.8 VERIFICATION OF THE ASPHALTENE PRECIPITATION MODEL

In this section, we compare the precipitation model of UTCOMP against the Burke et al. (1990) fluid experimental data and WinProp Module of CMG (WinProp user's guide, 2011). Table 5.4 summarizes the mixture properties and overall composition of the fluid and Table 5.5 presents the binary interaction coefficients of the Burke et al. (1990) fluid. The asphaltene onset pressure is considered to be 4600 psi at reservoir temperature (212 °F). Figure 5.11 compares the results of UTCOMP for asphaltene precipitation versus pressure with experimental data and CMG. As can be observed, the results of UTCOMP and CMG are in good agreement. The minor differences below the bubble point are due to dissimilarities in the flash calculation algorithms of UTCOMP and CMG. Both UTCOMP and CMG predict the bubble point pressure correctly, which is reported to be about 3000 psi at reservoir temperature (212 °F). As can be seen, the precipitation models of UTCOMP and CMG reasonably catch the behavior of asphaltene. The maximum amount of precipitation is estimated to be around the bubble point by both CMG and UTCOMP. However, the experimental data shows that the amount of precipitation reaches its maximum slightly below the bubble point pressure. In order to get a better match between the precipitation model and the experimental data, we need to sacrifice the accuracy of the bubble point prediction.

5.9 VERIFICATION OF THE ASPHALTENE DEPOSITION MODEL

In this section, we compare the asphaltene deposition model of UTCOMP against the Minssieux (1997) experimental data and the results of Kohse and Nghiem (2004). Minssieux (1997) performed a set of oil core flood experiments on different rock samples to investigate the effect asphaltene deposition on the rock permeability reduction. Minssieux (1997) injected 50 to 100 pore volumes of asphaltic Weyburn stock tank oil

(Huang and Dyer, 1993; Srivastava et al., 1995) into different rock samples, and measured the permeability of the rock at different conditions. Kohse and Nghiem (2004) matched the parameters of the Wang and Civan (2001) deposition model for three of the experiments presented by Minssieux (1997). Table 5.6 presents the fluid composition of the Weyburn dead oil (Kohse and Nghiem, 2004) and Table 5.7 summarizes the core data for the three different oil core-flood experiments. Table 5.8 shows the tuned parameters of the Wang and Civan (2001) deposition model for these three experiments matched by Kohse and Nghiem (2004).

We simulate these three oil core floods (GF3, GF1, and GV5) to verify the Wang and Civan (2001) deposition model implemented in UTCOMP. Since the dead oil is used in the experiments, we assume that all the asphaltenes precipitate from oil at any condition in the core and instantaneously transform into flocculated asphaltenes. For the sake of consistency with the Kohse and Nghiem (2004) simulations, we assume that asphaltene precipitation, flocculation, and deposition do not affect the oil viscosity and the wettability of the rock.

Figure 5.12 compares the results of UTCOMP for the permeability resistance factor (permeability over the initial permeability) versus pore volume injected against the experimental data and the results of Kohse and Nghiem (2004) for the GF3 core flood. Similarly, Figures 5.13 and 5.14 presents the results for GF1 and GV5 core floods, respectively. As can be seen, there is a good agreement between the results of UTCOMP and both the experimental data and the Kohse and Nghiem (2004) results.

The GF3 core flood is only matched by the surface deposition rate. The results suggest that pore-throat plugging and entrapment has little (or no) contribution in the deposition process. On the other hand, in addition to surface deposition, pore-throat plugging contributes to asphaltene deposition for GF1 core flood, and entrapment

contributes to asphaltene deposition for GV5 core flood. In Figure 5.12, we observe that the permeability resistance curve for GF3 sample is concave-up shaped and the rate of decline decreases slightly over time. For GF1 sample, the permeability resistance curve for GF3 sample is concave-down shaped and the rate of decline decreases over time. Small surface deposition rate and increase in the effect of pore-throat plugging over time are the reasons for the concave-down behavior of the permeability resistance factor curve. For GV5 sample, the permeability resistance curve for GF3 sample is concave-up shaped with a rapid decline in the beginning. The permeability of the rock dropped by about 80 % after 20 pore-volume oil injection. Afterward, the decline rate of permeability decreases significantly. Kohse and Nghiem (2004) suggested that the rapid initial decline in GV5 experiment is due to high clay content of the sample. High initial surface deposition rate incorporated with entrainment of asphaltene particles at high oil velocities explains the concave-up with a rapid initial decline behavior of GV5 sample.

5.10 SUMMARY

In this chapter, we discussed different components of the asphaltene model in UTCOMP. We provided details on the asphaltene precipitation, flocculation, and deposition models as well as the permeability, porosity, and oil viscosity reduction models. In addition, we proposed a wettability alteration model due to asphaltene deposition. Table 5.9 summarizes all the necessary parameters of the asphaltene model of UTCOMP. Furthermore, we discussed the solution scheme and the modifications that have been performed in the governing equations of UTCOMP.

Table 5.1 Properties of the five crude oils that are used in the Al-Maameri and Buckley (2003) set of experiments.

Oil	Density [g/cm ³]	Asphaltenes wt%	RI _{oil}	PR _i
A-93	0.8891	4.00	1.5168	1.4436
Mars-Yellow	0.8783	1.86	1.4950	1.4316
Mars-Pink	0.9474	6.50	1.5383	1.4291
Lagrange-97 + α -MN (70:30)	0.8936	5.40	1.5193	1.4608
Tensleep + α -MN (65:35)	0.9175	2.46	1.5322	1.4469

Table 5.2 Properties of the brines that are used in the Al-Maameri and Buckley (2003) set of experiments.

pH	Ionic Strength (M)	Salts	Notation
4	0.01	NaC ₂ H ₃ O ₂ .3H ₂ O HC ₂ H ₃ O ₂	{4,0.01}
8	1.00	Na ₂ HPO ₄ .7H ₂ O NaH ₂ PO ₄ .H ₂ O	{8,1}

Table 5.3 Tuned parameters of proposed wettability alteration model for the five crude oils that are used in the Al-Maameri and Buckley (2003) set of experiments.

Oil	θ_i	θ_f	a	b
A-93	70	155	0.003	-0.014
Mars-Yellow	56	71	0.004	-0.01
Mars-Pink	53	133	0.002	0
Lagrange-97 + α -MN (70:30)	154	162	0.001	0
Tensleep + α -MN (65:35)	71	165	0.003	-0.006

Table 5.4 Mixture properties and overall composition of the Burke et al. (1990) fluid.

	Pc [psi]	Tc [°R]	Vc [ft ³ /lb-mol]	Molecular Weight	Acentric Factor	Composition
CO ₂	1070.09	547.56	1.5071	44.01	0.225	0.0246
C ₁ -C ₂	668.51	360.61	1.6431	17.417	0.015127	0.4041
C ₃ -C ₅	573.15	732.89	3.8098	53.516	0.179313	0.0755
C ₆ -C ₁₉	291.41	1135.31	13.7197	164.423	0.655007	0.2719
C ₂₀ -C ₃₀	175.41	1419.29	29.033	340.927	1.064023	0.1064
C _{31+A}	143.17	1682.93	56.5486	665.624	1.371778	0.0774
Asphaltene	143.17	1682.93	56.5486	665.624	1.371778	0.0401

Table 5.5 Binary interaction coefficients for the Burke et al. (1990) fluid.

	CO₂	C₁-C₂	C₃-C₅	C₆-C₁₉	C₂₀-C₃₀	C_{31+A}	Asphaltene
CO₂	0						
C₁-C₂	0.0001	0					
C₃-C₅	0.0068	0.0056	0				
C₆-C₁₉	0.0375	0.0347	0.013	0			
C₂₀-C₃₀	0.0651	0.0616	0.0319	0.0045	0		
C_{31+A}	0.0945	0.0905	0.0548	0.0158	0.0035	0	
Asphaltene	0.22	0.22	0.22	0	0	0	0

Table 5.6 Weyburn dead oil composition (Kohse and Nghiem, 2004).

Component	Molecular Wight	Composition
CO ₂	44.010	0.00409
N ₂ +C ₁	17.930	0.00321
C ₂ -C ₃	39.448	1.75432
C ₄ -C ₅	64.552	11.14261
C ₆ -C ₉	124.491	36.27861
C ₁₀ -C ₁₉	217.808	35.16170
C ₂₀ -C ₂₉	364.176	11.54219
C _{30+A}	622.538	2.43375
Asphaltene	622.538	1.67952

Table 5.7 Oil core flood data of Minssieux (1997) experiments.

	GF3	GF1	GV5
Fluid	Weyburn	Weyburn	Weyburn
Core type	Fontainebleau	Fontainebleau	Vosges
Initial permeability, [md]	77.4	107	29
Initial porosity, [%]	13.7	13.1	24.7
Length, [cm]	6	6	6
Diameter, [cm]	2.3	2.3	2.3
Flow rate, [cm ³ /hr]	10	50	10
Back pressure, [kPa]	1000	1000	1000

Table 5.8 Deposition model parameters for oil core flood simulations (Kohse and Nghiem, 2004).

	GF3	GF1	GV5
α , [day ⁻¹]	6.0	0.1	13.0
β , [ft ⁻¹]	0.0	0.0	0.15
$V_{cr,o}$, [ft/day]	0.0	0.0	11.5
γ , [ft ⁻¹]	0.0	0.09	0.0
σ	0.0	150	0.0

Table 5.9 Necessary parameters of the asphaltene model of UTCOMP.

Parameter	Description
P^* , [psi]	Onset point of asphaltene precipitation at any condition
$v_{asph.}$, [lb-mol/ft ³]	Molar volume of asphaltene
k_{cf} , [day ⁻¹]	Forward rate of flocculation
k_{fc} , [day ⁻¹]	Backward rate of flocculation
g	Porosity-permeability correlation exponent
θ_i	Initial contact angle (before deposition)
θ_f	Final contact angle (after deposition)
a and b	Tuning parameters of the wettability alteration model
α , [day ⁻¹]	Adsorption constant
β , [ft ⁻¹]	Entrainment constant
$V_{cr,o}$, [ft/day]	Critical velocity for entrainment
γ , [ft ⁻¹]	Pore-throat plugging constant
σ	Snowball-effect deposition constant

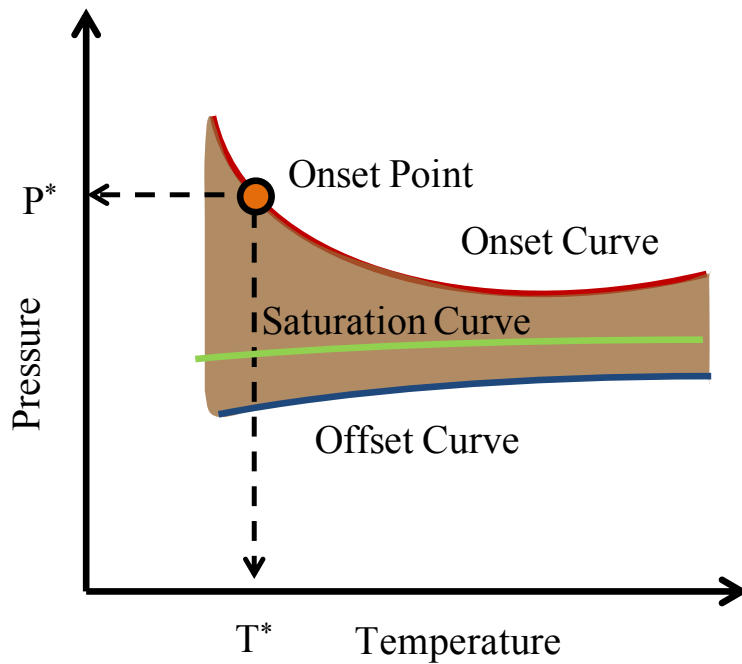


Figure 5.1 Schematic views of the P-T diagram of a fluid and the asphaltene precipitation envelope (APE).

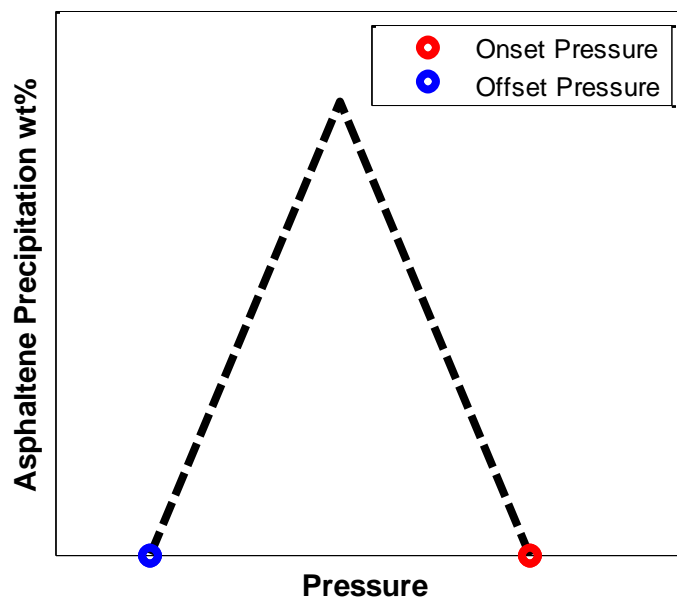


Figure 5.2 Schematic views of asphaltene precipitation curve at a constant temperature.

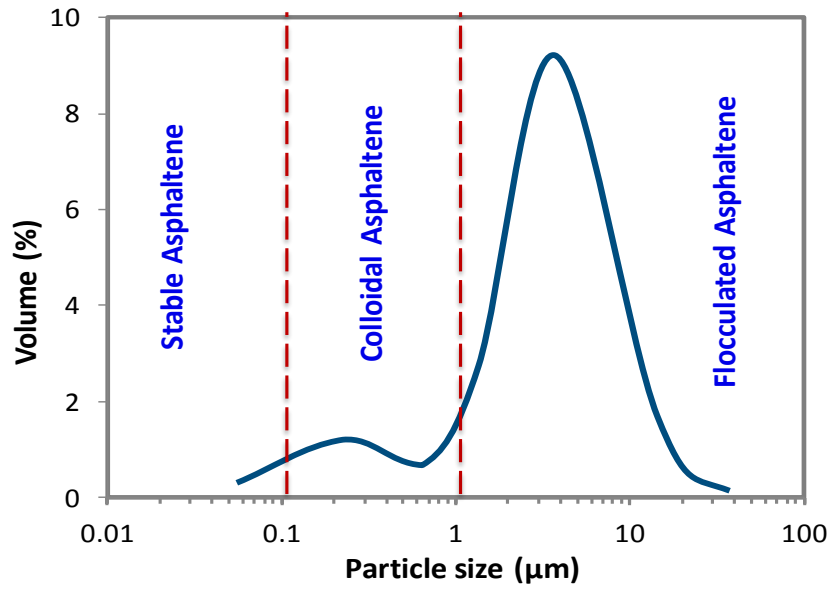


Figure 5.3 Asphaltene particle size distribution, reproduced from Kraiwattanawong et al., 2009.

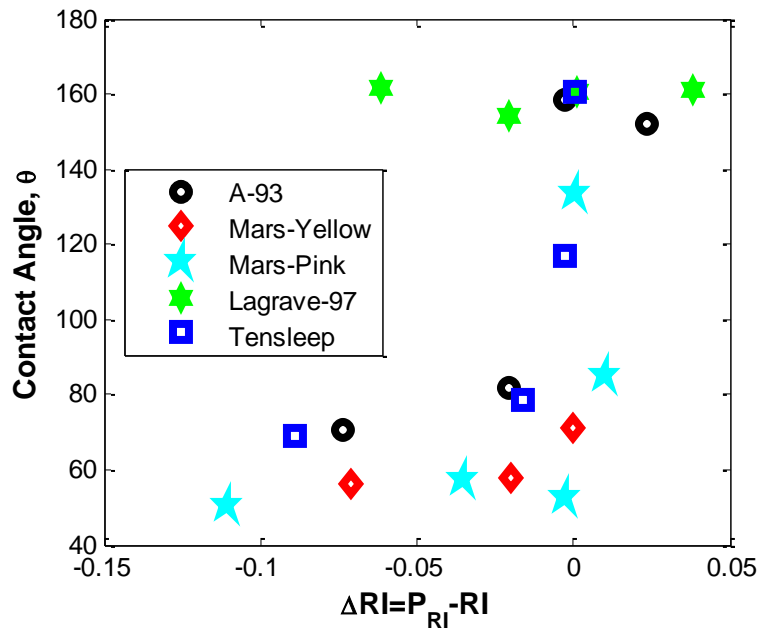


Figure 5.4 Results of the Al-Maamari and Buckley experiments for the five mentioned crude oils in the presence of the unstable brine ($pH = 4$ and $M = 0.01$).

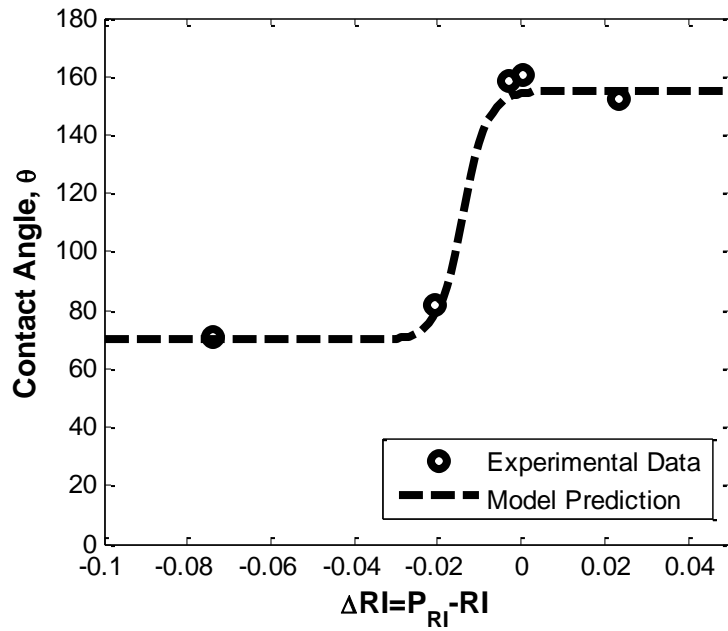


Figure 5.5 Comparison of the proposed wettability alteration model's prediction and the experimental data for the A-93 oil.

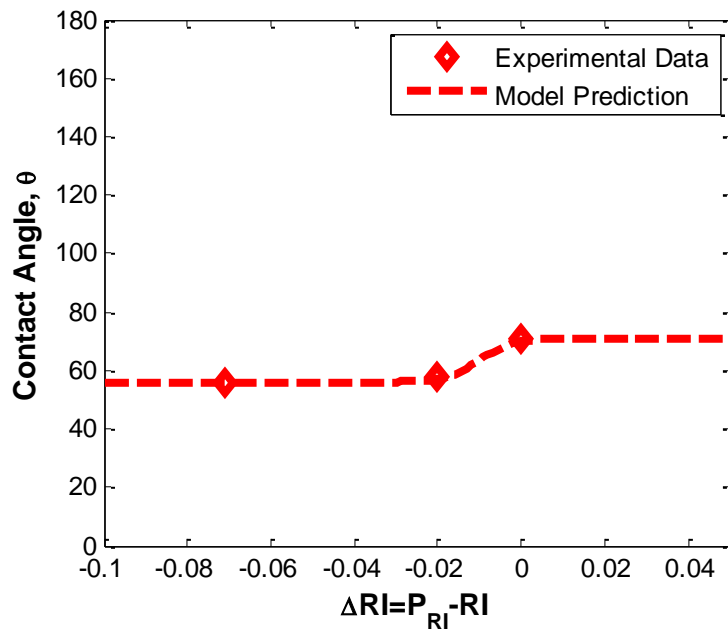


Figure 5.6 Comparison of the proposed wettability alteration model's prediction and the experimental data for the Marse-Yellow oil.

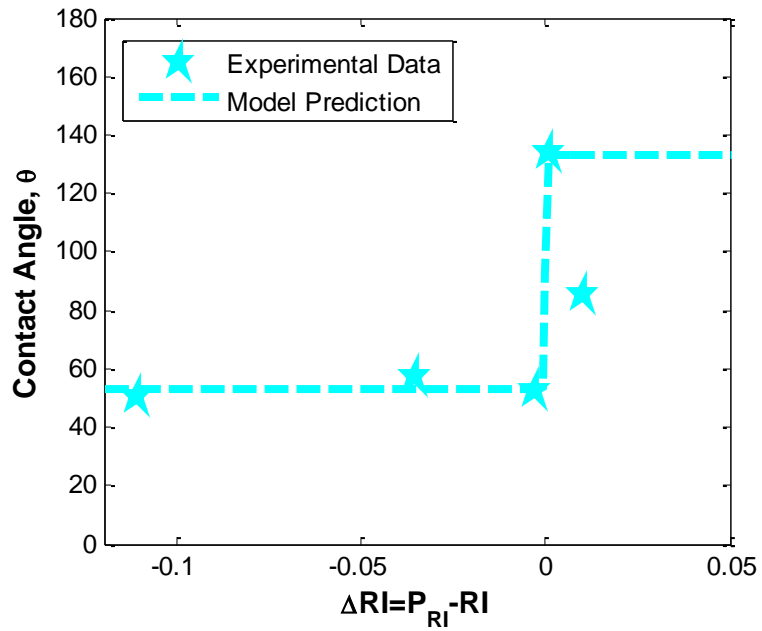


Figure 5.7 Comparison of the proposed wettability alteration model's prediction and the experimental data for the Mars-Pink oil.

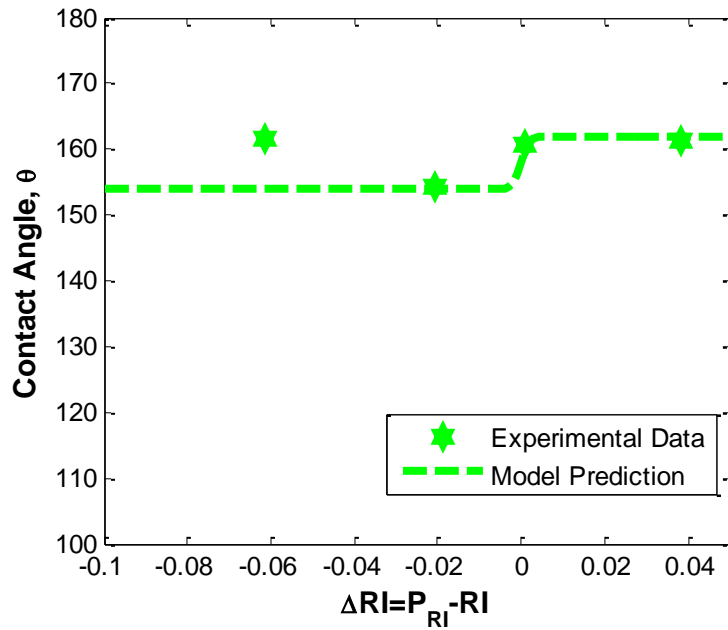


Figure 5.8 Comparison of the proposed wettability alteration model's prediction and the experimental data for the Legrave-97 oil.

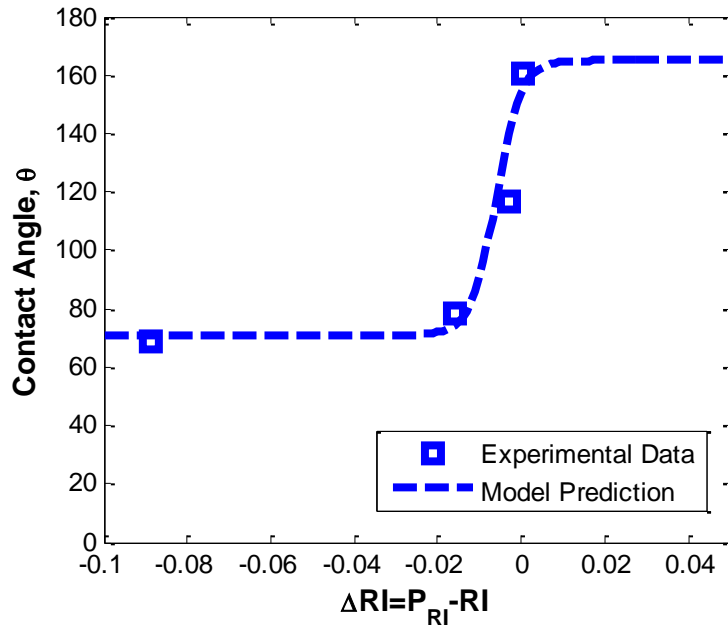


Figure 5.9 Comparison of the proposed wettability alteration model's prediction and the experimental data for the Tensleep oil.

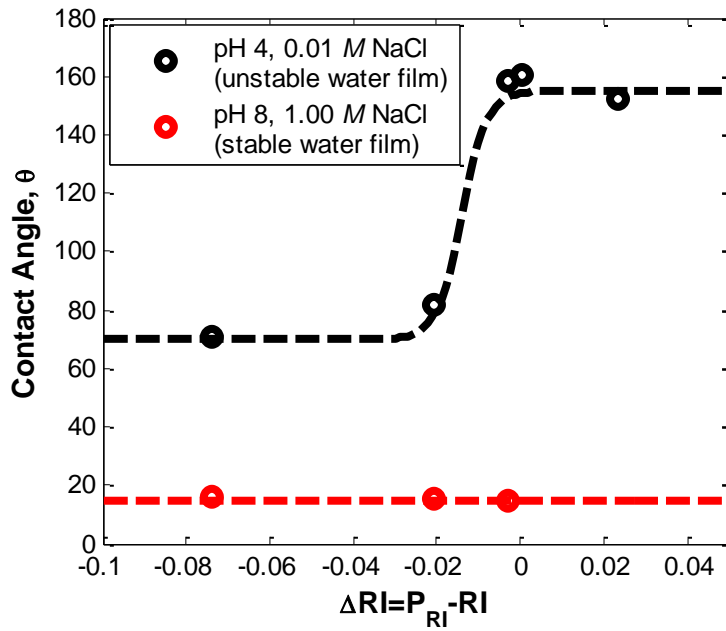


Figure 5.10 Comparison of the results of Al-Maamery and Buckley (2003) experiments for the A-93 oil in the presence of two different brines: (1) unstable brine (pH = 4 and $M = 0.01$), and (2) stable brine (pH = 8 and $M = 1.00$).

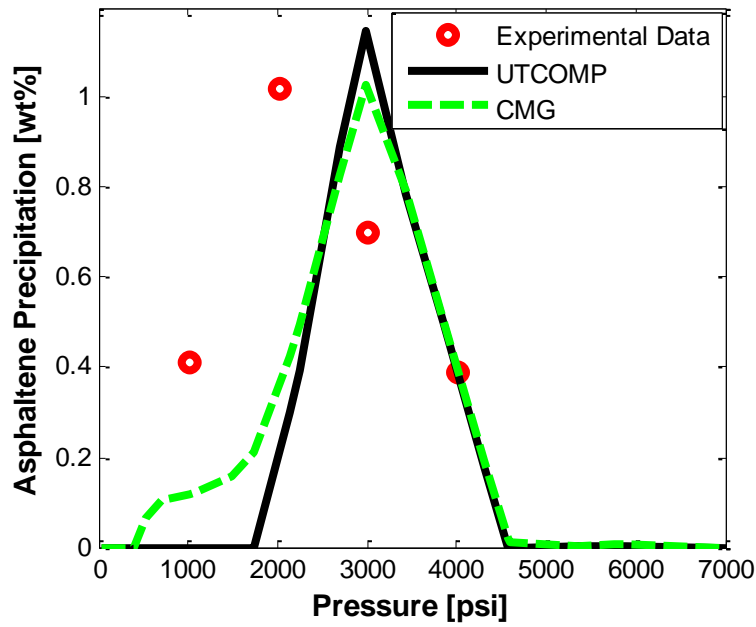


Figure 5.11 Comparison of asphaltene precipitation model of UTCOMP with Burke al. (1990) experimental data and WinProp module of CMG.

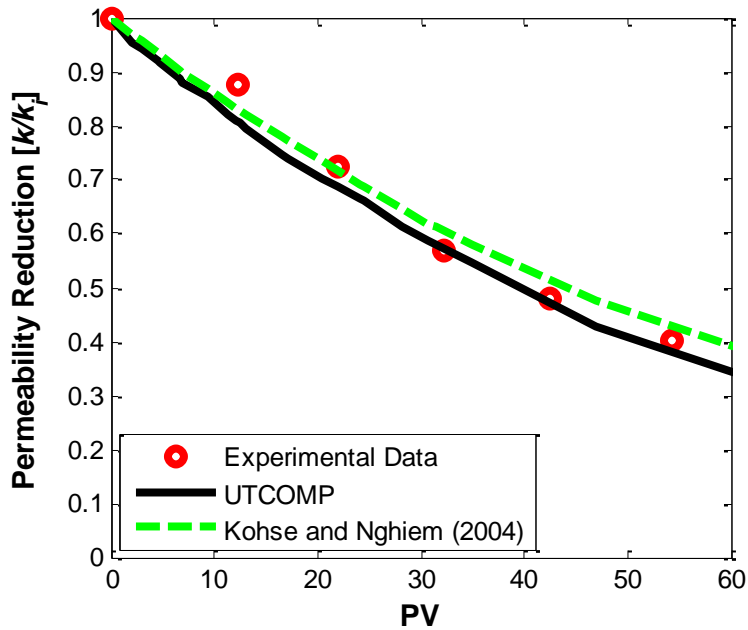


Figure 5.12 Permeability resistance factor for the GF3 sample; comparison between experimental data, UTCOMP, and Kohse and Nghiem (2004).

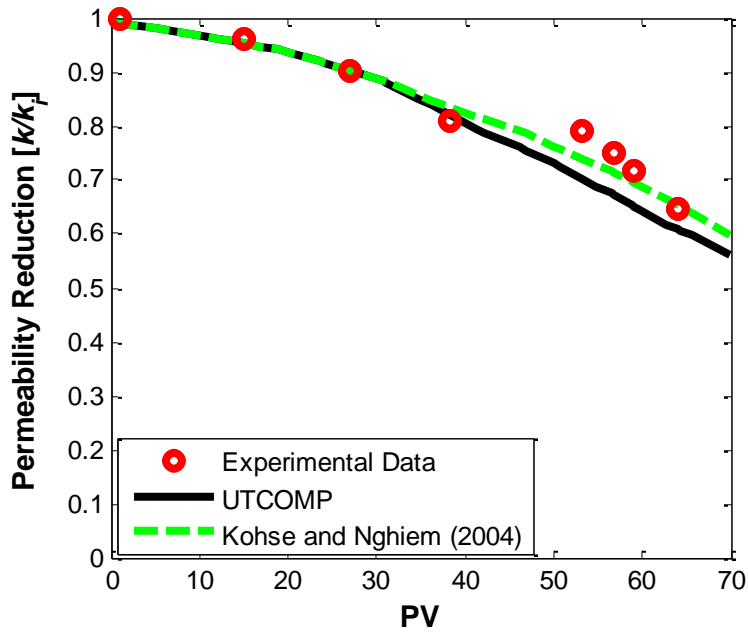


Figure 5.13 Permeability resistance factor for the GF1 sample; comparison between experimental data, UTCOMP, and Kohse and Nghiem (2004).

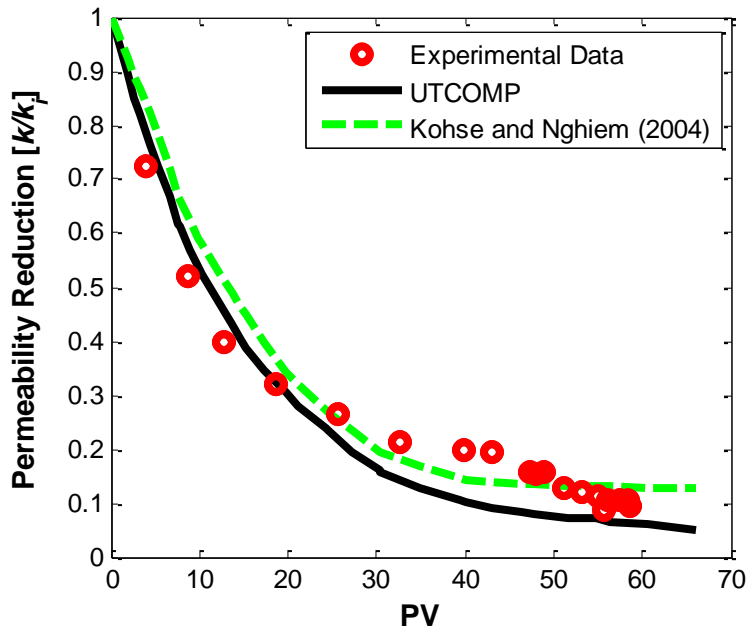


Figure 5.14 Permeability resistance factor for the GV5 sample; comparison between experimental data, UTCOMP, and Kohse and Nghiem (2004).

Chapter 6: Results

In this chapter, we present some case studies using the asphaltene model in UTCOMP. First, the characterization process of a Middle East oil will be discussed. Then, different case studies will be presented to investigate the effects of pressure, temperature, and composition variations, and that of wettability alteration on the dynamics of asphaltene precipitation, flocculation, and deposition.

6.1 FLUID CHARACTERIZATION

Fluid characterization is the first step in preparing any compositional simulation case. In this section, we present a guideline on characterization of an asphaltic fluid for appropriate modeling of asphaltene precipitation. In addition, we present the necessary data for the static modeling of asphaltene precipitation for a Middle East fluid. We use this characterized fluid throughout this chapter for various simulations.

6.1.1 Characterization Procedure

Asphaltic fluid characterization includes tuning of all the parameters of the phase behavior model (see Section 5.1) to reproduce the experimental data. Normally, the experimental data include bubble point pressure, separator test, liberations tests, etc. In the case of asphaltic oils, SARA (Saturate, Aromatic, Resin, and Asphaltene) test usually will be performed to determine the asphaltene content of the fluid. In addition, asphaltene onset pressure at different conditions (pressure, temperature, and composition in the case of gas injection) will be measured. Occasionally, the amount of precipitation at different conditions will also be measured. In this case, the precipitation model should be able to predict the amount of precipitation at different conditions. However, these data are very

expensive and are not usually available. In this section, we provide a guideline for asphaltic fluid characterization for our precipitation model (see Section 5.1) as follows:

- (1) Gather all the experimental data including bubble point pressure, asphaltene onset pressure at different conditions, SARA analysis, etc.
- (2) Split the heaviest component into heavy fractions. The fluid data are usually available up to C_{7+} . However, the average molecular weight of asphaltene is larger than a typical C_{7+} component in a mixture. Usually, a component between C_{30+} to C_{40+} can be a good representation of the asphaltene component.
- (3) Split the heaviest component (e.g. C_{30+}) into two components: a non-precipitating component (C_{30+A}) and a precipitating component (C_{30+B}). The precipitating component is also referred to as asphaltene. The properties of these two components are identical, except for their binary interaction coefficients with the lighter components.
- (4) Select the tuning parameters. Tuning parameters are the ones that we manipulate during characterization to match the results of the phase behavior calculation with the experimental data. In the case of asphaltic oils, the tuning parameters include the numbers of lumping groups (n_L), binary interaction coefficients, volume shift parameters, and molar volume of asphaltene.
- (5) Reduce the number of components with lumping some of the middle components together.
- (6) Perform phase behavior calculation presented in Section 5.1.
- (7) Compare the results of the phase behavior calculation with the experimental data.

- (8) Exit the procedure if the errors between the results of the phase behavior calculation and experimental data are less than the user defined criteria. Otherwise, update the values of tuning parameters (using trial and error or an optimization algorithm) and go to step (5).

6.1.2 Middle East Oil Characterization

Based on the procedure provided in the previous section, we characterized an asphaltic Middle East fluid. Table 6.1 presents the overall composition of the fluid. Table 6.2 summarizes the characterized fluid properties and Table 6.3 presents tuned binary interaction coefficients. At the reservoir temperature (212 °F), the bubble point pressure of the fluid is reported to be 2200 psi and the onset pressure of asphaltene is reported to be 3100 psi. The onset pressure of the asphaltene is an input parameter of the asphaltene phase behavior model. The tuned phase behavior model predicts the value of the bubble point pressure of the mixture to be about 2200 psi, which is in a good agreement with the experimental data. Figure 6.1 shows asphaltene precipitation curve at the reservoir temperature (212 °F) generated using the batch calculation of UTCOMP. As can be observed, the asphaltene onset pressure is 3100 psi, the maximum precipitation is around the bubble point (2200 psi), and the offset point is estimated about 1850 psi. Figure 6.1 shows that asphaltene precipitates between 1850 psi (offset point) and 3100 psi (onset point), if the composition of the fluid and temperature do not change. However, onset pressure, bubble point, and offset pressure change with temperature and composition variations.

Temperature of the reservoir changes during hot/cold fluid injection. As a result, onset pressure, bubble point, and offset pressure change during simulation. Our

asphaltene precipitation model requires onset pressure data at different temperatures to predict the asphaltene precipitation curve. Fortunately, the onset pressure data for the Middle East fluid was reported at 212 °F, 170 °F and 150 °F. We use linear interpolation and extrapolation for the points for which experimental data is not available. Figure 6.2 presents the onset experimental data against the linear interpolation curve of onset pressure at various temperatures. In Figure 6.2, the black and blue dashed lines are the calculated bubble points and offset points at various temperatures using the batch calculation of UTCOMP. Figure 6.3 compares the asphaltene precipitation curves at various temperatures, which are calculated using the batch calculation of UTCOMP. As can be observed in Figures 6.2 and 6.3, bubble point pressure slightly decreases as the temperature decreases. In addition, asphaltene onset pressure increases and asphaltene offset pressure decreases with a decrease in temperature. Therefore, the asphaltene precipitation curve expands from both sides (onset and offset points) due to the temperature drop; as a result, the asphaltene instability range inflates.

Composition variations during miscible gas flooding (e.g. CO₂ injection) affect the onset pressure, bubble point, and offset pressure of the mixture. Figure 6.4 presents the onset experimental data and the linear interpolation curve of onset pressure at various CO₂ concentrations. Black and blue dashed lines are the calculated bubble points and offset points at various CO₂ mole fractions calculated using the batch calculation of UTCOMP. Figure 6.5 presents the asphaltene precipitation curves at various CO₂ concentrations. As can be seen in Figures 6.4 and 6.5, bubble point pressure increases as CO₂ concentration increases. In addition, both asphaltene onset pressure and offset pressure increase with an increase in CO₂ concentration. However, the rate of growth for the onset point is much higher than the offset point. Thus, similar to the temperature

reduction case, the range of asphaltene instability expands as we introduce CO₂ to the fluid.

6.2 EFFECT OF PRESSURE VARIATIONS

In this section, we present three case studies to investigate the effect of pressure variations on asphaltene behavior.

Case 1: Primary Production, Constant Rate Producer. In this case study, we set up a three-dimensional simulation case to investigate the effect of pressure variations on asphaltene precipitation, flocculation, and deposition. We use the Middle East oil presented in Section 6.1.2 as the reservoir fluid. Table 6.4 summarizes the simulation input data and Table 6.5 presents the relative permeability data. The reservoir is homogenous with the size of 600×600×60 ft³. Initial water saturation is 0.2, and the rock porosity and horizontal permeability are 0.1 and 20 md, respectively. Initial temperature of the reservoir is 212 °F and initial pressure is 3100 psi. As shown in Figure 6.1, the onset pressure of asphaltene at temperature of 212 °F is 3100 psi. Therefore, the fluid is initially at its asphaltene onset pressure. There is one production well at the corner of the reservoir, which is a constant oil rate well with the production rate of 200 STBD. The asphaltene flocculation and deposition parameters are set as follows: forward rate of flocculation (k_{cf}) is 12 lb-mol/day, backward rate of flocculation (k_{fc}) is zero, porosity-permeability correlation exponent is 7, adsorption rate (α) is 8 day⁻¹, entrainment rate (β) is zero, and pore throat plugging coefficient is 1 ft⁻¹. We use the Einstein correlation with constant a equal to 2.5 to model oil viscosity reduction due to asphaltene.

Figure 6.6 compares the well-block pressure profiles for two scenarios when asphaltene is ignored and is considered in the simulation. Figure 6.6 shows that asphaltene deposition has a minor effect on well-block pressure, initially. However, the well-block pressure reduces from 1600 psi to 1280 psi after 400 days due to asphaltene deposition. Figures 6.7 (a) through (g) show the pressure, asphaltene precipitation, asphaltene flocculation, asphaltene deposition, porosity, horizontal permeability, and oil viscosity maps after 300 days of simulation. As we move away from the producer, we initially have an increase in the amount of asphaltene precipitation. However, the amount of precipitation decreases after reaching its maximum. Figure 6.7 (d) shows that asphaltene deposits all over the reservoir, and the maximum amount of asphaltene deposition is around the production well. Moreover, the porosity and horizontal rock permeability are reduced in the reservoir due to asphaltene deposition. The maximum decrease is at the producer well-block, where permeability dropped from 20 md to 14 md (30 %) after 300 days. In addition, the porosity is at its minimum value of 0.12 at the well-block. It should be noted that the rock is slightly compressible and that both pressure and asphaltene deposition affect the rock porosity. Figure 6.7 (g) shows that as we move away from the production well, the oil viscosity initially decreases, reaches a minimum, and then increases.

Asphaltene precipitation, flocculation and deposition are dynamic processes that depend on many factors. Since the reservoir temperature and fluid composition are constant in this case study, asphaltene behavior is controlled by pressure variations in the reservoir. As can be observed in Figures 6.7 (a) and 6.7 (b), pressure and asphaltene precipitation maps are in harmony with the asphaltene precipitation envelope (Figure 6.1). Maximum amount of precipitations is around 2200 psi. We have asphaltene precipitation, flocculation and deposition all over the reservoir, because the pressure

response of the production well quickly reaches the boundaries of the reservoir. As a result, pressure falls below the onset pressure of the asphaltene in every grid-block. Furthermore, since the maximum pressure drop always takes place around the production well, the maximum precipitation occurs near the producer as long as the well-block pressure is above 2200 psi (see Figure 6.1). The maximum precipitation around the producer and the dynamics of the flow of precipitated and flocculated asphaltene particles toward the producer are the reasons for the maximum asphaltene deposition around the wellbore. Moreover, oil viscosity is a function of pressure and asphaltene deposition. In the absence of the asphaltene particles, oil viscosity should monotonically decrease toward the producer due to the pressure drop. However, as shown in Figure 6.7 (g), oil viscosity reaches its maximum around the producer due to asphaltene precipitation, flocculation and deposition.

Case 2: Primary Production, Constant Bottom-hole Pressure Producer. In this case study, we set up a three-dimensional case with one constant bottom-hole pressure producer well located at the corner of the reservoir. Table 6.6 summarizes the operating condition of the production well. We initially set the bottom-hole pressure of the producer at 2900 psi. Then, we decrease the bottom-hole pressure 200 psi once every 100 days for five cycles. The other simulation input data and relative permeability curves are the same as case 1 (see Tables 6.1 through 6.5).

Figures 6.8 through 6.12 present the pressure, asphaltene deposition, porosity, and horizontal permeability profiles after 100, 200, 300, 400 and 500 days of simulation (at the end of each cycle), respectively. As can be observed, the maximum amount of asphaltene deposition, and the maximum porosity and permeability reduction occur around the production well. The well-block permeability drops from 20 md to 19.54,

18.47, 16.78, 14.71, and 12.54 md after 100, 200, 300, 400 and 500 days of simulation, correspondingly. Figure 6.13 compares the average reservoir pressure for two scenarios of considering and of neglecting asphaltene modeling in the simulation. Similarly, Figures 6.14 and 6.15 show oil production rate and cumulative oil production curves. As can be observed, the average reservoir pressure, oil production, and cumulative oil production curves for these two scenarios are initially almost the same (in the first and second cycle). However, these curves deviate from each other as time proceeds, and the maximum deviation is at the end of the fifth cycle. Oil production rate and cumulative oil production decrease, and the average reservoir pressure increases due to asphaltene deposition. As shown in Figure 6.14, there is a peak in oil production at the beginning of each cycle due to the sudden decrease in the bottom-hole pressure of the producer. In the absence of asphaltene particles, oil production rates corresponding to each of these peaks are almost the same (between 2100 and 2200 STBD). However, oil production rates at these peaks drastically decrease from one cycle to another cycle due to asphaltene deposition. In Figure 6.15, we observe that the cumulative oil production is reduced by about 4 % after 500 days due to asphaltene deposition. Considering only the fifth cycle, we observe that oil production dropped about 8.6 % in the fifth cycle.

Case 3: Effect of Wettability Alteration during Primary Production. In the case study 2, we assumed that the wettability of the rock does not change due to asphaltene deposition. In that condition, the ultimate recovery of the two scenarios of ignoring and considering asphaltene modeling would be the same, since the residual oil and water saturations do not change. However, as stated in Chapters 2 and 5, the wettability of the rock alters toward oil-wet condition because of asphaltene deposition. In case study 2, the reservoir rock is water-wet with initial contact angle of $\theta_i = 30^\circ$. In this case study, we

consider three different values for the final contact angle due to asphaltene deposition: $\theta_f = 60^\circ$, 90° , and 150° .

Figure 6.16 illustrates the initial and final water/oil relative permeability curves when the initial contact angle (θ_i) is 30° and final contact angle (θ_f) is 60° . The rock is still water-wet. Figures 6.17 through 6.19 compare the average reservoir pressure, oil production, and cumulative oil production profiles for the three scenarios of ignoring asphaltene, considering asphaltene and ignoring wettability, and considering asphaltene with wettability alterations from $\theta_i=30^\circ$ to $\theta_f=60^\circ$, respectively. As can be observed, the oil production rate and cumulative oil production decrease due to wettability alteration, while the average reservoir pressure increases. We observe that the cumulative oil production decreased by about 7.2 % due to combined effects of asphaltene deposition and wettability alteration. In other words, wettability alteration to $\theta_f=60^\circ$ caused additional 3.2 % decrease in the cumulative oil production after 500 days.

Figure 6.20 illustrates the initial and final water/oil relative permeability curves when the wettability of the rock changes to neutral condition ($\theta_f=90^\circ$). Likewise to the previous scenario, Figures 6.21 through 6.23 compare the average reservoir pressure, oil production rate, and cumulative oil production curves for the three scenarios: ignoring asphaltene, considering asphaltene and ignoring wettability alteration, and considering asphaltene with wettability alteration. As can be seen, in this case, the cumulative oil production decreased by about 13.3 % due to combined effects of asphaltene deposition and wettability alteration.

Figure 6.24 presents the initial and final water/oil relative permeability curves when the wettability of the rock changes to oil-wet condition ($\theta_f=150^\circ$). Similarly, Figures 6.25 through 6.28 compare the average reservoir pressure, oil production rate, and cumulative oil production curves for the three scenarios of ignoring asphaltene,

considering asphaltene and ignoring wettability alteration, and considering asphaltene with wettability alteration. In this case, the combined effects of asphaltene deposition and wettability alteration resulted in 33.1 % drop in oil production after 500 days; 29.1% of this drop in oil production is associated with the wettability alteration.

Figure 6.28 summarizes the cumulative oil production curves from all of the scenarios: ignoring asphaltene, considering asphaltene with no wettability alteration, and considering asphaltene with wettability alteration to $\theta_r = 60^\circ$, 90° , and 150° . As can be observed, the wettability alteration of the rock significantly affects the performance of the reservoir in the case of asphaltene deposition. In this case, the increase in residual oil saturation and the decrease in the relative permeability of the oil are the main reasons for the reduction in the oil production.

6.3 EFFECT OF TEMPERATURE VARIATIONS

In this section, we present two case studies to investigate the effect of temperature variations on asphaltene behavior.

Case 4: Secondary Production, Cold Water Injection. In this case study, we set up a three-dimensional case of displacing oil with cold water to investigate the effect of temperature variations on the asphaltene precipitation, flocculation, and deposition. The fluid data, relative permeability curves, and asphaltene model parameters are similar to case 1 (see Tables 6.1 through 6.5). Table 6.6 summarizes other necessary simulation input data. The reservoir is homogenous with the size of $600 \times 600 \times 60$ ft³. Initial water saturation is 0.2, and the rock porosity and horizontal permeability are 0.2 and 20 md, respectively. Initial temperature of the reservoir is 212 °F and initial pressure is 3100 psi.

Cold water is injected into the reservoir at a constant pressure of 4200 psi and temperature of 90 °F. The producer is a constant bottom-hole pressure well set at 3100 psi. To consider the effect of temperature, water viscosity is calculated using the Brill and Beggs correlation and water density is calculated using the Kell correlation. In addition, we consider the heat loss to the underburden and overburden layers. The volumetric heat capacity and thermal conductivity of the reservoir rock are assumed constant: 0.18 (Btu/lb-°R) and 67.2 Btu/(ft-day-°R), respectively. Similarly, the volumetric heat capacity and the thermal conductivity of the cap/base rock are 0.18 (Btu/lb-°R) and 72 Btu/(ft-day-°R).

Figure 6.29 shows (a) pressure, (b) water saturation, (c) temperature, (d) asphaltene deposition, (e) asphaltene concentration, (f) horizontal permeability, (g) water viscosity, and (h) oil viscosity maps after 500 days of simulation. Similarly, Figures 6.30 and 6.31 show the results after 1000 days (around the water breakthrough time) and 1500 days, respectively. As can be observed, pressure of the reservoir is between 4200 psi and 3100 psi, which has a decreasing trend from the injector to the producer. Water saturation is almost 0.9 everywhere before the water front, and decreases rapidly to the initial water saturation (0.1) after the water front near the producer. After 1500 days, there is almost no movable oil left in the reservoir. In addition, we observe that the injection well-block temperature drops from 212 °F to about 160 °F. As we move from the injector to the producer, temperature slightly increases initially. Then, we observe a rapid incline in temperature. Afterward, temperature stabilizes around the initial temperature of the reservoir. In other words, if we draw a line from the injector to the producer, temperature profile at this line is an increasing "S" shape curve. The differences in the temperatures in the area between the temperature front and the producer are very small (less than 5 °F). Moreover, we observe that the temperature front is behind the water front, which is due

to the heat exchange of the cold injecting fluid with the reservoir rock, surroundings, and initial fluid of the reservoir. As can be seen, even after 1500 days (500 days after the water breakthrough), temperature in more than half of the reservoir has remained almost unchanged. Figures 6.29 (d), 6.30 (d), and 6.31 (d) show that asphaltene mainly deposits before the temperature front near the injection well. As a result, the horizontal rock permeability is reduced in this region. The maximum decrease is at the injector well-block, where permeability dropped from 20 md to 18.75 md (a 6 % drop). If we compare the permeability profiles at 500, 1000, and 1500 days, we observe that the injector well-block permeability did not reduce that much over time. In other words, the permeability of a grid-block located before the temperature front reaches a minimum after a short period of asphaltene deposition. As can be seen in Figures 6.29 (e), 6.30 (e) and 6.31 (e), the molar concentration (overall composition) of the asphaltene component significantly decreases due to asphaltene deposition. The molar concentration includes the sum of precipitated asphaltenes, flocculated asphaltenes, and number of moles of the asphaltene component in the oil and gas phases. We observe that the overall composition of the asphaltene component in the injector well-block is reduced from the initial value of 0.02021 to 0.00230, 0.00019, and 0.00002 [moles of asphaltene/moles of hydrocarbons] after 500, 1000, and 1500 days of simulations, correspondingly. Figures 6.29 (f), 6.30 (f), and 6.31 (f) show that the water viscosity increased near the injection well due to the temperature drop. Similarly, the oil viscosity decreased around the injector due to the temperature drop, and asphaltene precipitation, flocculation, and deposition.

Figure 6.32 compares the oil rates for the simulations of the two scenarios: considering and ignoring asphaltene modeling. In addition, Figures 6.33 and 6.34 present water/oil ratio and cumulative oil production curves, respectively. As can be observed, the oil production rate slightly decreases due to asphaltene deposition. However, the

ultimate oil recovery does not change. In addition, asphaltene deposition postpones the water breakthrough from 970 to 1030 days.

As mentioned before, asphaltene precipitation, flocculation and deposition are dynamic processes that depend on many parameters. In the current case study, temperature variations control the behavior of asphaltene during the lifespan of the reservoir. If the temperature of the reservoir were constant, no asphaltene would precipitate in the reservoir, since the reservoir pressure (between 3100 and 4200 psi) is always higher than the asphaltene onset pressure (3100 psi) at initial temperature (212 °F). As shown in Figure 6.2, as the temperature of the reservoir decreases, the asphaltene onset pressure increases, and at some point, the condition (temperature and pressure) in some of the grid-blocks falls inside the asphaltene precipitation envelope. Therefore, there is no asphaltene precipitation after the temperature front near the production well. Since water and oil move slowly in the reservoir, most of the flocculated asphaltenes deposit before the temperature front. In addition, the precipitated asphaltenes dissolve in the oil after they pass the temperature front due to the sudden decrease in the asphaltene onset pressure. The amount of deposition in a grid-block does not increase that much during water injection, since all of the asphaltene particles precipitate from oil in a short period, and deposit on the rock surface. Therefore, the concentration of the asphaltene component significantly decreases (reaches zero), and there will be no more asphaltene particles left in the oil to precipitate. Moreover, asphaltene starts to precipitate from oil, when the oil is already at its residual saturation. Remember that the temperature front is behind the water front. Thus, very little amount of asphaltene is available to precipitate from the oil behind the temperature front. Therefore, the amount of deposition is not high compared to the primary production case. Consequently, the maximum permeability reduction is only 6 % in this case compared to 30 % in the primary production case (case

study 2). Small decrease in permeability and increase in water viscosity around the injection well decrease the injectivity of water. Therefore, water breakthrough time slightly increases and oil production rate slightly decreases.

Case 5: Effect of Wettability Alteration during Secondary Production. In this case study, we look into the effect of wettability alteration due to asphaltene deposition on the performance of the water flood presented in case study 4. We consider three scenarios of changing wettability from initial value of $\theta_i = 30^\circ$ to final values of $\theta_f = 60^\circ$, 90° , and 150° (see Figures 6.16, 6.20, and 6.24).

Figure 6.35 compares the oil production rates of the five scenarios: ignoring asphaltene, considering asphaltene and ignoring wettability alteration, and considering asphaltene with wettability alteration from $\theta_i = 30^\circ$ to $\theta_f = 60^\circ$, 90° , and 150° . In addition, Figures 6.36 and 6.37 show the results for the water/oil ratio and cumulative oil production curves, respectively. As can be observed, as the wettability of the rock changes toward oil-wet condition, the oil production rate increases and the water breakthrough time decreases. However, the ultimate oil recovery does not change. Figure 6.38 shows the water saturation, temperature, water relative permeability, and oil relative permeability maps after 500 days of simulation when the final contact angle is $\theta_f = 60^\circ$. Similarly, Figures 6.39 and 6.40 show the results when the final contact angle is $\theta_f = 90^\circ$ and 150° , correspondingly. We observe that the water relative permeability increases around the injection well as the wettability in this area changes toward oil-wet condition. However, the oil relative permeability is zero everywhere behind the water front.

Due to the increase in the water relative permeability around the injection well, the injectivity of water increases. Thus, the oil production rate increases and the water breakthrough time decreases. Moreover, except for a couple of the grid-blocks around the

injection well, asphaltene starts to deposit on the rock surface when the oil is at its residual saturation. Therefore, when wettability of the rock changes due to asphaltene deposition, oil saturation is at its initial residual saturation. Thus, wettability alteration towards oil-wet condition does not increase the residual oil saturation in this case, and ultimate recovery remains almost constant.

6.4 EFFECT OF COMPOSITION VARIATIONS

In this section, we present three case studies to investigate the effect of composition variations on asphaltene behavior.

Case 6: CO₂ Injection. In this case, we investigate the effect of composition variations on asphaltene precipitation, flocculation, and deposition during CO₂ flooding. The fluid data, relative permeability curves, and asphaltene model parameters are similar to case 1 (see Tables through 6.5). Table 6.8 summarizes other necessary simulation input data. The reservoir is homogenous with the size of 600×600×60 ft³. Initial water saturation is 0.2, and the rock porosity and horizontal permeability are 0.2 and 20 md, respectively. Initial temperature of the reservoir is 212 °F and initial pressure is 3100 psi. CO₂ is injected into the reservoir with a constant pressure of 3300 psi. Moreover, the producer is a constant bottom-hole pressure well set at 3100 psi.

Figure 6.41 shows the results after 100 days of simulation for (a) pressure, (b) CO₂ concentration, (c) asphaltene precipitation, (d) asphaltene flocculation, (e) asphaltene concentration, (f) asphaltene deposition, and (g) horizontal permeability maps. Similarly, Figure 6.42 shows the results after 420 days of simulation, which is around the breakthrough time of CO₂. As can be observed, pressure of the reservoir is between 3300

psi and 3100 psi, which has a decreasing trend from the injector to the producer. In addition, asphaltene precipitation occurs in a small interface region of CO₂ front. Figures 6.41 (e) and 6.42 (e) show the asphaltene concentration map, which is the total moles of asphaltene component including precipitated and flocculated asphaltene particles over the total moles of hydrocarbon in a grid-block. We observe that the asphaltene concentration significantly decreases behind the front near the injection well. The maximum drop occurs at the injection well, where the asphaltene concentration reaches zero. In addition, we observe that asphaltene deposits on the rock surface from the injection well-block to the front. The amount of deposition is low around the injection well, and increasingly higher toward the front. Maximum amount of asphaltene deposition occurs at the front sides closer to the reservoir boundaries. In addition, we observe that the amount of deposition is higher at 420 days compared to 100 days. As can be seen, there is an elliptical zone in the middle of the reservoir close to the producer where asphaltene deposition is very low compared to its surrounding. Moreover, we observe that the permeability reduction in the reservoir is in correspondence to the asphaltene deposition.

In this case study, the temperature of the reservoir is constant (212 °F) and the pressure is always above the onset point of asphaltene (3100 psi) at the reservoir temperature. Therefore, if the composition of the original fluid does not change, we will not have any asphaltene precipitation, flocculation, and deposition in the reservoir. Thus, composition variations control the behavior of asphaltene in the current case study. In the region between the front and the producer, the oil composition is similar to the initial composition, and therefore, asphaltene does not precipitate from the oil. In the small region behind the front, CO₂ dissolves in the fresh oil and increases the asphaltene onset pressure. In the region between the injector and the front, asphaltene concentration is very low because asphaltene particles have been carried away by the moving front. In

addition, in the region behind the front, the offset pressure is very high with respect to the original oil composition and asphaltene will not precipitate any further. The behavior of asphaltene precipitation in the reservoir is in harmony with the asphaltene precipitation envelope and asphaltene precipitation curves at various CO₂ concentrations presented in Figures 6.4 and 6.5, correspondingly. As can be observed, at CO₂ concentration of 0.45, the asphaltene offset pressure is around 3500 psi, which is higher than the reservoir pressure over all of the grid-blocks. Since asphaltene deposition is a time dependent process, the velocity of the front dictates the asphaltene deposition profile in the reservoir. Around the injection well, the amount of deposition is minimum, because of the fast movement of the front. As we move away from the injector, the front velocity decreases and more asphaltene deposits on the rock surface. The maximum amount of deposition is at the front sides near the reservoir boundaries, where the front movement is very low. The low asphaltene deposition in the elliptical region can be explained by the very high front velocity in the middle section of the reservoir.

Figure 6.43 shows the results after 1000 days of simulation for (a) CO₂ concentration, (b) asphaltene concentration, (c) asphaltene deposition, and (d) horizontal permeability maps. We observe that after the breakthrough, asphaltene deposition and permeability reduction mostly occur around the producer and close to the reservoir boundaries. In addition, Asphaltene concentration decreases significantly all over the reservoir, and reaches zero in most of the grid-blocks. In other words, most of the asphaltene component either deposited on the rock surface or was produced through the wellbore.

Figures 6.44 and 6.45 compare the oil production rate and cumulative oil production in the presence and absence of the asphaltene deposition. As can be observed, before the breakthrough of CO₂ (420 days), asphaltene deposition has a minor effect on

the oil production. However, oil production rate decreases after the breakthrough of the CO₂. We observe that oil production drops about 2.6 % after 1000 days of simulation. Figure 6.46 compares the after breakthrough cumulative oil production in the presence and in the absence of the asphaltene deposition. Considering only the after breakthrough period, we have a 6.3 % drop in oil production.

Before the breakthrough of CO₂, the oil located in the middle part of the reservoir is produced, where the asphaltene deposition has a minor effect on the permeability. The maximum permeability reduction before the breakthrough is 12.5 %, which only occurs in a couple of grid-blocks near the boundaries of the reservoir. However, after the breakthrough, the permeability drastically decreases near the boundaries close to the production well. Therefore, the oil production rate decreases.

Case 7: Effect of Wettability Alteration during CO₂ Injection. In this case study, we investigate the effect of wettability alteration due to asphaltene deposition on the performance of the CO₂ flooding presented in case study 6. We consider three scenarios of changing wettability from the initial value of $\theta_i = 30^\circ$ to the final values of $\theta_f = 60^\circ$, 90° and 150° (see Figures 6.16, 6.20, and 6.24).

Figures 6.47 and 6.48 compare the oil production rates and cumulative oil productions of five scenarios: ignoring asphaltene, considering asphaltene and ignoring wettability alteration, and considering asphaltene with wettability alteration from $\theta_i = 30^\circ$ to $\theta_f = 60^\circ$, 90° , and 150° . As can be observed, with wettability of the rock changing toward oil-wet condition, oil production rate decreases. Due to the oil relative permeability reduction, we have 7.6 %, 14.4 %, and 25.9 % drops in oil production after 1000 days for three scenarios of $\theta_f = 60^\circ$, 90° , and 150° , correspondingly. However, wettability alteration has a minor effect on the CO₂ breakthrough time. As mentioned

earlier, asphaltene deposition has a minor effect on the reservoir absolute permeability before the CO₂ breakthrough. In addition, wettability alteration does not affect the gas relative permeability.

Case 8: Effect of Gas Override during CO₂ Injection. In this case study, we investigate the effect of gas override on the behavior of asphaltene in case study 6. The vertical permeability is assumed to be very low (0.01 md) in the case study 6 to ignore the effect of gas override. However, in the current case, the vertical permeability of the reservoir is assumed to be equal to the horizontal permeability of the reservoir (20 md) to allow vertical flow. Other simulation input data are identical to case study 6.

Figure 6.49 compares the oil production rates of the three scenarios of ignoring asphaltene, considering asphaltene and ignoring gas override, and considering asphaltene with gas override. As can be observed, the oil production rate drop occurs earlier (around 350 days) when we have a gas override, which is due to earlier breakthrough of CO₂. However, gas override does not affect the ultimate recovery.

Figures 6.50 and 6.51 show the results after 300 and 1000 days of simulation for (a) CO₂ concentration, (b) top layer permeability, (c) middle layer permeability, and (d) bottom layer permeability maps. We observe that asphaltene deposition has a minor effect on permeability of the top layer of the reservoir. Permeability reduction is only noticeable in a small region near the boundaries of the reservoir. After 1000 days, the lowest permeability in the top layer is around 15 md. However, in the bottom layer, the permeability reduction is noticeable all over the reservoir, except near the injection well. In addition, permeability has a more smooth profile in the bottom layer compared to the top layer. Permeability in the middle section and the boundaries are almost the same.

However, near the production well, amount of permeability reduction is the maximum at the boundaries, where permeability dropped up to 60 %.

The differences between permeability profiles of the top and bottom layers are due to the effect of gas override. The velocity of oil is much higher in the upper layer compared to the lower layer due to the upward flow. Consequently, the front velocity decreases in the bottom layer, and asphaltene particles have more time to deposit on the rock. On the other hand, the front velocity increases in the upper layer, and only part of asphaltene particles have the chance to deposit.

6.5 SUMMARY AND CONCLUSIONS

In this chapter, we provided a guideline on the characterization of an asphaltic fluid. A Middle East oil was characterized and used throughout the case studies of this chapter. Asphaltene precipitation curves of the Middle East oil at different temperatures and CO₂ concentrations were calculated using UTCOMP. Our results showed that asphaltene onset point increases and asphaltene offset point decreases due to the temperature drop. However, CO₂ flooding increases both onset and offset points of asphaltene precipitation.

We presented different case studies to investigate the effect of asphaltene precipitation, flocculation, and deposition on the performance of the reservoir during primary production, water flooding, and CO₂ injection. In the first three case studies, the effect of pressure variations on the behavior of asphaltene was studied. Constant bottom-hole pressure and constant rate production wells were considered. In addition, the effect of wettability alteration due to asphaltene deposition was examined. Our results showed that most of the asphaltene deposition occurred around the production well during

primary production. In the constant rate producer case, the well-block pressure dropped about 20 % after 400 days because of asphaltene deposition. In the constant bottom-hole pressure producer case, the cumulative oil recovery decreased about 4 % after 500 days. The maximum permeability reduction was 30 %, which occurred around the production well. However, our simulations showed that wettability alteration toward oil-wet condition considerably decreased oil production. The cumulative oil production drop was 7.2, 13.3, and 33.1 % when the wettability of the rock changed from $\theta_i = 30^\circ$ to $\theta_f = 60^\circ$, 90° and 150° , correspondingly.

We investigated the effect of temperature variations on asphaltene behavior through the water injection case studies. Initial condition and operating conditions were selected in a way that no asphaltene would precipitate if the temperature of the reservoir were constant. Cold water was injected in the reservoir to initiate asphaltene precipitation. Our results showed that the asphaltene mainly deposited behind the temperature front. The maximum permeability reduction was only 6 % after 1500 days, which occurred around the injection well. The amount of asphaltene deposition was almost homogeneous behind the temperature front, which is due to the very low oil velocity (almost zero velocity). Our results showed that oil production rate slightly decreased due to asphaltene deposition. However, ultimate oil recovery remained constant. In addition, asphaltene deposition postponed the water breakthrough time from 970 days to 1030 days. In case study 5, we investigated the effect of wettability alteration on the performance of the water flood. We showed that the oil production rate increased and the water breakthrough time decreased due to wettability alteration toward oil-wet condition. The reasons are the increase in the water relative permeability around the injection well and the increase in the water injectivity. However, since the asphaltene

starts to deposit on the rock surface and change wettability when oil is almost at its residual saturation, the ultimate recovery remained almost constant.

We investigated the effect of composition variations on asphaltene behavior through the CO₂ flooding case studies. Initial condition and operating conditions were selected in a way that no asphaltene would precipitate if the composition of the oil were the same as the initial composition. Our results showed that asphaltene mainly precipitated in an interface region behind the CO₂ front. The amount of deposition was at its maximum at the front sides near the boundaries. After CO₂ breakthrough, the maximum deposition and permeability reduction were around the production well near the boundaries. The oil production decreased about 2.6 % after 1000 days due to asphaltene deposition. However, asphaltene deposition had a minor effect on the oil production before the breakthrough. In addition, we observed 7.6 %, 14.4 %, and 25.9 % drops in oil production due to wettability alteration to $\theta_f = 60^\circ$, 90° , and 150° , correspondingly. Furthermore, our results showed that CO₂ breakthrough time decreased due to gas override. In the presence of gas override, the amount of deposition decreased in the top layer due to the higher oil velocity (upward flow). However, asphaltene deposition was considerable in the bottom layer. In addition, permeability reduced homogeneously behind the CO₂ front in the bottom layer, except near the injection well.

We summarize the conclusions of this chapter as follows:

1. Asphaltene precipitation, flocculation, and deposition are dynamic processes that depend on many factors such as oil velocity, pressure, temperature, oil composition, etc.
2. Asphaltene precipitation curves at different conditions (temperature and composition) control the static behavior of asphaltene precipitation.

3. Proper dynamic modeling of asphaltene precipitation requires consideration of all pressure, temperature, and composition variations. Each of these factors has a distinct effect on the precipitation; neglecting one of these effects may result in a significant error in the prediction of asphaltene behavior.
4. Asphaltene deposition is a time dependent process that mainly depends on the amount of flocculation in a grid-block and oil velocity.
5. Wettability alteration, if occurs, has a major effect on the performance of the reservoir, compared to the permeability reduction.
6. During primary production, most of asphaltene deposition occurs around the production well.
7. During hot/cold water injection, asphaltene deposits mostly behind the temperature front, if we assume that asphaltene precipitation is only controlled by temperature variations. In this case, almost all the asphaltene particles precipitated from oil, deposit on the rock surface. In addition, wettability alteration toward oil-wet condition has a positive effect on the performance of the water flood in this situation.
8. During CO₂ injection, asphaltene mostly precipitates in a small interface region before the front. Moreover, asphaltene mostly deposits at the front sides near the boundaries, where the front velocity is minimum.
9. Asphaltene deposition has a minor effect on the oil production before the CO₂ breakthrough, if the wettability of the rock does not change.
10. In the presence of gas override, asphaltene mostly deposits in the bottom layer due to the lower velocity of the front in the bottom layer compared to the upper layer.

Table 6.1 Overall composition of the Middle East oil.

Components	Composition	Component	Composition
N ₂	0.005	C ₅	0.034
CO ₂	0.051	C ₆ - C ₇	0.116
H ₂ S	0.017	C ₈ - C ₁₁	0.094
C ₁	0.281	C ₁₂ - C ₃₅	0.167
C ₂	0.096	C _{36+A}	0.004
C ₃	0.068	Asphaltene	0.020
C ₄	0.044		

Table 6.2 Properties of the Middle East oil.

	P _c [psi]	T _c [°F]	V _c [ft ³]	Molecular Weight	Acentric Factor	Parachor	Volume Shift
N ₂	492.3143	227.16	1.433654	28.013	0.04	41	0
CO ₂	1069.865	547.56	1.505737	44.01	0.225	78	0
H ₂ S	1296.183	671.76	1.577821	34.08	0.1	80.1	0
C ₁	667.1961	343.08	1.58583	16.043	0.008	77	0
C ₂	708.3448	549.72	2.370736	30.07	0.098	108	0
C ₃	615.7603	665.64	3.251752	44.097	0.152	150.3	0
C ₄	546.4167	758.819	4.11129	58.124	0.18946	188.1508	0
C ₅	489.9309	839.3414	4.881039	72.151	0.242439	229.1813	0
C ₆ - C ₇	382.5528	992.8737	7.236641	105.7747	0.366792	328.0892	0.024091
C ₈ - C ₁₁	328.3834	1089.267	8.966265	132.6863	0.444136	397.9012	0.070258
C ₁₂ - C ₃₅	128.6837	1532.574	24.51612	388.0596	1.071234	902.2087	0.29465
C _{36+A}	106.2811	1846.35	31.12391	645.624	1.335481	1156.9	0.283504
Asphaltene	106.2811	1846.35	31.12391	645.624	1.335481	1156.9	0.283504

Table 6.3 Binary interaction coefficients for the Middle East oil.

Asph	C _{36+A}	C ₁₂ - C ₃₅	C ₈ - C ₁₁	C ₆ - C ₇	C ₅	C ₄	C ₃	C ₂	C ₁	H ₂ S	CO ₂	N ₂
0.120	0.120	0.120	0.105	0.100	0.095	0.095	0.091	0.042	0.031	0.176	-0.020	0.000
0.150	0.150	0.150	0.121	0.118	0.125	0.130	0.135	0.130	0.103	0.096	0.000	CO ₂
0.000	0.000	0.000	0.017	0.040	0.060	0.060	0.070	0.070	0.080	0.000		H ₂ S
0.099	0.132	0.113	0.048	0.037	0.021	0.015	0.009	0.003	0.000			C ₁
0.235	0.102	0.085	0.029	0.021	0.009	0.005	0.002	0.000				C ₂
0.188	0.080	0.064	0.017	0.011	0.003	0.001	0.000					C ₃
0.083	0.065	0.051	0.010	0.006	0.000	0.000						C ₄
0.055	0.055	0.042	0.006	0.003	0.000							C ₅
0.035	0.035	0.025	0.001	0.000								C ₆ -C ₇
0.026	0.026	0.017	0.000									C ₈ -C ₁₁
0.001	0.001	0.000										C ₁₂ -C ₃₅
0.000	0.000											C _{36+A}
0.000												Asph

Table 6.4 Reservoir properties and the simulation input data for case 1.

Parameters	Value
Number of grid-blocks (x,y,z)	30×30×3
Grid-block size	20 ×20×20 ft ³
Initial reservoir pressure	3100 psi
Reservoir temperature	212 °F
Producer oil rate	200 STB/D
Water density	62.4 lb/ft ³
Initial water saturation	0.2
Porosity	0.1
Vertical permeability	0.01 md
Horizontal permeability	20 md
k_{cf}	12 lb-mol/day
k_{fc}	0 lb-mol/day
g	7
a	2.5
α	8 day ⁻¹
β	0 ft ⁻¹
γ	1 ft ⁻¹

Table 6.5 Relative permeability data for case 1.

	Water	Oil	Gas
Residual saturation	0.2	0.1	0.0
End point	0.4	0.9	1.0
Exponent	3.0	2.0	2.0

Table 6.6 Operating conditions of the production well for case 2.

Period	Bottom-hole Pressure
Start of simulation – 100 days	2900
100 days – 200 days	2700
200 days – 300 days	2500
300 days – 400 days	2300
400 days – 500 days	2100

Table 6.7 Reservoir properties and the simulation input data for case 4.

Parameters	Value
Number of grid-blocks (x,y,z)	30×30×3
Grid-block size	20 ×20×20 ft ³
Injection temperature	90 °F
Reservoir temperature	212 °F
Initial water saturation	0.2
Initial reservoir pressure	3100 psi
Bottom-hole injector pressure	4200 psi
Bottom-hole producer pressure	3100 psi
Reservoir rock thermal conductivity	67.2 Btu/(ft-day-°R)
Reservoir rock density	171.36 lb/ft ³
Reservoir rock heat capacity	0.18 Btu/(lb -°R)
Porosity	0.1
Vertical permeability	0.01 md
Horizontal permeability	20 md

Table 6.8 Reservoir properties and the simulation input data for case 6.

Parameters	Value
Number of grid-blocks (x,y,z)	30×30×3
Grid-block size	20 ×20×20 ft ³
Reservoir temperature	212 °F
Initial water saturation	0.2
Initial reservoir pressure	3100 psi
Bottom-hole injector pressure	3300 psi
Bottom-hole producer pressure	3100 psi
Porosity	0.1
Vertical permeability	0.01 md
Horizontal permeability	20 md

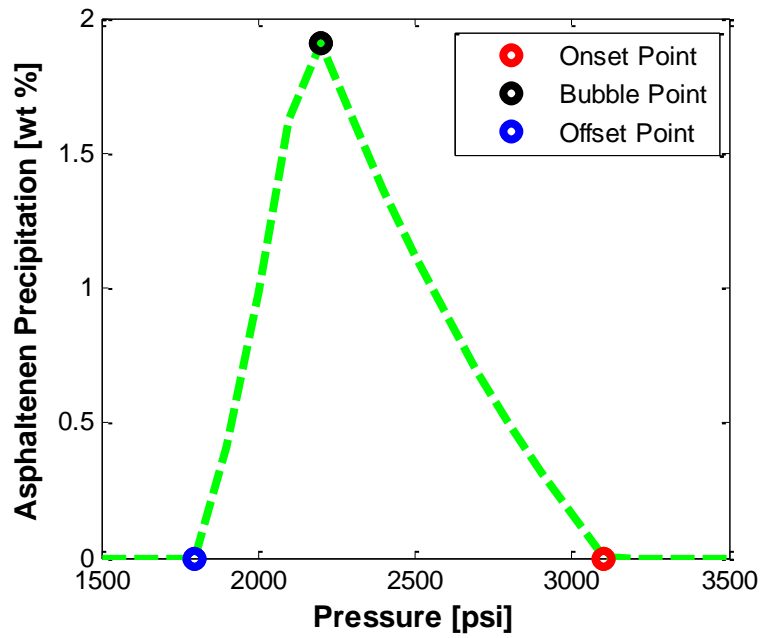


Figure 6.1 Asphaltene precipitation curve at reservoir temperature (212 °F) for the Middle East oil, generated by batch calculation of UTCOMP.

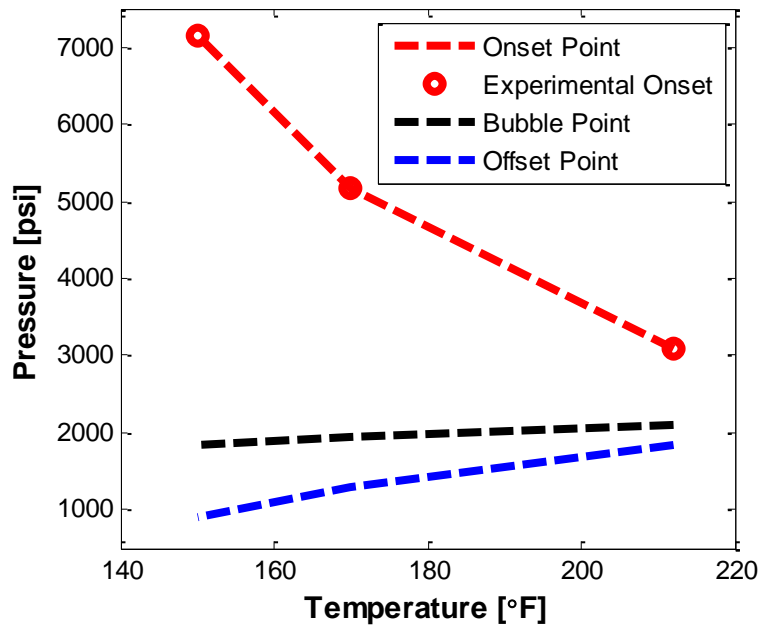


Figure 6.2 Experimental onset points, and calculated bubble points and offset points at different temperatures.

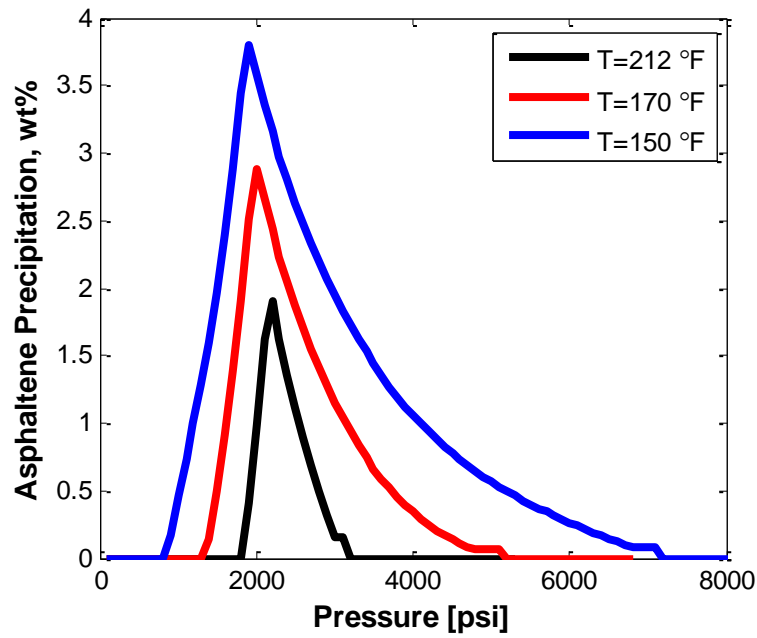


Figure 6.3 Comparison of asphaltene precipitation curves at various temperatures that are calculated using the batch calculation of UTCOMP.

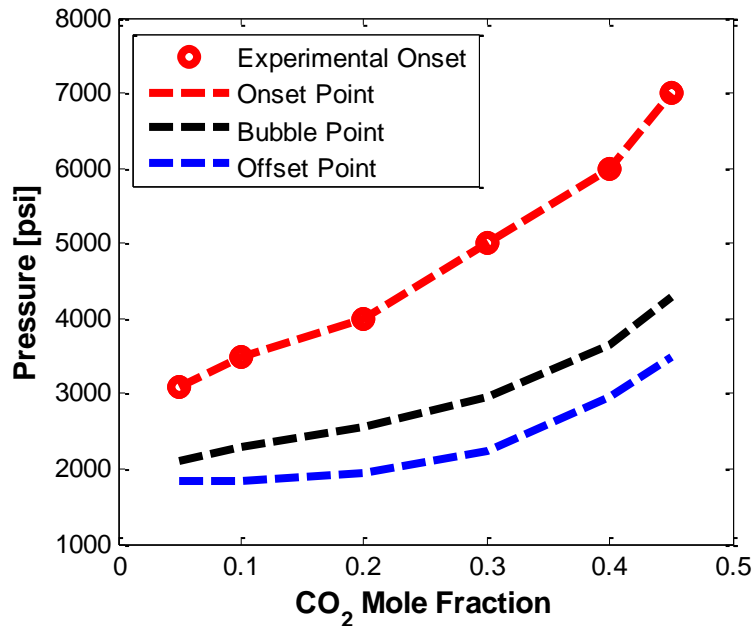


Figure 6.4 Experimental onset points, and calculated bubble points and offset points at different CO₂ mole fractions.

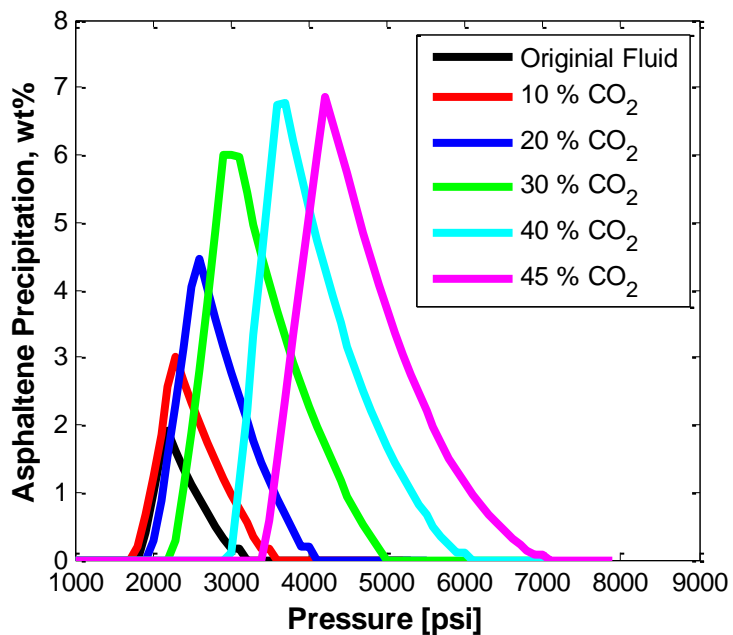


Figure 6.5 Comparison of asphaltene precipitation curves at various CO₂ concentrations that are calculated using the batch calculation of UTCOMP.

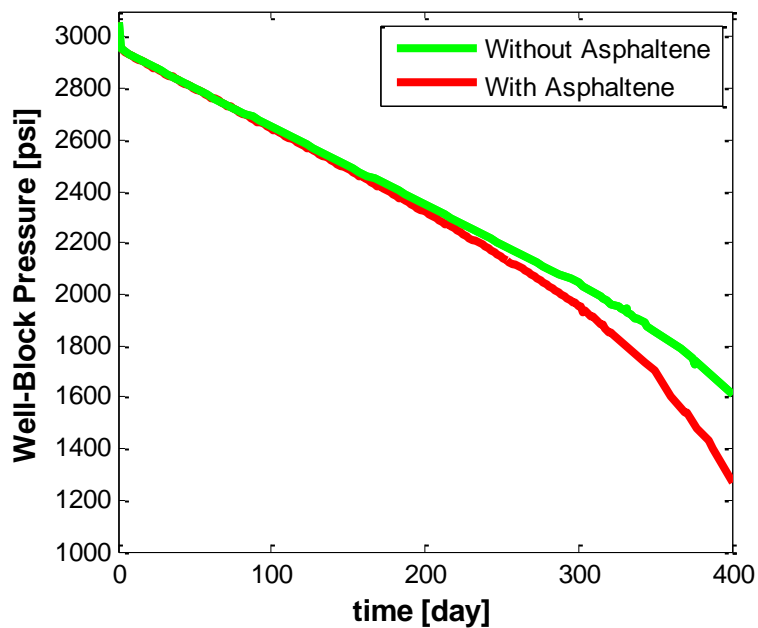
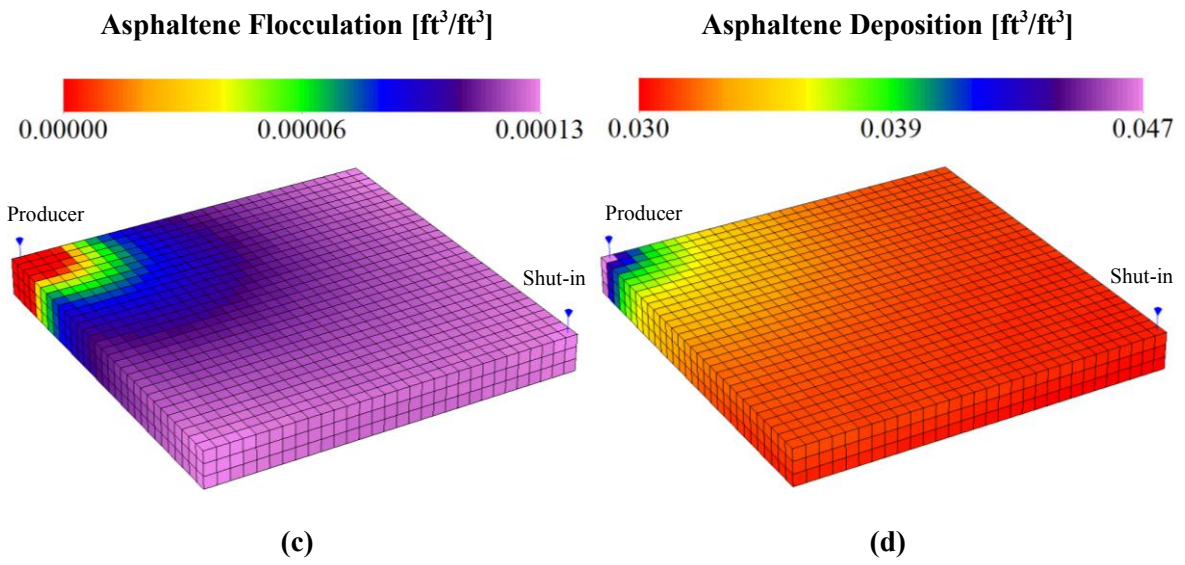
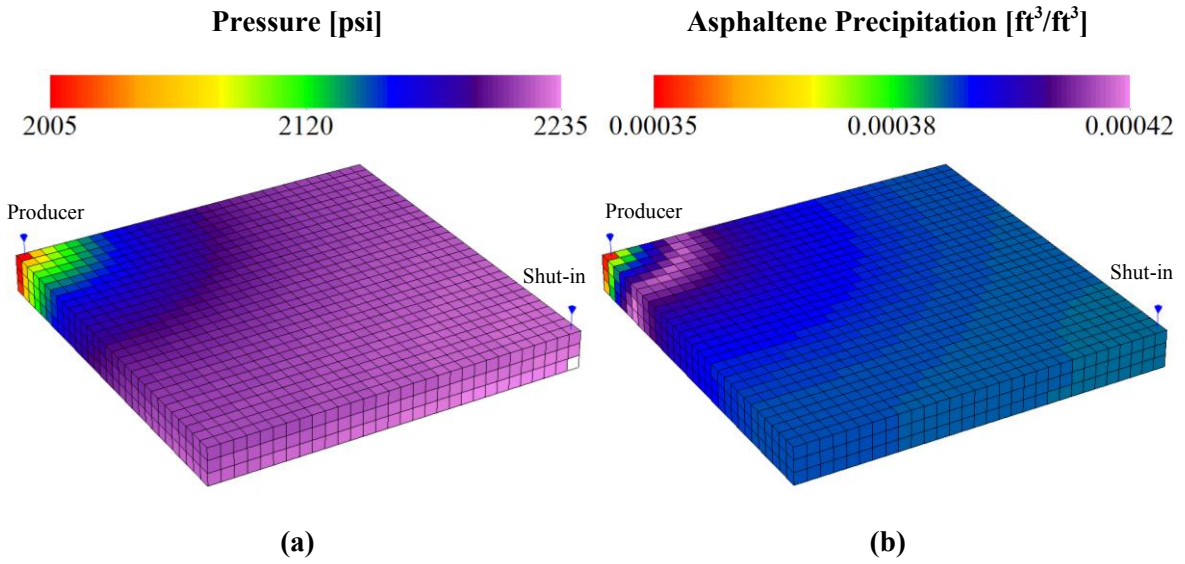


Figure 6.6 Well-block pressures for simulations of two cases of considering and ignoring asphaltene modeling.



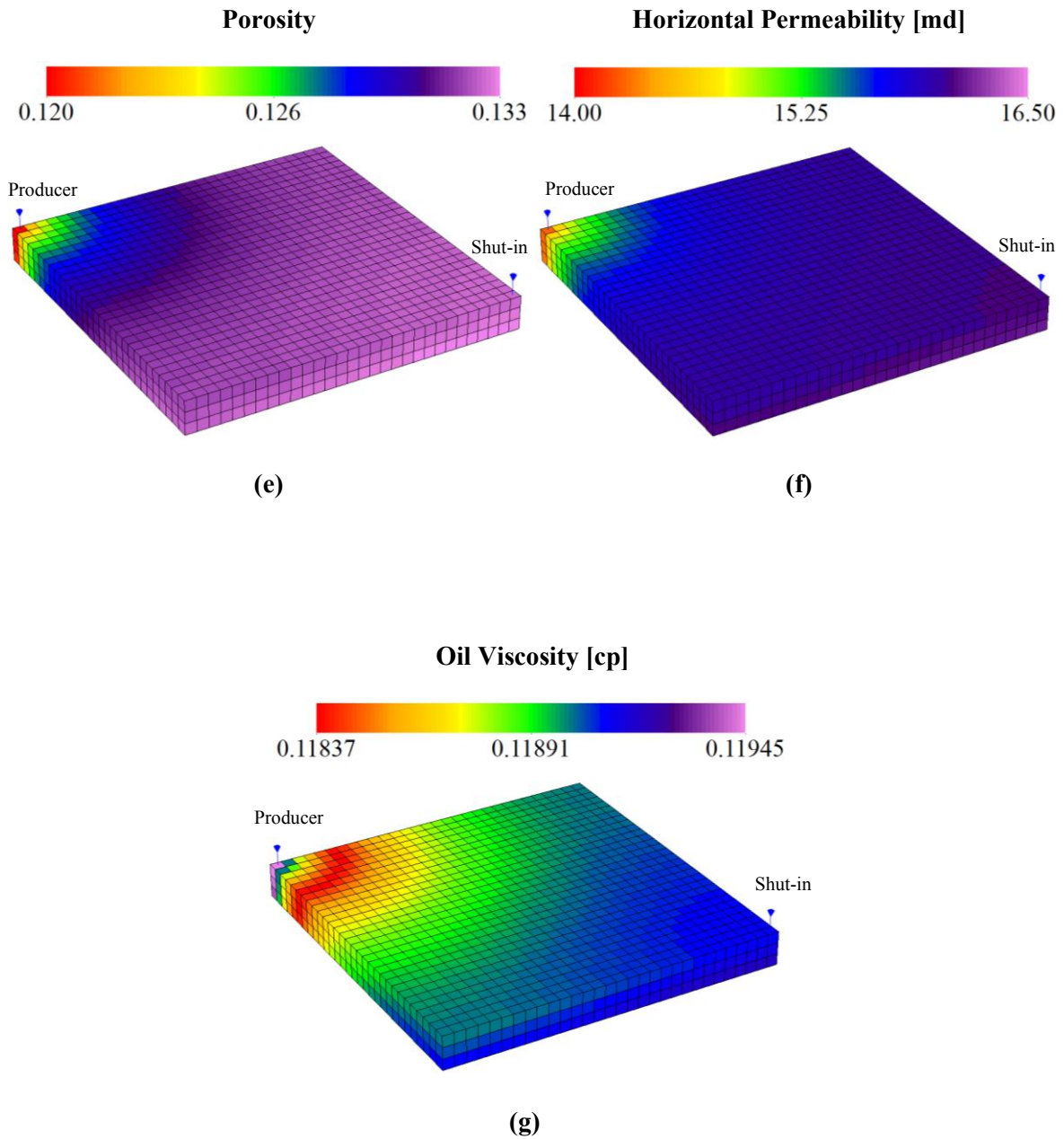


Figure 6.7 Results after 300 days of simulation for case 1: (a) pressure, (b) asphaltene precipitation, (c) asphaltene flocculation, (d) asphaltene deposition, (e) porosity, (f) horizontal permeability, and (g) oil viscosity profiles.

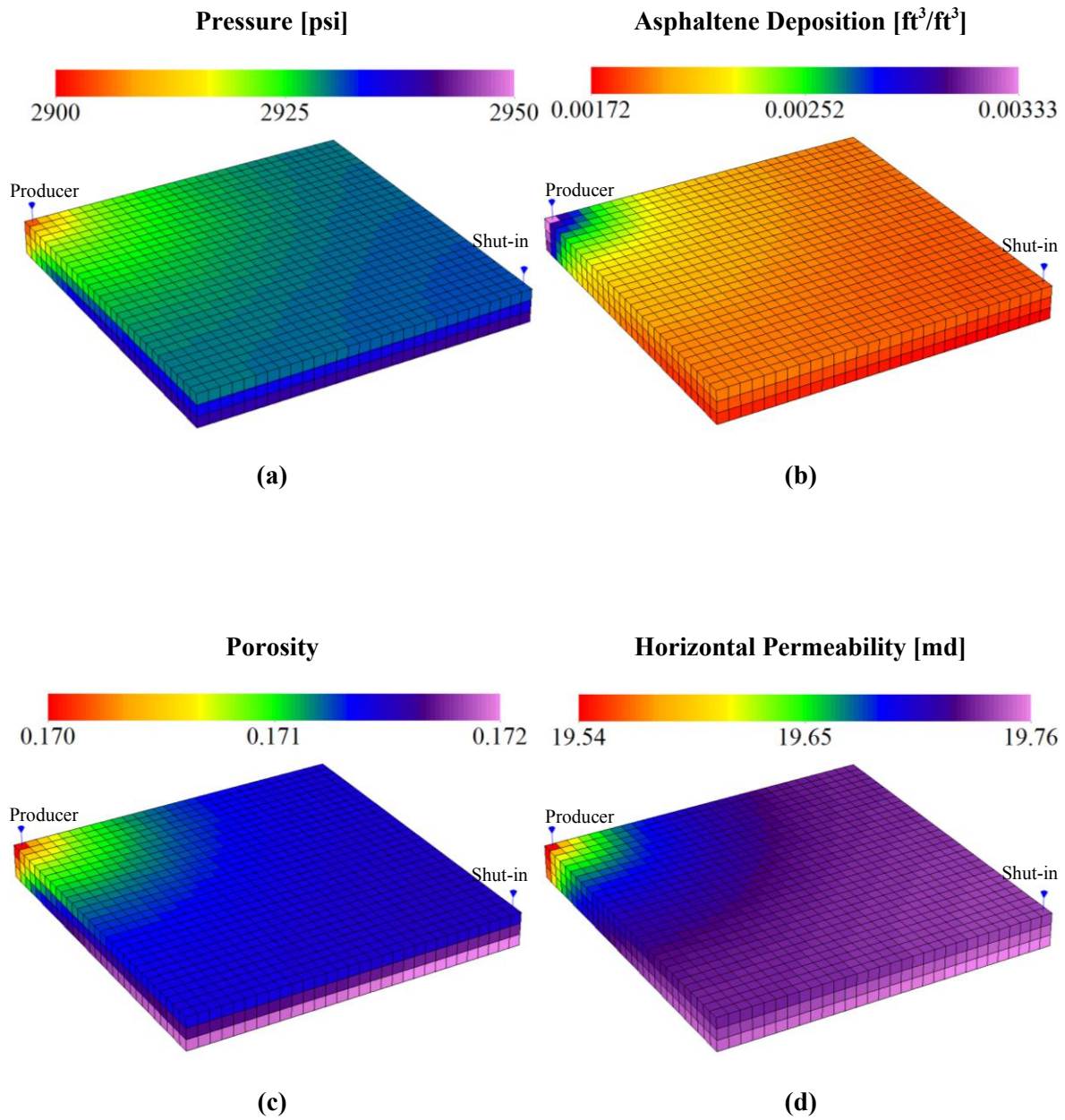


Figure 6.8 Results after 100 days of simulation for case 2: (a) pressure, (b) asphaltene deposition, (c) porosity, and (d) horizontal permeability profiles.

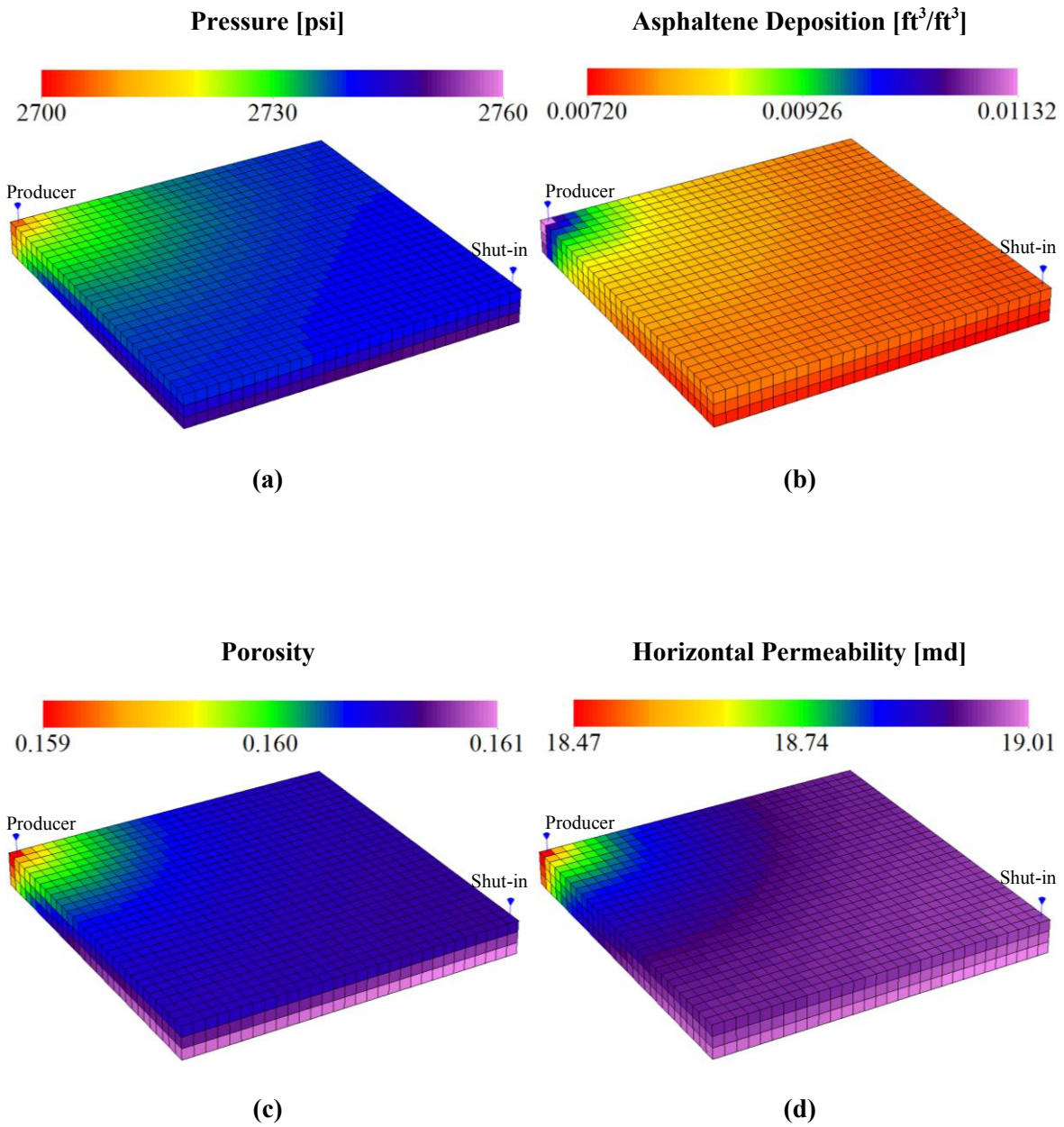


Figure 6.9 Results after 200 days of simulation for case 2: (a) pressure, (b) asphaltene deposition, (c) porosity, and (d) horizontal permeability profiles.

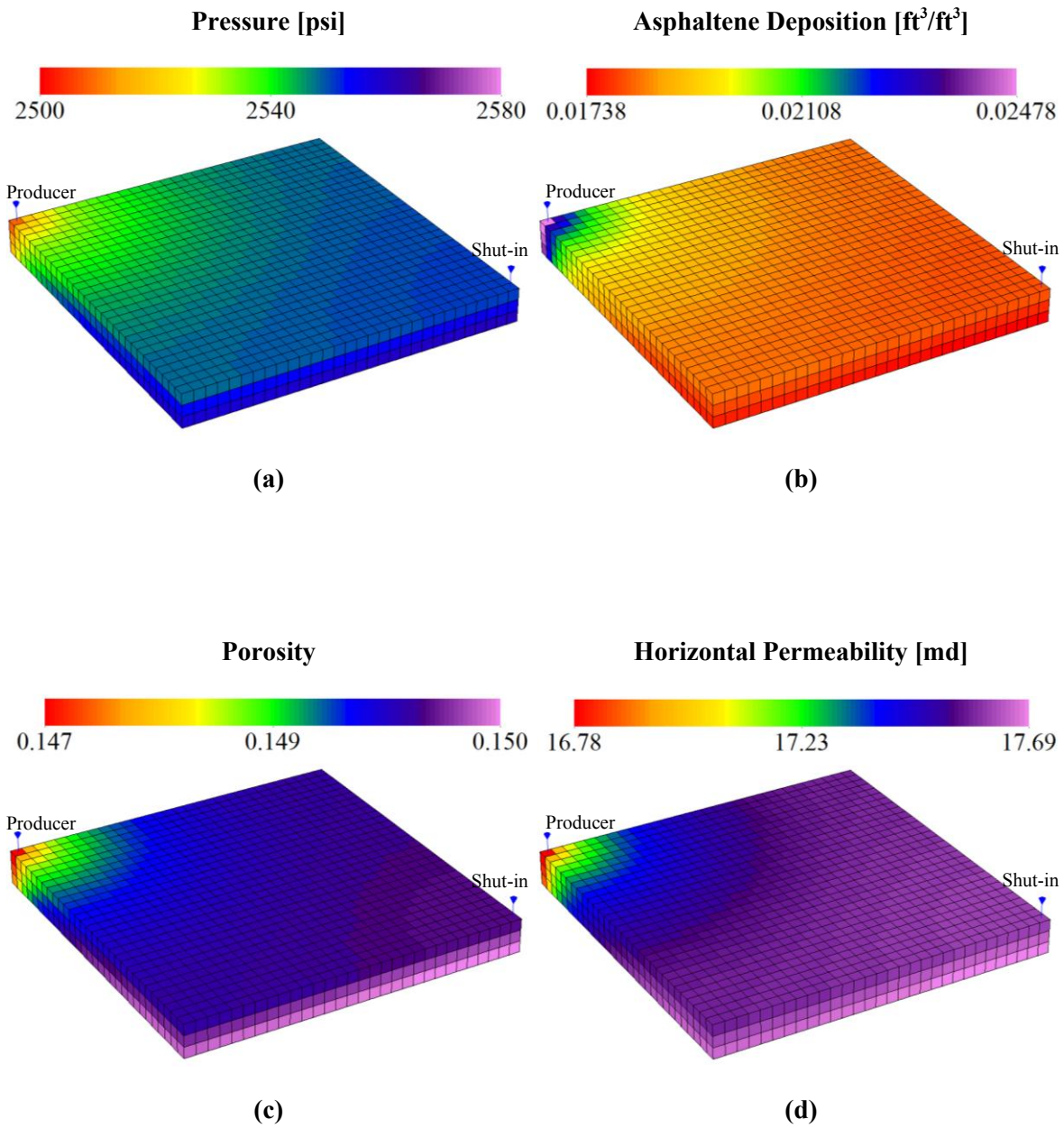


Figure 6.10 Results after 300 days of simulation for case 2: (a) pressure, (b) asphaltene deposition, (c) porosity, and (d) horizontal permeability profiles.

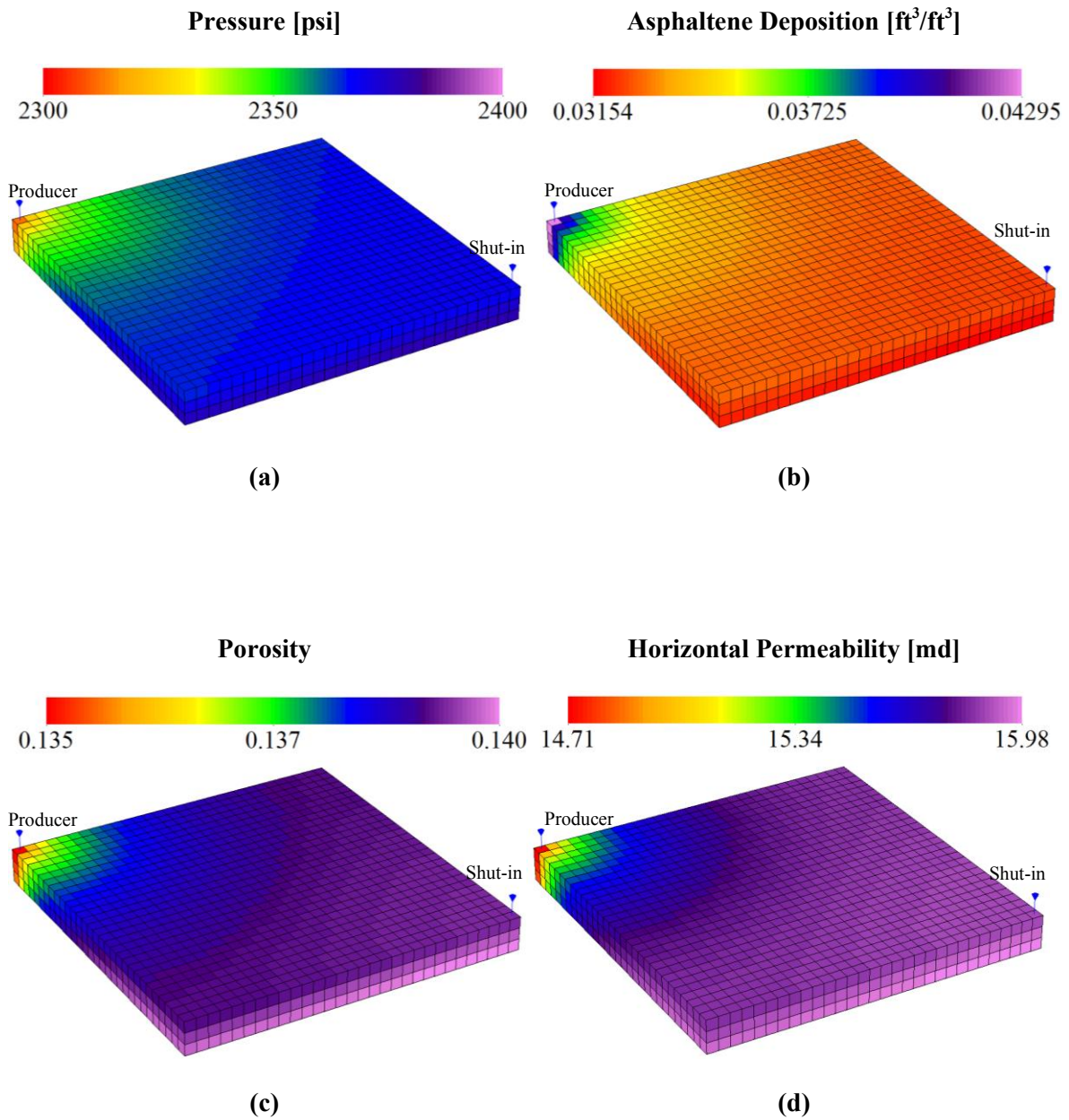


Figure 6.11 Results after 400 days of simulation for case 2: (a) pressure, (b) asphaltene deposition, (c) porosity, and (d) horizontal permeability profiles.

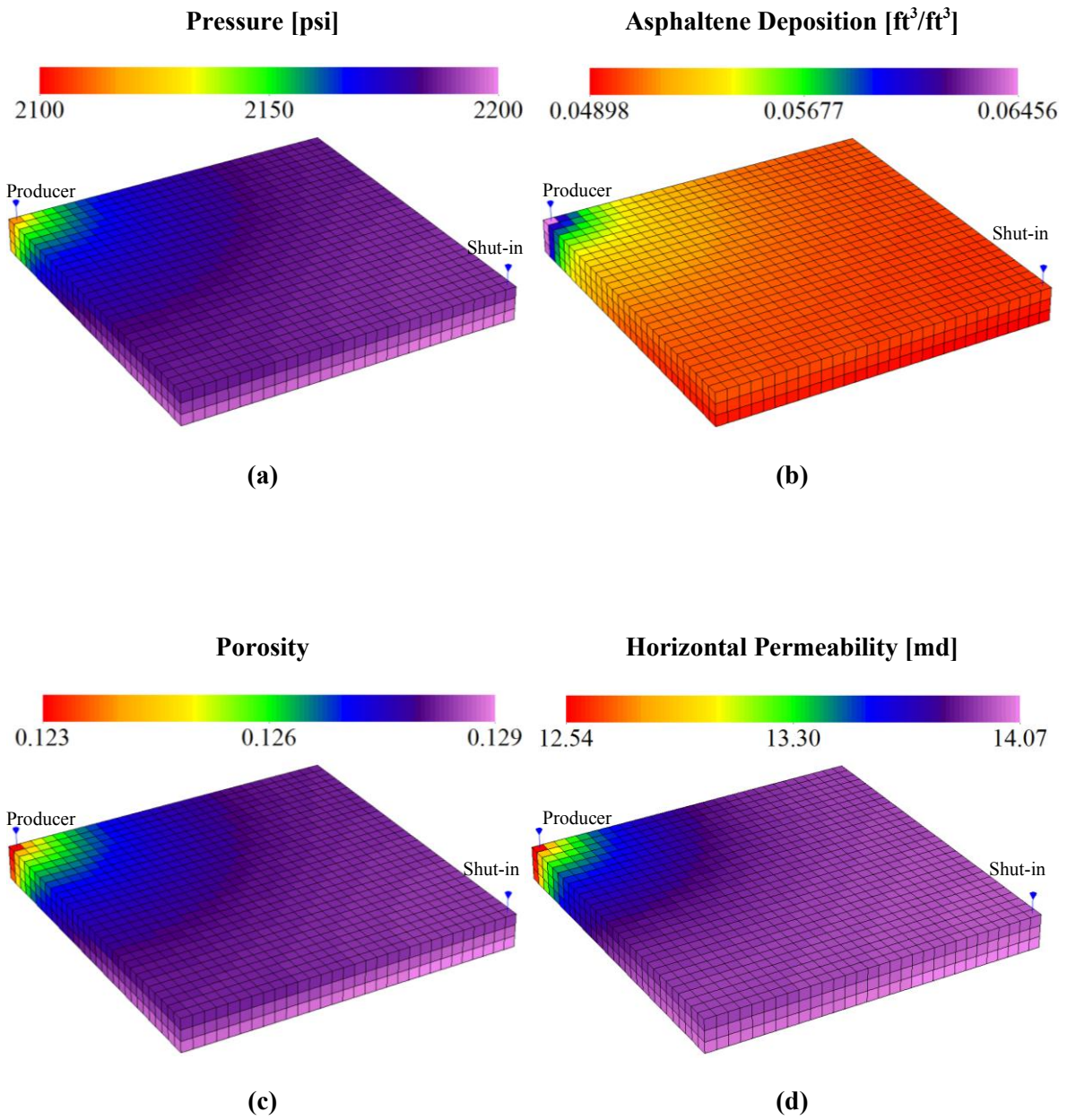


Figure 6.12 Results after 500 days of simulation for case 2: (a) pressure, (b) asphaltene deposition, (c) porosity, and (d) horizontal permeability profiles.

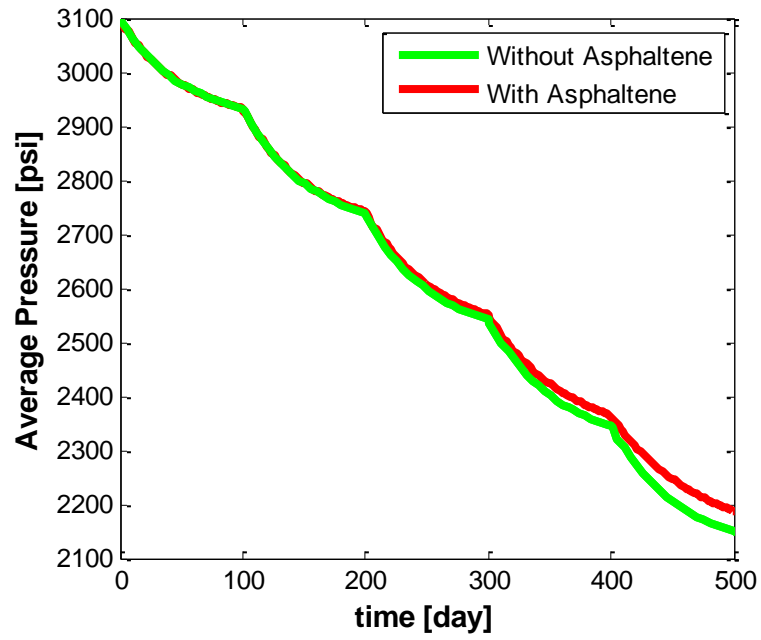


Figure 6.13 Average reservoir pressures for simulations of two cases of considering and ignoring asphaltene modeling; case 2.

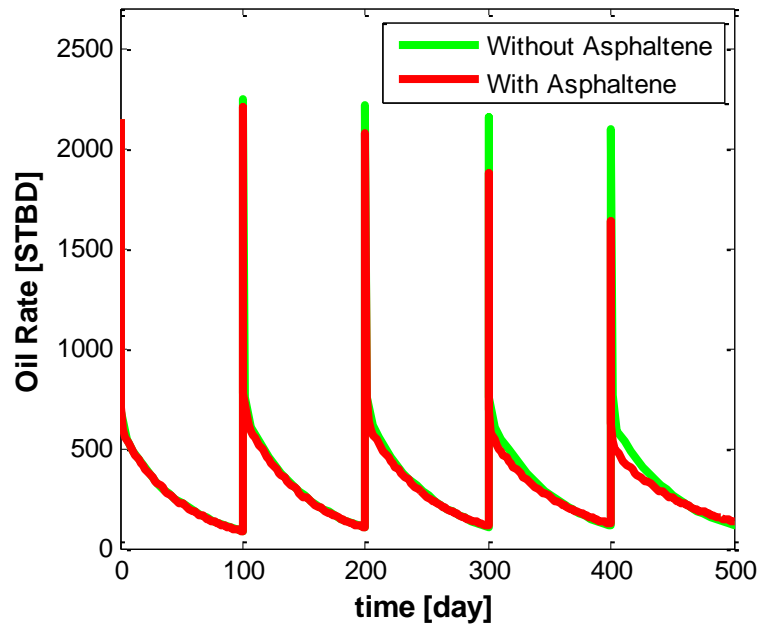


Figure 6.14 Oil rates for simulations of two cases of considering and ignoring asphaltene modeling; case 2.

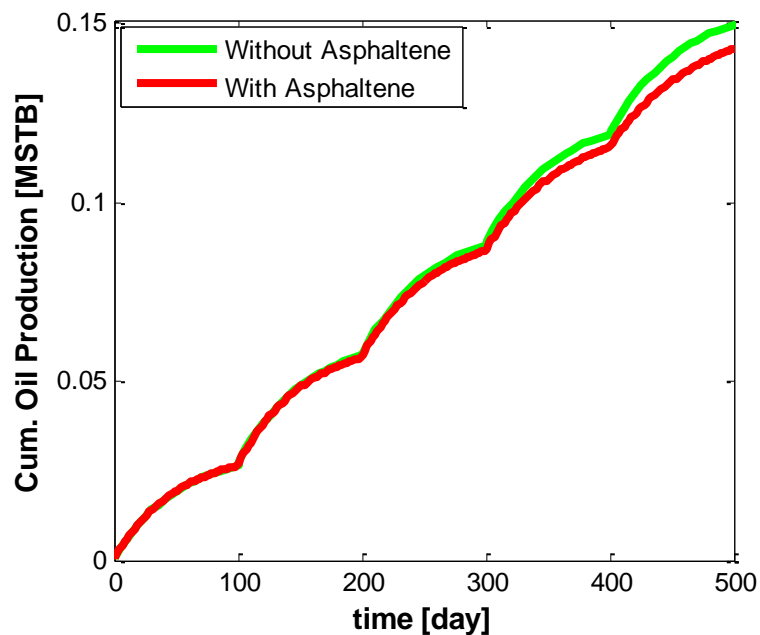


Figure 6.15 Cumulative oil productions for simulations of two cases of considering and ignoring asphaltene modeling; case 2.

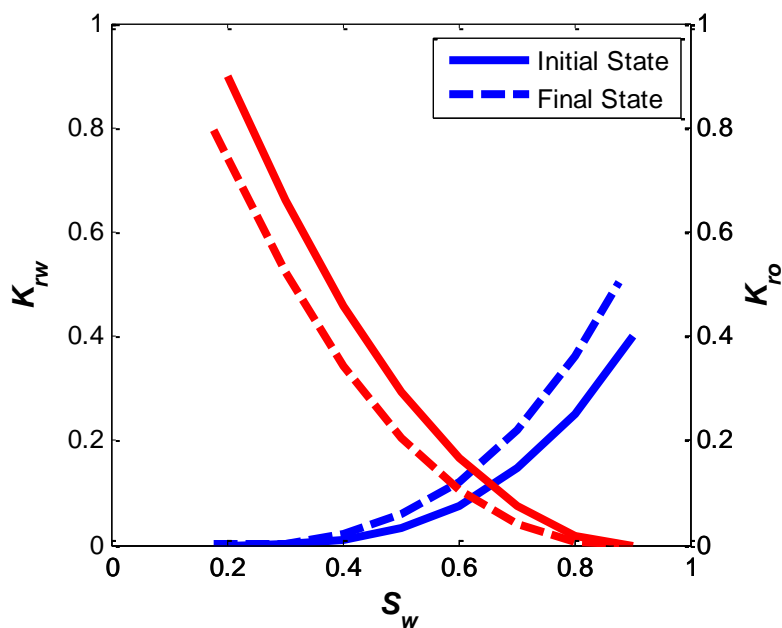


Figure 6.16 Initial and final water/oil relative permeability curves for case 3; initial contact angle is (θ_i) is 30° and final contact angle (θ_f) is 60° .

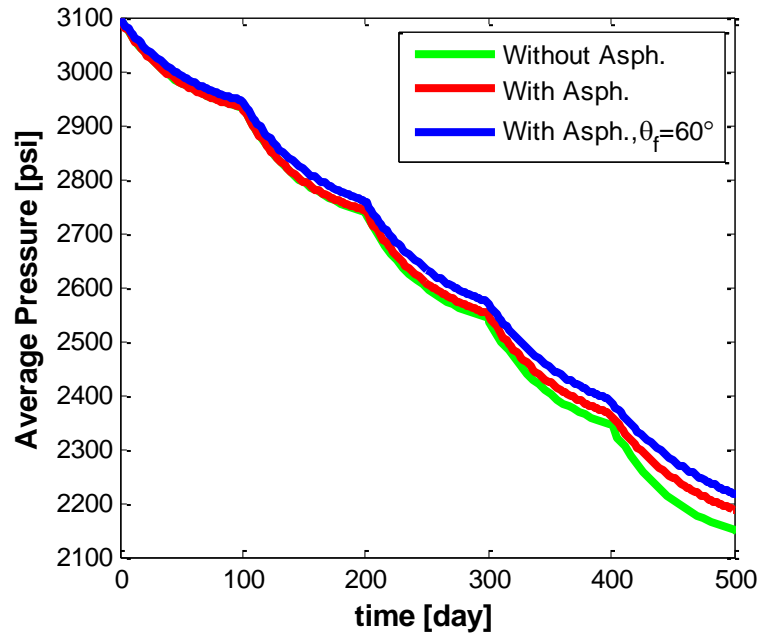


Figure 6.17 Comparison of the average reservoir pressures of three scenarios: ignoring asphaltene, considering asphaltene with no wettability alteration, and considering asphaltene with wettability alteration from $\theta_i=30^\circ$ to $\theta_f=60^\circ$.

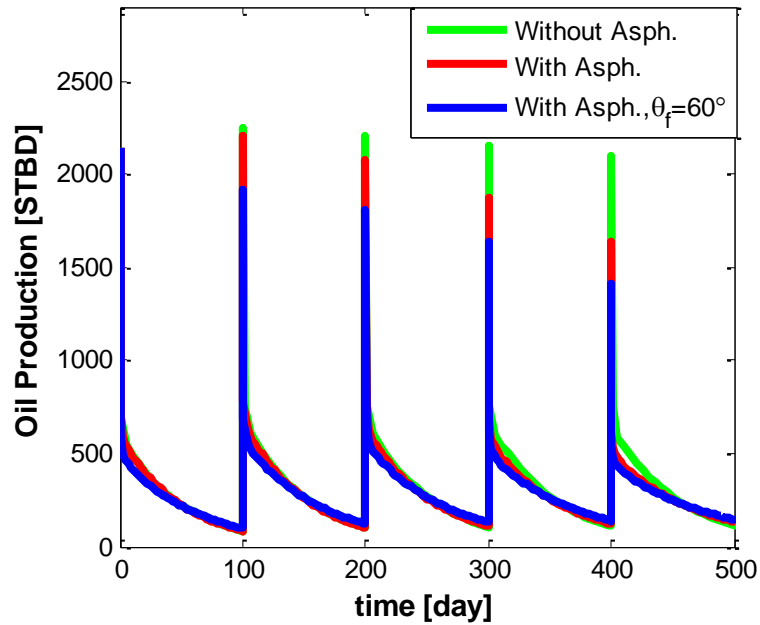


Figure 6.18 Comparison of the oil productions of three scenarios: ignoring asphaltene, considering asphaltene with no wettability alteration, and considering asphaltene with wettability alteration from $\theta_i=30^\circ$ to $\theta_f=60^\circ$.

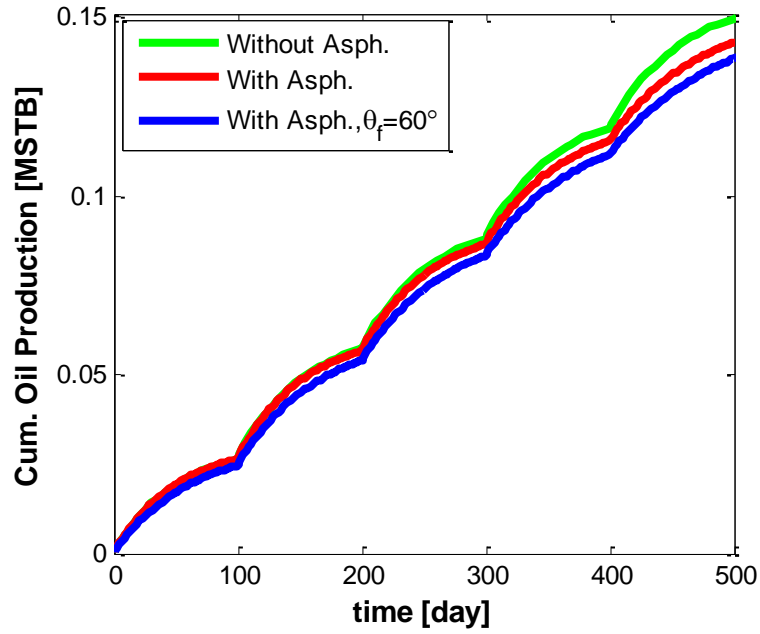


Figure 6.19 Comparison of the cumulative oil productions of three scenarios: ignoring asphaltene, considering asphaltene with no wettability alteration, and considering asphaltene with wettability alteration from $\theta_i=30^\circ$ to $\theta_f=60^\circ$.

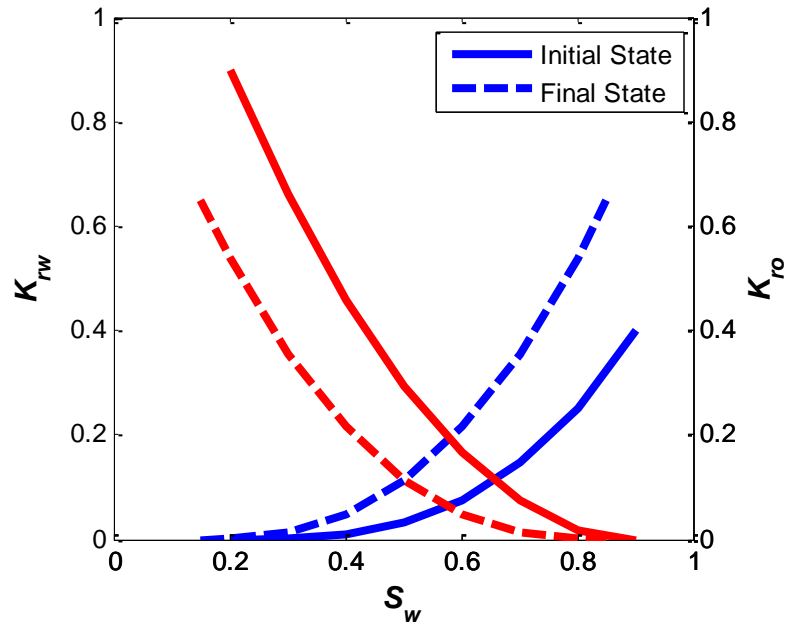


Figure 6.20 Initial and final water/oil relative permeability curves for case 3; initial contact angle is (θ_i) is 30° and final contact angle (θ_f) is 90° .

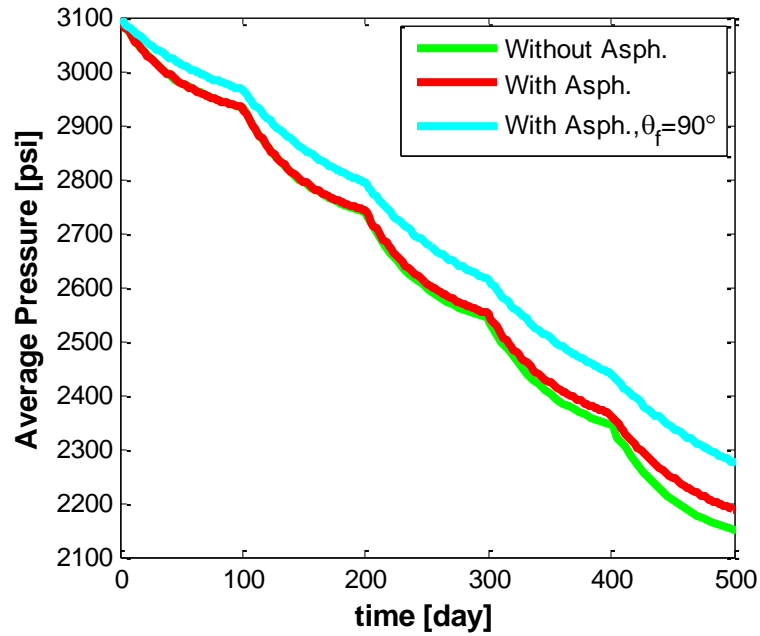


Figure 6.21 Comparison of the average reservoir pressures of three scenarios: ignoring asphaltene, considering asphaltene with no wettability alteration, and considering asphaltene with wettability alteration from $\theta_i=30^\circ$ to $\theta_f=90^\circ$.

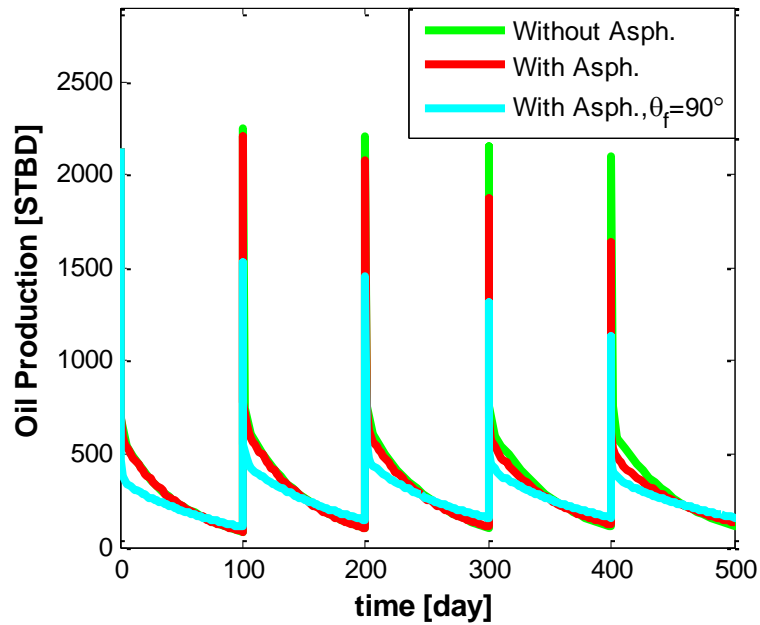


Figure 6.22 Comparison of the oil productions of three scenarios: ignoring asphaltene, considering asphaltene with no wettability alteration, and considering asphaltene with wettability alteration from $\theta_i=30^\circ$ to $\theta_f=90^\circ$.

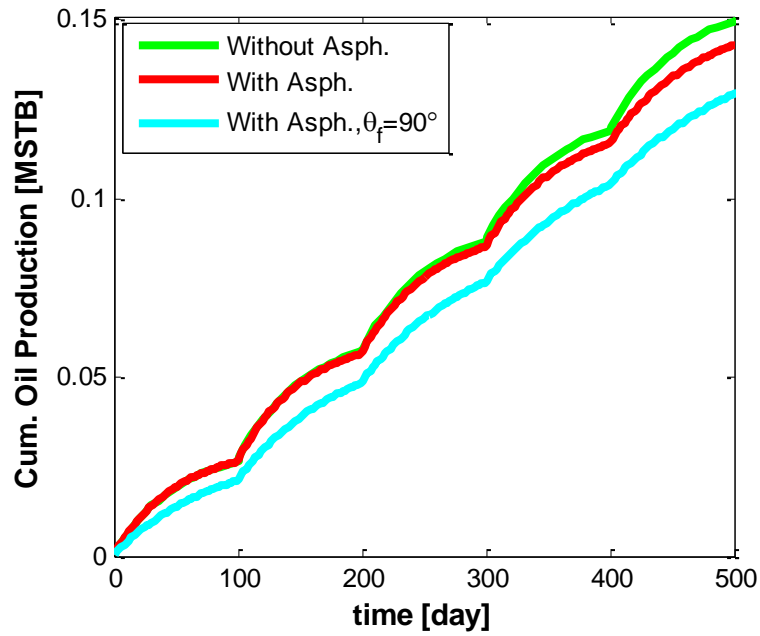


Figure 6.23 Comparison of the cumulative oil productions of three scenarios: ignoring asphaltene, considering asphaltene with no wettability alteration, and considering asphaltene with wettability alteration from $\theta_i=30^\circ$ to $\theta_f=90^\circ$.

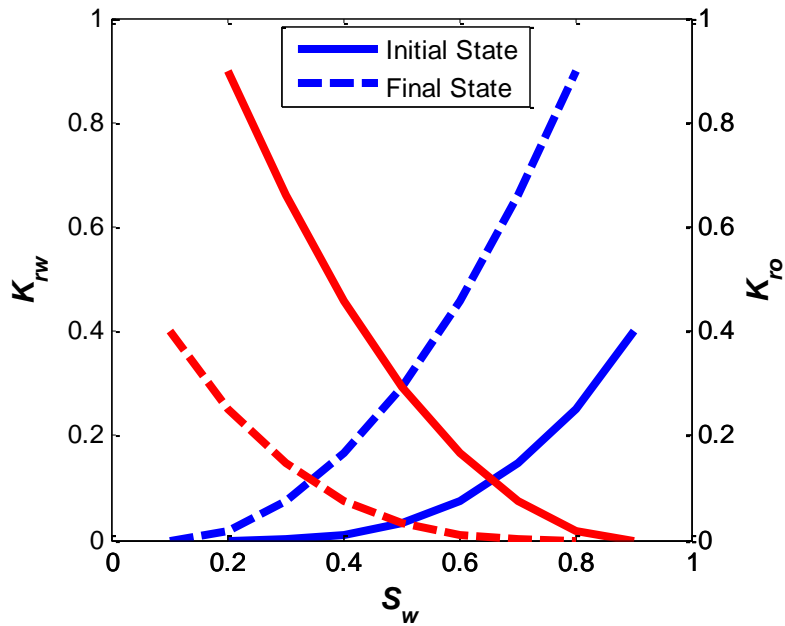


Figure 6.24 Initial and final water/oil relative permeability curves for case 3; initial contact angle is (θ_i) is 30° and final contact angle (θ_f) is 150° .

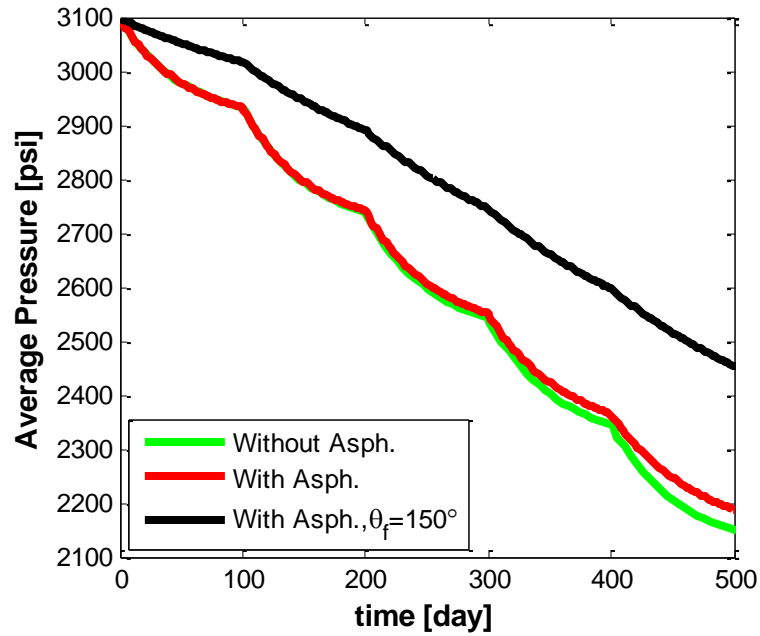


Figure 6.25 Comparison of the average reservoir pressures of three scenarios: ignoring asphaltene, considering asphaltene with no wettability alteration, and considering asphaltene with wettability alteration from $\theta_i=30^\circ$ to $\theta_f=150^\circ$.

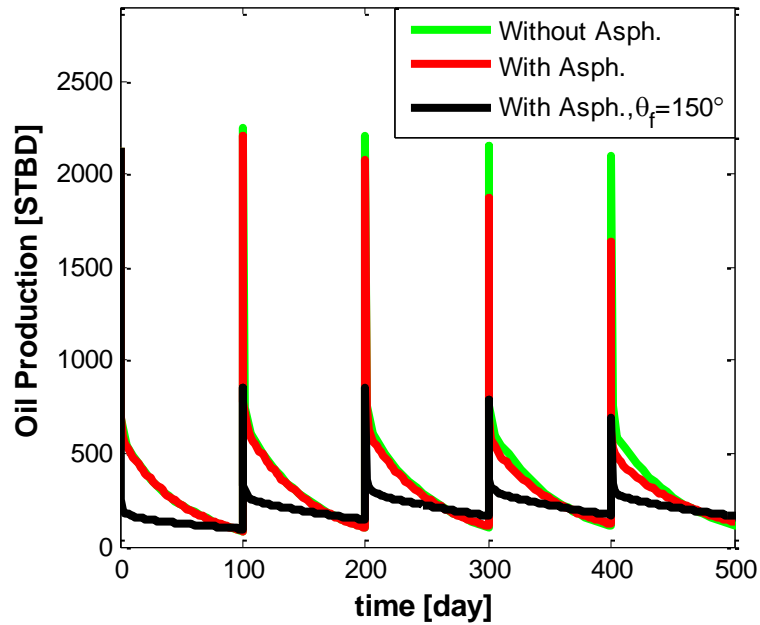


Figure 6.26 Comparison of the oil productions of three scenarios: ignoring asphaltene, considering asphaltene with no wettability alteration, and considering asphaltene with wettability alteration from $\theta_i=30^\circ$ to $\theta_f=150^\circ$.

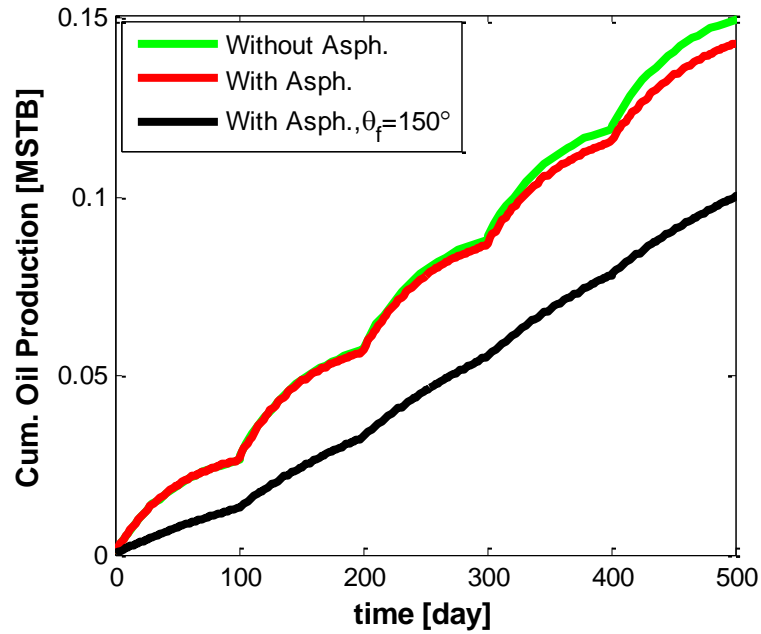


Figure 6.27 Comparison of the cumulative oil productions of three scenarios: ignoring asphaltene, considering asphaltene with no wettability alteration, and considering asphaltene with wettability alteration from $\theta_i=30^\circ$ to $\theta_f=150^\circ$.

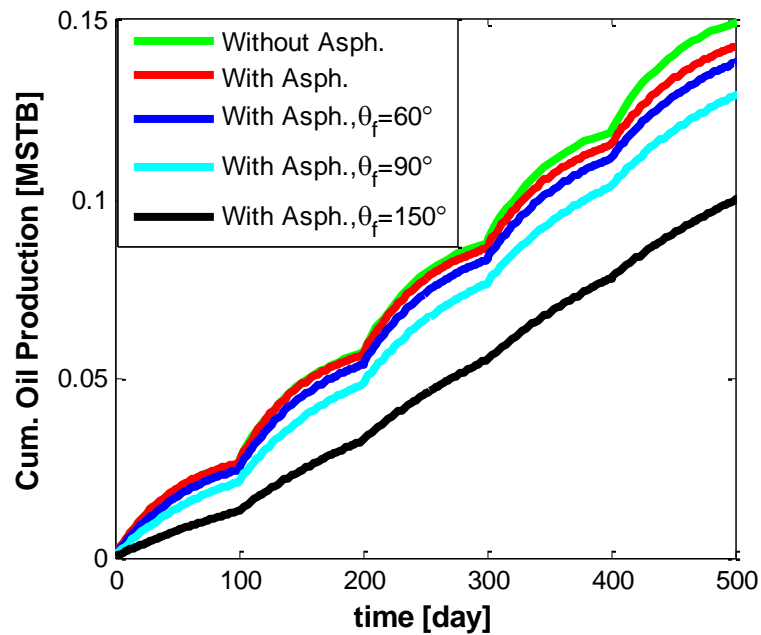
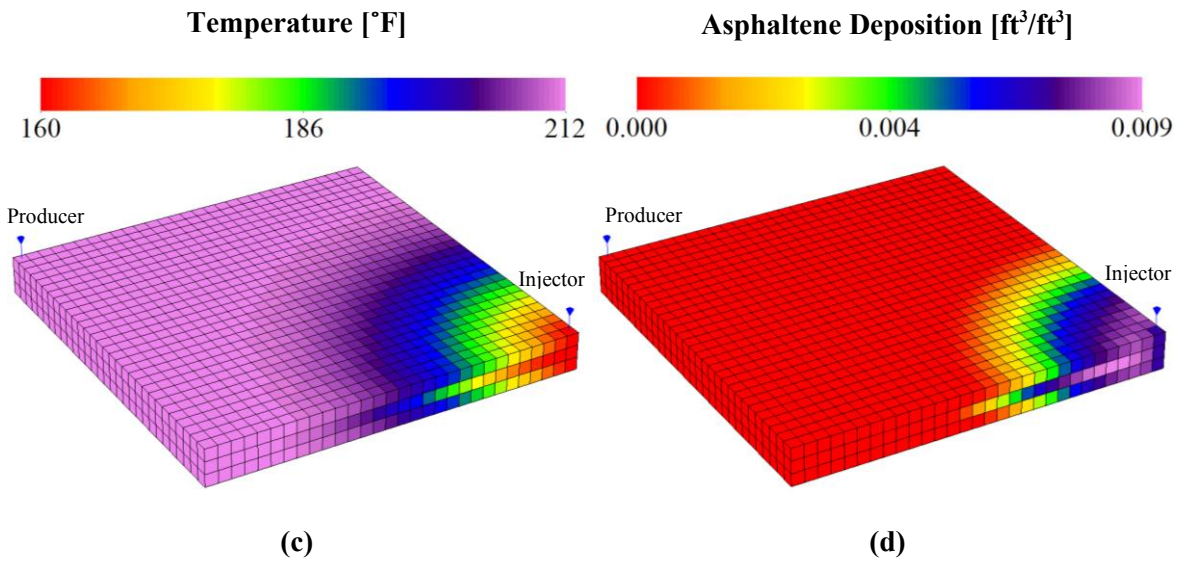
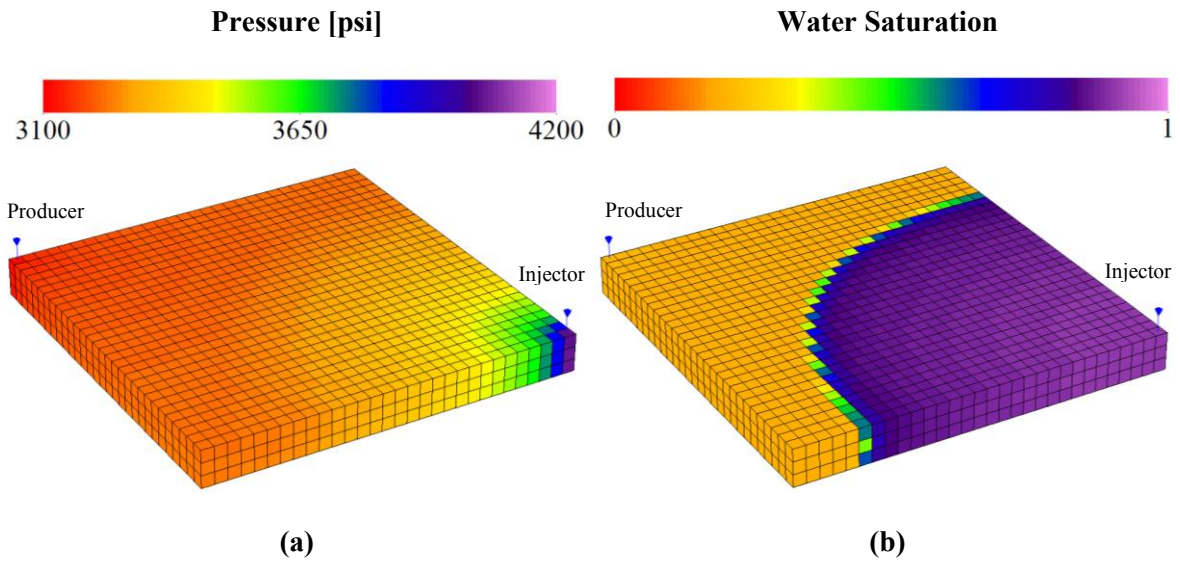


Figure 6.28 Comparison of the cumulative oil productions of five scenarios: ignoring asphaltene, considering asphaltene, and considering asphaltene with wettability alteration from $\theta_i=30^\circ$ to $\theta_f=60^\circ$, 90° , and 150° .



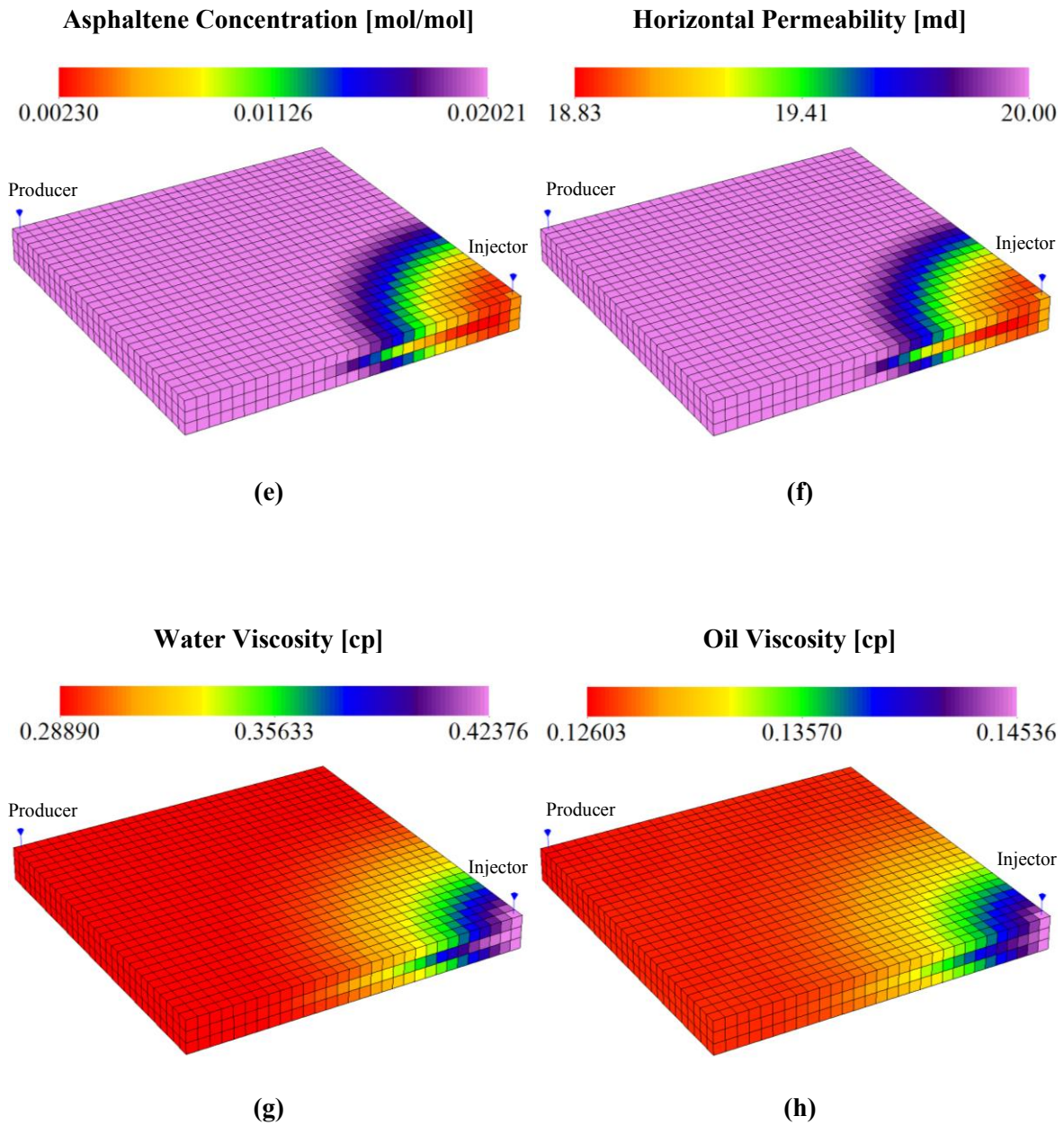
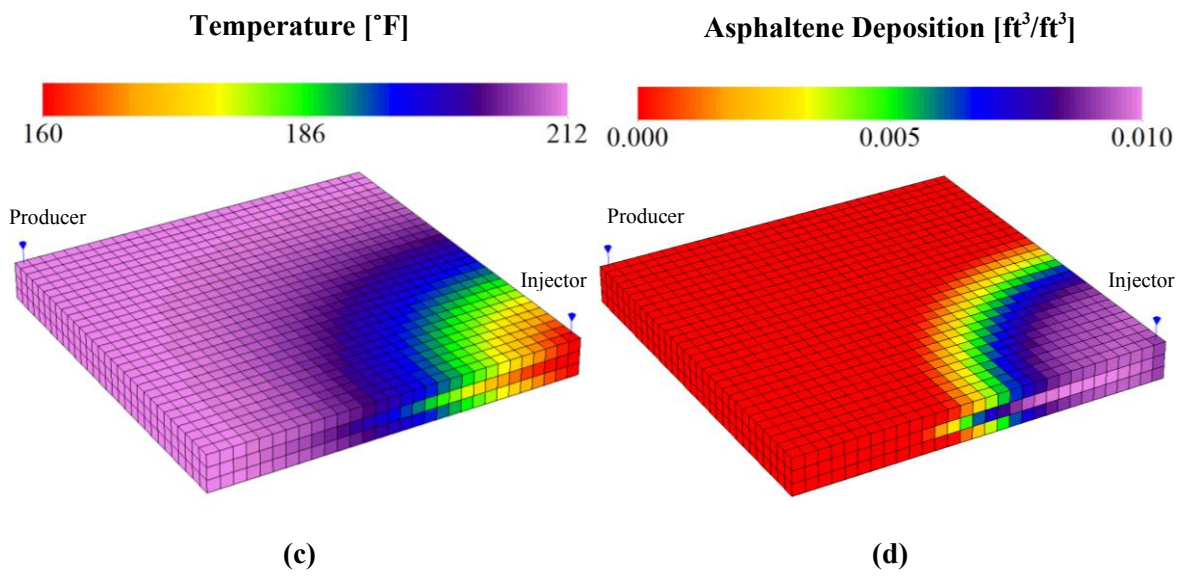
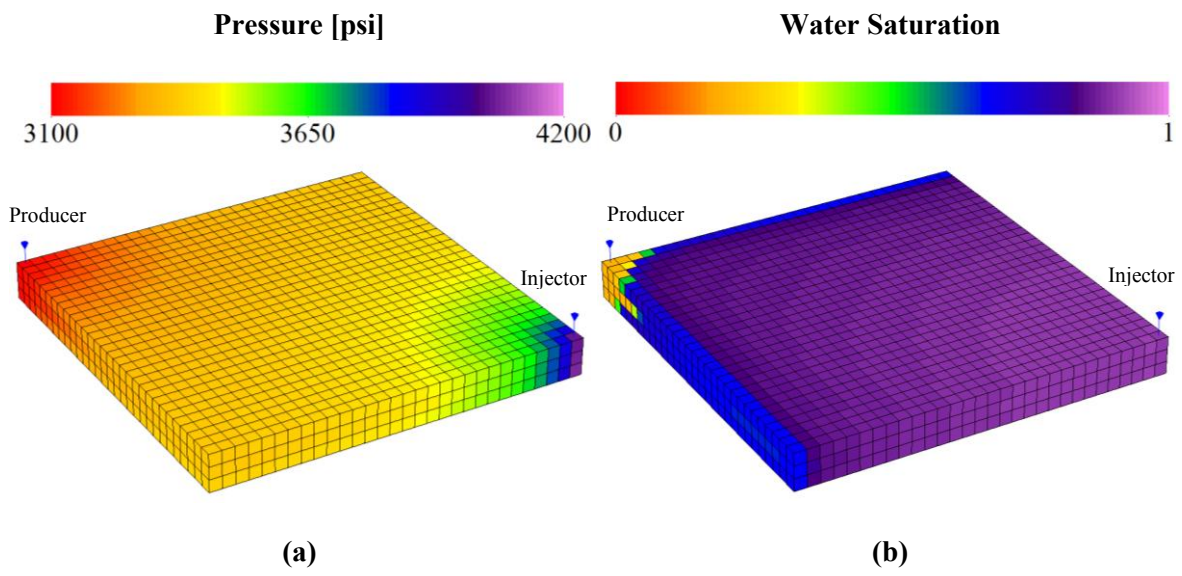


Figure 6.29 Results after 500 days of simulation for case 4; (a) pressure, (b) water saturation, (c) temperature, (d) asphaltene deposition, (e) asphaltene concentration, (f) horizontal permeability, (g) water viscosity, and (h) oil viscosity maps.



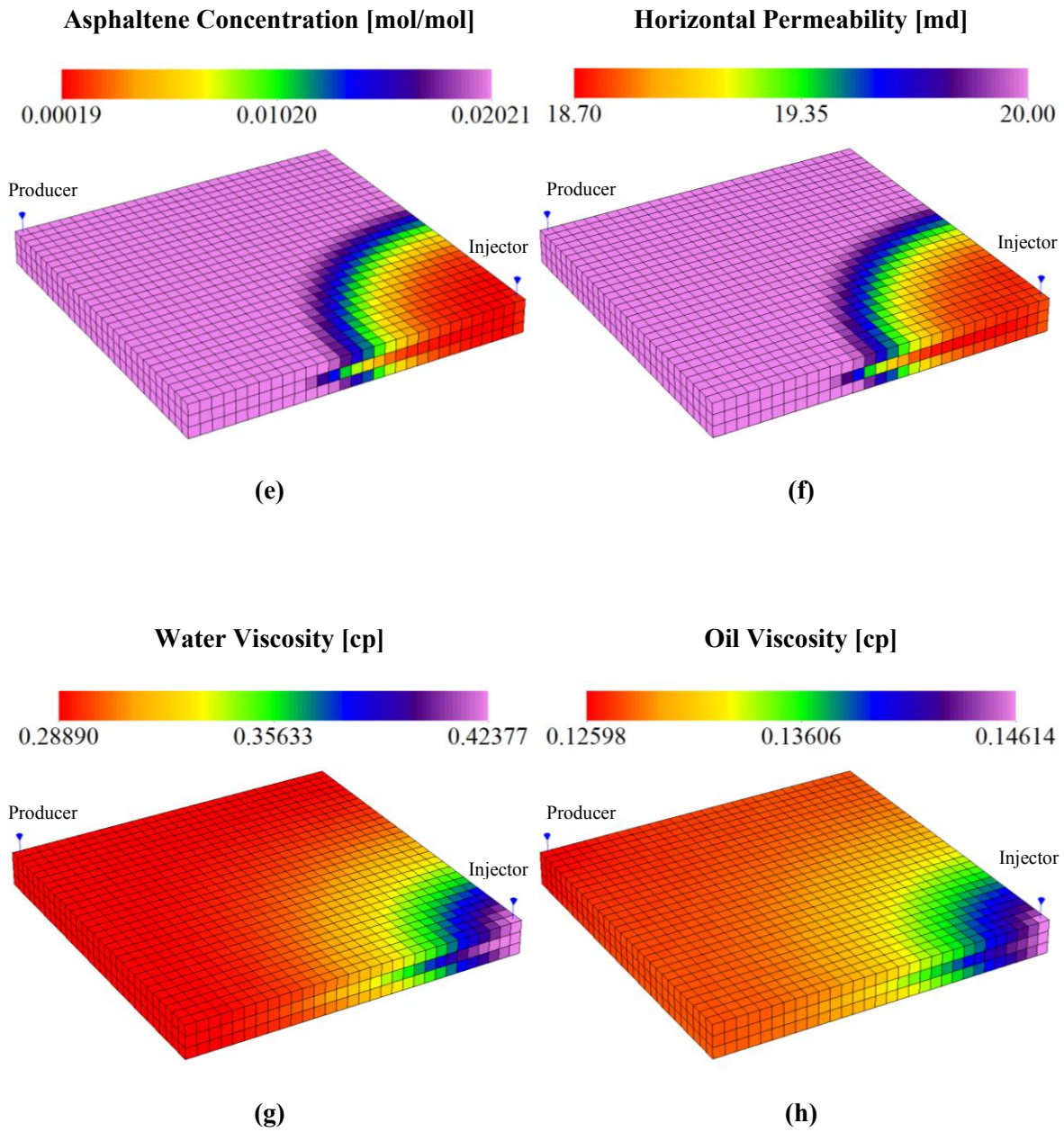
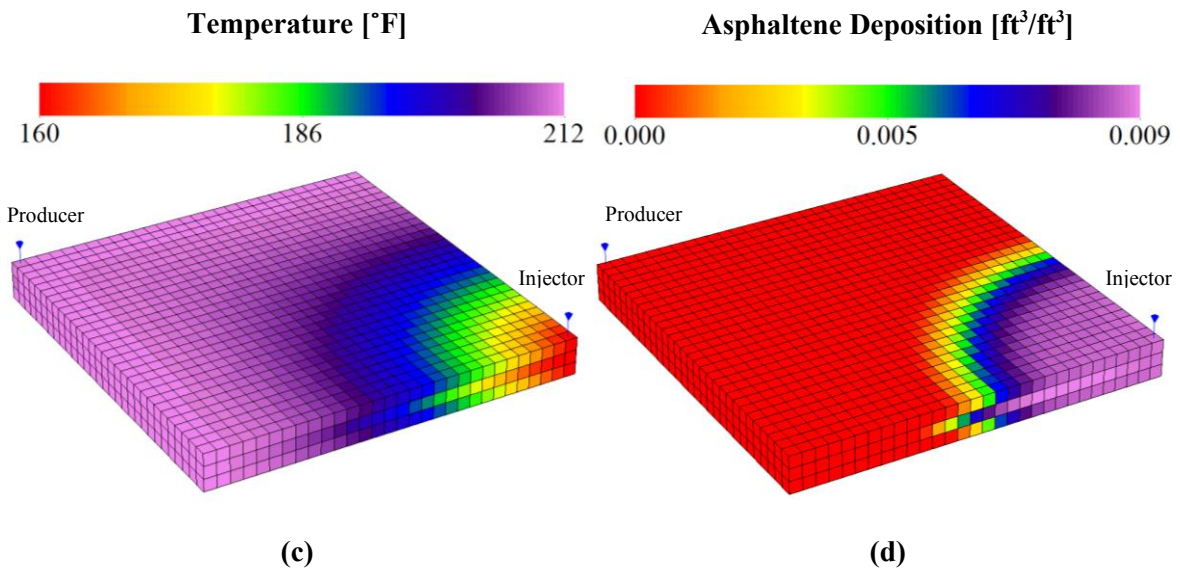
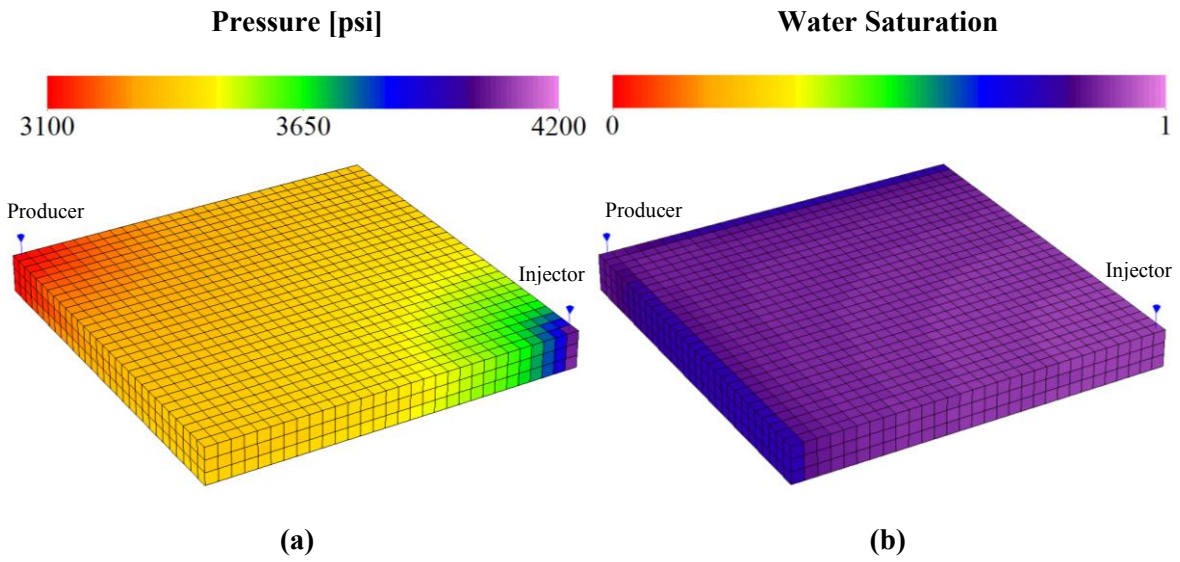


Figure 6.30 Results after 1000 days of simulation for case 4; (a) pressure, (b) water saturation, (c) temperature, (d) asphaltene deposition, (e) asphaltene concentration, (f) horizontal permeability, (g) water viscosity, and (h) oil viscosity maps.



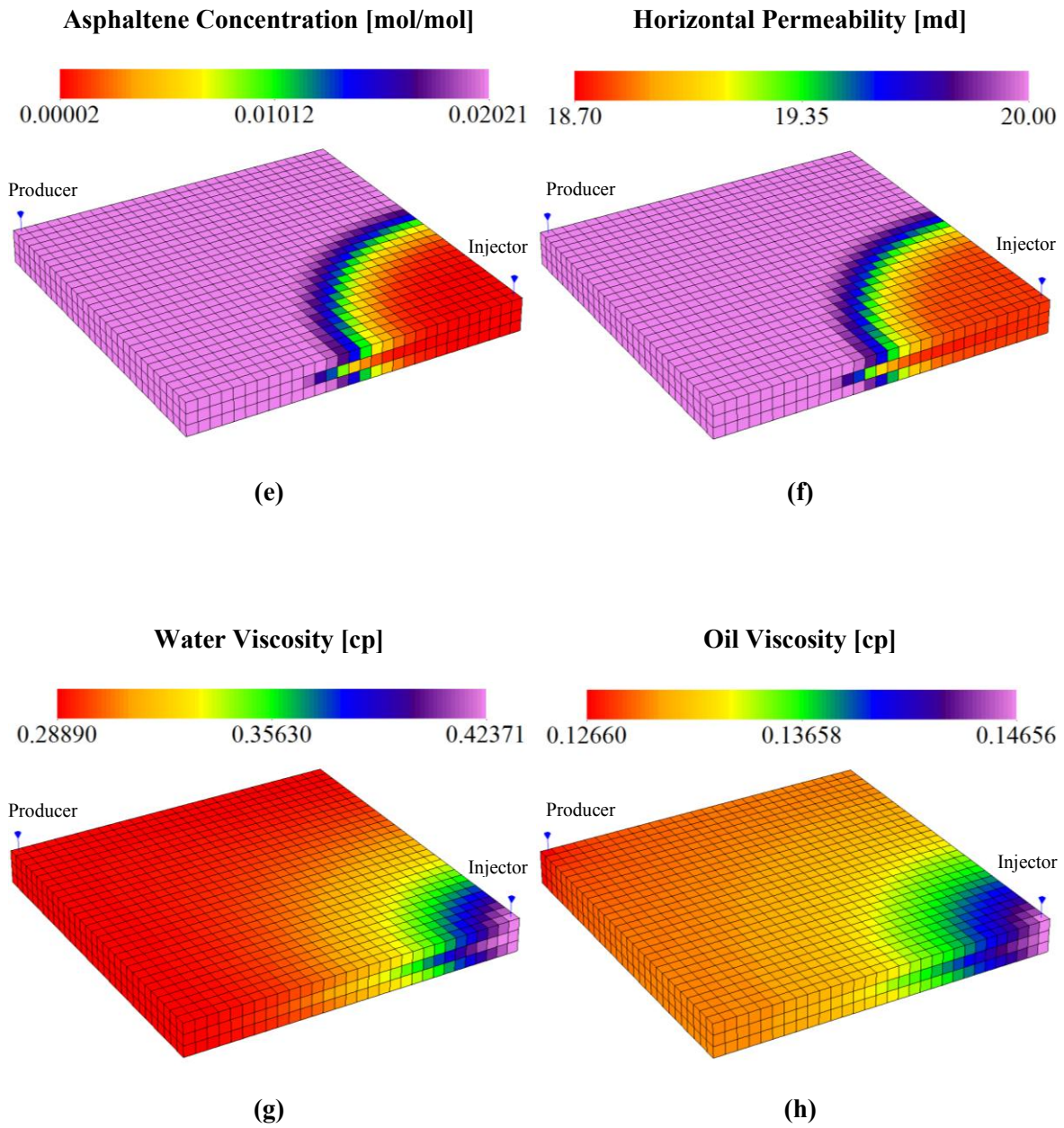


Figure 6.31 Results after 1500 days of simulation for case 4; (a) pressure, (b) water saturation, (c) temperature, (d) asphaltene deposition, (e) asphaltene concentration, (f) horizontal permeability, (g) water viscosity, and (h) oil viscosity maps.

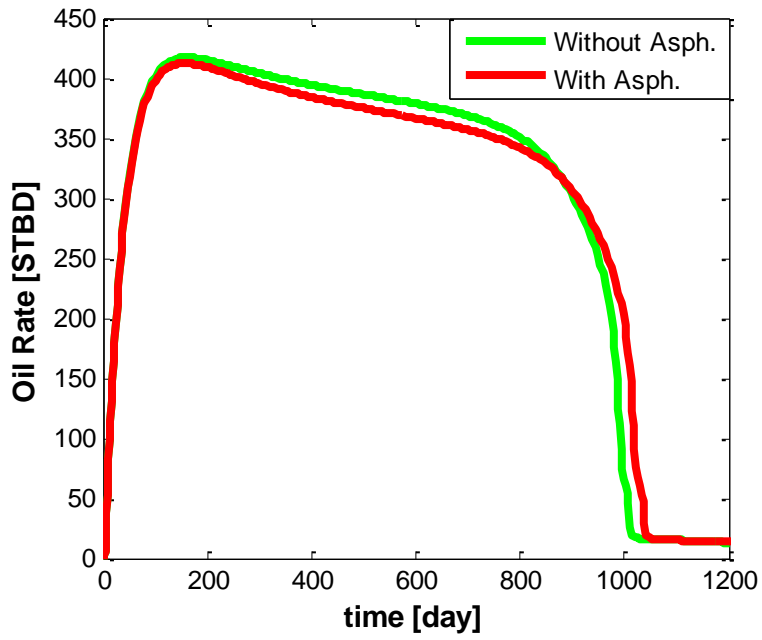


Figure 6.32 Oil rates for simulations of two scenarios of considering and ignoring asphaltene modeling; case 4.

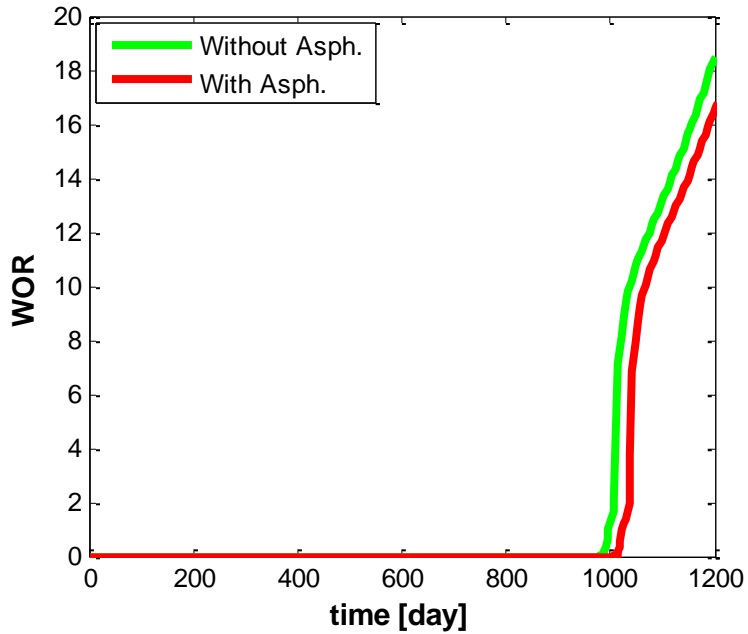


Figure 6.33 Water/oil ratios for simulations of two scenarios of considering and ignoring asphaltene modeling; case 4.

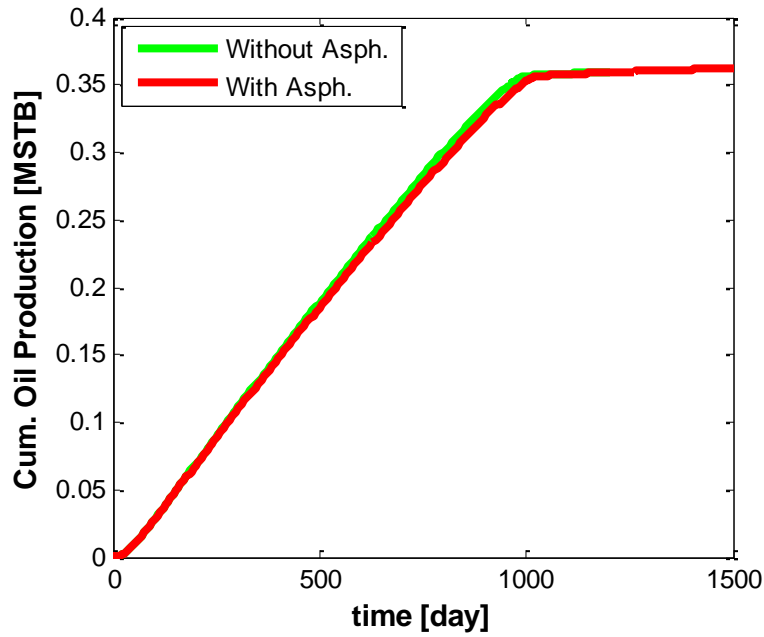


Figure 6.34 Cumulative oil productions for simulations of two scenarios of considering and ignoring asphaltene modeling; case 4.

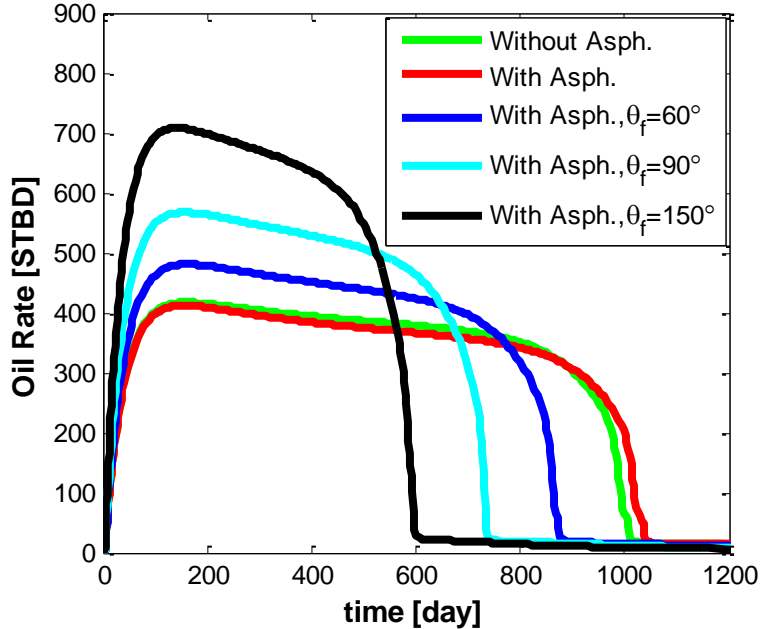


Figure 6.35 Comparison of the oil production rates of five scenarios: ignoring asphaltene, considering asphaltene, and considering asphaltene with wettability alteration from $\theta_i=30^\circ$ to $\theta_f=60^\circ$, 90° , and 150° .

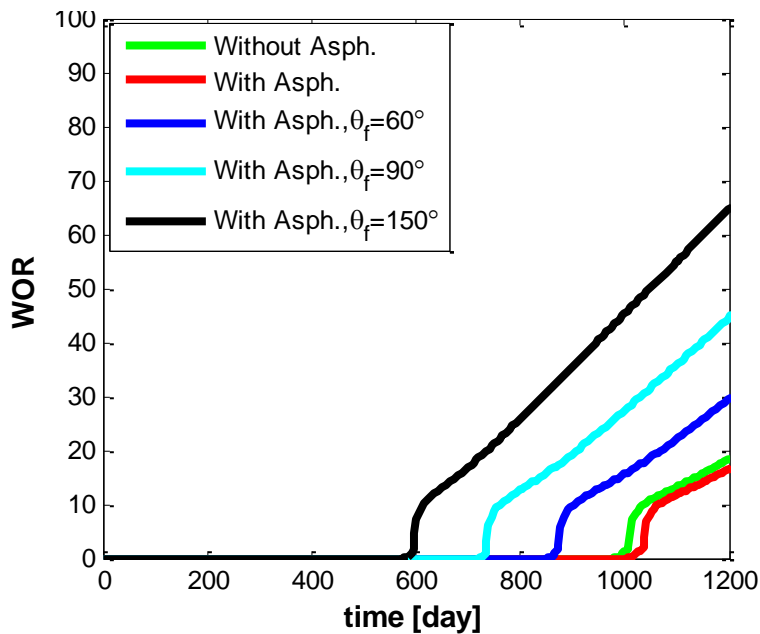


Figure 6.36 Comparison of the water/oil ratios of five scenarios: ignoring asphaltene, considering asphaltene, and considering asphaltene with wettability alteration from $\theta_i=30^\circ$ to $\theta_f=60^\circ$, 90° , and 150° .

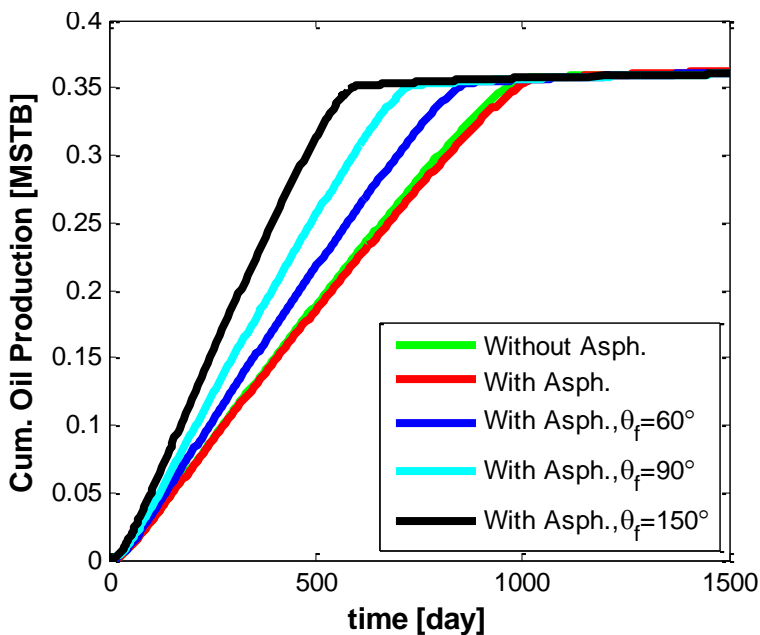


Figure 6.37 Comparison of the cumulative oil productions of five scenarios: ignoring asphaltene, considering asphaltene, and considering asphaltene with wettability alteration from $\theta_i=30^\circ$ to $\theta_f=60^\circ$, 90° , and 150° .

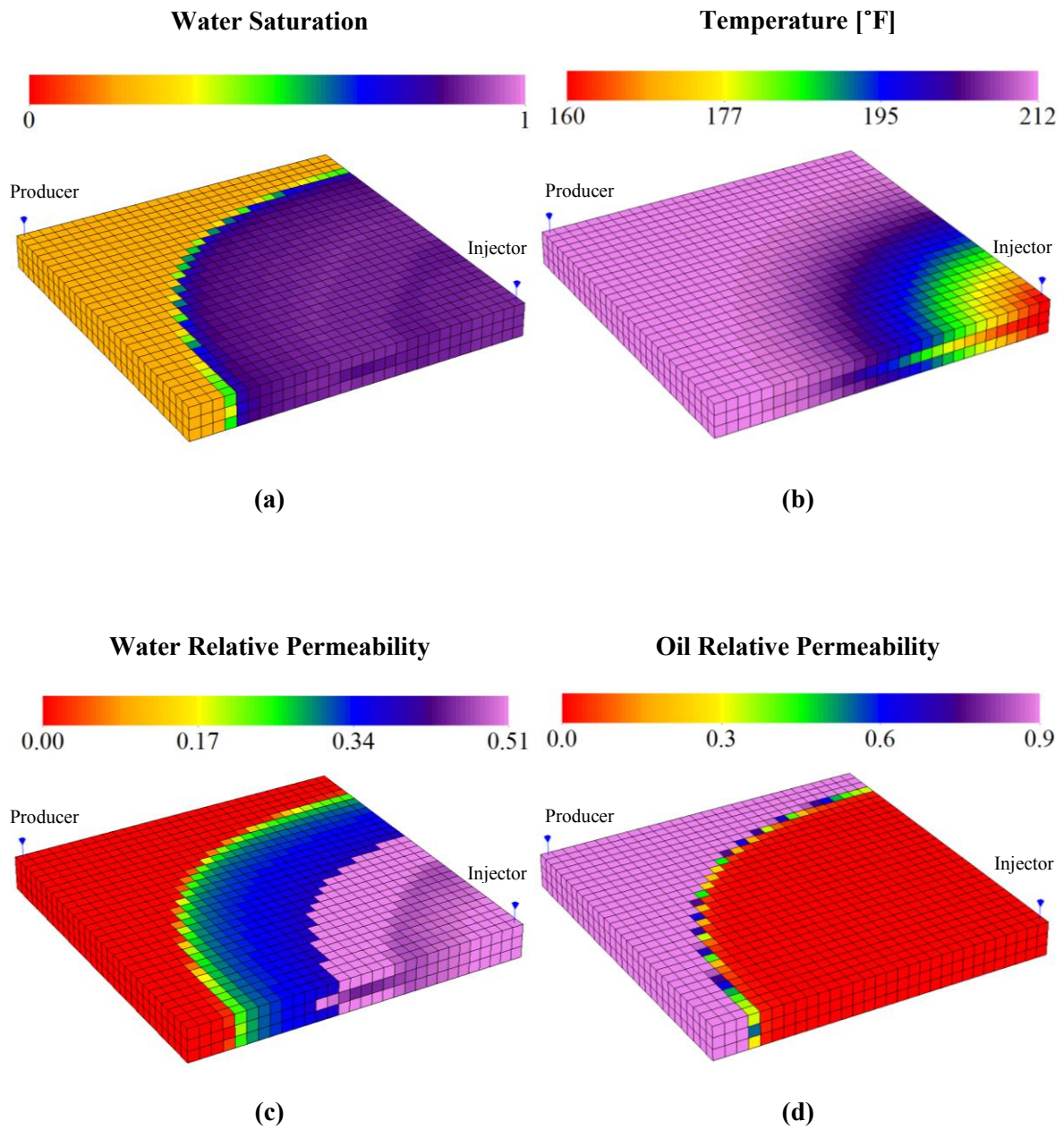


Figure 6.38 Results after 500 days of simulation for case 5 when $\theta_r = 60^\circ$: (a) water saturation, (b) temperature, (c) water relative permeability, and (d) oil relative permeability maps.

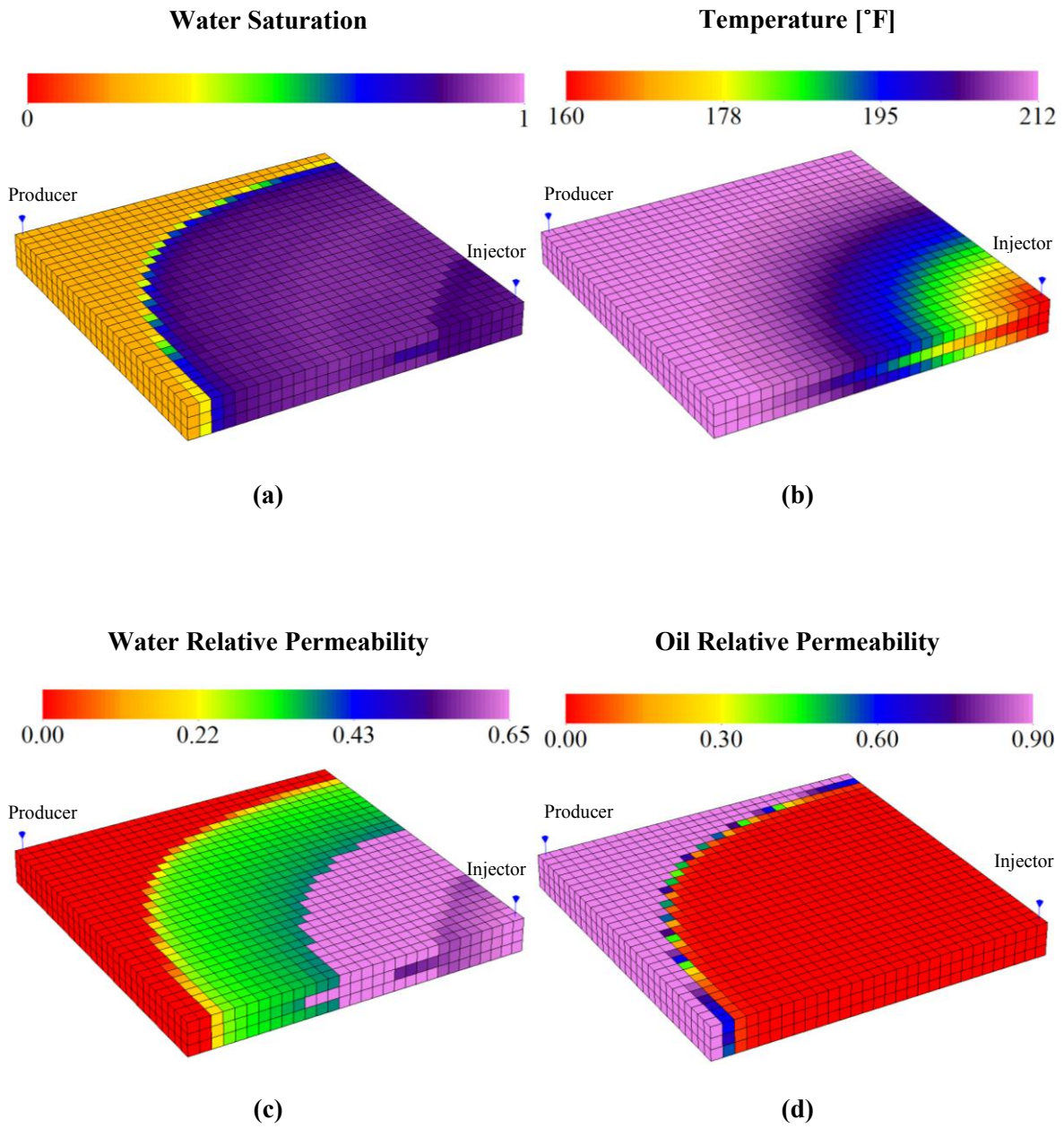


Figure 6.39 Results after 500 days of simulation for case 5 when $\theta_r = 90^\circ$: (a) water saturation, (b) temperature, (c) water relative permeability, and (d) oil relative permeability maps.

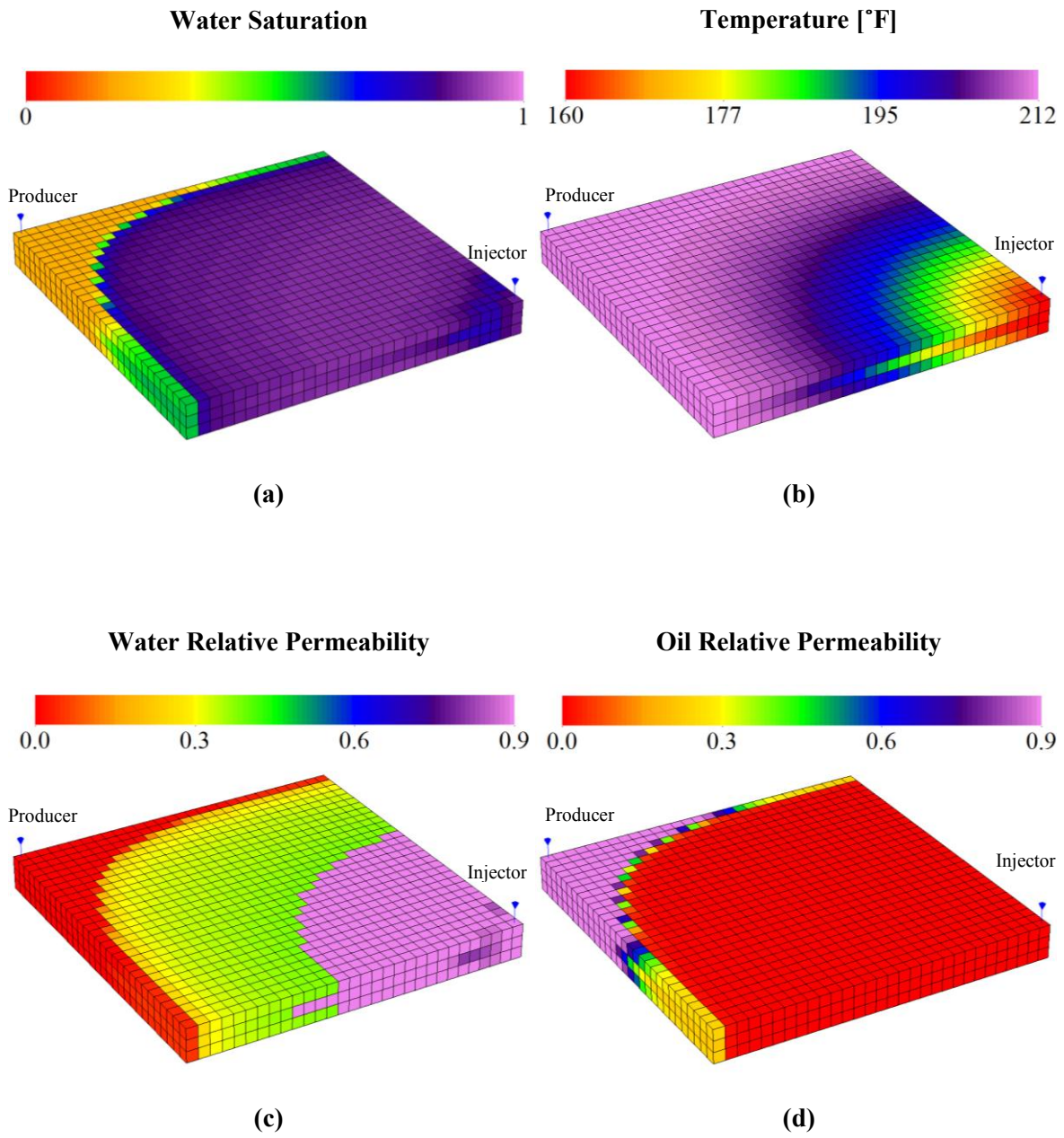
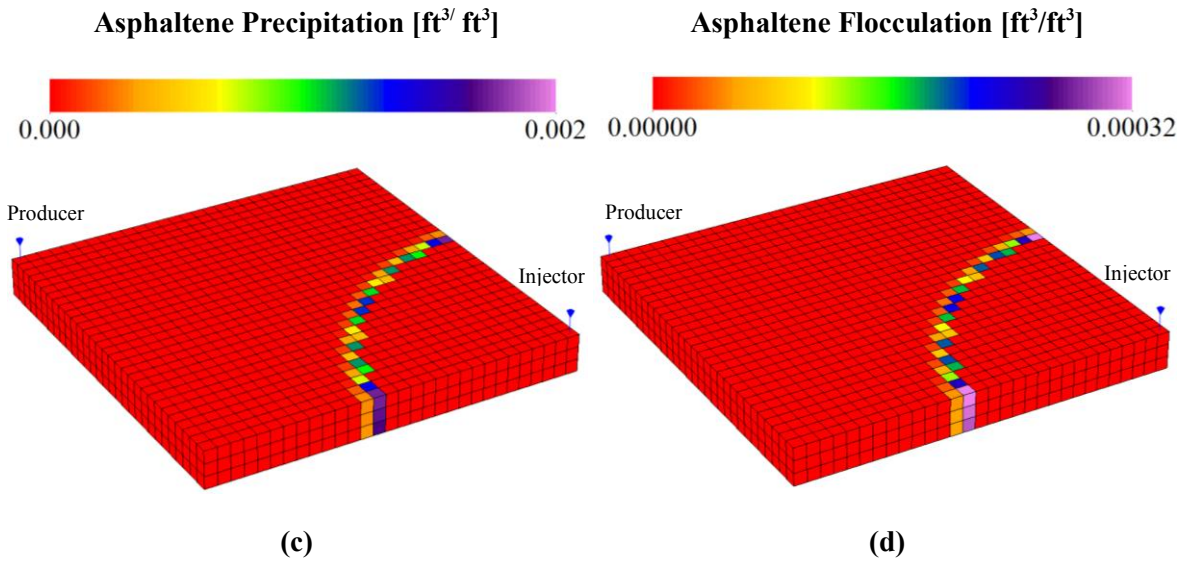
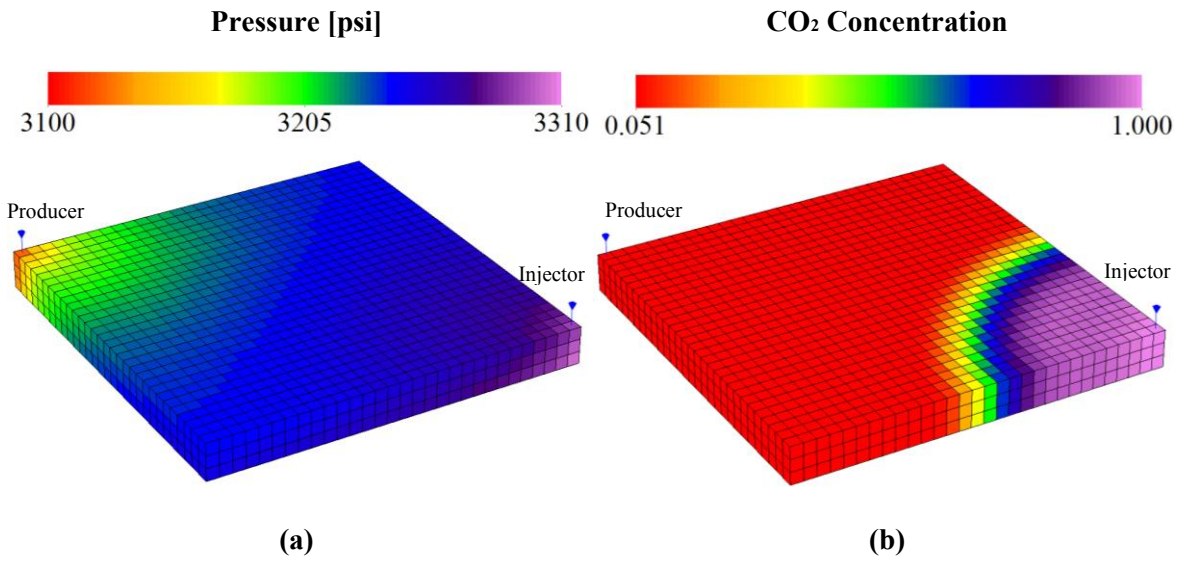


Figure 6.40 Results after 500 days of simulation for case 5 when $\theta_f = 150^\circ$: (a) water saturation, (b) temperature, (c) water relative permeability, and (d) oil relative permeability maps.



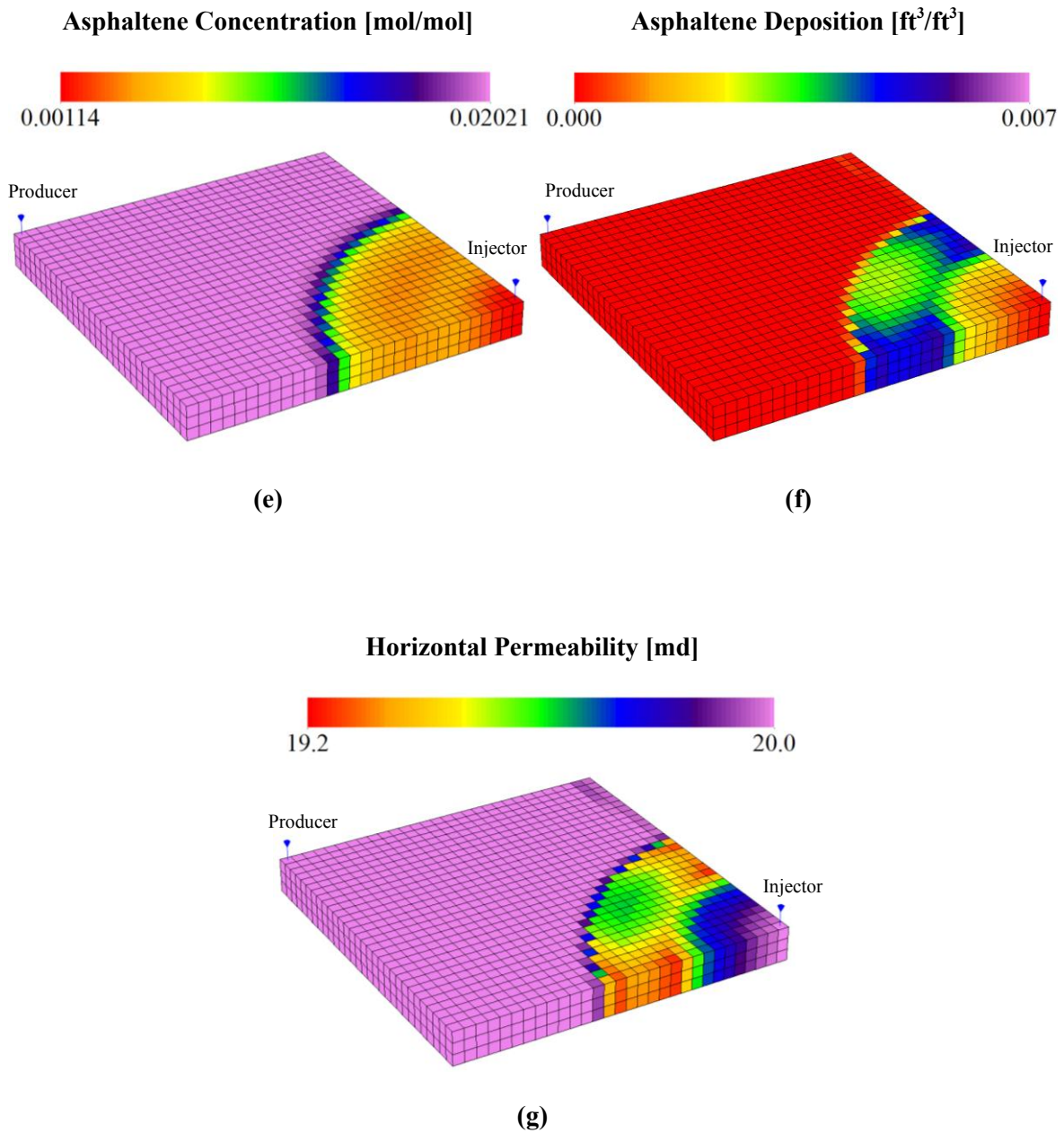
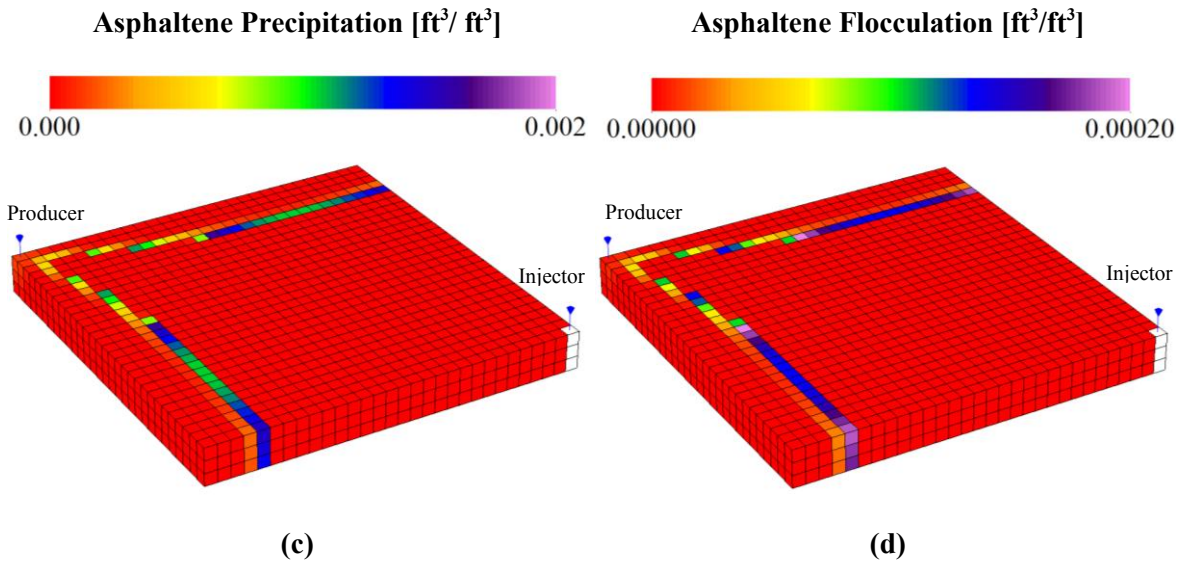
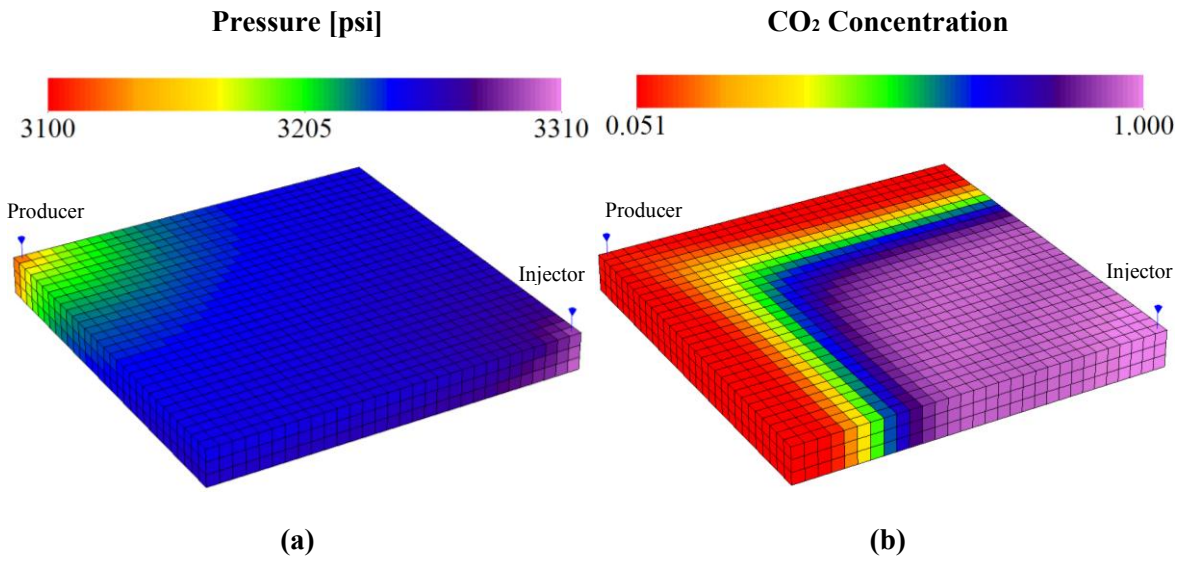


Figure 6.41 Results after 100 days of simulation for case 6: (a) pressure, (b) CO₂ concentration, (c) asphaltene precipitation, (d) asphaltene flocculation, (e) asphaltene concentration, (f) asphaltene deposition, and (g) horizontal permeability maps.



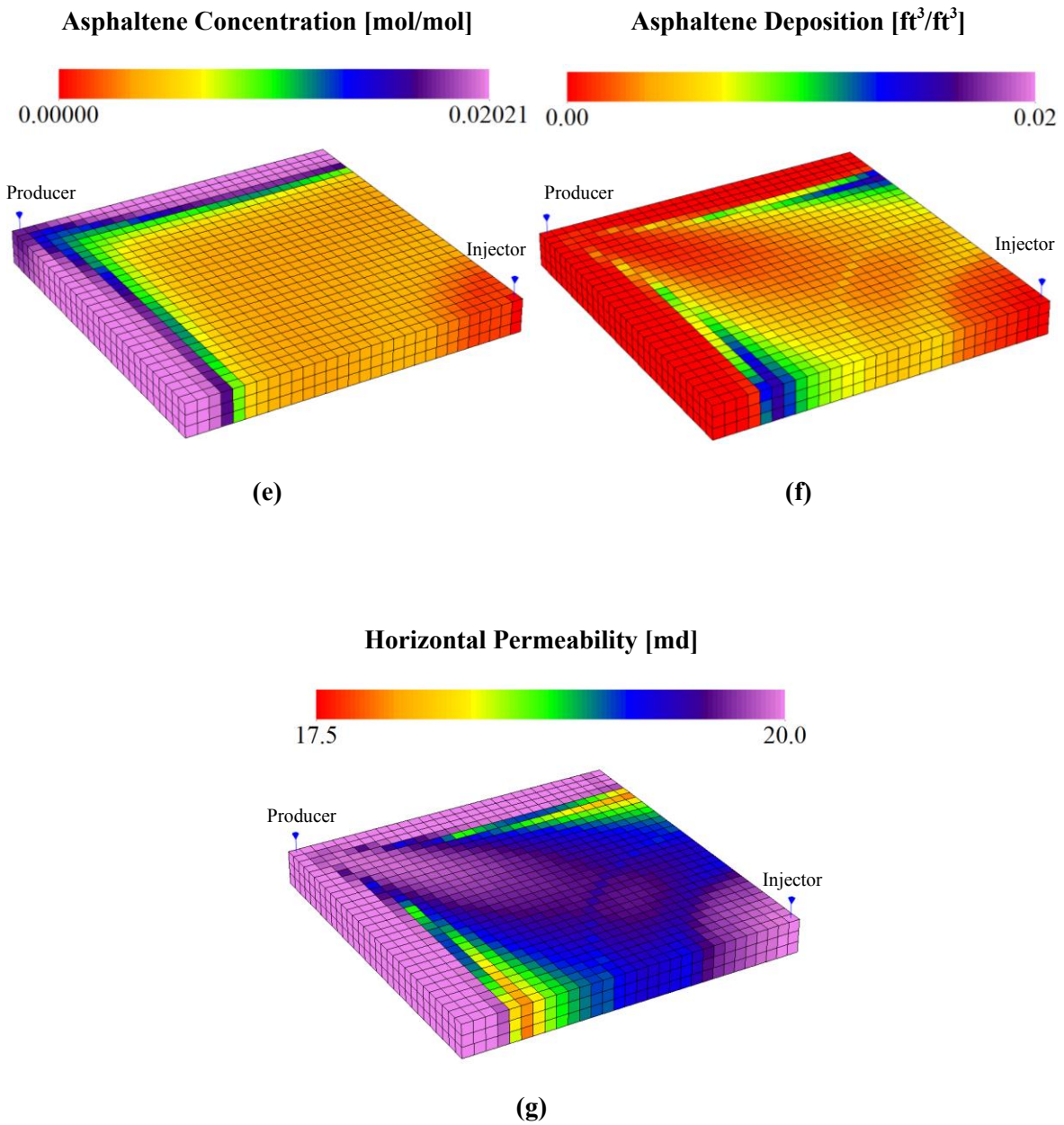


Figure 6.42 Results after 420 days of simulation (around CO₂ breakthrough) for case 6: (a) pressure, (b) CO₂ concentration, (c) asphaltene precipitation, (d) asphaltene flocculation, (e) asphaltene concentration, (f) asphaltene deposition, and (g) horizontal permeability maps.

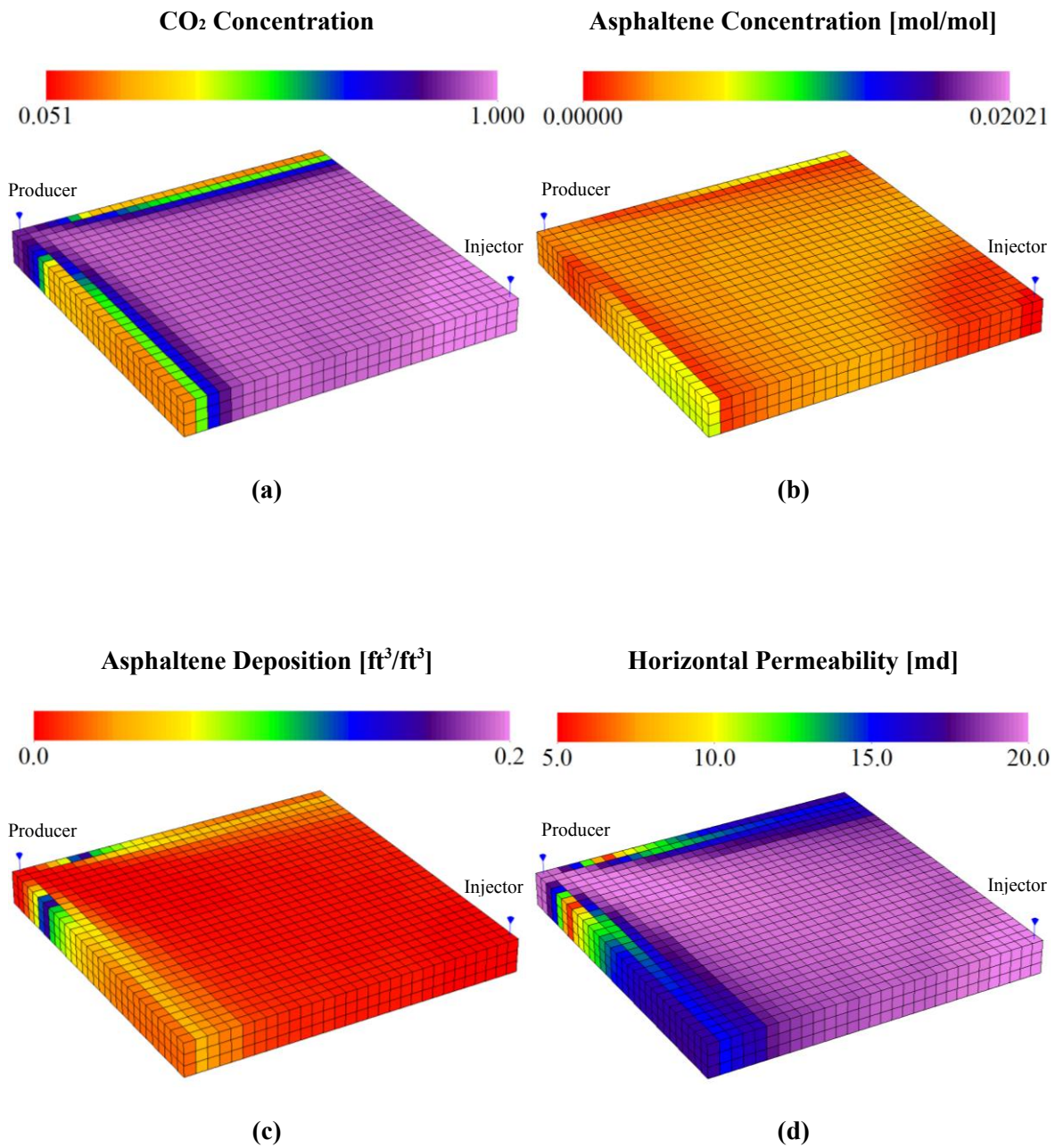


Figure 6.43 Results after 1000 days of simulation for case 6: (a) CO₂ concentration, (b) asphaltene concentration, (c) asphaltene deposition, and (d) horizontal permeability maps.

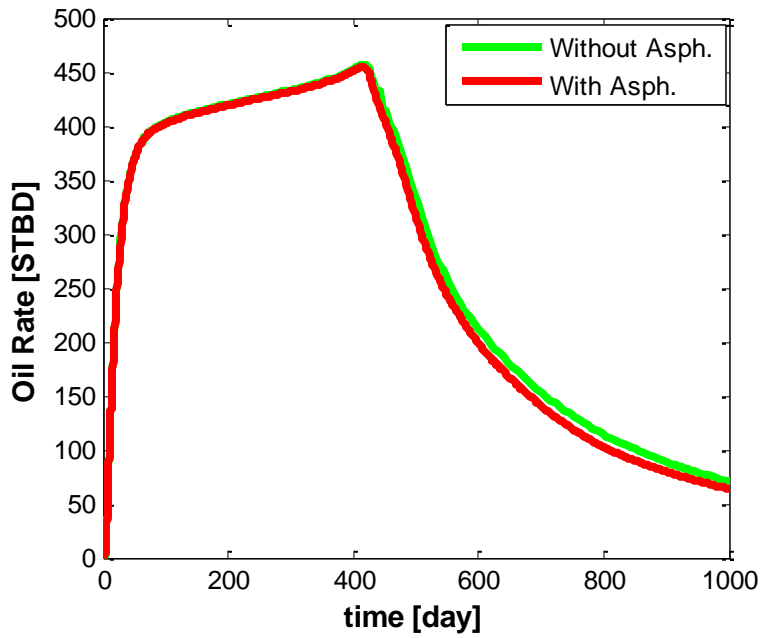


Figure 6.44 Comparison of the oil production rates in the presence and absence of the asphaltene deposition.

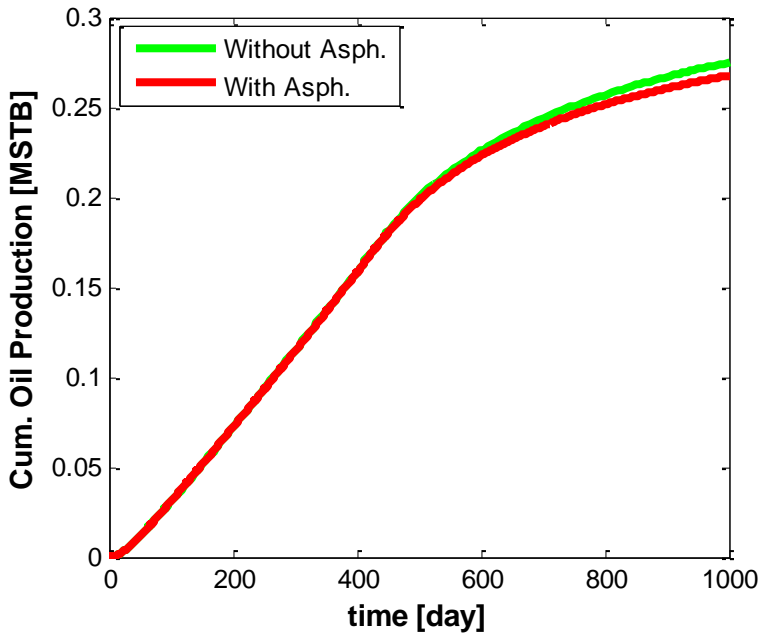


Figure 6.45 Comparison of the cumulative oil productions in the presence and absence of the asphaltene deposition.

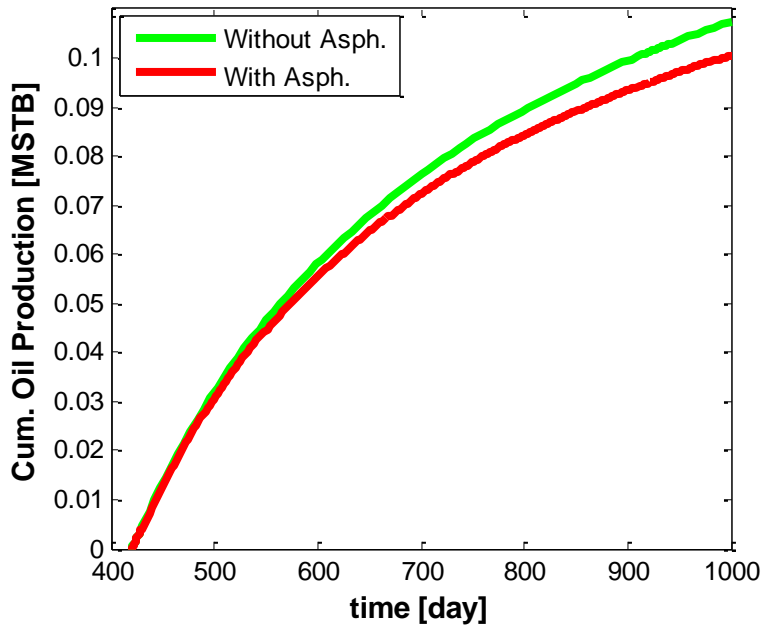


Figure 6.46 Comparison of the after breakthrough cumulative oil productions in the presence and absence of the asphaltene deposition.

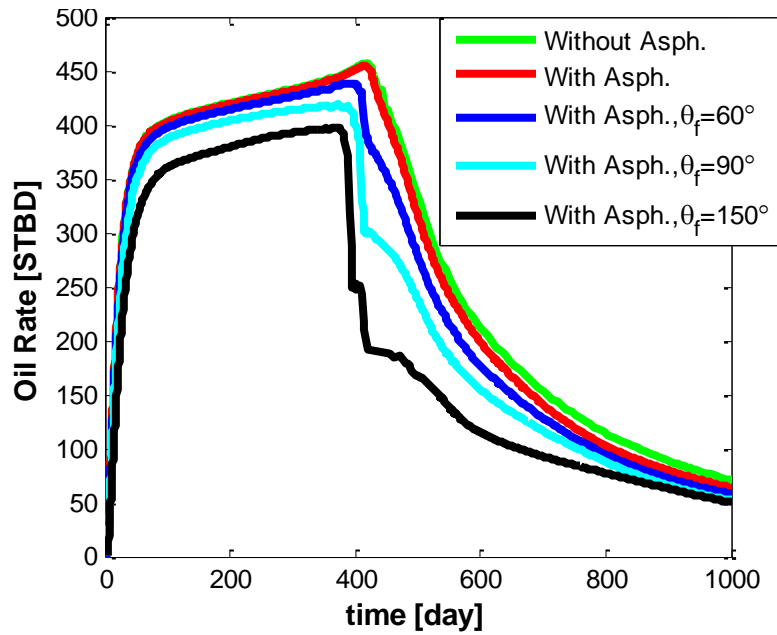


Figure 6.47 Comparison of the oil production of the five scenarios: ignoring asphaltene, considering asphaltene and ignoring wettability alteration, and considering asphaltene with wettability alteration to $\theta_f=60^\circ$, 90° , and 150° .

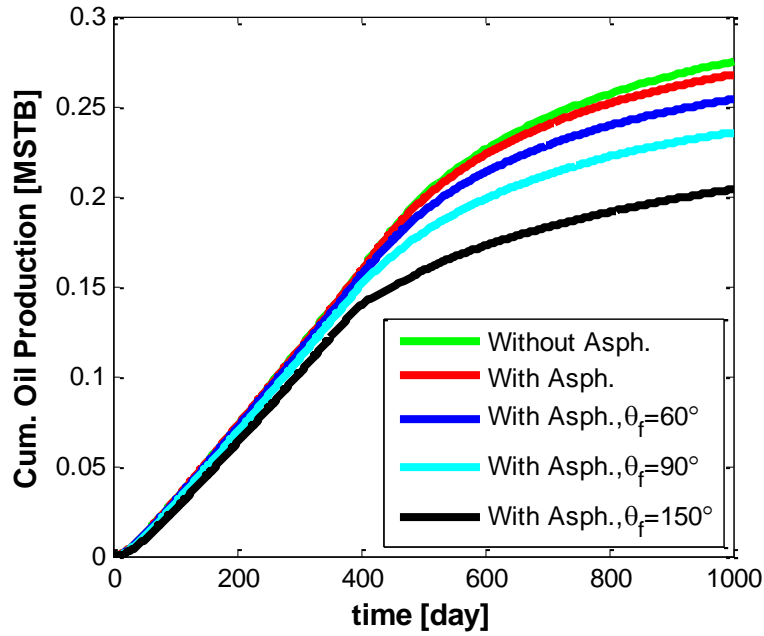


Figure 6.48 Comparison of the cumulative oil productions of the five scenarios: ignoring asphaltene, considering asphaltene and ignoring wettability alteration, and considering asphaltene with wettability alteration to $\theta_f=60^\circ$, 90° , and 150° .

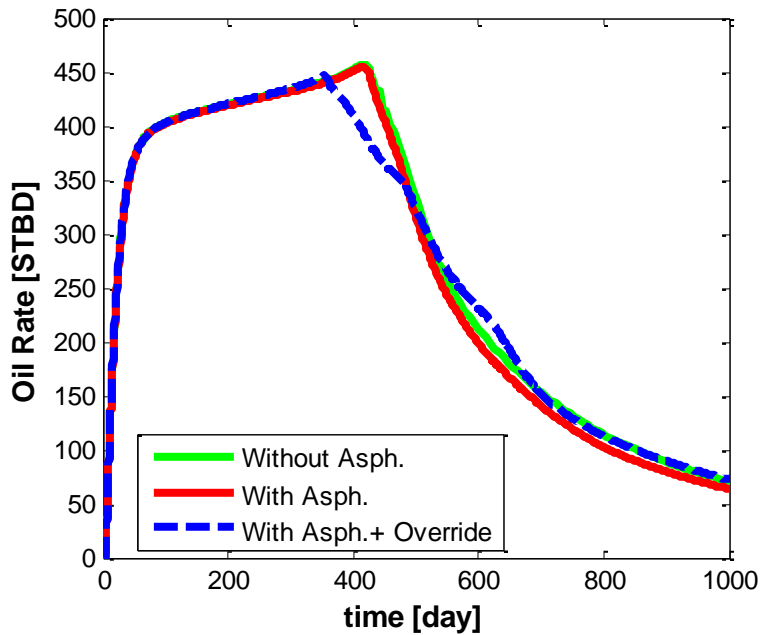


Figure 6.49 Comparison of the cumulative oil production of the three scenarios: ignoring asphaltene, considering asphaltene and ignoring gas override, and considering asphaltene with gas override.

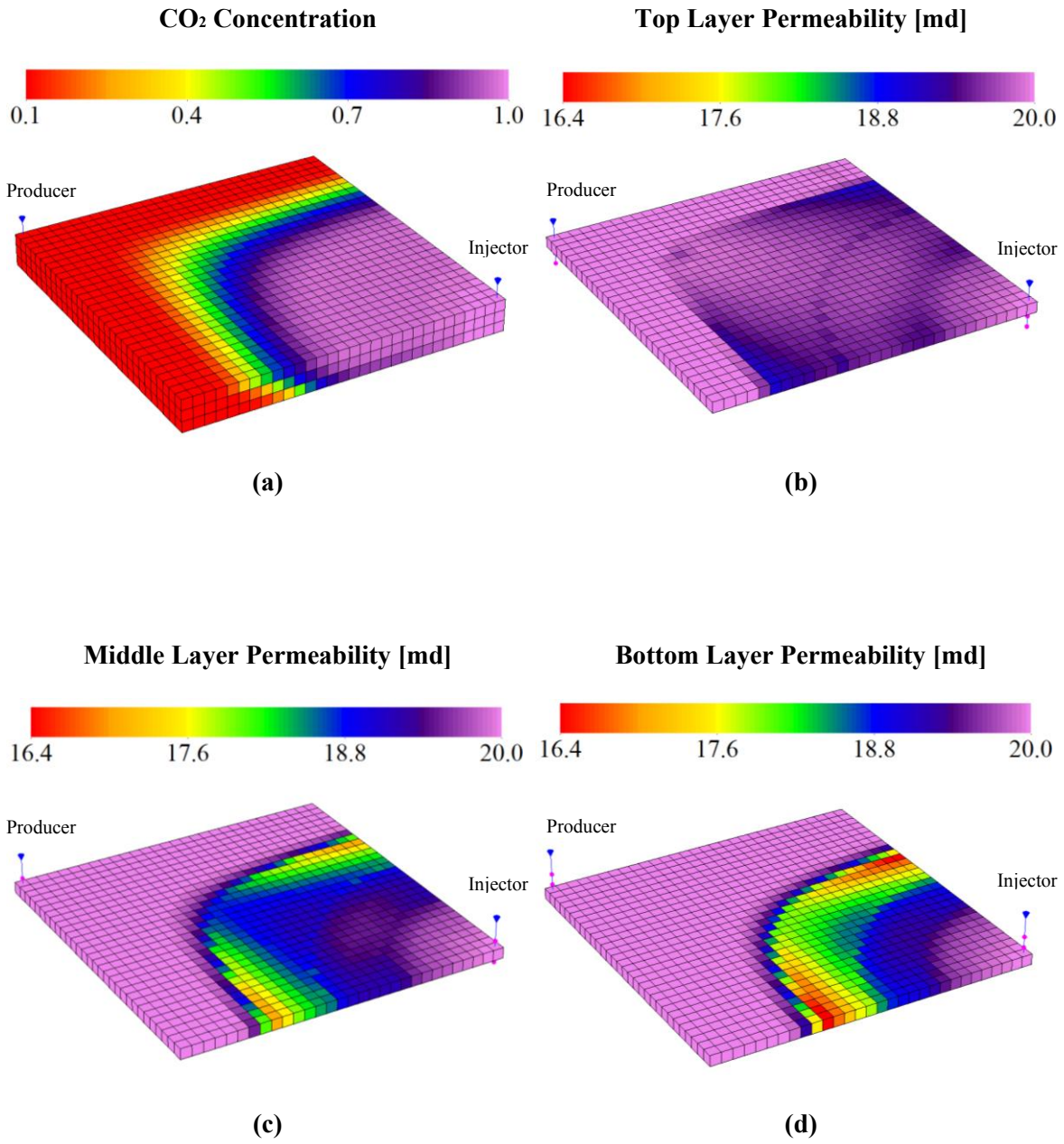


Figure 6.50 Results after 300 days of simulation for case 8: (a) CO₂ concentration, (b) top layer permeability, (c) middle layer permeability, and (d) bottom layer permeability maps.

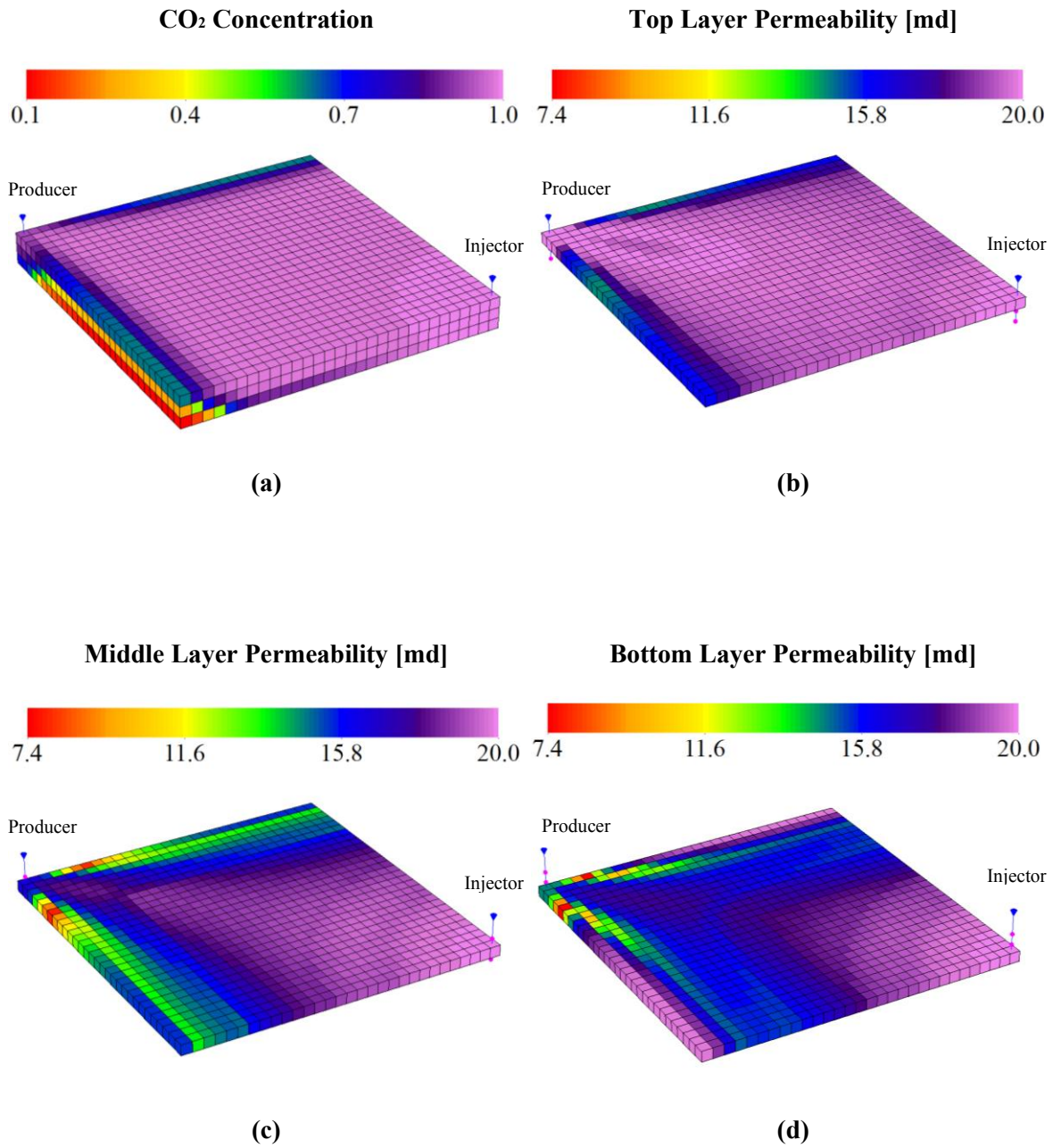


Figure 6.51 Results after 1000 days of simulation for case 8: (a) CO₂ concentration, (b) top layer permeability, (c) middle layer permeability, and (d) bottom layer permeability maps.

Chapter 7: Coupled Reservoir/ Wellbore Model

In this Chapter, a comprehensive thermal compositional coupled wellbore/reservoir simulator with the capability of modeling asphaltene phase behavior in the reservoir and in the wellbores is presented to address the wellbore/reservoir interaction, the effect of asphaltene deposition on the flow prediction and long-term reservoir performance. Indeed, the simulator models multiphase fluid flow in the reservoir and the wellbore to enable comprehensive production system analysis.

We present primary production and CO₂ flood simulation cases to investigate the effect of asphaltene deposition on oil recovery. Results show that injection of the light components into the reservoir significantly increases the instability of asphaltene components in the reservoir where they can precipitate further around the wellbore and in the wellbore. The precipitated asphaltene in the reservoir can be carried into the wellbore and be combined with excess asphaltene formation and deposit in the wellbore.

The materials presented in this chapter are the results of the joint work by me and Mahdy Shirdel, who graduated from The University of Texas at Austin in August, 2013 (Darabi et al., 2014). Shirdel's dissertation concentrated on asphaltene modeling in the wellbore (Shirdel, 2013).

7.1 INTRODUCTION

According to field reports (Leontaritis and Mansoori, 1988), asphaltene precipitation and deposition is a very serious problem that occurs during oil production and processing. Although the problem has been usually observed in the wellbore and the production system, asphaltene precipitation and deposition may occur anywhere in the reservoir-wellbore system, including near-wellbore region and inside the wellbore.

Therefore, a coupled wellbore-reservoir simulator is required to study asphaltene problem in a field. In the past, many researchers have performed experiments to understand the mechanism of asphaltene precipitation and deposition in the reservoir and the wellbore (Burke et al., 1990; Rassamdana et al., 1996; Hammami et al., 2000; Buckley, 2012). There are several standalone reservoir and wellbore simulators that are widely used to model asphaltene precipitation and deposition. However, to the best of our knowledge, application of coupled wellbore-reservoir simulator to model the entire process has not been fully addressed. In this chapter, we present a coupled wellbore-reservoir simulator that can model asphaltene precipitation and deposition due to pressure, temperature, and composition variations.

7.2 REVIEW OF WELLBORE MODELS

Asphaltene and wax precipitation in the tubing and surface facilities are the most common flow assurance issues during the production of hydrocarbon reservoirs. Applications of CO₂ and light hydrocarbon gas injection have also introduced additional issues to the asphaltene formation in the reservoirs as well as surface facilities (Tuttle, 1983). Several researchers have investigated the parameters affecting asphaltene precipitation and deposition in the production system; yet only few developed wellbore asphaltene simulators. Ramirez-Jaramillo et al. (2006) proposed a multiphase, multicomponent wellbore model to predict asphaltene deposition in the standalone wells. They discussed an asphaltene deposition model along with the effect of asphaltene particle on the rheology of the flowing fluid. Ramirez-Jaramillo et al. (2006) used asphaltene deposition models similar to wax deposition. Vargas (2009) developed a simulation tool that predicts the asphaltene precipitation and deposition in the pipelines.

In this model, a single-phase flow model was developed that accounts for the kinetics of asphaltene deposition, precipitation, and aggregation. Vargas (2009) showed fairly good agreement of the simulation results with test tube experimental data. Furthermore, Shirdel (2013) developed a fully compositional wellbore simulator that can model asphaltene precipitation and deposition in the wellbore. In this work, we use Shirdel (2013) wellbore model in our coupled wellbore-reservoir simulator to address the entire process from injection well to the producer.

7.3 WELLBORE MODEL

In this section, the overall procedure of the wellbore model, and the asphaltene deposition model in the wellbore will be presented.

7.3.1 Wellbore Simulator

The wellbore simulator used in this study was developed by Shirdel (2013) to model pressure and temperature distribution in multiphase flow, and flow assurance problems such as asphaltene, wax and scale deposition. In the current version of the wellbore model, N_c+6 transport equations are solved corresponding to N_c hydrocarbon components' mass conservations plus water and geochemical scale mass conservations, liquid momentum conservation, gas momentum conservation, and mixture energy conservation. Accordingly, hydrocarbon phases' velocities, water phase velocity, pressure, holdup, and temperature are solved as the primary flow variables.

Shirdel (2013) made the following assumptions to derive the governing equations:

- One-dimensional flow is assumed along the trajectory of the well in either horizontal, deviated, or vertical inclinations. This assumption is reasonable for the wellbores and pipelines with small diameter. Considering a long well in the order of 1000 ft with a small diameter in the order of 1 ft, one-dimensional assumption for the flow path is reasonable.
- Eulerian time and spatial averaging are applied.
- The liquid phase consists of oil/water mixture. In case, where water exists in the flow, liquid properties are calculated by volumetric and mass averaging between water and oil. This assumption is valid when the slippage between oil and water is negligible. For the cases where oil viscosity is not very large, no slip assumption is reasonable for the liquid mixture. However, for heavy oil systems the oil/water slippage should be considered.
- For the three-phase flow cases, oil/water slippage is included using a drift-flux correlation for the liquid mixture.
- In addition to source or sink mass flow rate, another term is also considered which is calculated by well indices values for each phase.
- Interface shear force, wall shear force, and spatial geometry of flow are modified for different flow regimes. A smooth transition is required for drag force changes in the momentum equations.
- Both gas and liquid phases have identical pressure and temperature. This is a reasonable assumption in many cases. In the cases that gas flow rate is not much larger than liquid, and gas expansion effect is not significant, temperature and pressure of different phases are approximately the same.
- Local thermodynamic equilibrium is considered between the phases. Compositional and black oil approaches are applied to calculate the fluid

properties and state relations. In fact, this assumption is reasonable as long as gas and liquid slippage effect is not very large.

Details of the wellbore model formulation can be found in Shirdel (2013) and Shirdel and Sepehrnoori (2009).

7.3.2 Deposition Model in the Wellbore

Asphaltene precipitation and flocculation models in the wellbore are the same as the reservoir models (see Chapter 5). One of the terms that appear in the compositional wellbore model equations is the solid particle deposition rate. Solid particle deposition in the flow stream consists of two steps. The first step is particles transportation from fluid bulk toward the wall surface, and the second step is the adhesion of the particles on the surface. Disregarding the electrostatic forces and thermophoresis effects between wall and particles, we have three different mechanisms for particles transportation from the fluid bulk toward the wall. Shirdel (2013) defined these mechanisms as diffusion, inertia, and impaction.

The diffusion mechanism becomes dominant for small particles (usually, less than 1 μm). In this mechanism, the particles' stopping distance is small. Hence, the particles are carried by Brownian motion of the fluid molecules, and transferred to the wall. By increasing particle size, the inertia effect is also incorporated in the deposition process. In this mechanism, the particles can obtain sufficient momentum by turbulent eddies to reach the wall. Finally, for the large particles size, the impaction mechanism is dominant. In this mechanism, the stopping distance is of the same order as the pipe diameter where we may observe solid slugs flow. In addition, the particles no longer respond to the

turbulent flow eddies. Figure 7.1 shows the schematic view of the different deposition mechanisms.

Considering particles transportation and adhesion probability effects, the complete equation for particle deposition flux becomes

$$\dot{m}_d = K_t SP (C_b - C_s). \quad (7.1)$$

In Equation (7.1), K_t is a global mass transfer coefficient which considers the macroscopic (convective) and microscopic (molecular diffusion) mechanisms, SP is sticking probability and $(C_b - C_s)$ is the concentration gradient between the fluid bulk and the wall surface.

Many researchers such as Lin et al. (1953), Friedlander and Johnstone (1957), Beal (1970), Davies (1983), and Escobedo and Mansoori (1995) use the classical approach to calculate K_t . However, several other researchers, like Hutchinson et al. (1971), and Cleaver and Yates (1975) use stochastic approaches to estimate K_t . In the development of the deposition model, Shirdel (2013) considered both approaches to allow different options to tune the particles deposition rate.

For the sticking probability factor, Watkinson (1968) also introduced an expression as follows:

$$SP \propto \frac{\text{Adhesion Force Between Particles and Wall}}{\text{Drag Force on Particles on the Surface}}. \quad (7.2)$$

Assuming an Arrhenius-type expression and using the drag coefficient to calculate the adhesion force and the drag force, respectively, we can show that SP is

$$SP = S_0 \frac{F_0 e^{(-E_a/RT_s)}}{C_D A_p \rho_p V_{avg}^2} = k_d \frac{e^{(-E_a/RT_s)}}{V_{avg}^2}. \quad (7.3)$$

In the above equation, k_d and E_a can be tuned by experimental data.

Moreover, the deposited solid can also be removed from the surface of the well due to shear forces. For this reason, the rate of solid deposit removal is defined as

$$\frac{d\delta}{dt} = k_r \delta \tau^a, \quad (7.4)$$

where δ is the asphaltene deposit thickness, k_r is the shear removal factor, τ is the shear stress, and a is the shear coefficient. Removed solid thickness can be converted to the removed mass as

$$\dot{m}_r = \pi D \frac{d\delta}{dt} dz \rho_s. \quad (7.5)$$

Attachment and detachment of solid on the surface of the well can also change the roughness of the well surface. Increasing the roughness can contribute to more pressure drop in the wellbore, especially in the turbulent flows. In the deposition model, to incorporate the roughness effect, Shirdel (2013) considered the roughness of contaminated zones by solid deposits as a user defined value.

7.4 WELLBORE/RESERVOIR COUPLING APPROACH

In the literature, two different approaches have been introduced for wellbore-reservoir coupling. One method is the iterative explicit coupling, where the wellbore and

reservoir systems are solved separately. The other method fully couples the wellbore and reservoir systems.

In the iterative method, the reservoir and wellbore pressure results are iteratively conveyed to each system, along with calculation of productivity indices, to obtain the influx/outflux rates to the wellbore. One of the advantages of the iterative coupling is that the wellbore model can be coupled to any reservoir simulator.

In fully coupled wellbore-reservoir simulations, wellbore and reservoir models are simultaneously solved. Behie et al. (1985) explained a mathematical approach to solve a modified Jacobian matrix in the case where the well crosses multiple blocks of the reservoir grid. They did not present the wellbore model to calculate the perforation pressure. However, they discussed a method to implement a fully coupled wellbore-reservoir system. They claimed that the fully coupled method was more stable than the explicit wellbore pressure coupling.

In our study, we apply explicit coupling scheme for our wellbore/reservoir model. The communicating parameter between wellbore and the reservoir is the rate for mass influx/out-flux.

We define the influx parameters as ψ_{jk} , which is the component k in phase j mass flux per unit length of the cell. This parameter is calculated as below:

$$\psi_{jk} = PI_j \rho_j \frac{Mw_k}{Mw_j} x_{jk} (P_{res} - P), \quad (7.6)$$

where PI_j is the productivity index of each phase (water, oil and gas). This parameter is calculated as follows for the coupled wellbore/reservoir model:

$$PI_j = \frac{2\pi\sqrt{k_x k_y} \Delta z}{0.15802 \left(\ln \frac{r_o}{r_w} + S \right)}, \quad (7.7)$$

where r_o is the equivalent radius of well block which is calculated by either Peaceman (1983) or Babu and Odeh (1989) models for vertical and horizontal wells, k_x and k_y are the permeability in x and y directions, Δz is the grid-block size, r_w is the wellbore size in perforation zone, and S is the skin factor. Asphaltene plugging in the perforation zones also changes r_w in the productivity index calculation.

Other issues remaining in the explicit coupling of wellbore and reservoir simulators are the time-step sizing and tight coupling for the convergence of both systems. Since the time-step sizes in the transient wellbore models are very small (in order of several seconds) in comparison to the reservoir models, synchronization between these two domains is necessary. For this purpose, an additional criterion is included in the time-step control method of both models to select the minimum time-step sizes of all calculations. Thus, for the coupled transient wellbore model time-step sizes are in the order of several seconds at the beginning of the simulation.

Moreover, for steady-state wellbore model coupling, an iterative solution must be used to match large time-step sizes in the simulation. The reservoir simulator is an IMPEC simulator. For this reason, convergence issues may occur if the wellbore model is not tightly coupled. In our tight coupling, we perform iterations for pressure solution with the new feeds of wellbore model. In fact, the solution of wellbore model changes the bottom-hole pressure of the well and the amount of influx. Several iterations should be performed until complete convergence is observed for both wellbore and reservoir systems mass influx/outflux. Our experience shows that without tight coupling the

reservoir time-steps should be very small to overcome the numerical instabilities. Otherwise, oscillatory results are obtained, which may stop the simulation progress.

7.5 RESULTS OF COUPLED WELLBORE/RESERVOIR MODEL

In this section, we present primary production and CO₂ injection simulation case studies to investigate the effect of pressure, temperature, and composition variations on asphaltene deposition in the reservoir and the wellbore. We use the Middle East crude oil composition presented in Chapter 6 in our simulation case studies (See Tables 6.1 through 6.3).

Case 1: Primary Production Case Study. In this case, we investigate asphaltene deposition in the reservoir and wellbore for initial oil composition during primary production. Table 7.1 presents the simulation input data. We assume a quarter of five spot with 20×20×3 grid-blocks, which the injection well is shut-in. Figure 7.2 shows our reservoir model. The initial pressure of the reservoir is 4000 psi, and the production well operates at a constant wellhead pressure of 2000 psi. We maintain the wellhead pressure of around 2000 psi to avoid gas production due to bubble point flash. The initial horizontal permeability of the reservoir is 20 md and the initial porosity is 0.3. Figure 7.3 also shows the water and oil relative permeability curves for primary production. The initial wellbore tubing diameter is 3 inches and wellbore length is 5000 ft. In our simulation, we monitor the behavior of asphaltene in the entire reservoir-wellbore system for 6 months of production.

Figures 7.4(a) and 7.4(b) show asphaltene deposition and permeability map, respectively at the end of 6 months of production. As can be seen, there is no asphaltene

deposition in the reservoir in this period, and the absolute permeability of the reservoir remains constant. Since the reservoir grid-blocks pressure never falls inside the asphaltene precipitation envelope, we do not observe asphaltene in the reservoir. However, if we change the producer operating condition we may have asphaltene deposition in the reservoir.

Figures 7.5(a) through 7.5(e) show the pressure, temperature, oil superficial velocity, asphaltene concentration, and asphaltene thickness profiles along the wellbore at the 1, 10, 50, and 100 days of simulation, respectively. Figure 7.5(a) shows that pressure profile linearly changes from top to the bottom of the well and the bottom-hole pressure increases about 100 psi after 100 days. Figure 7.5(b) shows that temperature does not significantly change along the wellbore initially; however, after 100 days wellhead temperature drastically drops from 212 °F to 95°F. Figure 7.5(c) shows oil superficial velocity profiles after 1, 10, 50, and 100 days of simulation. At the early stages of production, the oil superficial velocity is very large (4.5 ft/sec) along the wellbore. After 10 days the shape of the velocity profile starts to change. The velocity is higher at the top and then smoothly declines to the lower part of the well. In addition, the velocity decreases in front of the perforation zone. In 100 days, the velocity profile decreases significantly in the perforation zone and then drastically increases to a maximum value of about 3 ft/sec at the depth of 2000 ft. In Figure 7.5(d), we observe the asphaltene precipitates concentration from surface to a depth around 4000 ft. We do not have any asphaltene precipitation between 4000 ft and 5000 ft and around the perforation zone. Finally, asphaltene partially deposits in the upper part of the well and starts to change the inner diameter of the tubing. Figure 7.5(e) shows the tubing inner radius at different simulation times. As can be seen, after 50 days the inner diameter has decreased to about half of the initial diameter of the pipe and then it decreases more in the depth interval

between 0-4500 ft. In our model, we consider the effect of detachment of asphaltene solids due to shear stress. Therefore, at some point the deposition rate and the detachment rate can balance out the change of inner radius diameter. For this reason, the maximum tubing radius reduction is not necessarily where the maximum asphaltene concentration is.

Asphaltene deposition in the wellbore is a dynamic process in that every parameter can influence the trend of the entire process and the performance of the production system. For instance, when the fluid conditions fall in the asphaltene precipitation window, it continues with deposition process and changes the wellbore diameter. At the same time, diameter change affects the wellbore hydraulics pressure and velocity profiles. Consequently, energy balance is also affected by wellbore hydraulics and fluid velocity profiles. These sequences of change can potentially feed back to the asphaltene phase behavior as well.

Figures 7.6 through 7.8 were plotted to compare the oil production rate, bottom-hole pressure, and cumulative oil production of our model in the presence and in the absence of the asphaltene deposition. The blue lines are the results of our simulation if no asphaltene precipitates and deposits exist in the reservoir and wellbore. The red lines are the results of our simulation when we consider asphaltene precipitation and deposition in the entire system. The black lines are the results for the cases that we perform workover job in the producer after 50 days. One of the practical methods in the field to reduce asphaltene problems in the producers is using scraper to clean the wellbore. In our simulation case study, we could successfully assign a workover schedule at 50 days to the producer to shut down the well for one day and clean the wellbore, and put the well back on operation.

Figure 7.6 compares the oil production between the three mentioned scenarios. As can be seen, the producer dies earlier due to asphaltene deposition compared to the well with cleaning job or well without asphaltene deposition problem. Figure 7.7 shows that in the case of no asphaltene deposition, the bottom-hole pressure slightly decreases (3290 psi to 3250 psi over six months) due to friction loss; however, in the case of asphaltene deposition bottom-hole pressure increases drastically with time. At early stages of production, when only a thin asphaltene layer is deposited on the surface of the wellbore, bottom-hole pressure decreases slightly which means that the asphaltene layers has no (or very low) effect on the bottom-hole pressure and oil production rate. As time progresses (after 20 days of production), the deposited asphaltene layer grows very rapidly as discussed earlier. Therefore, bottom-hole pressure increases quickly, and reaches up to 3370 psi. If we perform a workover procedure to completely cleanup the well after 50 days we observe that we can prevent or delay the increment of the bottom-hole pressure for several months. Finally, Figure 7.8 compares cumulative oil production for the three cases. It is shown that oil recovery can be decreased up to 16 %, only because of asphaltene deposition. Moreover, with workover job and cleaning the producer we can save about 52 % of the oil that would be lost without workover.

Furthermore, Figure 7.6 shows that there is a jump in oil production right after workover job. Corresponding to this jump in production, there is a jump in bottom-hole pressure when dropped from 3300 psi to 3250 psi. The reason for this jump could be (1) the radius of the wellbore increases suddenly because of the workover job, and therefore oil production increases. (2) The accumulated oil bank around the producer is released when the flow path is cleaned.

To observe the reservoir response to the asphaltene deposition in the wellbore we plot the reservoir pressure profiles in Figure 7.9. Figure 7.9(a) shows the pressure map of

the reservoir when we have no workover job. As can be observed, well-block pressure increases due to an increase in bottom-hole pressure. After 100 days, the reservoir is almost stabilized around 3400 psi, and it is shown in Figure 7.6 that the oil production approaches zero. Figure 7.9(b) shows the pressure map of the reservoir when we have asphaltene workover job after 50 days of production. In this figure, we observe that after 50 days pressure is released from the reservoir. However, the well-block pressure increases again after 100 days because of the formation of asphaltene in the wellbore for the second time. In this case, the reservoir is stabilized around 3340 psi after 100 days of production, which is lower than 3400 psi (no workover case). We suggest that a second workover job is required to deplete the reservoir more using the existing operating condition.

Case 2: CO₂ Injection Case Study. In this case, we investigate the effect of composition variation on asphaltene deposition during CO₂ flooding. The reservoir input data and water and oil relative permeability curves are the same as in case 1. We use the Corey model with exponents equal to one for our gas relative permeability curves. The residual gas saturation is zero and the gas end point relative permeability is one. After 100 days of primary production, we start CO₂ injection (see Figure 3(a)). The injection well operates at a constant wellhead pressure of 3400 psi. Since asphaltene plugs the wellbore and kills the production well, we set up a workover schedule for the producer. Whenever the radius of the wellbore of producer falls below a critical radius (half of the initial radius), we shut in the well for one day, and clean up the asphaltene, then we put the production well on the operation.

CO₂ breakthroughs in the producer after about 700 days of injection (800 days of simulation). Figures 7.10 and 7.11 show CO₂ concentration, asphaltene precipitation,

asphaltene deposition, and permeability maps of the reservoir after 300 days and 800 days of simulation. The unit for asphaltene precipitation and deposition is $[\text{ft}^3/\text{ft}^3]$, which is volume of asphaltene per pore volume of the grid-block. As can be seen, asphaltene precipitation occurs in the small interface region of the CO_2 front. However, asphaltene deposits on the rock surface between the injection well-block and the front. The amount of deposition is low around the injection well, and increasingly higher toward the front. Asphaltene deposition reaches the maximum in the front sides closer to the reservoir boundaries. Comparing the amount of asphaltene deposition in the front for various simulation times (300 days and 800 days), we observe that the amount of deposition is higher at 800 days. As can be seen, there is an elliptical zone close to the producer at 800 days of simulation where asphaltene deposition is very low compared to its surrounding. Moreover, we observe that the permeability reduction in the reservoir is in correspondence to the asphaltene deposition.

Asphaltene precipitation and deposition in the reservoir are dynamic processes in that many parameters can affect their trend. In the region between front and the producer, the oil composition is similar to the initial composition. Therefore, like the primary production case, no asphaltene precipitation occurs in this region. In the small region before the front, CO_2 dissolves in the fresh oil and increases the asphaltene onset pressure. In the region between injector and the front, asphaltene concentration is very low because asphaltene particles have been carried away by the moving front. In addition, in the region behind the front, the offset pressure is very high with respect to the original oil composition and no further asphaltene will precipitates in this region. Since asphaltene deposition is a time dependent process, the velocity of the front dictates the asphaltene deposition profile in the reservoir. Around the injection well, the amount of deposition is minimum because of the fast movement of the front. As we move away

from the injector, the front velocity decreases and more asphaltene deposits on the rock surface. The maximum amount of deposition is at the front sides near the reservoir boundaries, where the front movement is very low. The low asphaltene deposition in the elliptical region before the production well can be explained by very high front velocity at that area during breakthrough of CO₂.

Figure 7.12 shows CO₂ concentration and permeability maps of the reservoir after 900 days of simulation (100 days after breakthrough). We observe that, after the breakthrough, asphaltene deposition and permeability reduction occur mostly around the producer well and close to the reservoir boundaries.

Before breakthrough of CO₂, the composition of the fluid in the wellbore is similar to the initial composition. Therefore, asphaltene precipitation and deposition occurs because of pressure and temperature variations, similar to the primary production case. However, after the breakthrough, composition variation affects asphaltene precipitation and deposition. We performed an asphaltene cleaning workover job at the breakthrough time (800 days of simulation), and monitored the behavior of asphaltene along the wellbore after the well was put back on operation. Figures 7.13(a) through (e) show the pressure, temperature, oil superficial velocity, asphaltene concentration, and asphaltene thickness profiles along the wellbore at the 800, 850, and 900 days of simulation, respectively. Figure 7.13(a) shows that pressure profile linearly changes from the top to the bottom of the well and remains almost constant after 100 days of breakthrough. Figure 7.13(b) shows that temperature does not considerably change along the wellbore at early stages; however, after 100 days wellhead temperature drastically decreases to 125°F. In addition, there is a bump in the temperature profile in 850 days of simulation at around 3600 ft. In Figure 7.13(c), we observe that oil superficial velocity is very high initially (4 ft/sec); however it drastically drops (lower than 1 ft/sec) along the

wellbore after 50 days. Figure 7.13(d) shows that initially asphaltene precipitates from the bottom of the producer to a depth around 4000 ft. We do not have any asphaltene precipitation between the surface and depth of 4000 ft. After 50 days, we observe an asphaltene precipitation profile from the surface to a depth around 1000 ft, and no asphaltene precipitation is observed below this depth. After 100 days, no asphaltene precipitation exists along the wellbore. Figure 7.13(e) shows the tubing inner radius at different simulation times. We observe that a thin layer of asphaltene deposits in front of the perforation zone at early stages. As time progresses, a thicker deposition layer grows in the top section of the wellbore, above 1000 ft. As can be seen, the inner diameter of the wellbore dropped by about 30 % of its initial diameter after 100 days.

To explain the dynamic behavior of asphaltene along the wellbore, we should consider the effects of temperature, pressure, composition variation, oil velocity, and the reservoir effects. After breakthrough, the oil that flows from the reservoir into the wellbore has already lost some of its asphaltene content in the reservoir. Severe drop in temperature, and pressure and the bump in the temperature profile are due to the release of gas from oil. Because of the huge temperature drop, in 850 days, the top section of the reservoir falls inside the precipitation envelope. However, in 900 days, CO₂ concentration increases significantly, and no asphaltene precipitates long the wellbore. Because of high oil velocity, asphaltene deposition is low initially; however, asphaltene deposition rate significantly increases by time due to the huge drop in oil velocity.

Figures 7.14 and 7.15 compare the oil production rate and cumulative oil production in the presence and in the absence of asphaltene deposition after the breakthrough of CO₂. The blue lines are the results of our simulation if no asphaltene precipitates and deposits in the reservoir and wellbore. The red lines are the results of our simulation when we consider asphaltene precipitation and deposition in the reservoir and

ignore asphaltene deposition in the wellbore. The black lines are the results of our simulation when we consider asphaltene precipitation and deposition in the entire system. We observe that cumulative oil production decreases up to 12 % because of the combined effects of asphaltene deposition in the wellbore and in the reservoir. Ignoring asphaltene deposition in the wellbore, we observe that cumulative oil production decreases up to 10 % because of asphaltene deposition in the reservoir. In other words, this indicates that even if we perform an asphaltene cleaning workover job in the wellbore, we still have at least 10 % drop in cumulative oil production. In this case, clean up of the asphaltene is not very helpful, since the reservoir is already damaged.

7.6 SUMMARY AND CONCLUSIONS

We developed a comprehensive thermal compositional coupled wellbore/reservoir simulator, specifically to monitor asphaltene behavior in the wellbore/reservoir system. This coupled wellbore/reservoir simulator is able to handle the effects of pressure, temperature, and composition variations on asphaltene precipitation and deposition. We model asphaltene precipitation using a solid model, and flocculation using a reversible chemical reaction. In the reservoir, we consider asphaltene deposition, wettability alteration, and porosity and permeability reduction. In the wellbore, we consider multiphase flow and asphaltene deposition in different flow regimes in the tubing. We presented primary production and CO₂ injection simulation case studies to investigate the effect of pressure, temperature, and composition variations on asphaltene deposition in the reservoir and in the wellbore. We characterized a Middle East crude oil to use in our simulation case studies. In the primary production case, asphaltene was not produced in the reservoir, while the oil recovery decreased up to 16 % because of asphaltene

deposition in the wellbore. An asphaltene cleaning workover job saved about 50 % of the loss in oil recovery due to asphaltene deposition. In the CO₂ injection case study, we observed a 10 % loss in the cumulative oil recovery after the breakthrough because of asphaltene deposition in the reservoir. Additional 2 % drop in cumulative oil production was observed because of wellbore related asphaltene problems.

We summarize the conclusions of this chapter as follows:

1. The behavior of asphaltene in the wellbore and reservoir are fully coupled with each other. Therefore, a standalone reservoir or wellbore simulator is not able to predict the asphaltene behavior properly in the entire system.
2. Asphaltene precipitation and deposition in the wellbore and reservoir is a dynamic process. Many parameters, such as oil velocity and pressure, temperature, and composition variations influence the trend of these processes. Hence, the asphaltene model should be comprehensive to consider the combined effects of these important parameters on the asphaltene behavior.
3. The coupled wellbore/reservoir simulator is able to aid in selecting asphaltene inhibition and remediation strategies. For example, when the problem in the well is pronounced, asphaltene cleaning workover job might be very useful. In this case, we can optimize the place and the time that a workover job would be needed to maximize the oil production, save us a lot of time and money. However, when the source of the problem is the reservoir, the asphaltene cleaning workover job in the wellbore is not effective, and we need to use other inhibition and remediation techniques (such as chemical injection).

4. During CO₂ flooding, asphaltene precipitation occurs mostly at the front, and asphaltene deposition is at its maximum where the front velocity is at its minimum.

Table 7.1 Simulation input data.

Parameter	Value
Number of grid-blocks	20×20×3
Reservoir dimension	400 ×400×60 ft ³
Reservoir temperature	212 °F
Initial water saturation	0.2
Initial reservoir pressure	4000 psi
Well-head pressure	2000 psi
Porosity	0.2
Horizontal permeability	20 md
Vertical permeability	1 md
Wellbore radius	0.11 ft
Wellbore length	5000 ft
k_{ef}	8 day ⁻¹
k_{fc}	0
g	7
α	5 day ⁻¹
β	0
γ	1 ft ⁻¹

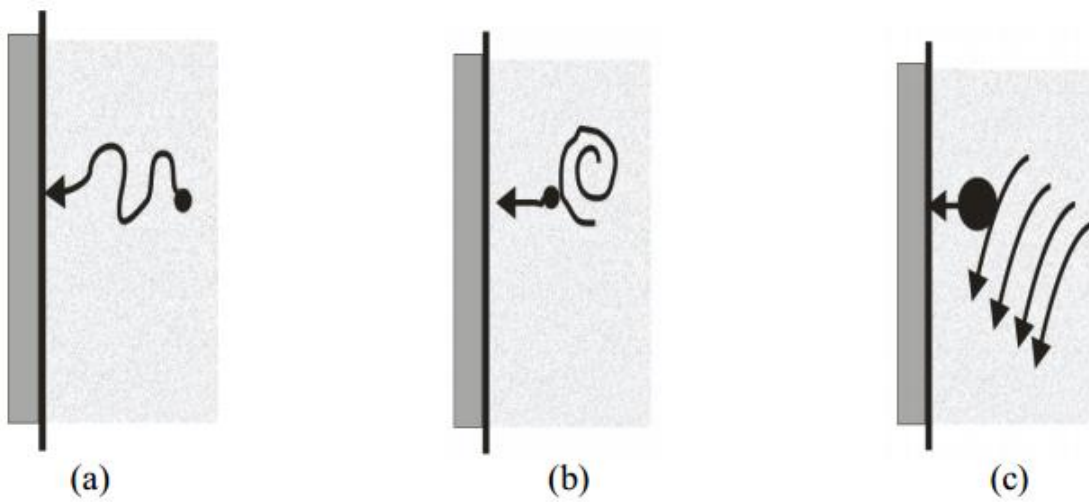


Figure 7.1 Schematic views of the deposition mechanisms: (a) diffusion, (b) inertia, and (c) impaction.

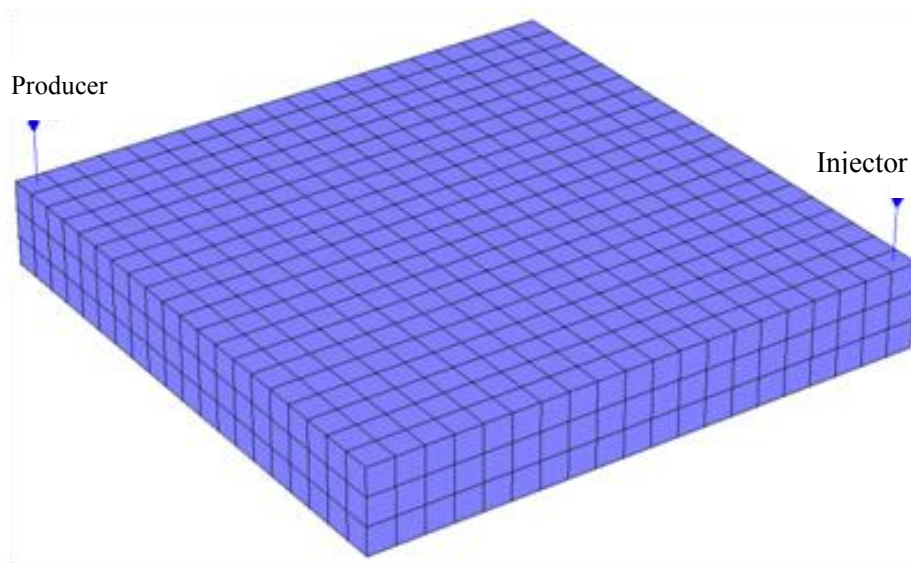


Figure 7.2 Illustration of the reservoir model.

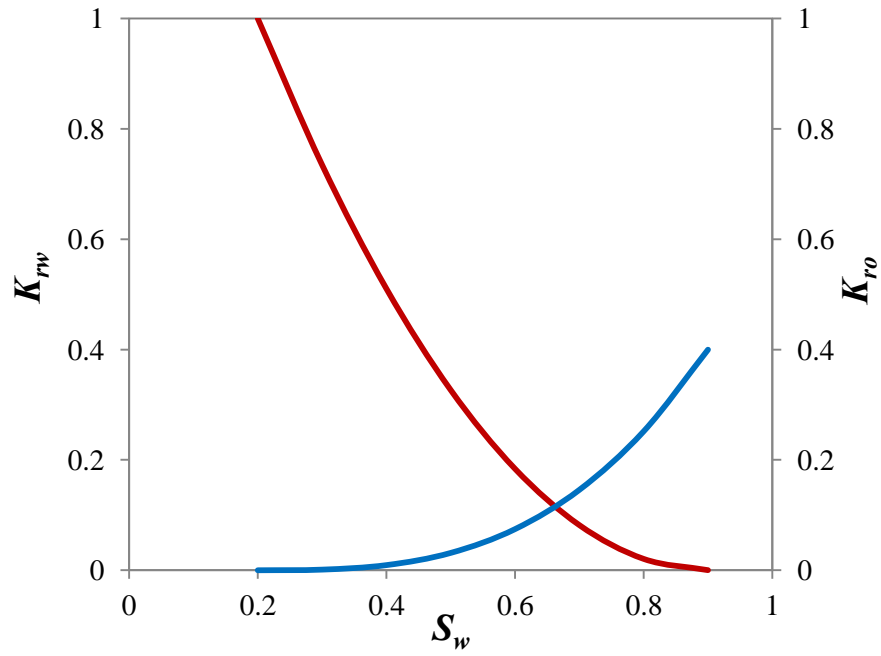


Figure 7.3 Oil and water relative permeability curves.

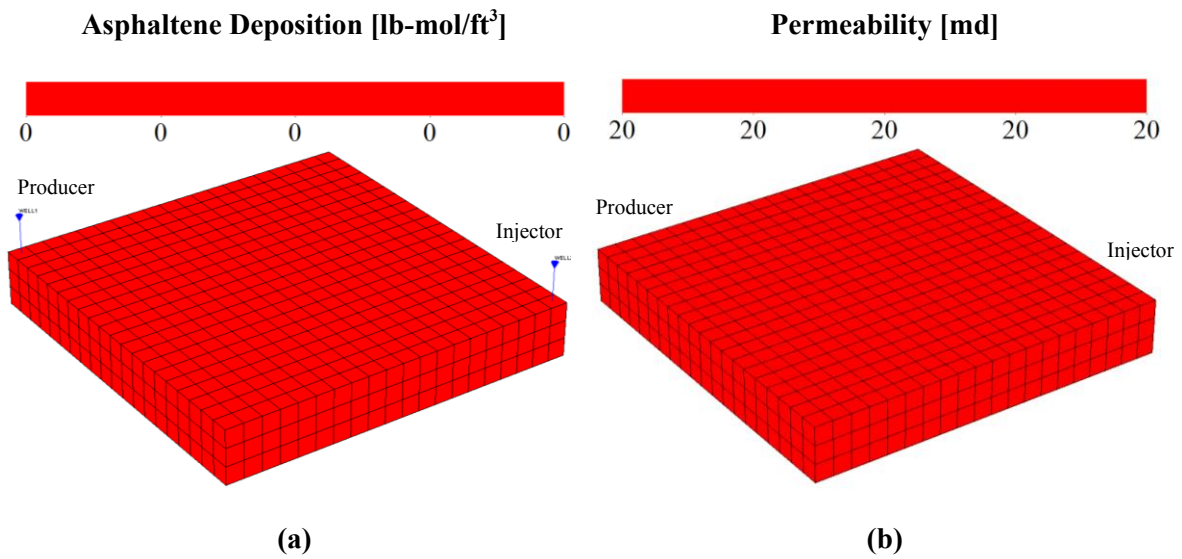
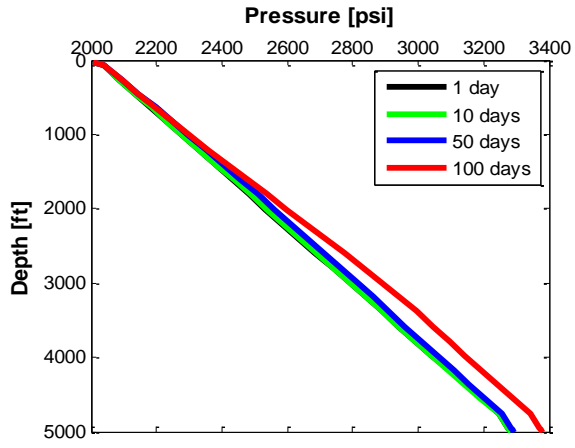
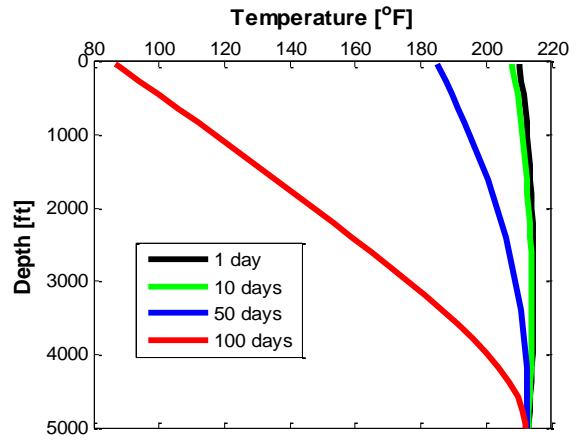


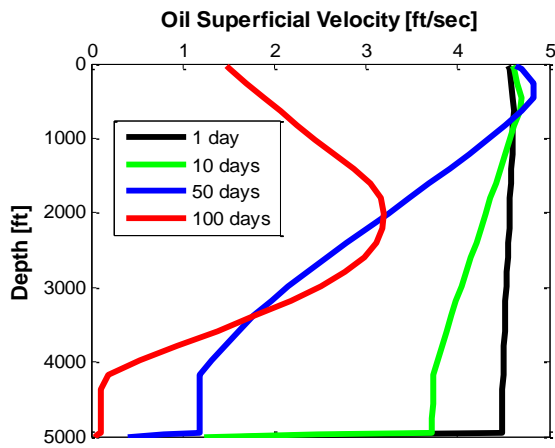
Figure 7.4 (a) Asphaltene deposition and (b) permeability maps after 6 months in the reservoir.



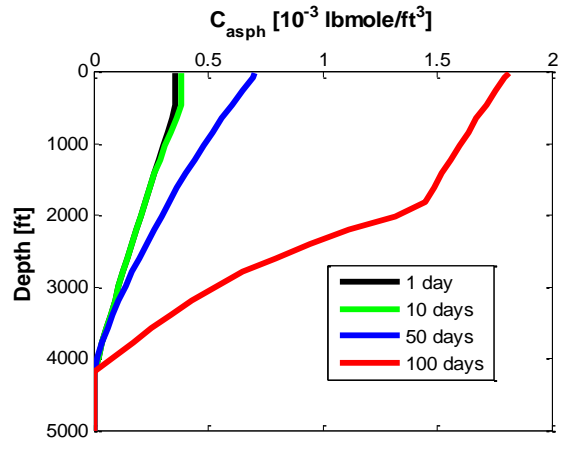
(a)



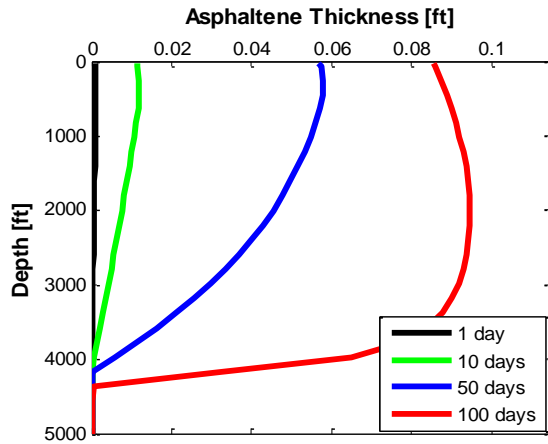
(b)



(c)



(d)



(e)

Figure 7.5 (a) Pressure, (b) temperature, (c) oil superficial velocity, (d) asphaltene concentration, and (e) asphaltene thickness profiles in the wellbore after 1, 10, 50, and 100 days of simulation.

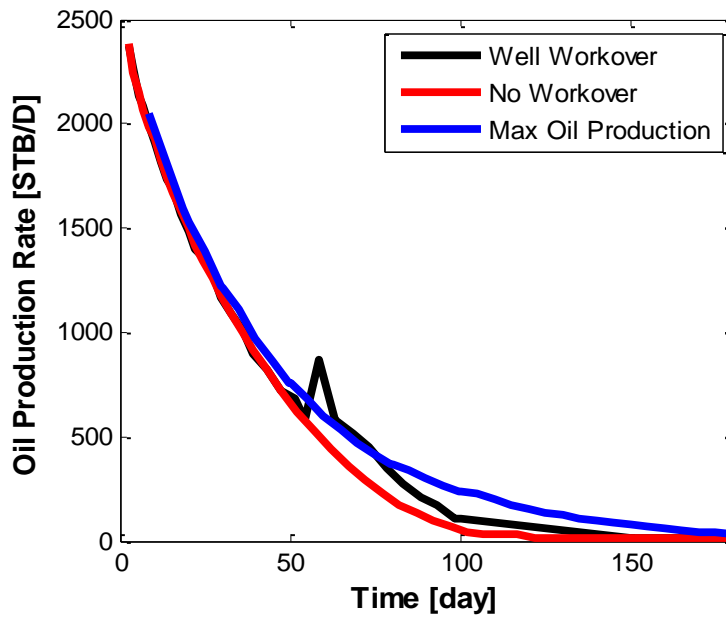


Figure 7.6 Oil production rates over six months of production.

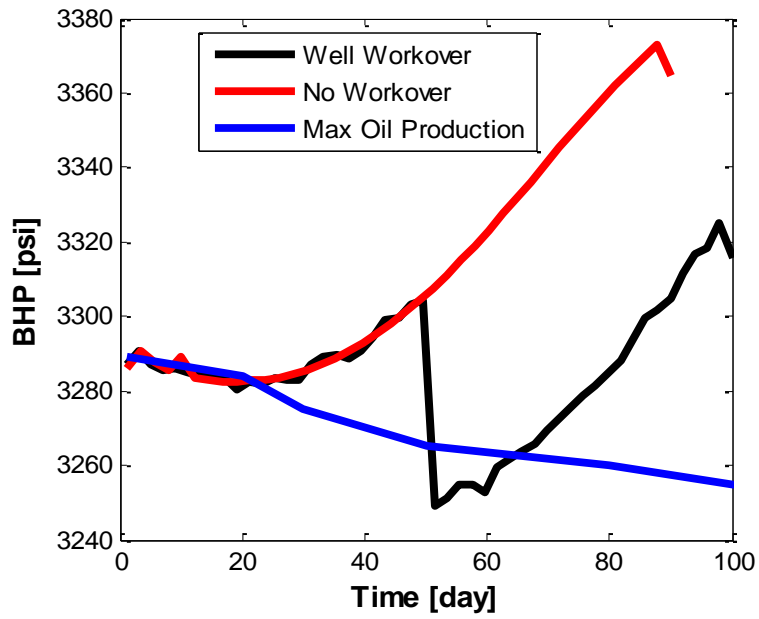


Figure 7.7 Bottom-hole pressures over six months of production.

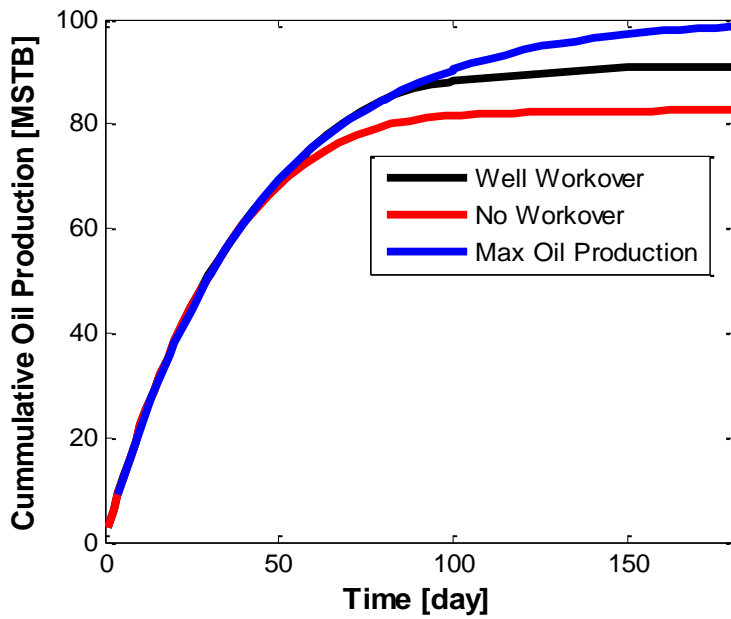


Figure 7.8 Cumulative oil productions over six months of production.

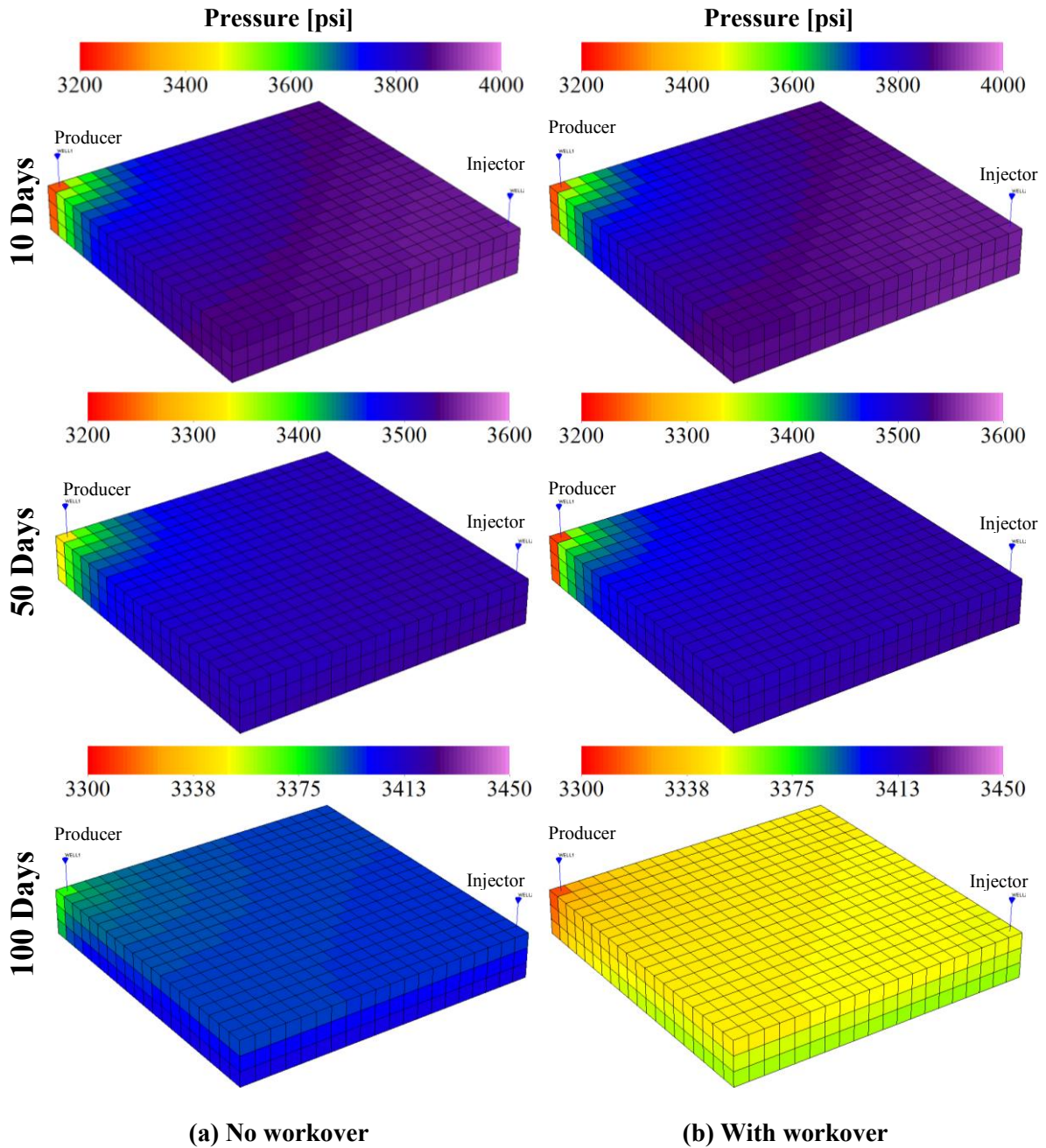


Figure 7.9 Pressure response of the reservoir because of asphaltene deposition in the wellbore after 10, 50, 100 days of production; (a) no workover, (b) with workover.

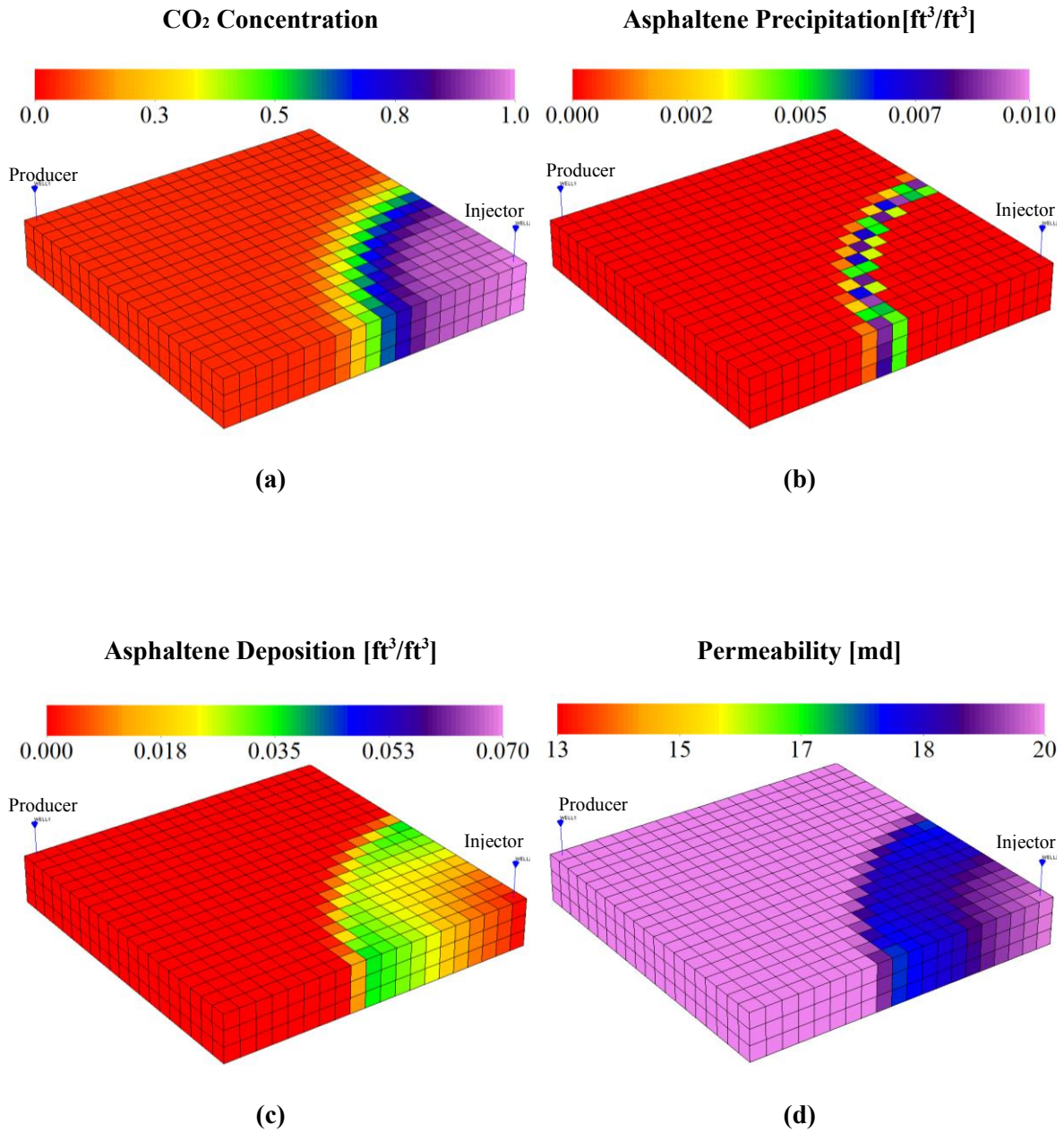


Figure 7.10 (a) CO₂ concentration, (b) asphaltene precipitation, (c) asphaltene deposition, and (d) permeability maps of the reservoir after 300 days of simulation.

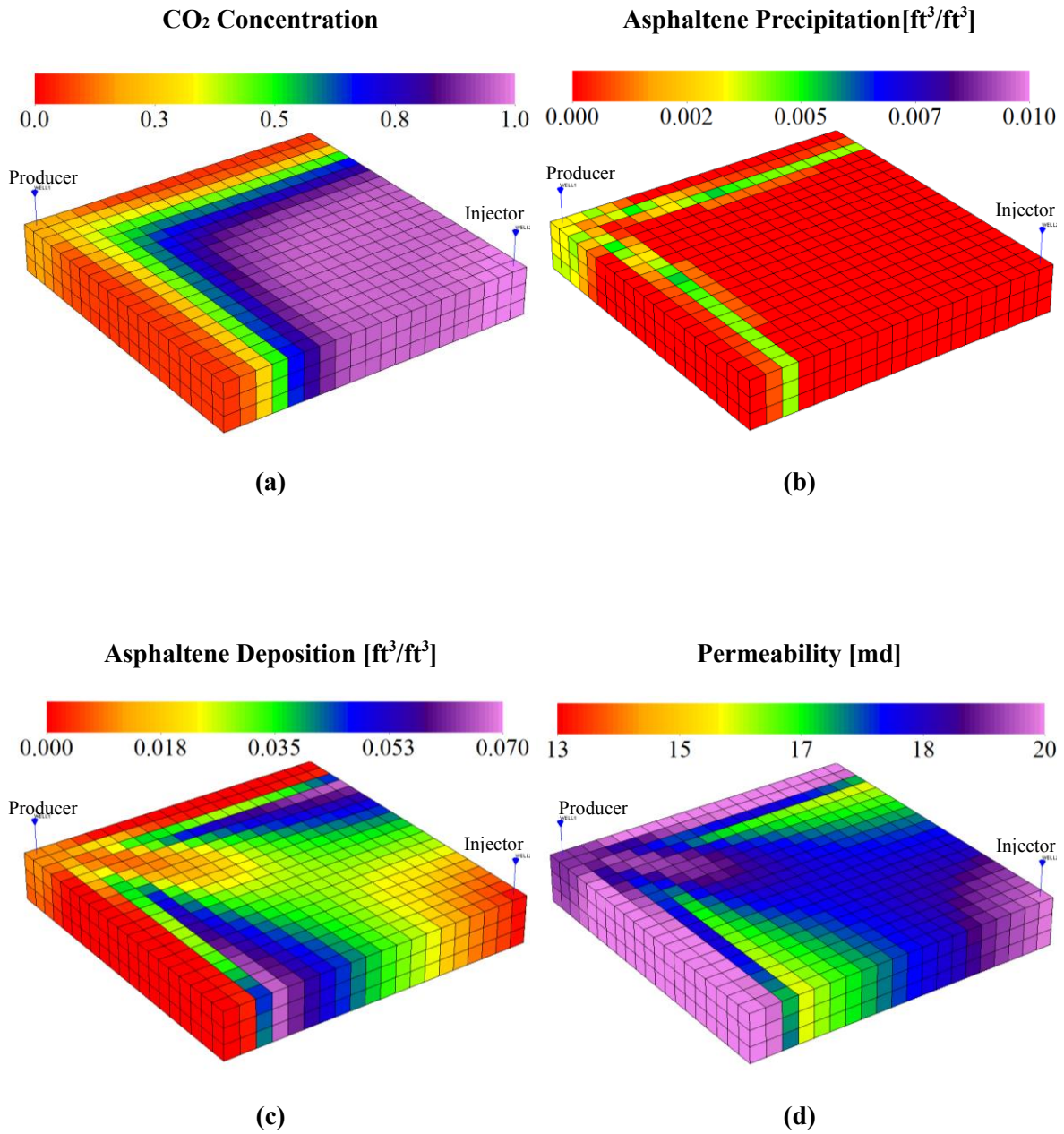


Figure 7.11 (a) CO₂ concentration, (b) asphaltene precipitation, (c) asphaltene deposition, and (d) permeability maps of the reservoir after 800 days of simulation.

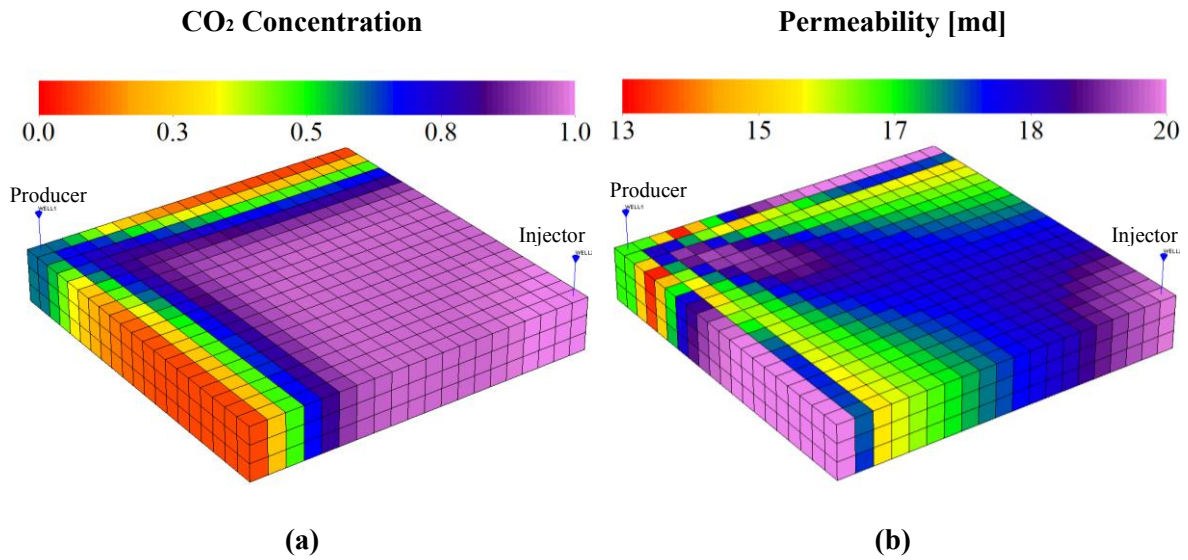
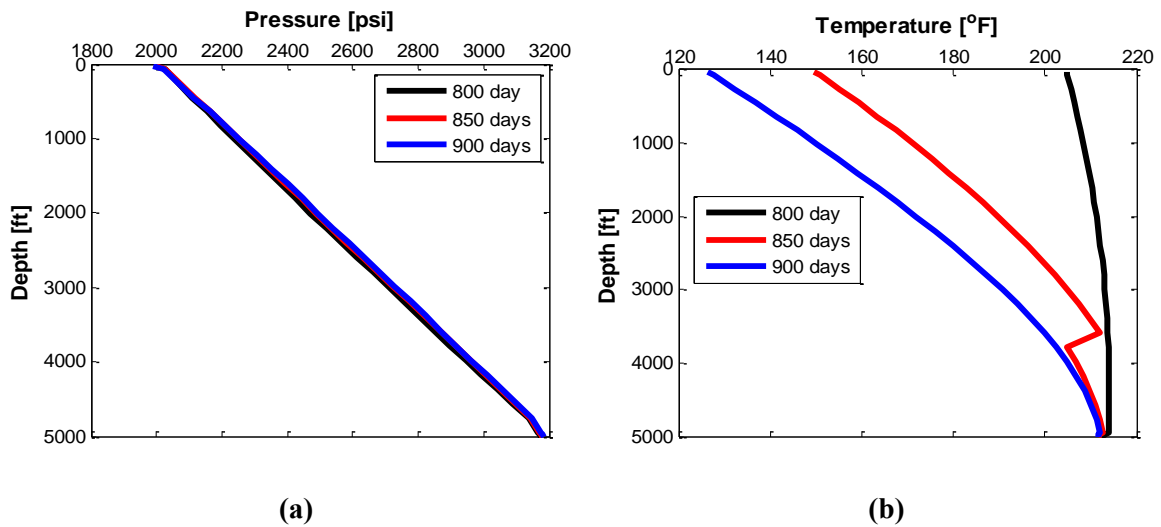
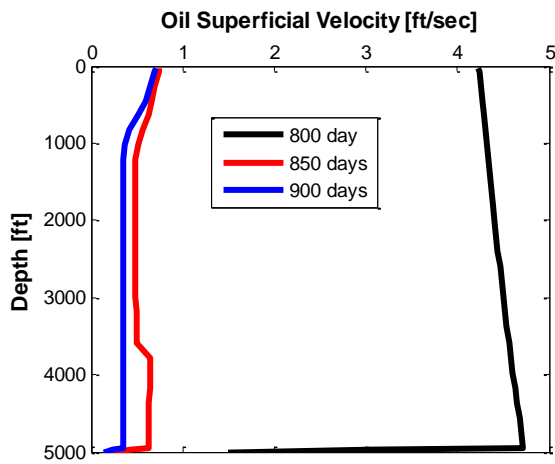
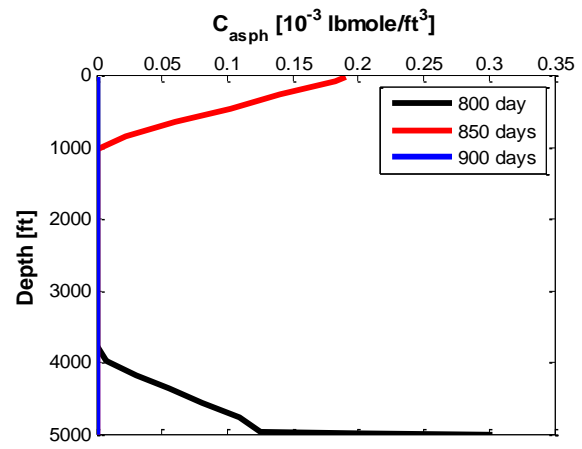


Figure 7.12 (a) CO₂ concentration and (b) permeability maps of the reservoir after 900 days of simulation.

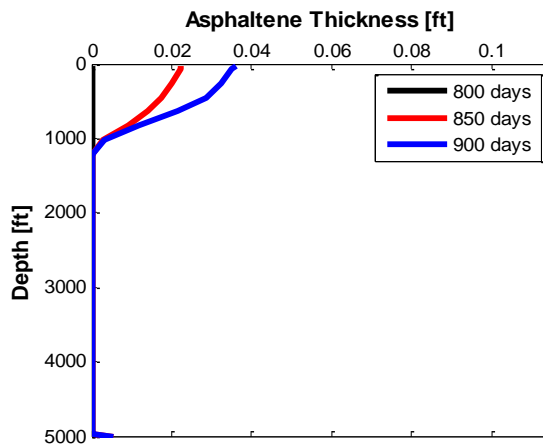




(c)



(d)



(e)

Figure 7.13 (a) Pressure, (b) temperature, (c) oil superficial velocity, (d) asphaltene concentration, and (e) asphaltene thickness profiles in the wellbore after 800, 850, and 900 days of simulation.

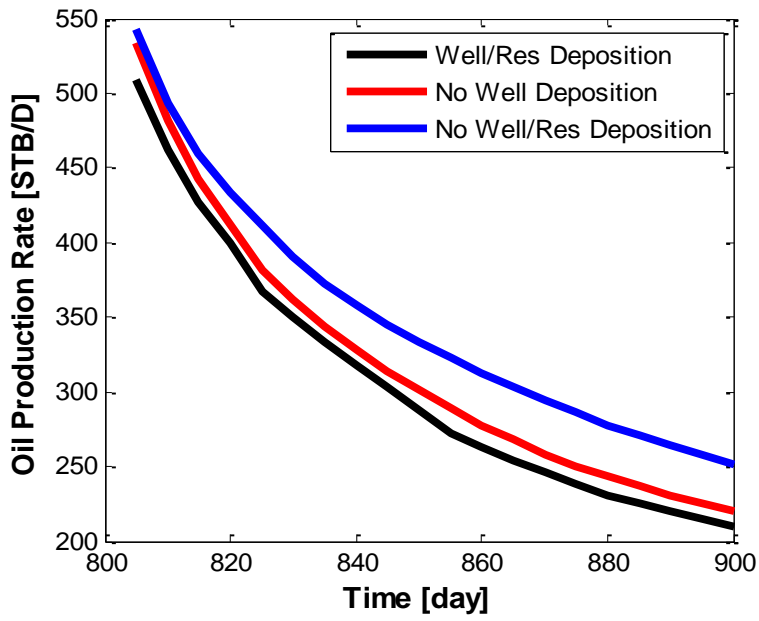


Figure 7.14 Oil production rates after 100 days of CO₂ breakthrough.

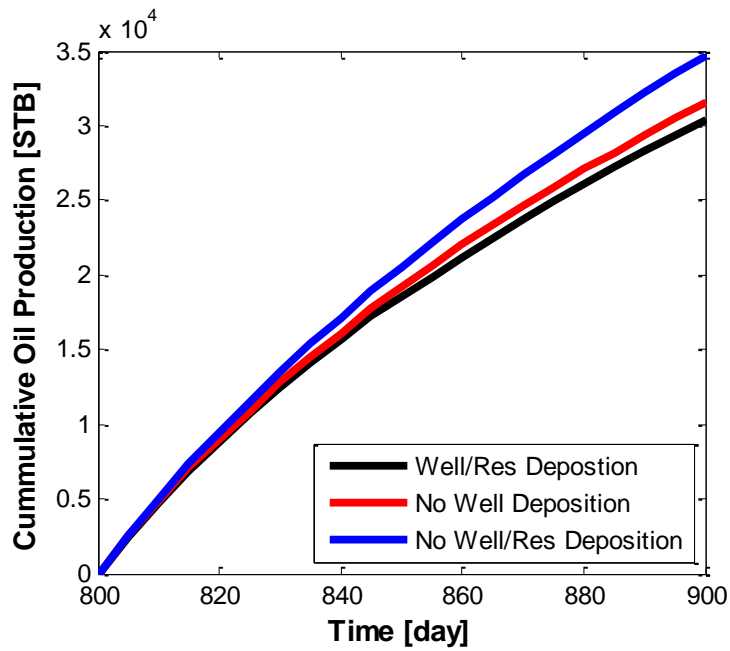


Figure 7.15 Cumulative oil productions after 100 days of CO₂ breakthrough.

Chapter 8: Asphaltene Inhibition and Remediation

In this chapter, we review available asphaltene inhibition and remediation procedures for the wellbore and reservoir. Then, we present various field case trials of chemical remediation for the reservoirs that have experienced asphaltene deposition problems. In addition, we discuss the mechanism of asphaltene-dispersant interactions and related reactions. Afterward, we introduce the first near wellbore asphaltene remediation model that is developed in this work. This remediation model is incorporated into the UTCOMP asphaltene model. Finally, we present different simulation cases to investigate the effectiveness of chemical treatment jobs on asphaltene dissolution. The results show that the type of dispersant, the amount of dispersant, soaking time, number of treatment jobs, and the time period between two treatment jobs affect the efficiency of an asphaltene treatment plan.

8.1 INTRODUCTION

Asphaltene inhibition and remediation techniques are very complex and expensive processes. Usually, companies spend a lot of money to design their own asphaltene inhibition and remediation procedures for the fields with asphaltene problems. However, due to the complexity of the problem and the lack of knowledge on the asphaltene problems in a field, these asphaltene inhibition and remediation programs are not always successful. For instance, Kuwait Oil Company spent a lot of money on Downhole Asphaltene Remediation Treatment (DART) project (Al-Qabandi and Al-Naqi, 2003) to reduce the major asphaltene problems that they had experienced in different fields. Although DART project reduced asphaltene problems in some of the wells, the project was not truly successful in all of the wells. The variation in the

effectiveness of the DART project was claimed to be due to the lack of a clear, consistent process for deciding on when to perform toluene washes and a variation in the effectiveness of toluene washes/soaks (Al-Qabandi and Al-Naqi, 2003).

The first step in asphaltene remediation is a comprehensive system analysis. At this stage, necessary information should be gathered to identify the source of the problem. We need to know whether the asphaltene deposition problem occurs in the reservoir, wellbore, or production facility. The coupled wellbore/reservoir asphaltene simulator presented in Chapter 8 is a very helpful tool that can diagnose the asphaltene deposition problems in the wellbore and reservoir.

The second step is to decide the remediation strategy and perform necessary laboratory tests. For example if the problem is in the wellbore or production facilities, mechanical cleaning might be a good option. However, in the reservoir we need to utilize other methods such as chemical treatments.

In this Chapter, we focus on the modeling of near wellbore chemical remediation of the asphaltene deposition. Having such a model, we can save a lot of time and money by optimizing the chemical treatment process.

8.2 ASPHALTENE INHIBITION AND REMEDIATION PROCEDURES

In the wellbore, asphaltene remediation methods are mechanical cleaning of the well, chemical cleaning of the well, and manipulation of the operating conditions.

One of the common asphaltene cleaning methods in the wellbore is scrapping the wellbore by coil tubing. However, this method can be very time consuming and impractical if the asphaltene deposition in the well blocks a large section of the wellbore.

For instance, Haskett and Tartera (1965) reported that the coil tubing that was performed in the Hassi-Messaoud field was very time-consuming and operationally unsuccessful.

Chemical cleaning by circulation of solvents is another asphaltene remediation technique in the wellbore. This method is usually used when the mechanical cleaning of a well is unsuccessful. However, due to the costs, environmental issues, and safety risks of flammability, these solvents have limited applicability (Shirdel, 2013).

Manipulating the operating condition is another method that significantly affects the evolution of asphaltene deposition in the wellbore and reservoir. For instance, asphaltene problems were significantly reduced in Hassi Messaoud field in Algeria, Ventura field in California, and Lake Maracaibo field in Venezuela by changing the operating conditions (Leontaritis and Mansoori, 1987). However, this method requires specialized laboratory tests and appropriate modeling tools to obtain the asphaltene instability conditions (e.g. see Figure 6.2). Once the asphaltene precipitation model is tuned using the experimental data, the coupled wellbore/reservoir simulator presented in Chapter 7 can be used to estimate where and when asphaltene problems occur. Then, by simulation of various scenarios, we can optimize the operating conditions during the lifespan of a well to minimize the asphaltene problems and maximize the oil recovery.

Besides manipulation of the operating conditions, chemical treatment is another method to inhibit or remediate asphaltene deposition in the reservoir. Washing the asphaltene deposits using aromatic-based solvents such as toluene and xylene is an effective method that has been tried (Kraiwattanawong et al., 2009). However, due to requirement of large quantity of solvent, this procedure is not economical, unless in a refinery where solvent recovery is plausible. To overcome this issue, usually different chemicals that are known as asphaltene inhibitors (or asphaltene dispersants) are mixed with aromatic-based solvents to increase the efficiency of the process.

Chang and Fogler (1993, 1994(a), and 1994(b)) studied various alkyl-benzene-derived amphiphiles that are known to be asphaltene inhibitors. The results of their experiments showed that amphiphiles are very effective in dispersing large asphaltene deposits. They showed that asphaltene deposits could be completely dissolved back into the solution, depending on the type and concentration of amphiphiles. Permuskarome et al. (1997) performed multiple experiments on the dissolution process of asphaltene using two known alkyl-benzene-derived amphiphiles: dodecylbenzenesulfonic acid (DBSA, $n\text{-C}_{12}\text{H}_{25}\text{-C}_6\text{H}_4\text{-SO}_3\text{H}$) and nonylphenol (NP, $n\text{-C}_9\text{H}_{19}\text{-C}_6\text{H}_4\text{-OH}$). They found that the dissolution rate of asphaltene follows a Langmuir-Hinshelwood equation. Feustel et al. (2000) showed that ethercarboxylic acids could disperse asphaltene deposits in crude oils. Miller et al. (2001(a) and 2001(b)) used mixtures of alkylphenol-formaldehyde resins with oxalkylated amines and mixtures of phosphoric esters with carboxylic derivatives to disperse asphaltene deposits in crude oils. Mukkamala (2006) and Banavali and Mukkamala (2006) showed that carbonyl, thiocarbonyl, or imine compounds or amide and carboxyl groups compounds can disperse asphaltene deposits. Wilkes and Davies (2008) showed that co-polymers are able to disperse large asphaltene particles.

The term “asphaltene inhibitor” is commonly used in the oil and gas industry rather than “asphaltene dispersant”. However, the asphaltene inhibitor chemicals usually stabilize small asphaltene particles (sub-micrometer size) and keep the particles dispersed in the crude oil, rather than inhibiting phase separation of asphaltene from oil. Karan et al. (2003) performed a set of experiments to investigate the effectiveness of various asphaltene inhibitors on two South America oil samples. They concluded that asphaltene inhibitors do not prevent asphaltene precipitation (phase separation). However, the amount of deposition reduced using those inhibitors. Kraiwattanawong et al. (2009) performed a comprehensive study to investigate the effectiveness of different available

asphaltene inhibitor chemicals. They used 3 known chemical compounds (4-dodecyl resorcinol (DR), 4-dodecyl phenol (DP), and 4-dodecylbenzenesulfonic acid (DBSA)) and 11 proprietary blends (X1, X2, X3, Y1, Y2, Y3, Y4, Z1, Z2, Z3, and Z4) in their experiments. The proprietary blends were obtained from different oil field chemical companies. Four different techniques including an automatic titration, an optical microscopy, a turbidity measurement, and a particle size distribution measurement were utilized in their study. Kraiwattanawong et al. (2009) concluded that all of the chemical additives were asphaltene dispersants and not asphaltene inhibitors. None of the chemicals stopped the phase separation stage. However, the chemicals were successful in dispersing/stabilizing the asphaltene particles. They showed that the stability of asphaltenes in the solution depends on the type and concentration of asphaltene dispersants.

In order to avoid confusion, we use the term “asphaltene dispersant” from now on throughout the chapter.

8.3 FILED EXPERIENCES OF CHEMICAL TREATMENT

Since chemical treatment of the reservoir for asphaltene inhibition/remediation purposes is relatively new and not that many published field cases are available in the literature, it is very hard to evaluate the efficiency of these processes. In this section, we review some field trials of chemical treatment of reservoir for asphaltene remediation purpose.

Case History 1. As mentioned earlier in this chapter, Kuwait Oil Company started a project called Downhole Asphaltene Remediation Treatment (DART) (Al-Qabandi and

Al-Naqi, 2003) to reduce the huge asphaltene problems in Kuwait fields. One of the outcomes of this project was the invention of an asphaltene dispersant chemical named DART. The field trial methodology of the DART chemical treatment was as follows:

1. Run caliper survey to measure asphaltene build-up.
2. Clean the well with Toluene, using Coil Tubing Unit (CTU).
3. Perform production well test, PLT, and Pressure Buildup Survey to obtain baseline records prior to the chemical injection.
4. Inject DART chemical into the formation and provide sufficient soaking period.
5. Return the well back to production and monitor the chemical flow back.
6. After the cleaning, obtain caliper survey to ensure that the asphaltene deposition had been fully removed.
7. Repeat production well test, PLT, and Pressure Buildup Survey, to compare the well performance post injection.
8. Post-chemical treatment monitoring of well-head pressure and chemical flow back.

It was reported that the chemical treatment was partially operationally successful (Al-Qabandi and Al-Naqi, 2003). The results of the caliper log indicated that asphaltene was still forming in the wells, but the amount of asphaltene deposition significantly reduced. On the other hand, the well test results showed that production rates and well productivity index remained unchanged at the pre-chemical treatment stage.

Case History 2. It was reported that one of the wells in the Comalcalco area of Mexico experienced a quick decline (about 35%) in production over six months (Newberry and Barker, 2000; Wang, 2000). Analysis of the crude oil showed that the oil was asphaltic. In addition, results of asphaltene stability tests indicated that the asphaltene was unstable. The experiments suggested that the quick production decline might be due to the asphaltene deposition in the reservoir. In order to reduce the asphaltene problems, a chemical treatment plan was designed to treat a single zone completion with 98 feet of perforations. A radial penetration of 28 feet was targeted by the chemical injection. A mixture of 880 gallons of dispersant and 6,700 gallons of solvent was injected in the reservoir through the production well with an overflush of 10,600 gallons of solvent. Afterwards, the well was shut-in for 24 hours to allow sufficient soaking time and then returned to production. Figure 8.1 presents the oil production profile of the well before and after the chemical treatment. As can be observed, the oil production increased to a maximum of 3,900 BOPD after the treatment job, and stabilized around 2,750 BOPD over the next 16 months. The cost of this large treatment job was estimated around \$50,000. Assuming oil price of \$15 per barrel of oil, Newberry and Barker (2000) estimated that the revenue from this chemical treatment job was \$9.3 million over the sixteen-month period.

Case History 3. It was reported that another production well in Mexico had also experienced a quick decline (around 22%) in production after six months (Newberry and Barker, 2000). Laboratory tests showed that the oil was asphaltic and the asphaltene was unstable in the formation. Similar to Case History 2, a chemical treatment plan was designed to treat single zone limestone formation with a perforated interval of 197 feet. A mixture consisting of 2,300 gallons of dispersant and 25,000 gallons of solvent was

injected into the reservoir. The radial penetration of the mixture was estimated at about seven feet. The well was shut-in for 24 hours after chemical treatment, and then returned to production. Figure 8.2 shows the oil production profile of the well before and after the chemical treatment. We observe that the oil production increased to a maximum rate of 13,900 BOPD after the treatment job, and stabilized around 13700 BOPD over the next four months. Newberry and Barker (2000) estimated that the revenue resulted from this chemical treatment job was \$6.5 million over the four-month period.

Case History 4. It was reported that a gas lift well in California experienced a steady production decline (Newberry and Barker, 2000). Laboratory tests showed that the production decline was due to asphaltene deposition in the reservoir. A mixture consisting of 980 gallons of dispersant and 980 gallons of solvent was injected into the reservoir through the production well. Due to the very low oil production rate of the well (around 24 BOPD), only a twelve-inch radial distance from the wellbore was targeted. Figure 8.3 presents the oil production profile of the well before and after the chemical treatment. As can be seen, the oil production increased to a maximum rate of 27 BOPD but decreased steadily with the decline rate similar to the pre-treatment job period. It was estimated that the revenue from this chemical treatment job was \$89,000 over 214 days (Newberry and Barker, 2000).

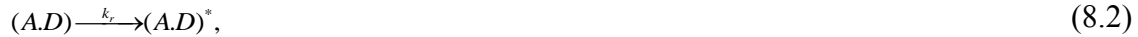
8.4 MODELING OF DISPERSANT INJECTION

As discussed in the previous section, asphaltene dispersants are used either separately or with aromatic solvents in a chemical treatment job for asphaltene

remediation. In this section, we focus on the dynamic modeling of dispersant injection and its effects on the asphaltene dissolution.

8.4.1 Mechanism of Asphaltene Dissolution using Asphaltene Dispersants

Dissolution of asphaltene particles using dispersants is a two-step process (Permsukarome et al., 1997; Jaoui et al, 1998; Leon et al., 1999): (1) the dispersants are adsorbed on the surface of the asphaltene particles and (2) the interactions between adsorbed dispersant and asphaltene becomes dominant, which results in formations of asphaltene-dispersant complexes. The reactions between the dispersants and asphaltene particles are as follows:



where A is asphaltene, D is dispersant, $(A.D)$ is dispersant molecule adsorbed on the surface of asphaltene, k_A is the forward rate of the first reaction, k_{-A} is the backward rate of the first reaction, $(A.D)^*$ is the asphaltene-dispersant transition state complex, and k_r is the reaction rate of the second reaction. The first reaction, Equation (8.1), is the fast step, and the second reaction, Equation (8.2), is the slow step or rate-determining step (Permsukarome et al., 1997).

Leon et al. (1999) measured the adsorption isotherms of various alkylbenzene-derived amphiphiles (that are asphaltene dispersants) on asphaltenes. They investigated the behavior of various commercial dispersants such as p-(sec-butyl)phenol (SBP), p-(tert-butyl)phenol (TBP), p-(tert-octyl)phenol (TOP), p-(n-nonyl)phenol (NP), p-(n-

dodecyl)phenol (DP), p-(n-nonyl)phenoethoxylated(6) (NPE6), and p-(n-dodecyl)benzene sulfonic acid (DBSA). Figures 8.4 and 8.5 show the adsorption isotherms for the different dispersants. As can be observed, all the adsorption isotherms follow a two-plateau type curve. These kinds of isotherms are related to a two-step adsorption mechanism mentioned earlier. In a separate study, Jaoui et al. (1998) measured the asphaltene isotherms for different combinations of dispersants-crude oils. Based on the results, they also concluded that the asphaltene-dispersant interaction is a two-step process.

The equilibrium constant in the first step, Equation (8.1), can be defined as

$$K_A = \frac{k_A}{k_{-A}}. \quad (8.3)$$

Determining the equilibrium constant requires understanding of the stoichiometry of the adsorption of the dispersants on the asphaltene particles, Equation (8.1). However, due to the complexity of the asphaltene molecules, it is very hard to determine the stoichiometry constants in Equation, (8.1). Usually, laboratory tests are required to determine the equilibrium constant in such a case. For instance, Figure 8.6 shows the percentage of DBSA dispersant on a specific asphaltene versus the weight ratio of asphaltene over DBSA (Chang and Fogler, 1994(b)). Based on these results, Chang and Fogler, (1994(b)) estimated that the stoichiometry of the interaction between asphaltenes and DBSA is about 1.8 mmol of DBSA/g of asphaltene.

By performing a comprehensive set of experiments, Permsukarome et al. (1997) showed that the formation of asphaltene-dispersant complex can be modeled using a first-order reaction model. Therefore, the rate of asphaltene dissolution becomes

$$-\frac{dC_M}{dt} = \frac{dC_{(A,D)}}{dt} = k_r C_{(A,D)}, \quad (8.4)$$

where C_M is the total concentration of asphaltene particles. Combining Equations (8.1) and (8.3), we have

$$C_{(A,D)} = K_A C_A C_D. \quad (8.5)$$

In addition, from the material balance of asphaltene particles, we have

$$C_M = C_{(A,D)} + C_A. \quad (8.6)$$

Combining Equations (8.5) and (8.6), we obtain

$$C_A = \frac{C_M}{1 + K_A C_D}. \quad (8.7)$$

Substituting Equations (8.5) and (8.7) in Equation (8.4), we have

$$-\frac{dC_M}{dt} = \frac{k_r C_D}{1 + K_A C_D} C_M = k C_M, \quad (8.8)$$

which is a Langmuir-Hinshelwood form.

Permsukarome et al. (1997) provided multiple experimental data to support the Langmuir-Hinshelwood form of asphaltene dissolution rate provided in Equation (8.8). As an example, Figure 8.7 shows the experimental data for the dissolution rate of asphaltene in DBSA dispersant for an asphaltic oil (Permsukarome et al., 1997).

8.4.2 Incorporating Asphaltene-Dispersant Reactions into the Asphaltene Model

In order to incorporate the asphaltene-dispersant reactions in our asphaltene reservoir model, we assume that dispersants dissolve flocculated and deposited asphaltenes and transform them to colloidal asphaltenes. In a study performed by Kraiwattanawong et al. (2009) on the effects of 14 dispersants on various asphaltic oils, it was shown that the dispersed/stabilized asphaltenes are in the form of colloidal asphaltenes (less than 1 μm). In addition, it was shown that all of the large asphaltene particles (flocculated and deposited asphaltenes) could transform into the colloidal asphaltenes, depending on the type and concentration of the dispersant.

As discussed in Chapter 5, in our asphaltene model, flocculated asphaltenes are the large asphaltene particles in the flow and deposited asphaltenes are the flocculated asphaltenes that are adsorbed on the rock surface. Considering all the reactions between colloidal, flocculated, and deposited asphaltenes, we have

$$\frac{dC_{coll.}}{dt} = -k_{cf}C_{coll.} + k_{fc}C_{floc.} + k_{dc}C_{dep.}, \quad (8.9)$$

$$\frac{dC_{floc.}}{dt} = k_{cf}C_{coll.} - k_{fc}C_{floc.} + \beta C_{dep.}(v_o - v_{cr,o}), \quad (8.10)$$

$$\frac{dV_{dep.}}{dt} = \alpha C_{floc.}\phi - \beta C_{dep.}(v_o - v_{cr,o}) + \gamma u_o C_{floc.} - \frac{V_o}{v_{asp}} k_{dc} C_{dep.}, \quad (8.11)$$

where k_{cf} is the reaction rate of the transformation of the colloidal asphaltenes to the flocculated asphaltenes, k_{fc} is the reaction rate for the transformation of the flocculated asphaltenes to the colloidal asphaltenes, k_{dc} is the reaction rate for the transformation of the deposited asphaltenes to the colloidal asphaltenes, V_o is the oil volume in a grid-block, and v_{asp} is the molar volume of asphaltene. Other parameters are defined in Chapter 5. k_{fc} and k_{dc} are Langmuir-Hinshelwood form similar to Equation (8.8),

$$k_{fc} = \frac{k_{\infty,f} C_D}{K_{S,f} + C_D}, \quad (8.12)$$

$$k_{dc} = \frac{k_{\infty,d} C_D}{K_{S,d} + C_D}, \quad (8.13)$$

where k_{∞} and K_s are matching parameters. Subscripts f and d refer to flocculated and deposited asphaltenes, respectively. Usually, $k_{\infty,d}$ is lower than $k_{\infty,f}$, since the dispersant needs to first deposit on the rock surface in order to dissolve the deposited asphaltenes. Therefore, the activation energy required to disperse deposited asphaltenes is more than the flocculated asphaltenes.

Equations (8.9) through (8.13) provide all the reactions (transformations) between colloidal, flocculated, and deposited asphaltenes. Other models, such as precipitation, wettability alteration, viscosity, porosity and permeability reduction, and flow of colloidal and flocculated asphaltenes are the same as in Chapter 5.

To consider material balance of the dispersant at each grid-block, we assume that the dispersant flows with the same velocity of the assisting fluid, which is water in our case studies. In addition, we assume that part of the dispersant instantaneously adsorbs on the asphaltene particles as is suggested by the equilibrium reaction in Equation (8.1). The amount of deposition of dispersant on the asphaltene particles is calculated by having the equilibrium constant (K_A). As mentioned earlier, K_A can be determined experimentally for a specific dispersant-asphaltene mixture (see Figure 8.6).

8.5 SIMULATION CASE STUDIES

In this section, we present simulation case studies to investigate the effectiveness of DBSA dispersant on asphaltene remediation.

Case 1: Single Treatment job. In this case study, we set up a two-dimensional simulation case to investigate the effectiveness of DBSA dispersant on asphaltene remediation. We use the Middle East oil presented in Section 6.1.2 as the reservoir fluid. Table 8.1 summarizes the simulation input data and Table 8.2 presents the relative permeability data. The reservoir is homogenous with the size of $1500 \times 1500 \times 20$ ft³. Initial water saturation is 0.2, and the rock porosity and horizontal permeability are 0.1 and 20 md, respectively. Initial temperature of the reservoir is 212 °F and initial pressure is 4000 psi. As can be observed in Figure 6.1, the onset pressure of asphaltene at the temperature of 212 °F is 3100 psi. Therefore, the reservoir is initially above the asphaltene onset pressure of the fluid. There is one production well at the corner of the reservoir, which is a constant bottom-hole pressure well set at 2000 psi. The asphaltene flocculation and deposition parameters are set as follows: forward rate of flocculation is 12 lb-mol/day, porosity-permeability correlation exponent is 7, adsorption rate (α) is 8 day⁻¹, entrainment rate (β) is zero, and pore throat plugging coefficient is 1 ft⁻¹. We use the Einstein correlation with constant a equal to 2.5 to model oil viscosity reduction due to asphaltene.

The green and red lines in Figure 8.8 compare the oil rate profiles for two scenarios when asphaltene is ignored and is considered in the simulation. Figure 8.9(a) shows permeability profile after 200 days of simulation when asphaltene precipitation, flocculation, and deposition are considered in the simulation. As can be observed, the permeability around the production well decreased up to 30 % after 200 days, due to asphaltene deposition around the wellbore. Consequently, oil production rate dropped about 10% after 200 days. To remove/reduce asphaltene deposition problem around the wellbore, we design a chemical treatment job to clean asphaltene deposits. The production well is treated with a mixture of 400 gallons of DBSA (dispersant) and 2500

gallons of water with a preflush of 7500 gallons of water. With the injection rate of 238.1 bbl/d, the treatment job including preflush took about 24 hours. Then, the well was shut-in for 24 hours and allowed to soak before resuming production. The asphaltene-dispersant reaction parameters are set as follows: $k_{\infty,d}$ and $k_{\infty,f}$ are 20 day^{-1} , and $K_{s,d}$ and $K_{s,f}$ are 0.05 lb-mol/ft^3 . Molecular weight of DBSA is 326.5 lb/lb-mol , and density of DBSA is 1.06 g/ml . The amount of deposition of dispersant on the asphaltene particles is calculated using the dashed line in Figure 8.6. In other words, the stoichiometry of the interaction between asphaltenes and DBSA is assumed to be $1.8 \text{ mmol of DBSA/g of asphaltene}$.

Figure 8.8 compares the oil rate profiles for three scenarios when asphaltene was ignored, asphaltene was considered, and the well was treated with chemical treatment. The blue dashed line is the production profile when we treat the well with remediation job after 200 days. Figure 8.9(b) shows the permeability profile after 202 days (right after the chemical treatment job). By comparing Figures 8.9(a) and 8.9(b), we observe that the treatment job affected about 50 feet around the wellbore. Since the amount of chemical was sufficient and enough soak time was allowed, treatment job was successful to dissolve all the deposited asphaltenes in a small region around the wellbore. However, as we move away from the production well, the effectiveness of the chemical decreases due to the lower concentration of dispersant. The weight ratio of deposited asphaltenes to DBSA is about one around the production well (well grid-block). Therefore, according to Figure 8.6, about 50 % of DBSA instantaneously adsorbs on the surface of asphaltene particles. In other words, only 50 % of dispersant can move further into the reservoir and dissolve asphaltenes. Before the treatment job, the minimum permeability of the reservoir is about 14 md. However, the minimum permeability of the reservoir is about 18 md after the chemical treatment job. Due to improving the skin around the well, we observe a

jump in oil production in Figure 8.8 right after we put the well back on production following the treatment job. At the peak, the oil production almost reaches to the case when we did not have any asphaltene deposition problem in the reservoir (green line in Figure 8.8). However, as time proceeds, we observe a quick decline in production, and the oil production profile approaches the red line (the case when we had asphaltene problem in the reservoir with no chemical treatment job). The quick decline in the production is due to the formation of the second asphaltene deposition bank around the wellbore. As can be observed in Figures 8.9(c) and 8.9(d), the well-block permeability decreased to about 14 md and 8 md after 400 and 600 days of simulation (200 days and 400 days after treatment job).

Case 2: Effect of Soaking Time. As mentioned earlier, soaking time plays a key role in the efficiency of an asphaltene chemical treatment job. In this case study, we investigate the effectiveness of the treatment job discussed in case 1, considering various soaking times of 6 hrs, 1 day, and 2 days.

Figure 8.10 compares the oil rate profiles for the treatment job discussed in case 1 with soaking times of 6 hrs, 1 day, and 2 days. As can be observed, the oil production rate improved when we increased the soaking time from 6 hrs to 1 day. However, increasing the soaking time from 1 day to 2 days does not affect the oil production. There is always an optimum value for the soaking time. Below the optimum value, the efficiency of the chemical treatment decreases and some of the dispersant will be produced from the well without reacting with the deposited asphaltenes. Above the optimum value, no more dispersant will be left in the reservoir to dissolve the asphaltenes and we lose money due to the shutdown of the well.

Case 3: Multiple Treatment Jobs. In order to design an effective treatment plan for a well, besides the type and amount of injecting dispersant and soaking time, we also need to optimize the number of treatment jobs and the time period between two treatment jobs. The optimization process requires evaluation of the treatment plan when we have multiple treatment jobs on a single well. In this case study, we present our simulation results for the reservoir in case 1, when the well is treated with multiple remediation jobs. We treat the well three times after 200, 400, and 700 days. For each job, we inject a mixture of 400 gallons of DBSA and 2500 gallons of water with a preflush of 7500 gallons of water through the production well. Then, the well is shut-in for 24 hours before resuming production.

Figure 8.11 compares the oil production profiles when asphaltene is ignored, asphaltene is considered, and asphaltene is considered with three remediation jobs. Similarly, Figure 8.12 presents the cumulative oil production profiles. As can be observed, there is a jump in oil production right after each treatment job. However, after a couple of months, the oil production quickly decreases and approaches the case when the well was not treated at all (red line). In Figure 8.12, we observe that the cumulative oil production decreased about 17.6 % after 1000 days due to asphaltene related problems, if we do not run any remediation job in the well. However, if we treat the well with the three mentioned chemical treatment jobs, we can recover 41 % of the lost production due to asphaltene deposition. The incremental oil recovery over 800 days after treatment jobs is about 38971 STB. Considering each treatment job costs about \$ 50,000 and oil price is \$80 per a barrel of oil, the revenue resulting from this treatment plan is about \$3 million over 800 days. Coupling the simulator with an optimization algorithm, we can design the best treatment plan that results in maximum revenue.

8.6 SUMMARY AND CONCLUSIONS

In this chapter, we reviewed various asphaltene inhibition and remediation methods in the wellbore and reservoir. Successful cases of field trials of the chemical treatment for the asphaltene remediation were reviewed. In addition, the mechanism of asphaltene-dispersant interactions were discussed. We incorporated the asphaltene-dispersant reactions in our asphaltene model and presented the first near wellbore asphaltene remediation model. Different simulation cases were provided to investigate the effectiveness of the chemical treatment jobs on asphaltene dissolution.

Based on the results of our simulation case studies, we summarize the conclusions of this chapter as follows:

1. The efficiency of an asphaltene remediation in the reservoir depends on many parameters, and requires dynamic asphaltene modeling.
2. The amount of dispersant, type of dispersant, soaking time, number of treatment jobs, and the time period between two treatment jobs affect the outcome of an asphaltene treatment plan.
3. By coupling of an optimization algorithm with the presented asphaltene remediation model, we can optimize the treatment plan and maximize the revenue.

Table 8.1 Reservoir properties and the simulation input data for case study 1.

Parameter	Value
Number of grid-blocks	60×60×1
Reservoir dimension	1500 ×1500×20 ft ³
Reservoir temperature	212 °F
Initial water saturation	0.2
Initial reservoir pressure	4000 psi
Bottom-hole pressure	2000 psi
Porosity	0.1
Horizontal permeability	20 md
Vertical permeability	1 md
k_{cf}	12 day ⁻¹
$k_{\infty, f}$	20 day ⁻¹
$k_{\infty, d}$	20 day ⁻¹
$K_{S, f}$	0.05 lb-mol/ft ³
$K_{S, d}$	0.05 lb-mol/ft ³
g	7
α	8 day ⁻¹
β	0
γ	1 ft ⁻¹

Table 8.2 Relative permeability data for case study 1.

	Water	Oil	Gas
Residual saturation	0.2	0.1	0.0
End point	0.4	0.7	1.0
Exponent	3.0	2.0	1.0

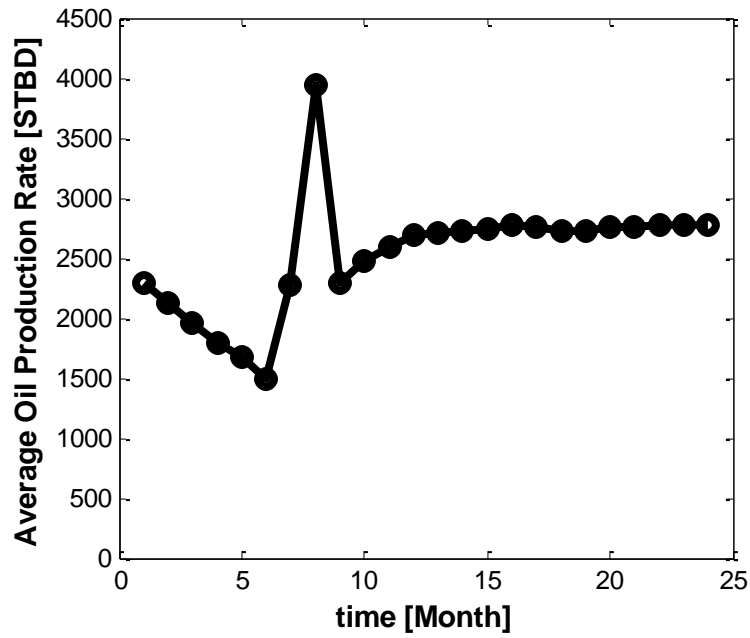


Figure 8.1 Oil production profile for the well in case history 2, reproduced from Newberry and Barker (2000).

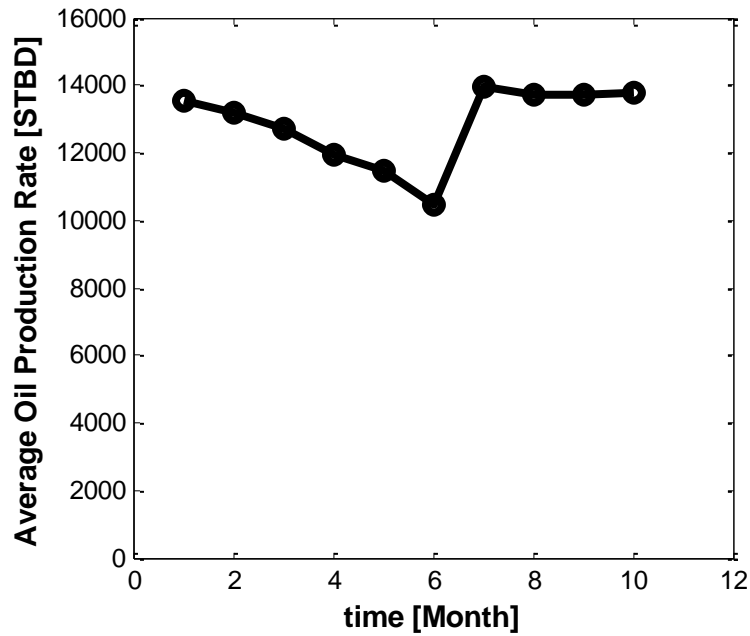


Figure 8.2 Oil production profile for the well in case history 3, reproduced from Newberry and Barker (2000).

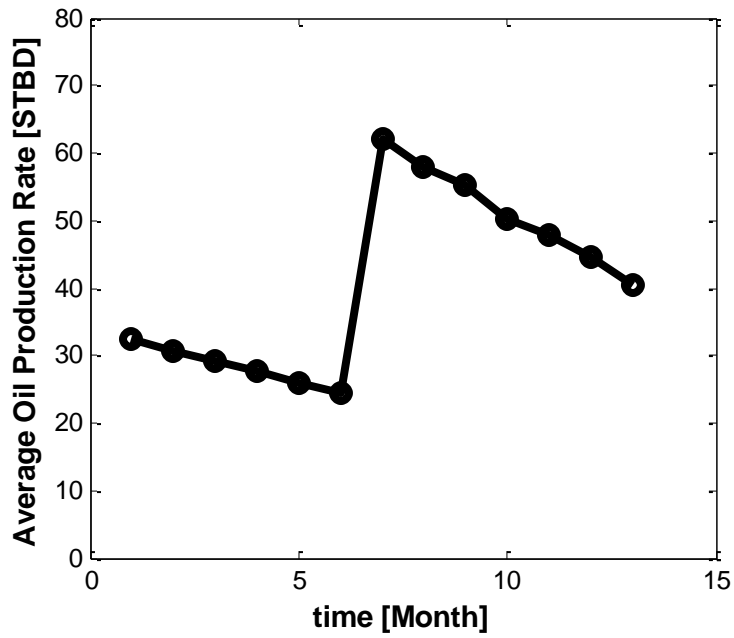


Figure 8.3 Oil production profile for the well in case history 4, reproduced from Newberry and Barker (2000).

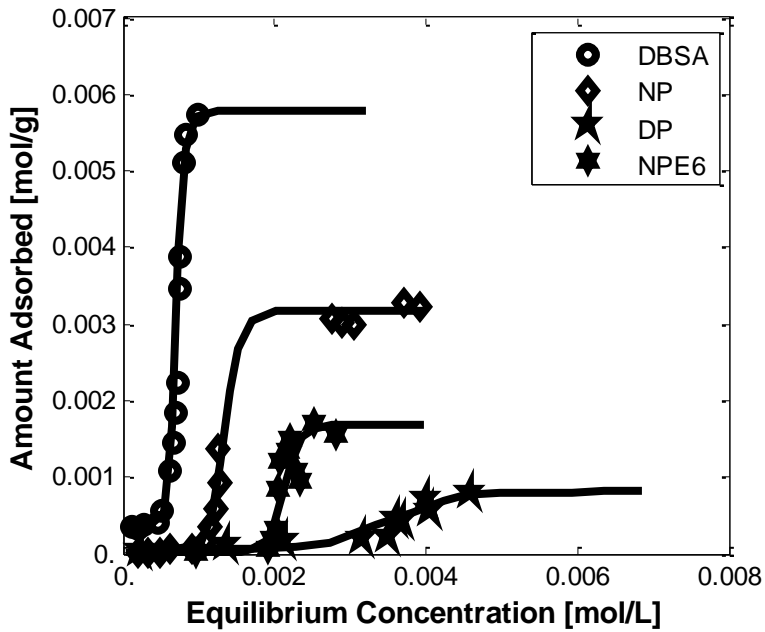


Figure 8.4 Adsorption isotherms for DBSA, NP, DP, and NPE6 dispersants, reproduced from Leon et al. (1999).

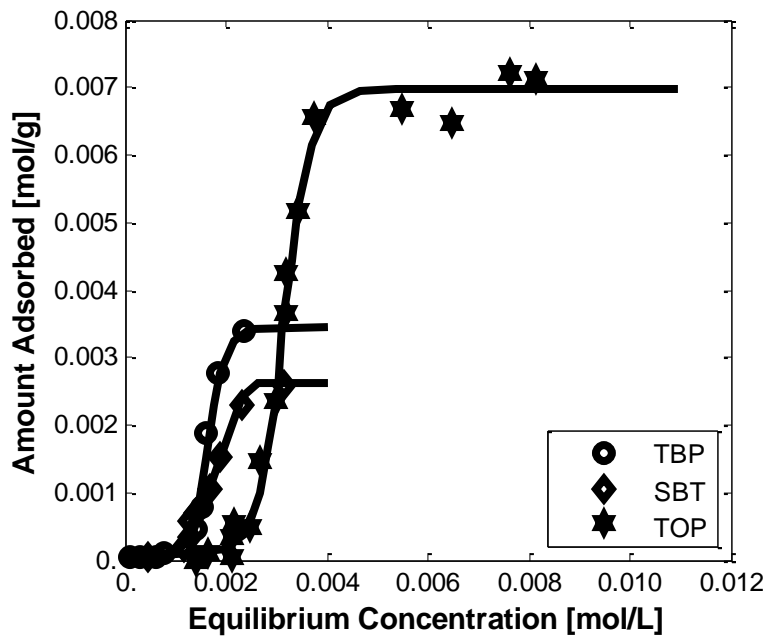


Figure 8.5 Adsorption isotherms for TBP, SBT, and TOP dispersants, reproduced from Leon et al. (1999).

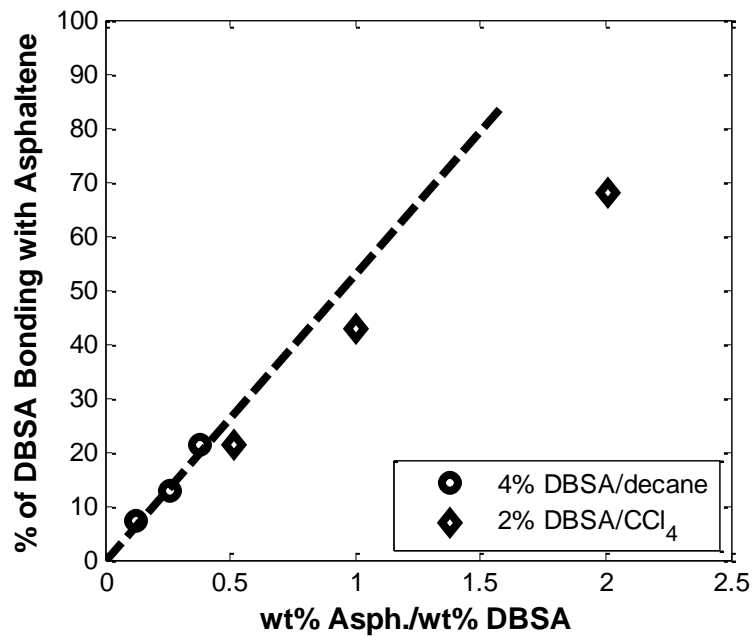


Figure 8.6 Amount of DBSA adsorbed on the asphaltene particles versus weight ratio of asphaltene over DBSA, reproduced from Chang and Fogler (1994(b)).

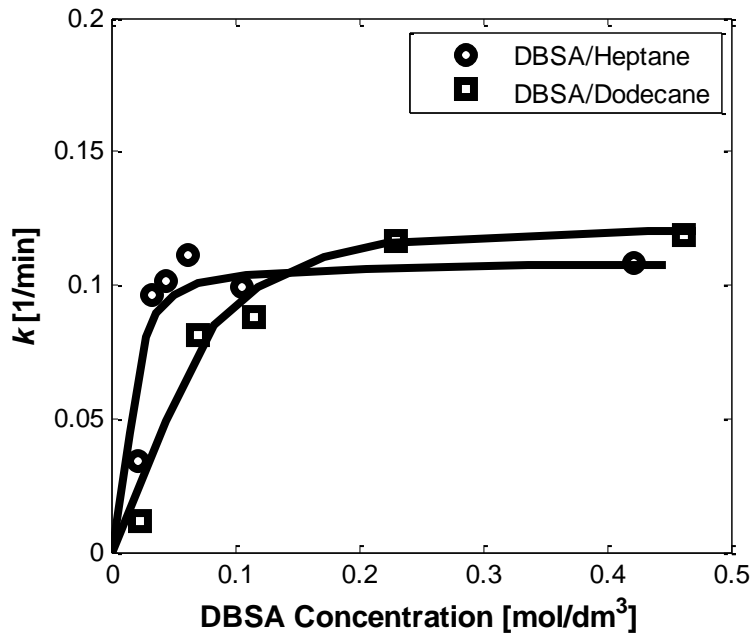


Figure 8.7 Specific dissolution rate constant, k , as a function of DBSA concentration in solution, reproduced from Permsukarome et al. (1997).

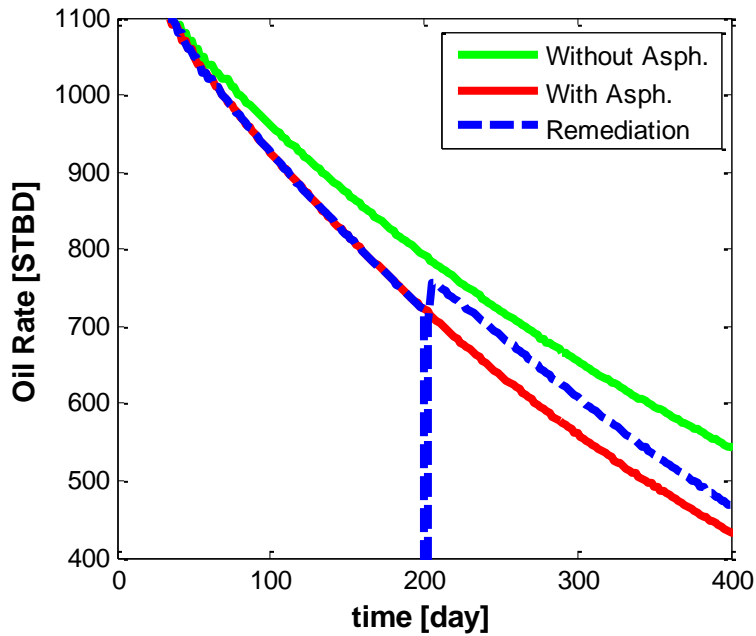


Figure 8.8 Oil production rates for three scenarios of ignoring asphaltene, considering asphaltene, and considering asphaltene with chemical treatment, case 1.

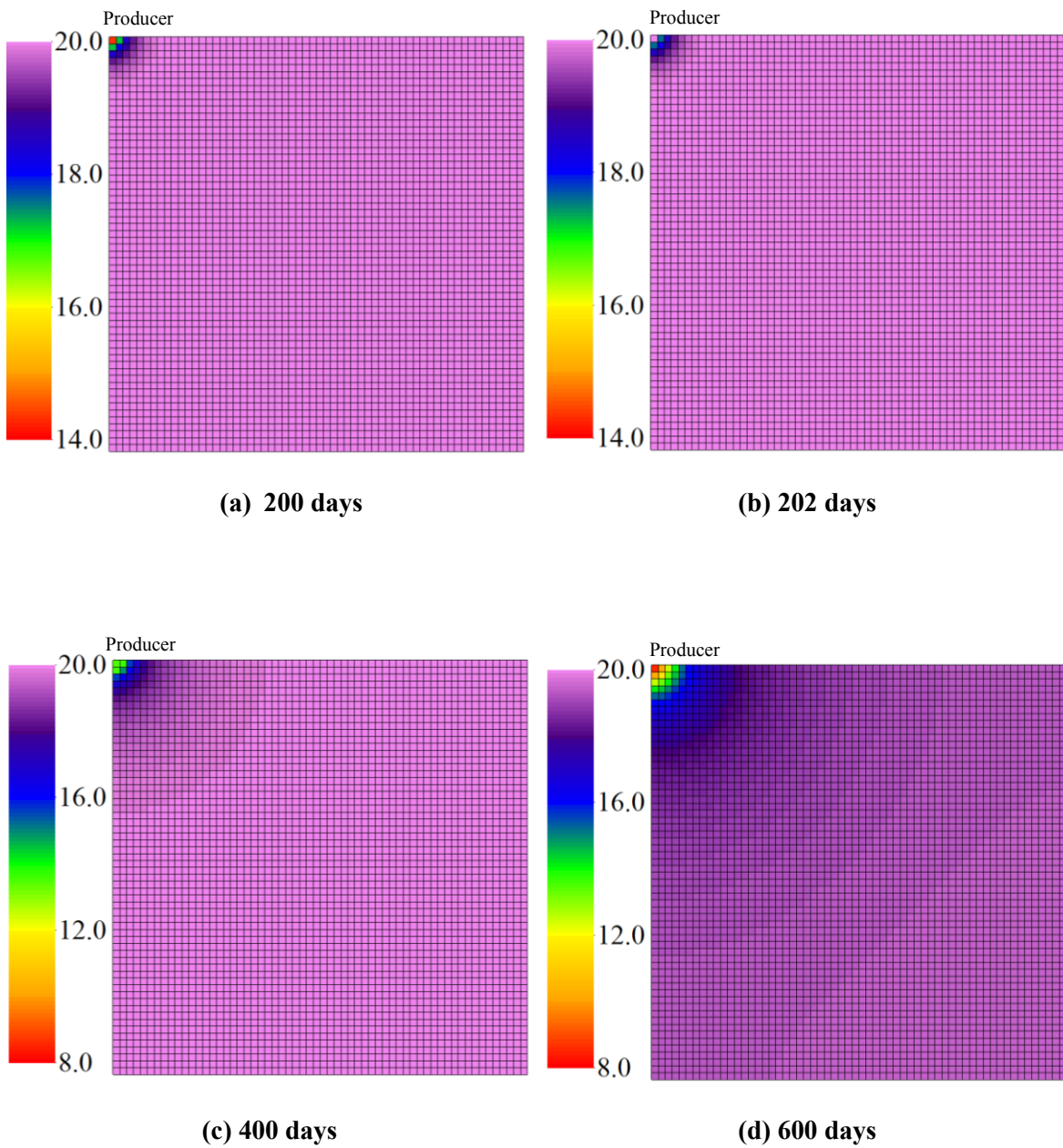


Figure 8.9 Permeability maps after (a) 200 days, (b) 202 days (after treatment), (c) 400 days, and (d) 600 days for case 1.

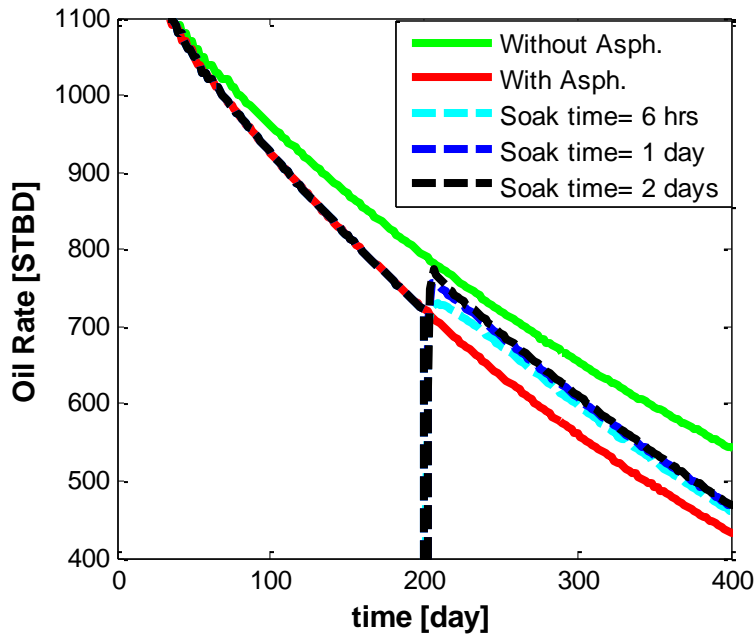


Figure 8.10 Comparison of oil production rates for three different soaking times of 6 hrs, 1 day, and 2 days for case 2.

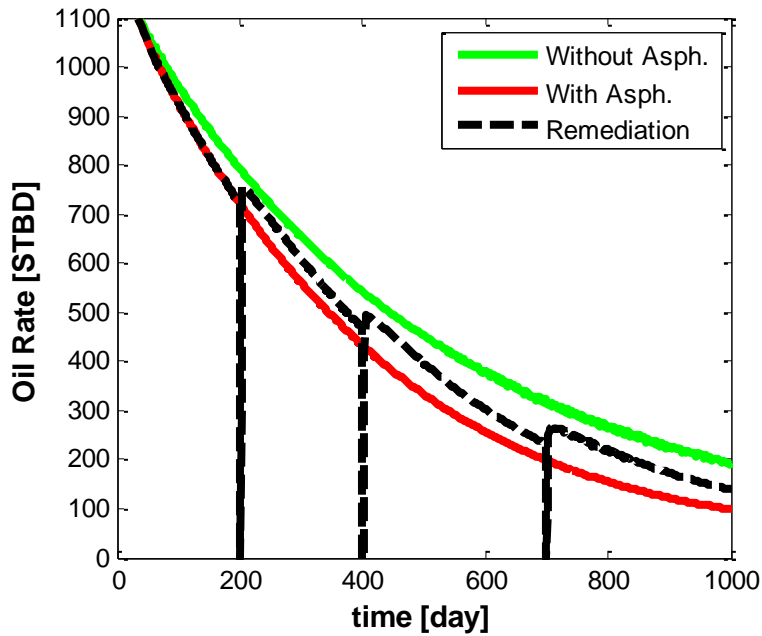


Figure 8.11 Oil production rates for three scenarios of ignoring asphaltene, considering asphaltene, and considering asphaltene with three chemical treatment jobs.

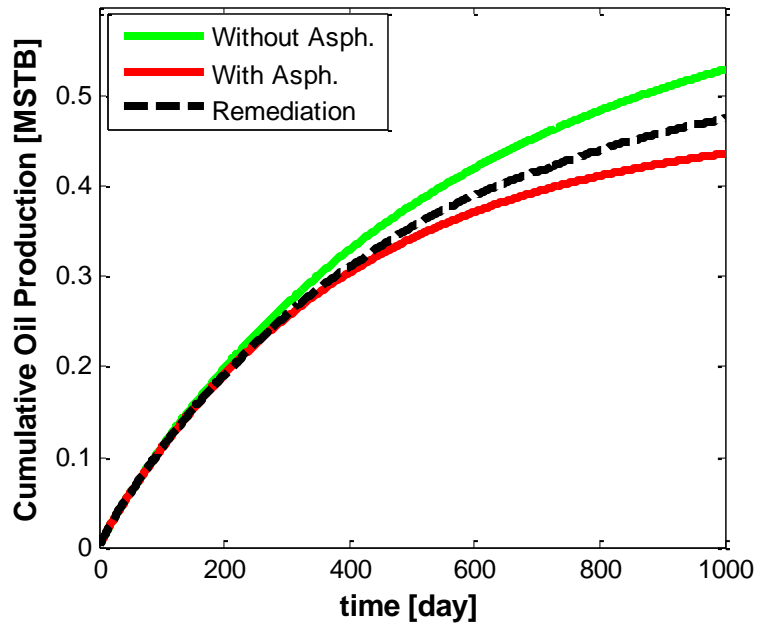


Figure 8.12 Cumulative oil productions for three scenarios of ignoring asphaltene, considering asphaltene, and considering asphaltene with three chemical treatment jobs.

Chapter 9: Summary, Conclusions, and Recommendations

In this chapter, we present the summary and the conclusions of this dissertation. In addition, recommendations for the future extension of this work will be presented.

9.1 SUMMARY

We list the summary of the tasks that were performed in this dissertation as follows:

- We implemented the energy equation in UTCOMP to consider the effect of temperature variations on asphaltene behavior. The non-isothermal UTCOMP is a three-dimensional compositional EOS-based reservoir simulator that can model hot/cold fluid injection. We calculated enthalpy and internal energy of each phase directly from the Peng-Robinson EOS. In addition, we considered heat loss to the underburden/overburden layers to include the exchange of heat by conduction between the reservoir and its surroundings. Moreover, we considered the density and viscosity variations of water, oil, and gas phases due to temperature variations. We solved the energy equation implicitly, isolated from pressure equation and material balance equations. Furthermore, an iterative, sequential, semi-implicit scheme was selected for the overall solution scheme of the non-isothermal UTCOMP. In addition, we implemented an automatic time-step selection in the non-isothermal UTCOMP to avoid numerical instability and to save computational time.
- We verified the enthalpy calculation of the non-isothermal UTCOMP against the WinProp module of the CMG simulator (WinProp, 2011).

- We verified the results of the non-isothermal UTCOMP against the Lauwarier (1955) analytical solution, the UTCHEM simulator (UTCHEM-10 Technical Documentation, 2003), and the GEM module of CMG simulator (GEM, 2011).
- A comprehensive dynamic asphaltene model was presented and implemented in UTCOMP to consider asphaltene precipitation, flocculation, and deposition. We used a solid model for asphaltene precipitation. The amount of precipitation was calculated using the Peng-Robinson EOS assuming a reversible process. We modeled flocculation using a reversible chemical reaction. We considered adsorption, pore throat plugging, and re-entrainment processes as the main mechanisms of asphaltene deposition. In addition, we considered porosity, permeability, and oil viscosity reduction due to asphaltene. In our asphaltene model, we assumed that asphaltene is not a continuous phase and exists in the oil phase in the form of colloids. In addition, we assumed that colloidal and flocculated asphaltene particles are carried in crude oil and move with the same velocity as the oil phase.
- Based on the available experimental data, a wettability alteration model due to asphaltene deposition was proposed and implemented in UTCOMP. The wettability alteration model was verified against a set of experimental data provided by Al-Maameri and Buckley (2003).
- We verified the precipitation model of UTCOMP against the Burke et al. (1990) fluid experimental data and WinProp Module of CMG (WinProp user's guide, 2011). In addition, we verified the asphaltene deposition model of UTCOMP against the Minssieux (1997) experimental data and simulation results of Kohse and Nghiem (2004).

- We provided a guideline on characterization of an asphaltic fluid for appropriate modeling of asphaltene precipitation. In addition, an asphaltic Middle East oil was characterized. The Peng-Robinson EOS parameters were tuned to reproduce the experimental data.
- Different case studies were presented to investigate the effects of pressure variations, temperature variations, composition variations, and wettability alteration on the dynamics of asphaltene precipitation, flocculation, and deposition. We included primary production, secondary production, and CO₂ injection scenarios in our simulation case studies. In addition, the effect of gas override on the behavior of asphaltene was investigated.
- The asphaltene reservoir simulator was coupled to a wellbore simulator to address the wellbore/reservoir interaction, the effect of asphaltene deposition on the flow prediction, and long-term reservoir performance. We performed simulations of primary production and CO₂ flood scenarios using the coupled reservoir/wellbore simulator to track the behavior of asphaltene in the entire production system, from the injection well to the production well.
- We reviewed available asphaltene inhibition and remediation procedures for the wellbore and reservoir. In addition, we reviewed various field case trials of chemical remediation for the reservoirs that have experienced asphaltene deposition problems.
- Based on the mechanisms of asphaltene-dispersant interactions, we proposed a dynamic model for the chemical remediation of the near-wellbore using asphaltene dispersants.

- We presented various simulation cases to investigate the effectiveness of the chemical treatment jobs on asphaltene dissolution. In addition, we investigated the effect of soaking time on the performance of the chemical remediation.

9.2 CONCLUSIONS

We summarize the conclusions of this research as follows:

- Proper dynamic modeling of asphaltene precipitation requires consideration of pressure, temperature, and composition variations. Each of these factors has a distinct effect on the precipitation, and neglecting one of these effects may result in a significant error in the prediction of asphaltene behavior.
- Asphaltene deposition is a time-dependent process that mainly depends on the amount of flocculation in a grid-block and oil velocity.
- Wettability alteration, if occurs, has a major effect on the performance of the reservoir, compared to the permeability reduction.
- During primary production, most of asphaltene deposition occurs around the production well.
- During hot/cold water injection, asphaltene mostly deposits behind the temperature front, if we assume that asphaltene precipitation is only controlled by temperature variations. In this case, almost all the asphaltene particles that precipitated from oil deposit on the rock surface.
- During CO₂ injection, asphaltene mostly precipitates in a small interface region before the front. Moreover, asphaltene mostly deposits at the front near the boundaries, where the front velocity is minimum.

- In the presence of gas override, asphaltene mostly deposits in the bottom layer due to the lower velocity of the front in the bottom layer compared to the upper layer.
- The behavior of asphaltene in the wellbore and reservoir are fully coupled with each other. Therefore, a standalone reservoir or wellbore simulator is not able to predict the asphaltene behavior properly in the entire system.
- Asphaltene precipitation and deposition in the wellbore and reservoir are dynamic processes. Many parameters, such as oil velocity and pressure, temperature, and composition variations influence the trend of these processes. Hence, the asphaltene model should be comprehensive to consider the combined effects of these important parameters on the asphaltene behavior.
- The coupled reservoir/wellbore model can be used to track asphaltene deposition, to diagnose the potential for asphaltene problems in the wellbore and reservoir, and to find the optimum operating conditions of the well that minimizes the asphaltene problems.
- In addition, the coupled wellbore/reservoir simulator is able to suggest the asphaltene inhibition and remediation strategies. For example, when the problem in the well is pronounced, asphaltene cleaning workover job might be very useful. In this case, we can optimize the place and time that workover job is needed to maximize the oil production, which saves us a lot of time and money.
- The efficiency of an asphaltene remediation in the reservoir depends on many parameters, and requires dynamic asphaltene modeling.
- The amount of dispersant, type of dispersant, soaking time, number of treatment jobs, and the time period between two treatment jobs affect the outcome of an asphaltene treatment plan.

9.3 RECOMMENDATIONS

We list the recommendations for the extension of this research as follows:

- Heterogeneity is an important factor that may significantly affect the dynamics of the asphaltene in the reservoir. In this research, we did not include the effect of heterogeneity in our simulation case studies. Since we can input any permeability distribution into UTCOMP, we only need to set up a couple of simulation cases with variable permeability over the grid-blocks to study the effect of heterogeneity. However, to verify the simulation results, we recommend conducting multiple experiments on different heterogeneous core samples using asphaltic oils, and track the asphaltene deposition evolution in the cores on high and low permeability zones. It would be interesting to inject various asphaltic oils into layered core samples and compare the amount of deposition on high and low permeability layers.
- Dispersion is another factor that may affect the behavior of asphaltene in the reservoir, specifically during miscible gas injection. During gas injection, the amount of precipitation depends on the amount of gas that mixed with oil. Introducing light components to a fluid increases both onset and offset pressures of asphaltene. As mentioned earlier, most of the asphaltene precipitation occurs in a small front region during gas injection. Since dispersion affects the shape and size of the gas front, asphaltene behavior may significantly change. We recommend performing several simulation studies to investigate the effect of physical dispersion on the behavior of asphaltene during gas injection. Since

UTCAMP already handles physical dispersion, completion of this task will be simple.

- In our simulation cases, we investigated the effect of water flooding and CO₂ injection separately, on asphaltene precipitation, flocculation and deposition. In many field cases, CO₂ is injected with water in a cyclic process that is called Water Alternative Gas (WAG) injection. Therefore, we recommend performing a series of simulations on the WAG cases to study the combined effects of CO₂ and water injections on the dynamics of asphaltene.
- To model asphaltene flocculation, we assumed a normal distribution for asphaltene aggregates, and we used an average diameter size of flocs that determines the parameters of the deposition model. It is fairly accepted that the particle size distribution of asphaltene aggregates is normal. However, evolution of the asphaltene aggregates at different times were neglected in this research. In other words, the particle size distribution of asphaltene aggregates grows as time proceeds. Since the aggregation of asphaltene particles is very fast (in order of minutes or hours), using the final particle size distribution of the flocs is a fairly valid assumption. However, we recommend incorporating the evolution of asphaltene aggregates in the asphaltene model to investigate the validity of this assumption. Recently, Maqbool et al. (2011) and Haji-Akbari et al. (2013) suggested a unified model for the aggregation of asphaltene nano-aggregates that considers the evolution of the asphaltene flocs. We recommend implementation of this model into the asphaltene model and compare the results with the existing flocculation model in the simulator.

- Although the wettability alteration model was verified against the Al-Maameri and Buckley (2003) experimental data, we recommend multiple experiments to be performed on different rock samples to investigate the effect of rock composition on the wettability of the rock. For instance, carbonates rocks may show a different behavior compared to what was observed in Al-Maameri and Buckley (2003). Having a wide-ranging experimental data set, we can test the validity of the wettability alteration model that was proposed in this research.
- In this dissertation, we modeled near-wellbore asphaltene remediation using asphaltene dispersants. As was mentioned in Chapter 8, sometimes a mixture of aromatic-based solvents and dispersants are used to remove the deposited asphaltene bank near the wellbore. As a future work, development of a solvent injection model that considers solvent-asphaltene interactions is recommended. Having this model, we can investigate the combined effects of solvents and dispersants on asphaltene remediation.
- Finally, we recommend coupling an optimization algorithm with the coupled wellbore/reservoir asphaltene simulator to optimize the operating conditions. Having this tool, we can minimize the asphaltene related problems in a field or provide the best remediation strategy for the field.

Appendix A: Peng-Robinson Equation-of-State

The equation of the Peng-Robinson EOS (Peng and Robinson, 1976) is

$$P = \frac{RT}{\bar{v} - b} - \frac{a}{\bar{v}(\bar{v} + b) + b(\bar{v} - b)}. \quad (\text{A.1})$$

The parameters a and b for a pure component are computed from

$$a = 0.45748 \frac{R^2 T_c^2}{P_c} \alpha(T), \quad (\text{A.2})$$

$$b = 0.07780 \frac{RT_c}{P_c}, \quad (\text{A.3})$$

$$\sqrt{\alpha} = 1 + f_w \left(1 - \sqrt{\frac{T}{T_c}} \right), \quad (\text{A.4})$$

$$f_w = \begin{cases} 0.37464 + 1.54226\omega - 0.26992\omega^2 & \omega < 0.49 \\ 0.379640 + 1.485030 \omega - 0.164423 \omega^2 + 0.016666 \omega^3 & \omega \geq 0.49 \end{cases}. \quad (\text{A.5})$$

For component i

$$a_i = \frac{0.45748 R^2 T_{c_i}^2}{P_{c_i}} [1 + f_{w_i} (1 - \sqrt{T_r})]^2, \quad (\text{A.6})$$

$$b_i = 0.07780 \frac{RT_{c_i}}{P_{c_i}}, \quad (\text{A.7})$$

For a multi-component mixture, the mixing rules for the two parameters are

$$a_{m,j} = \sum_{i=1}^{n_c} \sum_{k=1}^{n_c} x_{ij} x_{kj} a_{i,k} \quad \text{for phase } j, \quad (\text{A.8})$$

$$a_{i,k} = \sqrt{(a_i a_k)}(1 - \delta_{ik}) \quad , \quad (\text{A.9})$$

$$a_{m,j} = \sum_{i=1}^{n_c} \sum_{k=1}^{n_c} x_{ij} x_{kj} \sqrt{(a_i a_k)}(1 - \delta_{ik}) \quad \text{for phase } j, \quad (\text{A.10})$$

$$b_{m,j} = \sum_{i=1}^{n_c} x_{ij} b_i. \quad (\text{A.11})$$

The constant δ_{ik} is called the binary interaction coefficient between components i and k .

The Peng-Robinson EOS for phase j can be written in the form:

$$Z_j^3 + (B_j - 1)Z_j^2 + (A_j - 3B_j^2 - 2B_j)Z_j + (-A_j B_j + B_j^2 + B_j^3) = 0, \quad (\text{A.12})$$

where $Z_j = \frac{P\bar{v}_j}{RT}$ is the compressibility factor, and A_j and B_j are defined as

$$A_j = \frac{a_{m,j} P}{(RT)^2}, \quad (\text{A.13})$$

$$B_j = \frac{b_{m,j} P}{RT}. \quad (\text{A.14})$$

By including the related parameters for each phase, the compressibility factor for that phase is calculated from the above EOS.

The fugacity is calculated for each component in each phase as follows:

$$\text{Ln}\varphi_{ij} = \frac{b_i}{b} (Z_j - 1) - \text{Ln}(Z_j - B_j) - \frac{A_j}{2\sqrt{2}B_j} \left(\frac{2}{a_j} \sum_{m=1}^{n_c} x_{mj} a_{im} - \frac{b_i}{b_m} \right) \times \text{Ln} \left[\frac{Z_j + (1 + \sqrt{2})B_j}{Z_j + (1 - \sqrt{2})B_j} \right]. \quad (\text{A.15})$$

The enthalpy expression, which is the function of mole fraction, temperature, and pressure is

$$H_j = f(x_{ij}, T, P), \quad (\text{A.16})$$

$$H_j = \frac{T \frac{\partial a_{m,j}}{\partial T} - a_{m,j}}{2\sqrt{2}b_{m,j}} \ln \left(\frac{Z_j + (\sqrt{2} + 1)B_j}{Z_j - (\sqrt{2} - 1)B_j} \right) + RT(Z_j - 1) + H_j^\circ, \quad (\text{A.17})$$

$$H_j^\circ = \sum_{i=1}^n x_i h_i^\circ, \quad (\text{A.18})$$

$$U_j = H_j - PV_j, \quad (\text{A.19})$$

where U is internal energy of phase j . The derivative in Equation (A.17) are defined as

$$\frac{\partial a_{m,j}}{\partial T} = \frac{1}{2} \sum_{i=1}^{n_c} \sum_{k=1}^{n_c} x_{ij} x_{kj} (a_i a_k)^{-\frac{1}{2}} (a_i \frac{\partial a_k}{\partial T} + a_k \frac{\partial a_i}{\partial T}) (1 - \delta_{ik}), \quad (\text{A.20})$$

$$\begin{aligned} \frac{\partial^2 a_{m,j}}{\partial T^2} = & \sum_{i=1}^{n_c} \sum_{k=1}^{n_c} x_{ij} x_{kj} \left[-\frac{1}{4} (a_i a_k)^{-\frac{3}{2}} (a_i \frac{\partial a_k}{\partial T} + a_k \frac{\partial a_i}{\partial T}) + \right. \\ & \left. \frac{1}{2} (a_i a_k)^{-\frac{1}{2}} (a_i \frac{\partial^2 a_k}{\partial T^2} + 2 \frac{\partial a_i}{\partial T} \frac{\partial a_k}{\partial T} + a_k \frac{\partial^2 a_i}{\partial T^2}) \right] (1 - \delta_{ik}), \end{aligned} \quad (\text{A.21})$$

$$\frac{\partial a_i}{\partial T} = -\frac{0.45748 R^2 T_{C_i} f_{w_i}}{P_{C_i} \sqrt{T_{r_i}}} [1 + f_{w_i} (1 - \sqrt{T_{r_i}})], \quad (\text{A.22})$$

$$\frac{\partial^2 a_i}{\partial T^2} = \frac{0.45748 R^2 f_{w_i}}{2 P_{C_i} T_{r_i}^{1.5}} [1 + f_{w_i}], \quad (\text{A.23})$$

$$f_w = \begin{cases} 0.37464 + 1.54226\omega - 0.26992\omega^2 & \omega < 0.49 \\ 0.379640 + 1.485030 \omega - 0.164423 \omega^2 + 0.016666 \omega^3 & \omega \geq 0.49 \end{cases}, \quad (\text{A.24})$$

The derivative of the enthalpy expression for phase j with respect to temperature is

$$\begin{aligned}
\frac{\partial H_j}{\partial T} &= \frac{T \frac{\partial^2 a_{m,j}}{\partial T^2}}{2\sqrt{2} b_{m,j}} \operatorname{Ln} \left(\frac{Z_j + (\sqrt{2} + 1)B_j}{Z_j + (\sqrt{2} - 1)B_j} \right) + \frac{T \frac{\partial a_{m,j}}{\partial T} - a_{m,j}}{2\sqrt{2} b_{m,j}} \frac{2\sqrt{2} \left(Z_j \frac{\partial B_j}{\partial T} - B_j \frac{\partial Z_j}{\partial T} \right)}{(Z_j + (\sqrt{2} - 1)B_j)(Z_j + (\sqrt{2} + 1)B_j)} \\
&+ R[(Z_j - 1) + T \frac{\partial Z_j}{\partial T}] + \frac{\partial H_j^\circ}{\partial T}. \tag{A.25}
\end{aligned}$$

Nomenclature

a	shear coefficient or constant in the Einstein viscosity model
ASI	asphaltene stability index
C_0	drift flux profile parameter
C_b	average bulk particle concentration (lbm/ft ³)
C_s	average surface particle concentration (lbm/ft ³)
$C_{coll.}$	concentration of colloidal asphaltene in oil phase
$C_{floc.}$	concentration of flocculated asphaltene in oil phase
$Coll. Asph.$	colloidal asphaltene
$Floc. Asph$	flocculated asphaltene
$f_{asph.}^*$	fugacity of asphaltene in solid phase at temperature T and pressure P^*
g	porosity-permeability correlation exponent
K_t	transport coefficient
k	permeability
k_{cf}	rate of formation of flocculated asphaltenes from colloidal asphaltenes
k_{fc}	rate of formation of colloidal asphaltenes from flocculated asphaltenes
k_{dc}	rate of formation of colloidal asphaltenes from deposited asphaltenes
k_r	the shear removal factor or rate of reaction for asphaltene-dispersant complex
m_d	mass deposition flux (lbm/sec.ft ²)
N_T	trapping number
P^*	onset pressure of asphaltene
PI	productivity index
p_c	capillary pressure
SP	sticking probability
T	temperature

u_o	oil phase Darcy velocity
$V_{asph.}$	volume of deposited asphaltene per grid block volume
v_o	oil phase interstitial velocity
$v_{cr,o}$	critical oil phase interstitial velocity
α	surface deposition rate coefficient
β	entrainment coefficient
γ	pore throat plugging rate coefficient
δ	asphaltene deposit thickness
θ	contact angle
ρ	density
τ	shear stress
ϕ	porosity
ψ	influx parameters, mass flux per unit length of the cell

References

- Abdalla, A., and K. H. Coats. "A Three-Phase Experimental and Numerical Simulation Study of the Steam Flood Process." In *Fall Meeting of the Society of Petroleum Engineers of AIME*, Society of Petroleum Engineers, 1971.
- Abou-Kassem, J. H. "Investigation of Grid Orientation in a Two Dimensional, Compositional, Three-Phase Steam Model." PhD Dissertation, University of Calgary, 1981.
- Acs, G., S. Deleschall, and E. Farkas. "General Purpose Compositional Model." *Society of Petroleum Engineers Journal* 25, no. 4 (1985): 543-553.
- Adialalis, S. "Investigation of Physical and Chemical Criteria as Related to the Prevention of Asphalt Deposition in Oil Well Tubings." MSc Thesis, Imperial College of the University of London, 1982.
- Adibhatia, B., X. Sun, and K. Mohanty. "Numerical Studies of Oil Production from Initially Oil-Wet Fracture Blocks by Surfactant Brine Imbibition." In *SPE International Improved Oil Recovery Conference in Asia Pacific*, Society of Petroleum Engineers, 2005.
- Akbarzadeh, K., A. Hammami, A. Kharrat, D. Zhang, S. Allenson, J. Creek, S. Kabir, A. Jamaluddin, A.G. Marshall, R. P. Rodgers, O. C. Mullins, and T. Solbakken. "Asphaltenes- Problematic But Rich in Potential." *Oil Field Rev.*, (2007): 22–43.
- Al-Maamari, R. S. H., and J. S. Buckley. "Asphaltene Precipitation and Alteration of Wetting: The Potential for Wettability Changes during Oil Production." *SPE Reservoir Evaluation & Engineering* 6, no. 04 (2003): 210-214.
- Al-Qabandi, S., and A. Al-Naqi. "Field Trial of Downhole Asphaltene Remediation Treatment in a Deep Carbonate Reservoir Kuwait." In *Canadian International Petroleum Conference*, Petroleum Society of Canada, 2003.
- Ali, M. A., and M. R. Islam. "The Effect of Asphaltene Precipitation on Carbonate-Rock Permeability: An Experimental and Numerical Approach." *SPE Production & Facilities* 13, no. 03 (1998): 178-183.

- Amroun, H., and D. Tiab. "Alteration of Reservoir Wettability Due to Asphaltene Deposition in Rhourd-Nouss Sud Est Field Algeria." In *SPE Rocky Mountain Petroleum Technology Conference*, Society of Petroleum Engineers, 2001.
- Andrews, A. B., R. E. Guerra, O. C. Mullins, and P. N. Sen. "Diffusivity of Asphaltene Molecules by Fluorescence Correlation Spectroscopy." *The Journal of Physical Chemistry A* 110, no. 26 (2006): 8093-8097.
- Anisimov, M. A., I. K. Yudin, V. Nikitin, G. Nikolaenko, A. Chernoutsan, H. Toulhoat, D. Frot, and Y. Briolant. "Asphaltene Aggregation in Hydrocarbon Solutions Studied by Photon Correlation Spectroscopy." *The Journal of Physical Chemistry* 99, no. 23 (1995): 9576-9580.
- "ASTM D3279-97 Standard Test Method for *n*-Heptane Insolubles." American Society for Testing and Material, 2001.
- Babu, D. K., and A. S. Odeh. "Productivity of a Horizontal Well." *SPE Reservoir Engineering* 4, no. 04 (1989): 417-421.
- Banavali, R. M., and R. Mukkamala. "Compounds Containing Amide and Carboxyl Groups as Asphaltene Dispersants in Crude Oil." U.S. Patent 7,122,112, issued October 17, 2006.
- Beal, S. K. "Deposition of Particles in Turbulent Flow on Channel or Pipe Walls." *Nucl. Sci. Eng* 40, no. 1 (1970): 1-11.
- Behie, A., D. Collins, P. A. Forsyth Jr, and P. H. Sammon. "Fully Coupled Multiblock Wells in Oil Simulation." *Society of Petroleum Engineers Journal* 25, no. 04 (1985): 535-542.
- Boduszynski, M. M. "Asphaltenes in Petroleum Asphalts." *Advances in Chemistry Series* 195 (1981): 119-35.
- Boussingault, J. B. "Memoire sur la Composition des Bitumens." In *Annales de Chimie et de Physique*, vol. 64, p. 141, 1837.
- Brantferger, K. M., G. A. Pope, and K. Sepehrnoori. "Development of a Thermodynamically Consistent Fully Implicit Equation-of-State Compositional Steamflood Simulator." In *SPE Symposium on Reservoir Simulation*, Society of Petroleum Engineers, 1991.
- Brill J. P., H. D. Beggs. "*Two-Phase Flow in Pipes*." Lecture Notes, University of Tulsa, 1978.

- Buckley, J. S. "*Mechanisms and Consequences of Wettability Alteration by Crude Oils.*" PhD Dissertation, Heriot-Watt University, 1996.
- Buckley, J. S. "Asphaltene Deposition." *Energy & Fuels* 26, no. 7 (2012): 4086-4090.
- Burke, N. E., R. E. Hobbs, and S. F. Kashou. "Measurement and Modeling of Asphaltene Precipitation." *Journal of Petroleum Technology* 42, no. 11 (1990): 1440-1446.
- Burya, Y. G., I. K. Yudin, V. A. Dechabo, V. I. Kosov, and M. A. Anisimov. "Light-Scattering Study of Petroleum Asphaltene Aggregation." *Applied optics* 40, no. 24 (2001): 4028-4035.
- Carnahan, N. F. "Precipitation of Asphaltene in Heavy Oil and Tar Sands." *Developments in petroleum science* (2000): 319-333.
- Cenegy, L. M. "Survey of Successful World-Wide Asphaltene Inhibitor Treatments in Oil Production Fields." In *SPE Annual Technical Conference and Exhibition*, Society of Petroleum Engineers, 2001.
- Cicek, O. "Numerical Simulation of Steam Displacement of Oil in Naturally Fractured Reservoirs Using Fully Implicit Compositional Formulation: A Comparative Analysis of the Effects of Capillary and Gravitational Forces in Matrix/Fracture Exchange Term." In *SPE Annual Technical Conference and Exhibition*, Society of Petroleum Engineers, 2005.
- Cimino, R., S. Corraera, P. A. Sacomani, and C. Carniani. "Thermodynamic Modeling for Prediction of Asphaltene Deposition in Live Oil." In *SPE International symposium on oilfield chemistry*, Society of Petroleum Engineers, 1995.
- Civan, F. "A Multi-Purpose Formation Damage Model." In *International symposium on formation damage control*, Society of Petroleum Engineers, 1996.
- Chang, Y. B. "*Development and Application of an Equation of State Compositional Simulator.*" PhD Dissertation, The University of Texas at Austin, 1990.
- Chang, Y. B., G. A. Pope, and K. Sepehrnoori. "A Higher-Order Finite-Difference Compositional Simulator." *Journal of Petroleum Science and Engineering* 5, no. 1 (1990): 35-50.
- Chang, C. L., and H. S. Fogler. "Asphaltene Stabilization in Alkyl Solvents using Oil-Soluble Amphiphiles." In *SPE International Symposium on Oilfield Chemistry*, Society of Petroleum Engineers, 1993.

- Chang, C. L., and H. S. Fogler. "Stabilization of Asphaltenes in Aliphatic Solvents using Alkylbenzene-Derived Amphiphiles. 1. Effect of the Chemical Structure of Amphiphiles on Asphaltene Stabilization." *Langmuir* 10, no. 6 (1994-a): 1749-1757.
- Chang, C. L., and H. S. Fogler. "Stabilization of Asphaltenes in Aliphatic Solvents using Alkylbenzene-Derived Amphiphiles. 2. Study of the Asphaltene-Amphiphile Interactions and Structures using Fourier Transform Infrared Spectroscopy and Small-Angle X-ray Scattering Techniques." *Langmuir* 10, no. 6 (1994-b): 1758-1766.
- Chapman, W. G., K. E. Gubbins, G. Jackson, and M. Radosz. "New Reference Equation of State for Associating Liquids." *Industrial & Engineering Chemistry Research* 29, no. 8 (1990): 1709-1721.
- Chien, M. C. H., H. E. Yardumian, E. Y. Chung, and W. W. Todd. "The Formulation of a Thermal Simulation Model in a Vectorized General Purpose Reservoir Simulator." In *SPE Symposium on Reservoir Simulation*, Society of Petroleum Engineers, 1989.
- Cleaver, J. W., and B. Yates. "A Sub-layer Model for the Deposition of Particles from a Turbulent Flow." *Chemical Engineering Science* 30, no. 8 (1975): 983-992.
- Coats, K. H., W. D. George, C. Chu, and B. E. Marcum. "Three-Dimensional Simulation of Steamflooding." *Society of Petroleum Engineers Journal* 14, no. 06 (1974): 573-592.
- Coats, K. H. "Simulation of Steamflooding with Distillation and Solution Gas." *Society of Petroleum Engineers Journal* 16, no. 05 (1976): 235-247.
- Coats, K. H. "A Highly Implicit Steamflood Model." *Society of Petroleum Engineers Journal* 18, no. 05 (1978): 369-383.
- Corey, A. T., C. H. Rathjens, J. H. Henderson, and M. R. J. Wyllie. "Three-Phase Relative Permeability." *Journal of Petroleum Technology* 8, no. 11 (1956): 63-65.
- Darabi, H., K. Sepehrnoori, and M. H. Kalaei. "Modeling of Wettability Alteration Due to Asphaltene Deposition in Oil Reservoirs." In *SPE Annual Technical Conference and Exhibition*, Society of Petroleum Engineers, 2012.
- Darabi, H., M. Shirdel, M. H. Kalaei, and K. Sepehrnoori. "Aspects of Modeling Asphaltene Deposition in a Compositional Coupled Wellbore/Reservoir

- Simulator." In *SPE Improved Oil Recovery Symposium*, Society of Petroleum Engineers, 2014.
- Davies, J. T. "A New Theory of the Deposition of Colloidal Particles from Turbulent Fluids." *Annals of the New York Academy of Sciences* 404, no. 1 (1983): 313-326.
- De Boer, R. B., K. Leerlooyer, M. R. P. Eigner, and A. R. D. Van Bergen. "Screening of Crude Oils for Asphalt Precipitation: Theory Practice and the Selection of Inhibitors." *SPE Production & Facilities* 10, no. 01 (1995): 55-61.
- Delshad, M., and G. A. Pope. "Comparison of the Three-Phase Oil Relative Permeability Models." *Transport in Porous Media* 4, no. 1 (1989): 59-83.
- Eastman, J. A., S. R. Phillpot, S. U. S. Choi, and P. Keblinski. "Thermal Transport in Nanofluids 1." *Annu. Rev. Mater. Res.* 34 (2004): 219-246.
- Escobedo, J., and G. A. Mansoori. "Asphaltene and Other Heavy-Organic Particle Deposition during Transfer and Production Operation." In *SPE Annual Technical Conference and Exhibition*, Society of Petroleum Engineers, 1995.
- Fazelipour, W., G.A. Pope, and K. Sepehrnoori. "Development of a Fully Implicit Parallel EOS Compositional Simulator to Model Asphaltene Precipitation in Petroleum Reservoirs." In *SPE Annual Technical Conference and Exhibition*, Society of Petroleum Engineers, 2008.
- Ferrer, J. "A Three-Phase Two-Dimensional Compositional Thermal Simulator For Steam Injection Processes." *Journal of Canadian Petroleum Technology* 16, no. 01 (1977): 78-90.
- Ferworn, K. A., W. Y. Svrcek, and A. K. Mehrotra. "Measurement of Asphaltene Particle Size Distributions in Crude Oils Diluted with n-Heptane." *Industrial & Engineering Chemistry Research* 32, no. 5 (1993): 955-959.
- Feustel, M., P. Klug, D. Miller, and A. Vollmer. "Ethercarboxylic Acids as Asphaltene Dispersants in Crude Oils." U.S. Patent 6,063,146, issued May 16, 2000.
- Flory, P. J. "Thermodynamics of High Polymer Solutions." *The Journal of Chemical Physics* 10, no. 1 (1942): 51-61.
- Friedlander, S. K., and H. F. Johnstone. "Deposition of Suspended Particles from Turbulent Gas Streams." *Industrial & Engineering Chemistry* 49, no. 7 (1957): 1151-1156.

- Galoppini, M., and M. Tambini. "Asphaltene Deposition Monitoring and Removal Treatments: An Experience in Ultra Deep Wells." In *European Production Operations Conference and Exhibition*, Society of Petroleum Engineers, 1994.
- Geankoplis, C. J. "*Transport Processes and Unit Operations*, 3rd ed." Prentice Hall: Upper Saddle River, NJ, 1993.
- "GEM, CMG: Version 2011 User's Guide." Computer Modeling Group Ltd., Calgary, Alberta, 2011.
- Godderij, R. R., J. Bruining, and J. Molenaar. "A Fast 3D Interface Simulator for Steamdrives." *SPE Journal* 4, no. 04 (1999): 400-408.
- Gonzalez Rodriguez, D. L. "*Modeling of Asphaltene Precipitation and Deposition Tendency using the PC-SAFT Equation of State*." PhD Dissertation, Rice University, 2008.
- "GPAS: Technical Documentation for GPAS-3.5." Reservoir Engineering Research Program, Center for Petroleum and Geosystems Engineering, The University of Texas at Austin, 2005.
- Groenzin, H., and O. C. Mullins. "Molecular Size and Structure of Asphaltenes from Various Sources." *Energy & Fuels* 14, no. 3 (2000): 677-684.
- Gross, J., and G. Sadowski. "Perturbed-Chain SAFT; An Equation of State Based on a Perturbation Theory for Chain Molecules." *Industrial & Engineering Chemistry Research* 40, no. 4 (2001): 1244-1260.
- Gruesbeck, C., and R. E. Collins. "Entrainment and Deposition of Fine Particles in Porous Media." *Society of Petroleum Engineers Journal* 22, no. 6 (1982): 847-856.
- Gupta, A. K. "*A Model for Asphaltene Flocculation using an Equation of State*." MSc Thesis, Chemical and Petroleum Engineering, University of Calgary, 1986.
- Haji-Akbari, N., P. Masirisuk, M. P. Hoepfner, and H. S. Fogler. "A Unified Model for Aggregation of Asphaltenes." *Energy & Fuels* 27, no. 5 (2013): 2497-2505.
- Hammami, A., C. H. Phelps, T. Monger-McClure, and T. M. Little. "Asphaltene Precipitation from Live Oils: An Experimental Investigation of Onset Conditions and Reversibility." *Energy & Fuels* 14, no. 1 (2000): 14-18.

- Haskett, C. E., and M. Tartera. "A Practical Solution to the Problem of Asphaltene Deposits-Hassi Messaoud Field Algeria." *Journal of Petroleum Technology* 17, no. 04 (1965): 387-391.
- Hilbert A.D. "*Numerical Simulation of the Electric Pre-Heat and Steam Drive Bitumen Recovery Process for the Athabasca Oil Sands.*" PhD Dissertation, Department of Electrical Engineering, University of Alberta, 1986.
- Hirschberg, A., L. N. J. DeJong, B. A. Schipper, and J. G. Meijer. "Influence of Temperature and Pressure on Asphaltene Flocculation." *Society of Petroleum Engineers Journal* 24, no. 03 (1984): 283-293.
- Hortal, A. R., B. Martínez-Haya, M. D. Lobato, J. M. Pedrosa, and S. Lago. "On the Determination of Molecular Weight Distributions of Asphaltenes and Their Aggregates in Laser Desorption Ionization Experiments." *Journal of Mass Spectrometry* 41, no. 7 (2006): 960-968.
- Huang, S. S., and S. B. Dyer. "Miscible Displacement in the Weyburn Reservoir: a Laboratory Study." *Journal of Canadian Petroleum Technology* 32, no. 07 (1993): 42-52.
- Hutchinson, P. G. F. A. E., G. F. Hewitt, and A. E. Dukler. "Deposition of Liquid or Solid Dispersions from Turbulent Gas Streams: A Stochastic Model." *Chemical Engineering Science* 26, no. 3 (1971): 419-439.
- Ishimoto, K., G. A. Pope, and K. Sepehrnoori. "An Equation of State Steam Simulator." *In Situ* 11, no.1, (1987): 1-37.
- Jaoui, M., C. A., N. Hasnaoui, and M. Rogalski. "Adsorption Isotherms of Phenol and 4-Chlorophenol on Petroleum Asphaltenes." *Oil & Gas Science and Technology* 53, no. 1 (1998): 35-40.
- Jensen, O. K. "An Automatic Timestep Selection Scheme for Reservoir Simulation." In *SPE Annual Technical Conference and Exhibition*, Society of Petroleum Engineers, 1980.
- Joshi, N. B., O. C. Mullins, A. Jamaluddin, J. Creek, and J. McFadden. "Asphaltene Precipitation from Live Crude Oil." *Energy & Fuels* 15, no. 4 (2001): 979-986.
- Kaminsky, R., and C. J. Radke. "Asphaltenes Water Films and Wettability Reversal." *SPE Journal* 2, no. 04 (1997): 485-493.

- Karan, K., A. Hammami, M. Flannery, and B. A. Stankiewicz. "Evaluation of Asphaltene Instability and a Chemical Control during Production of Live Oils." *Petroleum Science and Technology* 21, no. 3-4 (2003): 629-645.
- Kell, G. S. "Density, Thermal Expansivity, and Compressibility of Liquid Water from 0. deg. to 150. deg.. Correlations and Tables for Atmospheric Pressure and Saturation Reviewed and Expressed on 1968 Temperature Scale." *Journal of Chemical and Engineering Data* 20, no. 1 (1975): 97-105.
- Kim, S. T., M. E. Boudh-Hir, and G. A. Mansoori. "The Role of Asphaltene in Wettability Reversal." In *SPE Annual Technical Conference and Exhibition*, Society of Petroleum Engineers, 1990.
- Kohse, Bruce F., Long X. Nghiem, Haruo Maeda, and Kenji Ohno. "Modelling Phase Behaviour Including the Effect of Pressure and Temperature on Asphaltene Precipitation." In *SPE Asia Pacific Oil and Gas Conference and Exhibition*, Society of Petroleum Engineers, 2000.
- Kohse, B. F., and L. X. Nghiem. "Modelling Asphaltene Precipitation and Deposition in a Compositional Reservoir Simulator." In *SPE/DOE Symposium on Improved Oil Recovery*, Society of Petroleum Engineers, 2004.
- Kokal, S. L., and S. G. Sayegh. "Asphaltenes: The Cholesterol of Petroleum." In *Middle East Oil Show & Conference*, Society of Petroleum Engineers, 1995.
- Kontogeorgis, G. M., E. C. Voutsas, I. V. Yakoumis, and D. P. Tassios. "An Equation of State for Associating Fluids." *Industrial & Engineering Chemistry Research* 35, no. 11 (1996): 4310-4318.
- Kraiwattanawong, K., H. S. Fogler, S. G. Gharfeh, P. Singh, W. H. Thomason, and S. Chavadej. "Effect of Asphaltene Dispersants on Aggregate Size Distribution and Growth." *Energy & Fuels* 23, no. 3 (2009): 1575-1582.
- Krieger, I. M., and T. J. Dougherty. "A Mechanism for Non-Newtonian Flow in Suspensions of Rigid Spheres." *Transactions of the Society of Rheology* 3, no. 1 (1959): 137-152.
- León, O., E. Rogel, A. Urbina, A. Andújar, and A. Lucas. "Study of the Adsorption of Alkyl Benzene-Derived Amphiphiles on Asphaltene Particles." *Langmuir* 15, no. 22 (1999): 7653-7657.
- Lauwerier, H. A. "The Transport of Heat in an Oil Layer Caused by the Injection of Hot Fluid." *Applied Scientific Research, Section A* 5, no. 2-3 (1955): 145-150.

- Leontaritis, K. J. "Asphaltene Near-Wellbore Formation Damage Modeling." In *International Symposium on Formation Damage Control*, Society of Petroleum Engineers, 1998.
- Leontaritis, K. J., and G. A. Mansoori. "Asphaltene Flocculation during Oil Production and Processing: A Thermodynamic Colloidal Model." In *Int. Symp. Oilfield Chemistry*, Society of Petroleum Engineers, 1987.
- Leontaritis, K. J., and G. A. Mansoori. "Asphaltene Deposition: A Survey of Field Experiences and Research Approaches." *Journal of Petroleum Science and Engineering* 1, no. 3 (1988): 229-239.
- Leontaritis, K. J., S. Kawanaka, and G. A. Mansoori. "Descriptive Accounts of Thermodynamic and Colloidal Models of Asphaltene Flocculation." In *Proc. Symp. Advances in Oil Field Chemistry, 3rd Chem. Congr.*, North American Continent, and 195th Nat. Mtg. Am. Chem. Soc., 1988.
- Lichaa, P. M. "Asphaltene Deposition Problem in Venezuela Crudes-Usage of Asphaltenes in Emulsion Stability." *Oil Sands* (1977): 609-624.
- Lichaa, P. M., and L. Herrera. "Electrical and Other Effects Related to the Formation and Prevention of Asphaltene Deposition Problem in Venezuelan Crudes." In *SPE Oilfield Chemistry Symposium*, Society of Petroleum Engineers, 1975.
- Lin, C. S., R. W. Moulton, and G. L. Putnam. "Mass Transfer between Solid Wall and Fluid Streams. Mechanism and Eddy Distribution Relationships in Turbulent Flow." *Industrial & Engineering Chemistry* 45, no. 3 (1953): 636-640.
- Lohrenz, J., B. G. Bray, and C. R. Clark. "Calculating Viscosities of Reservoir Fluids from Their Compositions." *Journal of Petroleum Technology* 16, no. 10 (1964): 1171-1176.
- Maqbool, T., S. Raha, M. P. Hoepfner, and H. S. Fogler. "Modeling the Aggregation of Asphaltene Nanoaggregates in Crude oil- Precipitant Systems." *Energy & Fuels* 25, no. 4 (2011): 1585-1596.
- Mehra, R. K., R. A. Heidemann, and K. Aziz. "An Accelerated Successive Substitution Algorithm." *The Canadian Journal of Chemical Engineering* 61, no. 4 (1983): 590-596.
- Merdrignac, I., B. Desmazieres, P. Terrier, A. Delobel, and O. Laprevote. "Analysis of Raw and Hydrotreated Asphaltenes Using Off-Line and On-Line SEC/MS

- Coupling." In *International Conference on Heavy Organics Deposition, Mexico*, 2004.
- Michelsen, M. L. "The Isothermal Flash Problem. Part I. Stability." *Fluid Phase Equilibria* 9, no. 1 (1982): 1-19.
- Miller, D., M. Feustel, A. Vollmer, R. Vybiral, and D. Hoffmann. "Synergistic Mixtures of Alkylphenol-Formaldehyde Resins with Oxalkylated Amines as Asphaltene Dispersants." U.S. Patent 6,180,683, issued January 30, 2001(a).
- Miller, D., A. Vollmer, M. Feustel, and P. Klug. "Synergistic Mixtures of Phosphoric Esters with Carboxylic Acids or Carboxylic Acid Derivatives as Asphaltene Dispersants." U.S. Patent 6,204,420, issued March 20, 2001(b).
- Minssieux, L. "Core Damage from Crude Asphaltene Deposition." In *SPE International Symposium on Oilfield Chemistry*, Society of Petroleum Engineers, 1997.
- Moritis, G. "Flow Assurance Challenge Production from Deeper Water." *Oil and Gas Journal* 99, (2001).
- Muhammad, M., N. Joshi, J. Creek, and J. McFadden, "Effect of Oil Based Mud Contamination on Live Fluid Asphaltene Precipitation Pressure." In *the 5th International Conference on Petroleum Phase Behavior and Fouling*, Bnaff, Alberta, Canada, 2004.
- Mukkamala, R. "Carbonyl, Thiocarbonyl or Imine Containing Compounds as Asphaltene Dispersants in Crude Oil." U.S. Patent 7,097,759, issued August 29, 2006.
- Newberry, M. E., and K. M. Barker. "Organic Formation Damage Control and Remediation." In *SPE International Symposium on Formation Damage Control*, Society of Petroleum Engineers, 2000.
- Ngheim, L. X. "*Phase Behavior Modeling and Compositional Simulation of Asphaltene Deposition in Reservoirs.*" PhD dissertation, University of Alberta, 1999.
- Nghiem, L. X., M. S. Hassam, R. Nutakki, and A. E. D. George. "Efficient Modeling of Asphaltene Precipitation." In *SPE Annual Technical Conference and Exhibition*, Society of Petroleum Engineers, 1993.
- Nielsen, L. E. "Generalized Equation for the Elastic Moduli of Composite Materials." *Journal of Applied Physics* 41, no. 11 (1970): 4626-4627.

- Nielsen, B. B., W. Y. Svrcek, and A. K. Mehrotra. "Effects of Temperature and Pressure on Asphaltene Particle Size Distributions in Crude Oils Diluted with n-Pentane." *Industrial & engineering chemistry research* 33, no. 5 (1994): 1324-1330.
- Novosad, Z., and T. G. Costain. "Experimental and Modeling Studies of Asphaltene Equilibria for a Reservoir Under CO₂ Injection." In *SPE Annual Technical Conference and Exhibition*, Society of Petroleum Engineers, 1990.
- Nor-Azlan, N., and M. A. Adewumi. "Development of Asphaltene Phase Equilibrium Predictive Model." In *SPE Eastern Regional Meeting*, Society of Petroleum Engineers, 1993.
- Pan, Huanquan, and A. Firoozabadi. "A Thermodynamic Micellization Model for Asphaltene Precipitation: Part I: Micellar Size and Growth." In *SPE Annual Technical Conference*, Society of Petroleum Engineers, 1996.
- Peaceman, D. W. "Interpretation of Well-Block Pressure in Numerical Reservoir Simulation with Non-square Grid Blocks and Anisotropic Permeability." *Journal of Petroleum Technology*, (1983): 531-543.
- Peng, D. Y., and D. B. Robinson. "A New Two-Constant Equation of State." *Industrial & Engineering Chemistry Fundamentals* 15, no. 1 (1976): 59-64.
- Permsukarome, P., C. Chang, and H. S. Fogler. "Kinetic Study of Asphaltene Dissolution in Amphiphile/Alkane Solutions." *Industrial & Engineering Chemistry Research* 36, no. 9 (1997): 3960-3967.
- Perschke, D. R. "*Equation of State Phase Behavior Modeling for Compositional Simulator*." PhD Dissertation, The University of Texas at Austin, 1988.
- Pope, G. A., W. Wu, G. Narayanaswamy, M. Delshad, M. M. Sharma, and P. Wang. "Modeling Relative Permeability Effects in Gas-Condensate Reservoirs with a New Trapping Model." *SPE Reservoir Evaluation & Engineering* 3, no. 02 (2000): 171-178.
- Qian, K., K. E. Edwards, M. Siskin, W. N. Olmstead, A. S. Mennito, G. J. Dechert, and N. E. Hoosain. "Desorption and Ionization of Heavy Petroleum Molecules and Measurement of Molecular Weight Distributions." *Energy & fuels* 21, no. 2 (2007): 1042-1047.

- Qin, X. "*Modelling Asphaltene Precipitation and Implementation of Group Contribution Equation of State into UTCOMP.*" MSc Thesis, The University of Texas at Austin, 1998.
- Qin, X., P. Wang, K. Sepehrnoori, and G. A. Pope. "Modeling asphaltene precipitation in reservoir simulation." *Industrial & Engineering Chemistry Research* 39, no. 8 (2000): 2644-2654.
- Ramirez-Jaramillo, E., C. Lira-Galeana, and O. Manero. "Modeling Asphaltene Deposition in Production Pipelines." *Energy & Fuels* 20, no. 3 (2006): 1184-1196.
- Rassamdana, H., B. Dabir, M. Nematy, M. Farhani, and M. Sahimi. "Asphalt Flocculation and Deposition: I. The Onset of Precipitation." *AIChE Journal* 42, no. 1 (1996): 10-22.
- Reis, J. C., and A. M. Acock. "Permeability Reduction Models for the Precipitation of Inorganic Solids in Berea Sandstone." *In Situ* 18, no. 3 (1994): 347-368.
- Rubin, B., and W. L. Buchanan. "A General Purpose Thermal Model." *Society of Petroleum Engineers Journal* 25, no. 02 (1985): 202-214.
- Scotti, R., and L. Montanari. "Molecular Structure and Intermolecular Interaction of Asphaltenes by FT-IR, NMR, EPR." In *Structures and Dynamics of Asphaltenes*. Springer US, 1998.
- Shirdel, M. "*Development of a Coupled Wellbore-Reservoir Compositional Simulator for Damage Prediction and Remediation.*" PhD Dissertation, The University of Texas at Austin, 2013.
- Shirdel, M., and K. Sepehrnoori. "Development of a Coupled Compositional Wellbore/Reservoir Simulator for Modeling Pressure and Temperature Distribution in Horizontal Wells." In *SPE Annual Technical Conference and Exhibition*, Society of Petroleum Engineers, 2009.
- Shutler, N. D. "Numerical Three-Phase Simulation of the Linear Steamflood Process." *Society of Petroleum Engineers Journal* 9, no. 02 (1969): 232-246.
- Soave, G. "Equilibrium Constants from a Modified Redlich-Kwong Equation of State." *Chemical Engineering Science* 27, no. 6 (1972): 1197-1203.

- Srivastava, R. K., S. S. Huang, S. B. Dyer, and F. M. Mourits. "Quantification of Asphaltene Flocculation During Miscible CO₂ Flooding In the Weyburn Reservoir." *Journal of Canadian Petroleum Technology* 34, no. 08 (1995): 31-42.
- Stone, H. L. "Estimation of Three-Phase Relative Permeability and Residual Oil Data." *Journal of Canadian Petroleum Technology* 12, no. 04 (1973): 53-61.
- Ting, D. L. "*Thermodynamic Stability and Phase Behavior of Asphaltenes in Oil and of Other Highly Asymmetric Mixtures.*" PhD Dissertation, Rice University, 2003.
- Thawer, R., D. C. Nicoll, and G. Dick. "Asphaltene Deposition in Production Facilities." *SPE Production Engineering* 5, no. 04 (1990): 475-480.
- Thomas, F. B., D. B. Bennion, D. W. Bennion, and B. E. Hunter. "Experimental and Theoretical Studies of Solids Precipitation from Reservoir Fluid." *Journal of Canadian Petroleum Technology* 31, no. 01 (1992): 22-31.
- Trangenstein, J. A. "Customized Minimization Techniques for Phase Equilibrium Computations in Reservoir Simulation." *Chemical Engineering Science* 42, no. 12 (1987): 2847-2863.
- Turek, E. A., R. S. Metcalfe, L. Yarborough, and R. L. Robinson Jr. "Phase Equilibria in CO₂-Multicomponent Hydrocarbon Systems: Experimental Data and an Improved Prediction Technique." *Society of Petroleum Engineers Journal* 24, no. 3 (1984): 308-324.
- Turta, A. T., J. Najman, A. K. Singhal, S. Leggitt, and D. Fisher. " Permeability Impairment due to Asphaltenes during Gas Miscible Flooding and its Mitigation." In *International Symposium on Oilfield Chemistry*, Society of Petroleum Engineers, 1997.
- Tuttle, R. N. "High-Pour-Point and Asphaltic Crude Oils and Condensates." *Journal of Petroleum Technology* 35, no. 06 (1983): 1192- 1196.
- "*UTCHEM: Technical Documentation for UTCHEM-10.*" Reservoir Engineering Research Program, Center for Petroleum and Geosystems Engineering, The University of Texas at Austin, 2003.
- "*UTCOMP: Technical Documentation for UTCOMP 3.8.*" Reservoir Engineering Research Program, Center for Petroleum and Geosystems Engineering, The University of Texas at Austin, 2003.

- Varavei, A. "*Development of an Equation-of-State Thermal Flooding Simulator.*" PhD Dissertation, The University of Texas at Austin, 2009.
- Vargas, F. M. "*Modeling Asphaltene Precipitation and Arterial Deposition.*" PhD Dissertation, Rice University, 2009.
- Verdier, S., H. Carrier, S. I. Andersen, and J. L. Daridon. "Study of Pressure and Temperature Effects on Asphaltene Stability in Presence of CO₂." *Energy & fuels* 20, no. 4 (2006): 1584-1590.
- Vinsome, P. K. W. "A Numerical Description of Hot-Water and Steam Drives By The Finite-Difference Method." In *Fall Meeting of the Society of Petroleum Engineers of AIME*, Society of Petroleum Engineers, 1974.
- Vinsome, P. K. W., and J. Westerveld. "A Simple Method For Predicting Cap And Base Rock Heat Losses in Thermal Reservoir Simulators." *Journal of Canadian Petroleum Technology* 19, no. 03 (1980): 87-90.
- Von Albrecht, C., W.M. Salathiel, and D.E. Nierode. "Stimulation of Asphaltic Deep Wells and Shallow Wells in Lake Maracaibo, Venezuela. Advances in Methods of Increasing Well Productivity and Injectivity." *Can. Pet. Technol. J., Oil Sands* 7, no. 1, (1977): 55-62.
- Wang, S. "*Simulation of Asphaltene Deposition in Petroleum Reservoirs during Primary Oil Recovery.*" PhD Dissertation, University of Oklahoma, 2000.
- Wang, S., and F. Civan. "Productivity Decline of Vertical and Horizontal Wells by Asphaltene Deposition in Petroleum Reservoirs." In *SPE International Symposium on Oilfield Chemistry*, Society of Petroleum Engineers, 2001.
- Wargadalam, V. J., K. Norinaga, and M. Iino. "Size and Shape of a Coal Asphaltene Studied by Viscosity and Diffusion Coefficient Measurements." *Fuel* 81, no. 11 (2002): 1403-1407.
- Watkinson, A. P. "*Particulate Fouling of Sensible Heat Exchangers.*" PhD Dissertation, University of British Columbia, 1968.
- Wilkes, M. F., and Davies, M. C. "Asphaltene Inhibition," U.S. Patent 20,080,096,772, issued April 24, 2008.
- "*WinProp, CMG: Version 2011 User's Guide.*" Computer Modeling Group Ltd., Calgary, Alberta, 2011.

Won, K. W. "Thermodynamics for Solid Solution-Liquid-Vapor Equilibria: Wax Phase Formation from Heavy Hydrocarbon Mixtures." *Fluid Phase Equilibria* 30 (1986): 265-279.

Yan, J., H. Plancher, and N. R. Morrow. "Wettability Changes Induced by Adsorption of Asphaltenes." *SPE Production & Facilities* 12, no. 04 (1997): 259-266.